THE UNIVERSITY OF MICHIGAN
JAN 3 1961
ENGINEERING

JOURNAL OF FLUID MECHANICS

VOLUME 9 PART 4

DECEMBER 1960

PUBLISHED BY

CAMBRIDGE UNIVERSITY PRESS

BENTLEY HOUSE, 200 EUSTON ROAD, LONDON, N.W.1

AMERICAN BRANCH: 32 EAST 57TH STREET, NEW YORK 22, N.Y.

Price 30*s.* (*U.S.A.* $5.00)

The JOURNAL OF FLUID MECHANICS exists for the publication of theoretical and experimental investigations of all aspects of the mechanics of fluids, and is issued in four parts per volume.

EDITOR

DR G. K. BATCHELOR

Department of Applied Mathematics and Theoretical Physics, University of Cambridge, Free School Lane, Cambridge, England

ASSISTANT EDITORS

DR T. B. BENJAMIN, DR I. PROUDMAN

Department of Applied Mathematics and Theoretical Physics, University of Cambridge, Free School Lane, Cambridge, England

ASSOCIATE EDITORS

PROF. G. F. CARRIER

Pierce Hall, Harvard University, Cambridge 38, *Massachusetts, U.S.A.*

DR W. C. GRIFFITH

Lockheed Missiles and Space Division, Palo Alto, California, U.S.A.

M. J. LIGHTHILL

Royal Aircraft Establishment, Farnborough, Hampshire, England

PROF. R. R. LONG

School of Engineering, The Johns Hopkins University, Baltimore 18, *Maryland, U.S.A.*

DR P. G. SAFFMAN

Department of Mathematics, King's College, London, W.C. 2, *England*

Authors wishing to have papers published in the JOURNAL should communicate them to any one of the persons named above, choosing one in their own country where possible.

Authors are urged to ensure that their papers are written clearly and attractively, in order that their work will be readily accessible to readers.

Manuscripts should be typed in double spacing on one side of the paper only, with references listed at the end in alphabetical order of authors. Drawings should be done on a large scale in Indian ink on tracing cloth or drawing paper, the lettering being shown clearly in pencil for reproduction by the printer; the list of captions should be typed at the end of the manuscript. Proofs of papers from overseas will usually be despatched to authors by airmail. There is no charge for publication. Authors are entitled to receive 50 offprints of a paper in the JOURNAL free of charge, and additional offprints can be purchased if ordered in advance.

SUBSCRIPTIONS

The subscription price for a volume of four parts is £5. 10*s*. net, post free, payable in advance; separate parts 30*s*. net, plus postage. Subscriptions may be sent to any bookseller, or to the Cambridge University Press, Bentley House, 200 Euston Road, London, N.W.1.

Subscribers in the United States should send their orders to the Cambridge University Press, American Branch, 32 East 57th Street, New York 22, N.Y. The subscription price per volume is $18.50, post free, payable in advance; separate parts $5.00, plus postage.

Quotations for available back volumes and parts may be obtained on application to the Cambridge University Press.

One-dimensional magnetogasdynamics in oblique fields

By J. A. SHERCLIFF
Department of Engineering, University of Cambridge

(Received 2 August 1960)

Earlier work on the dynamics of a perfectly conductive gas in situations where all variables depend on one space co-ordinate only is extended to the case where the magnetic field has a component in the direction of variation. The theory is developed for an arbitrary gas in equilibrium, subject only to certain reasonable restrictions.

The first main section studies the variation of the transverse field component in slow and fast simple waves and the tendency of compressive waves in which the transverse field does not change sign to steepen into shocks.

The next section develops a symmetrical treatment of the Rayleigh, Fanno and other processes of ordinary steady one-dimensional gasdynamics, generalized to allow for electromagnetic effects. The slow, fast and Alfvén wave speeds are critical. A particular case of this analysis is a generalization of ordinary gasdynamics which allows for the effect of transverse forces such as occur in turbomachinery.

The final section is an exhaustive study of shocks in the presence of a field component normal to the shock front. From the generalized Rayleigh line it is established that there are up to six different types of shocks, all compressive and distinguishable by the relative magnitudes of the upstream and downstream normal velocities in comparison with the local slow, fast and Alfvén wave speeds.

Some aspects of shock structure are discussed briefly.

1. Introduction

In an earlier paper (Shercliff 1960) the theory of one-dimensional magnetogasdynamics was developed for arbitrary, isotropic, conducting gases in thermodynamic equilibrium for the case where the magnetic field is transverse to the longitudinal direction, i.e. the direction in which variation occurs. In this paper we extend the analysis to the situation where there is also a longitudinal magnetic field component. This adds the complication that transverse momentum is no longer conserved.

The meanings of some of the less obvious symbols used in the paper are defined in the following list.

Notation

B = magnitude of magnetic field $\mathbf{B}$ $\quad$ B_x, etc., Cartesian components of $\mathbf{B}$

$b = B/(\mu\rho)^{\frac{1}{2}}$ $\quad$ $b_x = B_x/(\mu\rho)^{\frac{1}{2}}$, etc.

c = fast or slow sound speeds (c_f and c_s, respectively)

$F_x = p + \rho v_x^2 + B_y^2/2\mu$ $\quad$ $F_y = \rho v_x v_y - B_x B_y/\mu$

$f_x = p + \rho v_x^2$ $\quad$ $f_y = \rho v_x v_y$
$G = \rho v_x$ $\quad$ $H = h + \frac{1}{2}(v_x^2 + v_y^2)$
h = enthalpy; also $|\Delta B_y|/B$, upstream of shock
$s_0 = (a/b)^2$, upstream of shock $\quad$ u = internal energy
v = magnitude of velocity $\mathbf{v}$ $\quad$ v_x, etc., Cartesian components of $\mathbf{v}$
$X = v_x^4 - v_x^2(a^2 + b^2) + a^2 b_x^2$ $\quad$ $\theta_0 = \tan^{-1}(B_y/B_x)$, upstream of shock
$\rho_0 = 1/\tau_0$ $\quad$ $\tau = 1/\rho$, specific volume
$\tau_0 = B_x^2/\mu G^2$ $\quad$ $\tau_x = F_x/G^2$
Δ = difference across shock $\quad$ $\tau_y = F_y/G^2$
$\bar{\tau}$, etc., bar denotes mean between two sides of shock
1, 2 (suffices) upstream, downstream of shock

It is desirable to develop the theory so as to apply to any gas, since magnetogasdynamics often concerns partially ionized or reactive gases of variable mean molecular weight. It is, moreover, easier on the whole to treat a general gas rather than a perfect gas, for which the algebra becomes very complicated. The speed of sound, a, which appears in the analysis, refers to the speed of waves of low enough frequency for the maintenance of equilibrium of ionization and other effects. The only restrictions placed on the properties of the gas are: (i) stability; i.e. $(\partial p/\partial \rho)_s > 0$ and $c_p > 0$, and (ii) the conditions of Weyl (1949); $(\partial^2 p/\partial \tau^2)_s > 0$, and positive expansion coefficient, i.e. $(\partial \tau/\partial T)_p > 0$, $(\partial p/\partial s)_\tau > 0$, etc.

There are three main sections in the paper. Section 2 deals with the behaviour of simple waves in a perfect conductor, investigating particularly the changes of magnitude and sign of the transverse field component and the tendency of compressive waves in which the transverse field does not change sign to steepen into shocks.

Section 3 discusses steady flows in a perfect conductor caused by external influences such as gravity, energy release, etc. These are generalizations of the Rayleigh and other processes of classical one-dimensional gasdynamics. The crucial significance of the two sound speeds, fast and slow, is explored. A degenerate case of these flows is a generalization of the ordinary gasdynamics discussed in a previous communication (Shercliff 1958). Here the ordinary sound speed is dominant.

The final and most important section is an exhaustive but, it is hoped, simple treatment of magnetogasdynamic shocks in the presence of a field component normal to the shock front. For convenience this section is written so as to be intelligible by itself without reference to the rest of the paper. The approach is to exploit the properties of the generalized Rayleigh line, from which it is easy to establish such facts as the possibility of *six* different types of shock, all compressive. The results are reconciled with the work of earlier writers, most of whom performed numerical investigations of the case of a perfect gas with $\gamma = \frac{5}{3}$.

In terms of the distinction between approximate and strict one-dimensionality made in the earlier paper (Shercliff 1960), the motions studied herein are *strictly* one-dimensional. All quantities are strictly independent of the transverse co-ordinates and Maxwell's equations are obeyed. All quantities are assumed to vary sufficiently slowly with distance for finite electrical conductivity to have

negligible effect, i.e. the magnetic Reynolds number is assumed to be virtually infinite. This is not true within shocks, of course, but in this paper we are not primarily concerned with shock structure.

We select the x-axis in the longitudinal direction. The equations

$$\operatorname{curl} \mathbf{E} = -\partial \mathbf{B}/\partial t \quad \text{and} \quad \operatorname{div} \mathbf{B} = 0$$

then indicate that $\partial/\partial t$ and $\partial/\partial x$ of B_x vanish and $B_x = \text{const}$. We shall also assume it positive. In §§ 2 and 3 we restrict the investigation to cases where $\mathbf{B}$ and the fluid velocity $\mathbf{v}$ lie in xy-planes and $B_z = v_z = 0$.

The equation of continuity is

$$\frac{D\rho}{Dt} + \rho \frac{\partial v_x}{\partial x} = 0, \tag{1}$$

and the dynamic equations state that (in MKS units)

$$\rho \frac{Dv_x}{Dt} + \frac{\partial}{\partial x}\left(p + \frac{B_y^2}{2\mu}\right) = 0 \quad \text{and} \quad \rho \frac{Dv_y}{Dt} = \frac{B_x}{\mu}\frac{\partial B_y}{\partial x}, \tag{2}$$

in the absence of viscous stress or any additional force on the fluid. For a perfect conductor we have

$$\frac{DB_y}{Dt} = B_x \frac{\partial v_y}{\partial x} - B_y \frac{\partial v_x}{\partial x}, \tag{3}$$

while in the absence of viscous or Ohmic dissipation, heat exchange or relaxation processes (i.e. thermodynamic disequilibrium) we have

$$\frac{Ds}{Dt} = 0. \tag{4}$$

In steady flow this implies s is constant. We shall assume this is also true in unsteady cases, so that $dp = a^2 d\rho$.

2. Simple waves

It is well known (Kulikovsky 1958; Friedrichs & Kranzer 1958) that simple-wave solutions of the equations (1) to (4) exist, there being two wave speeds, the fast and the slow, in each direction. The Alfvén mode has been excluded by the restriction that v_z and B_z vanish. We remark in passing that Alfvén simple waves are three-dimensional and involve arbitrary rotations of a transverse field component of constant magnitude, the thermodynamic state being constant. Thus the wave speed $B_x/(\mu\rho)^{\frac{1}{2}}$ is constant and there is no steepening or spreading tendency.

For a simple wave in the xy-plane, travelling in the x-direction at a speed c, we may replace D/Dt by $-c\,\partial/\partial x$ in (1) to (3), which become, in differential form at a given instant in time,

$$\left.\begin{aligned} \rho dv_x = c\,d\rho, \quad -\rho c\,dv_x + a^2 d\rho + B_y dB_y/\mu = 0, \\ -\rho c\,dv_y = B_x dB_y/\mu, \quad -c\,dB_y = B_x dv_y - B_y dv_x. \end{aligned}\right\} \tag{5}$$

The eliminant of (5) is the familiar equation which gives the real fast and slow wave speeds

$$c^4 - c^2(a^2 + b^2) + a^2 b_x^2 = 0, \tag{6}$$

where $b_x = B_x/(\mu\rho)^{\frac{1}{2}}$, $b_y = B_y/(\mu\rho)^{\frac{1}{2}}$ and $b^2 = b_x^2 + b_y^2$. Equation (6) may usefully be rewritten

$$\frac{c^2-b^2}{a^2} = \frac{b_y^2}{c^2-a^2} = \frac{c^2-b_x^2}{c^2}. \tag{7}$$

These three quantities are positive for fast waves, negative for slow waves. From the first two equations (5) it follows that

$$\frac{d\rho}{\rho}\frac{a^2}{c^2-b^2} = \frac{dB_y}{B_y} = \frac{db_y}{b_y} + \frac{1}{2}\frac{d\rho}{\rho}. \tag{8}$$

This shows that compressive fast waves increase $|B_y|$ while compressive slow waves decrease $|B_y|$, the reverse being true for expansive waves. These facts have been pointed out by various authors (e.g. Friedrichs & Kranzer 1958).

A right-travelling simple wave of either type may be specified by an arbitrary distribution of density $\rho(x)$ at some initial instant, the other variables v_x, v_y and B_y then being determined by equations (5). If all four of ρ, v_x, v_y and B_y were chosen arbitrarily at an instant, the resultant motion would in general involve left- and right-travelling slow and fast waves, and these would not be simple waves any longer. Simple waves cannot be superposed as the problem is non-linear.

It is instructive to study the equation which determines B_y, given $\rho(x)$, in the case of simple waves. This can conveniently be obtained by eliminating c from (6) and (8), to give

$$\left(\frac{dB_y}{d\rho}\right)^2 - \left(\frac{B_x^2 + B_y^2 - \mu\rho a^2}{\rho B_y}\right)\frac{dB_y}{d\rho} - \frac{\mu a^2}{\rho} = 0. \tag{9}$$

This gives two real differential equations of the first order. For any values of B_y and ρ, the two values of $dB_y/d\rho$ have opposite signs, their product being $-\mu a^2/\rho$, and the two families of solutions may readily be identified as fast or slow, in accordance with the comment after (8). Typical trajectories of these solutions on the B_y/ρ plane are illustrated in figure 1. The resemblance of the curves to orthogonal confocal conics is striking. Indeed the curves have exactly this form in the case of a perfect gas for which $\gamma = 2$, but the curves have approximately this shape for any gas which satisfies the two conditions:

(i) $a^2 \to 0$ as $\rho \to 0$, isentropically. This ensures that $dB_y/d\rho \to 0$ as $\rho \to 0$ along the slow branches.

(ii) $(\partial/\partial\rho)(\rho a^2)_s = \{a^2 + \rho(\partial^2 p/\partial\rho^2)_s\}$ always positive. This is a slightly stronger condition than the Weyl condition and requires that $(\partial^2 p/\partial\tau^2)_s$ be greater than a^2/τ^3. This condition is necessary to secure that only one singular point X occurs. The density at this point is given by the condition $\rho a^2 = B_x^2/\mu$ which fixes ρ if ρa^2 varies monotonically with ρ.

Other facts which permit the establishment of the form of the branches are as follows:

(*a*) Equation (9) is even in B_y, which implies symmetry in the ρ-axis.

(*b*) $dB_y/d\rho$ cannot change sign while B_y and ρ are finite and non-zero.

(*c*) From (7) and (8) we have $1-(B_y/\rho)\,d\rho/dB_y = b_x^2/c^2$, positive. Hence $|B_y/\rho|$ increases with ρ on the fast branches and B_y, b_y and c (fast) $\to \infty$ as $\rho \to \infty$,

whereas $b_x \to 0$. Thus $(B_y/\rho)\,d\rho/dB_y \to 1$ and $B_y/\rho \to$ const. along the fast branches as $\rho \to \infty$. The fast waves are then tending towards the case treated earlier (Shercliff 1960 and others) where the field is essentially transverse, with $B_y \gg B_x$.

We observe that simple waves are either fast or slow throughout. The only exception to this occurs when $B_y = 0$ throughout, i.e. an ordinary simple wave for which $c = a$. When $B_y = 0$, $c = a$ or b_x. If $\rho < \rho_X$, $a < b_x$, and if $\rho > \rho_X$, $a > b_x$. In either case, the wave for which $dB_y/d\rho$ is infinite has $c = b_x$. The fact that the fluid enters or leaves a simple wave at a relative normal velocity of b_x where $B_y = 0$ makes an interesting contrast with the well-known result that the fluid enters or leaves a shock wave at a relative normal velocity of b_x when $B_y = 0$ *on the other side of the wave*, which is then a switch-on or switch-off shock.

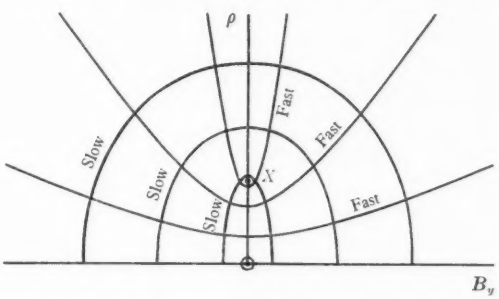

FIGURE 1. Trajectories on the B_y/ρ plane for simple waves.

In each slow wave there are upper limits on density and B_y, and in each fast wave a lower limit on density, except in the ordinary wave with $B_y = 0$.

If the pressure is negligible in comparison with the magnetic pressure, as in the ionosphere, we have the interesting degenerate case where $a = 0$. The slow and fast speeds then become zero and b, respectively. The fast waves still travel faster than the Alfvén speed b_x. Their trajectories on the B_y/ρ plane are the hyperbolae $B_y^2 + B_x^2 \propto \rho^2$, and along each trajectory $c \propto \rho^{\frac{1}{2}}$.

2.1. *Steepening of compressive simple waves*

From the preceding section we see that B_y cannot change sign in a wholly compressive wave and that a wave in which B_y does change sign must be partly expansive. But an expansive *and* compressive wave need not involve a change of sign of B_y unless the relevant extremum of ρ is reached.

It is natural to inquire whether compressive simple waves show the usual steepening tendency which leads to the creation of compressive shocks. At the same time expansive waves would show a spreading tendency. That this occurs has been stated by Liubarskii & Polovin (1958). The condition for its occurrence is that, for right-travelling waves,

$$\frac{d}{d\rho}(v_x + c) = \frac{c}{\rho} + \frac{dc}{d\rho}$$

be positive.

Differentiation of (6) and the use of (8) leads to the result

$$\frac{c}{\rho}+\frac{dc}{d\rho}=\frac{c}{2\rho}\frac{\left\{\tau^3\left(\frac{\partial^2 p}{\partial\tau^2}\right)_s+\frac{3(c^2-a^2)^2}{b_y^2}\right\}}{\left\{a^2+\frac{(c^2-a^2)^2}{b_y^2}\right\}}. \tag{10}$$

Granted Weyl's conditions, it follows from the form of (10) that $c/\rho+dc/d\rho$ is indeed positive and that fast or slow compressive waves, in which B_y does not change sign, do steepen, presumably into the fast or slow shocks that are discussed later. These too involve no change in sign of B_y. A simple wave in which B_y did change sign would not entirely steepen; the expansive parts would spread instead. Thus it is hard to see how the so-called intermediate shocks, in which B_y changes sign, could be created directly by a steepening process. This perhaps adds to the doubt which has been cast on the existence of intermediate shocks by Akhiezer *et al.* (1958) and Germain (1959) and others. Akhiezer *et al.* have shown that intermediate shocks, treated as discontinuities, are unstable to weak disturbances, while Germain has shown that intermediate shock structures cannot exist for certain values of the diffusivities. An obvious question deserving investigation is whether intermediate shocks could arise when a shock, newly formed from the compressive part of a simple wave, advances into an expansive part in which B_y is reversed.

In the degenerate cases where either the longitudinal or the transverse field component vanishes, condition (10) yields the results:

(i) If $B_x=0$, $c^2=a^2+b^2$ and $\dfrac{c}{\rho}+\dfrac{dc}{d\rho}=\dfrac{\tau^4}{2c}\left\{\left(\dfrac{\partial^2 p}{\partial\tau^2}\right)_s+\dfrac{3B^2\rho^2}{\mu}\right\}$,

in agreement with the earlier paper (Shercliff 1960).

(ii) If $B_y=0$, *either*

$$c=a \quad \text{and} \quad \frac{c}{\rho}+\frac{dc}{d\rho}=\frac{\tau^4}{2a}\left(\frac{\partial^2 p}{\partial\tau^2}\right)_s,$$

the usual result for ordinary simple waves, *or*

$$c=b \quad \text{and} \quad \frac{c}{\rho}+\frac{dc}{d\rho}=\frac{3b}{2\rho}.$$

This result also applies to the case where $a=0$. In all these degenerate cases compressive waves still steepen.

3. Steady motions

In this section we generalize the theory of strictly one-dimensional steady motions (Shercliff 1960) to include the effect of a longitudinal field component. This involves our considering variation of transverse momentum. We continue to take the gas as having perfect electrical conductivity, except in § 3.1.

In steady one-dimensional gasdynamics some influence must be exerted on the flow in order that any changes should occur at all. By 'influence' is meant the application of additional forces to the flow (by viscous stress, distributed

drag, actuator disks, gravity, etc.) or heat exchanges (by conduction, radiation or release or absorption of heat by chemical, nuclear, or thermonuclear reaction). It is possible to treat the resultant magnetogasdynamic processes in the symmetrical manner already developed for ordinary gasdynamics (Shercliff 1958). A difference here is that G, the mass flow per unit area, is constant because the motion is strictly one-dimensional.

Some of the processes may be difficult to achieve in reality, but nevertheless it can still be useful to consider them as mathematical loci since worthwhile results can be deduced from them, particularly about shocks. Germain (1959) goes further and considers mathematical loci where quantities such as G or the electric field E_z are varied. These cannot represent processes occurring in space, since G and E_z must be uniform by continuity and Maxwell's equations, as is pointed out below.

In steady motions, (1) degenerates to

$$\rho v_x = G \quad \text{(const.), assumed positive,}$$

and (2) gives

$$\rho v_x^2 + p + B_y^2/2\mu = F_x \quad \text{and} \quad \rho v_x v_y - B_x B_y/\mu = F_y,$$

where F_x and F_y are constant in the absence of additional forces or stresses in the x and y directions, respectively. Since $\mathbf{E} + \mathbf{v} \times \mathbf{B} = 0$, we see that E_z is the only component of electric field, and Maxwell's equation $\operatorname{curl} \mathbf{E} = -\partial \mathbf{B}/\partial t = 0$ here indicates that E_z is uniform. Since B_x is also uniform and non-zero, we can suppress any E_z by the choice of axes moving in the y-direction with a velocity E_z/B_x. Then $\mathbf{v} \times \mathbf{B} = 0$ and we have the simplification that the flow and field are everywhere parallel. Hence $B_y/\rho v_y = B_x/G = \text{const.}$

Another consequence of the vanishing of $\mathbf{E}$ is that no electrical energy exchange $\mathbf{E} \cdot \mathbf{j}$ occurs, and the stagnation enthalpy, $H = h + \frac{1}{2}v^2 = h + \frac{1}{2}(v_x^2 + v_y^2)$, is constant in the absence of any additional heat or work exchange.

The other major flow property which can be constant is the entropy s. This occurs in the absence of dissipation or heat exchange.

We thus have the situation where a flow characterized by known values of G and B_x may undergo changes in which some or all of the quantities F_x, F_y, H and s may be made to vary. For given values of G and B_x, *three* further quantities are necessary to specify the state of a flow-section (e.g. ρ, s and v_y). Another set of three quantities which may be used as co-ordinates is (F_x, F_y, H), but then the flow-state is not uniquely defined. We shall see that there may be up to four states having these co-ordinates, mutually accessible via stationary shocks, since across a stationary shock F_x, F_y and H are conserved (de Hoffman & Teller 1950). Note that across shocks G and B_x are also uniform and $\mathbf{v}$ can be made parallel to $\mathbf{B}$ on both sides. The fact that only three of the four quantities F_x, F_y, H and s are independent is expressible by the relation

$$v_x dF_x + v_y dF_y + GT\,ds = G\,dH, \tag{11}$$

which results from the relation $T\,ds = dh - dp/\rho$ for a gas in equilibrium.

We shall concentrate on the six processes which may be defined by keeping any two of F_x, F_y, H and s constant. The processes may be interpreted physically

in various ways. The most interesting case is the generalized Rayleigh process, in which F_x and F_y are conserved because no extra force is applied to the fluid, but H and s are changed by heat exchanges. Similarly we have a generalized Fanno process, in which F_y and H are constant while dissipative forces operate in the x-direction but no energy is exchanged. Another adiabatic case is that where gravity or other forces in the x-direction result in reversible energy exchange and F_y and s are constant. Alternatively there may be forces in the y-direction, causing F_y to vary.

Some simple, important relations are

$$(\tau-\tau_0)B_y = F_y B_x/G^2 \quad \text{and} \quad (\rho_0-\rho)v_y = \mu F_y G/B_x^2, \tag{12}$$

where

$$\tau_0 = B_x^2/\mu G^2 = \text{const.},$$

and

$$\tau/\tau_0 = v^2/b^2 = v_x^2/b_x^2 = v_y^2/b_y^2. \tag{13}$$

Relation (12) is particularly important when $F_y = \text{const.}$, as obviously the specific volume τ_0 is a singular value. Its importance has also been noted by Germain (1959). When $\tau = \tau_0$, $v_x = b_x$, i.e. the flow is travelling at the Alfvén speed.

In all six processes, the two of F_x, F_y, H and s which are not being kept constant are stationary whenever v_x equals the local fast or slow sound speed given by (6). This is easily demonstrated, for instance, in the case (H, s) const. We have

$$\left(\frac{\partial F_x}{\partial \rho}\right)_{Hs} = a^2 - v_x^2 + \frac{B_y}{\mu}\frac{dB_y}{d\rho}, \tag{14}$$

$$\left(\frac{\partial H}{\partial \rho}\right)_{Hs} = 0 = \frac{a^2}{\rho} - \frac{v_x^2}{\rho} + v_y\frac{dv_y}{d\rho},$$

and

$$\frac{dB_y}{B_y} = \frac{d\rho}{\rho} + \frac{dv_y}{v_y},$$

which together with (13) yield

$$\left(\frac{\partial F_x}{\partial \rho}\right)_{Hs} = -\frac{1}{v_x^2}\{v_x^4 - v_x^2(a^2+b^2) + a^2 b_x^2\} = -\frac{X}{v_x^2}, \quad \text{say},$$

where X vanishes whenever v_x equals either root of (6).

The values of all such derivatives are presented in table 1 as multiples of X. The quantity Y in the last line denotes the expression

$$\left\{1 - \left(1 - \frac{b_x^2}{v_x^2}\right)\frac{1}{T}\left(\frac{\partial h}{\partial s}\right)_\rho\right\}.$$

Since the gas has a positive expansion coefficient, $(\partial s/\partial p)_\rho$ and $(\partial s/\partial h)_\rho$ in table 1 are positive and $T(\partial s/\partial h)_\rho$ is less than unity. As a result Y can vanish, for example for a perfect gas when $\tau/\tau_0 = \gamma/(\gamma-1)$. We shall not investigate this complicated (F_x, H) case any further, despite the fact that it is one of the processes that link the two sides of shocks.

Not all parts of these processes may be physically meaningful. In the Rayleigh (F_x, F_y) process, B_y increases so much as $\tau \to \tau_0$ that $B_y^2/2\mu$ becomes larger than F_x and the pressure goes negative. Similarly, in the (F_x, s) process, B_y^2 and v_y^2 become negative whenever p or ρv_x^2 gets too large, at low and high values of τ, respectively.

In the processes with F_y constant the derivatives in table 1 increase without limit as τ passes τ_0, and v_y and B_y change sign via large values.

When F_y is not constant, the signs of F_y, v_y and B_y are to some extent arbitrary, because only the squares of v_y and B_y appear in F_x and H. We can either keep F_y constant in sign so that v_y and B_y change sign discontinuously as τ passes τ_0, although F_x and H would be continuous (this course would be appropriate if we were interested in states having the same value of F_y, for example, the two sides of a shock) or we can keep v_y and B_y (and b_y) positive and continuous, for convenience in discussing table 1. Then F_y changes sign via zero as τ passes τ_0.

Const.	$\partial F_x/\partial\rho$	$\partial F_y/\partial\rho$	$\partial H/\partial\rho$	$\partial s/\partial\rho$
H, s	$-\dfrac{1}{v_x^2}$	$\dfrac{1}{v_x v_y}$	0	0
F_x, s	0	$\dfrac{1}{b_x b_y}$	$\dfrac{1}{\rho b_x^2}$	0
F_y, s	$-\dfrac{1}{v_x^2-b_x^2}$	0	$-\dfrac{1}{\rho(v_x^2-b_x^2)}$	0
F_x, F_y	0	0	$T\left(\dfrac{\partial s}{\partial p}\right)_\rho \dfrac{1}{(v_x^2-b_x^2)}$	$\left(\dfrac{\partial s}{\partial p}\right)_\rho \dfrac{1}{(v_x^2-b_x^2)}$
F_y, H	$-T\left(\dfrac{\partial s}{\partial h}\right)_\rho \dfrac{1}{(v_x^2-b_x^2)}$	0	0	$\dfrac{1}{\rho}\left(\dfrac{\partial s}{\partial h}\right)_\rho \dfrac{1}{(v_x^2-b_x^2)}$
F_x, H	0	$\dfrac{1}{v_x v_y Y}$	0	$-\dfrac{1}{T\rho v_x^2 Y}$

TABLE 1. Derivatives expressed as multiples of X.

The next task is to establish whether the stationary values of F_x, F_y, H and s are maxima or minima. From relations such as

$$\left(\frac{\partial X}{\partial\rho}\right)_{F_y H} = \left(\frac{\partial X}{\partial\rho}\right)_{F_y s} + \left(\frac{\partial X}{\partial s}\right)_{\rho F_y}\left(\frac{\partial s}{\partial\rho}\right)_{F_y H},$$

we see that $\partial X/\partial\rho$ takes the same value in all the processes when $X = 0$. The quantities such as $(\partial X/\partial s)_{\rho F_y}$ which enter are finite for all likely gases. In fact

$$(\partial X/\partial s)_{\rho F_y} = (b_x^2 - v_x^2)\,\tau^2(\partial^2 T/\partial\tau^2)_s.$$

The common value of $\partial X/\partial\rho$ is most easily evaluated in the (H, s) case, using (7) with $v_x = c$ and the result

$$\frac{\partial b^2}{\partial\rho} = -\frac{b^2}{\rho} + \frac{2B_y}{\mu\rho}\frac{\partial B_y}{\partial\rho} = -\frac{b^2 + 2(v_x^2 - a^2)}{\rho} \quad \text{from (14) when } X = 0.$$

We find that

$$\frac{\partial X}{\partial\rho} = \frac{(b_x^2 - v_x^2)}{\rho}\left\{\tau^3\left(\frac{\partial^2 p}{\partial\tau^2}\right)_s + \frac{3(v_x^2 - a^2)^2}{b_y^2}\right\},$$

an expression reminiscent of the denominator of (10). We conclude that in each case $\partial X/\partial\rho$ has the same sign as $(b_x^2 - v_x^2)$ when $X = 0$. For slow roots of $X = 0$,

$(b_x^2 - v_x^2)$ and $(\rho - \rho_0)$ are positive, for fast, negative. We can thus compile table 2, with the convention that b_y, B_y and v_y are positive in the first two processes. They can be completed by changing the sign of b_y, B_y, v_y and F_y throughout.

It is easily verified that, in each process, the state is a single-valued function of ρ (apart from the ambiguity of sign of F_y already mentioned), provided the state of the gas is uniquely defined by ρ and any one of s, p or h. Each process will have only one sonic point of each kind, the fast when $\rho < \rho_0$, the slow when $\rho > \rho_0$. This is illustrated in figure 2. Extra sonic points such as P and Q are precluded because on each continuous branch, maxima and minima must occur alternately but the nature of the extrema are stated in table 2. Figure 2 shows the difference between cases such as (*a*) where F_y = const. and (*b*), (*c*) and (*d*) where F_y varies. In the latter case the ambiguity of sign of F_y, already discussed, is shown by the curves (*c*) and (*d*).

Const.	Slow sonic point	Fast sonic point
H, s	F_x max.; F_y min.	F_x min.; F_y max.
F_x, s	F_y min.; H min.	F_y max.; H max.
F_y, s	F_x min.; H min.	
F_x, F_y	H max.; s max.	
F_y, H	F_x min.; s max.	

TABLE 2

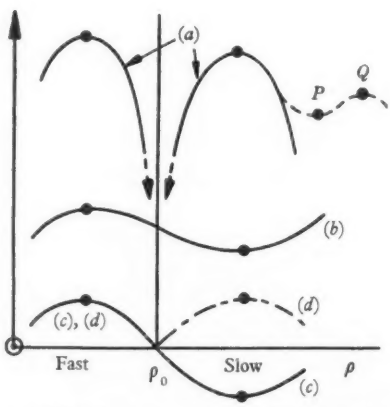

FIGURE 2. Typical graphs of the five processes. (*a*) H or s against ρ with (F_x, F_y) const. (Rayleigh line). (*b*) H against ρ with (F_x, s) const. (*c*) F_y against ρ with (F_x, s) const., B_y and v_y positive. (*d*) F_y against ρ with (F_x, s) const., F_y positive.

As in the earlier papers (Shercliff 1958, 1960) it is possible to explore the significance of the isothermal sound speeds, determined by (6) with a^2/γ replacing a^2. The most important result which emerges is that the temperature T is a maximum at the two isothermal-sonic points that occur in a Rayleigh process, which also straddle the point $\rho = \rho_0$. This requires the further assumption that $(\partial^2 p/\partial \tau^2)_T$ be positive, which is true for gases except near the critical point. As

with ordinary shocks, the Rayleigh process represents the shock structure in gases for which the thermal diffusivity is dominant. The isothermal fast and slow sound speeds are then critical for determining whether or not there is a shock-within-a-shock, in which the other diffusivities operate.

The properties of Rayleigh lines are more thoroughly exploited in the study of shock transitions in § 4.

3.1. *Ordinary generalized gas dynamics*

A degenerate case of the foregoing is worth studying briefly. This is the case which results from setting B_x and B_y to zero and which represents ordinary one-dimensional gas dynamics generalized to include transverse effects, but with the flow per unit area kept constant (although it is simple to waive this restriction). Again influences must be exerted on the fluid to cause changes to take place. These may still be electromagnetic in origin, just as electromagnetic effects were considered in the earlier work on ordinary gasdynamics (Shercliff 1958). As an example we can consider a flow at such low magnetic Reynolds number that the field may be taken to be uniform but at any inclination. Alternatively, we may imagine the processes as being somewhat idealized versions of the flows that occur in axial-flow turbo-machinery.

Adopting the previous techniques, we consider the quantities G (here constant), H and s, as usual, together with $f_x = p + \rho v_x^2$ and $f_y = \rho v_x v_y$. They are related by

$$v_x df_x + v_y df_y = G\,dH - GT\,ds. \tag{15}$$

We could generalize to three dimensions with a term $v_z df_z$. Again processes can be defined by taking two of H, s, f_x and f_y constant. Except in one case, the other two variables are then stationary when $v_x = a$ and the longitudinal Mach number is unity.

The six processes are:

f_x, s const. Here the state of the gas and v_x are constant and only v_y, f_y and H vary. This corresponds to flow through impulse blading. The condition $v_x = a$ is irrelevant.

f_y const. and one of s, f_x or H const. There are merely the three processes (G, s), (F, G) or (G, H) treated in the earlier paper (Shercliff 1958) with a constant transverse velocity v_y superposed. F and f_x are identical, but H in the earlier paper did not include the term $\frac{1}{2}v_y^2$. Now the condition $v_x = a$ is critical.

f_x, H const. This is a modification of the (F, G) Rayleigh process, in which p, ρ, s and v_x vary as usual, but in addition v_y varies in such a way that H is constant. The condition $v_x = a$ makes s and $(h + \frac{1}{2}v_x^2)$ a maximum and hence v_y and f_y a minimum. Indeed if H is too small, v_y will fall to zero before v_x reaches a. One way of realizing this process would be to have a uniform field in the longitudinal direction, the magnetic Reynolds number being low, and zero electric field. Then in this adiabatic, dissipative process the velocity v_y across the field would decay to zero or until choking occurred at $v_x = a$.

H, s const. This is a modification of the (G, s) process discussed in the earlier paper, in which p, ρ, s and v_x vary as usual, but v_y varies in such a way that H is constant. The condition $v_x = a$ makes f_x and $(h + \frac{1}{2}v_x^2)$ a minimum and hence

v_y and f_y a maximum. Instead of the external energy exchange in the original (G, s) process, the transverse kinetic energy now acts as a sink or source of energy. It is interesting to observe that this transverse energy is a maximum when the *longitudinal* velocity is sonic. The process can be imagined to be brought about by stationary cascades of blades which apply forces to the fluid in a direction perpendicular to its motion, so that

$$v_x df_x + v_y df_y = 0,$$

in accordance with (15). It is perhaps necessary to point out that turbine nozzle rows are not subject to an upper limit on v_y when $v_x = a$, because G is not usually constant in them.

The list of processes could be prolonged by putting other constraints on f_x, f_y, H and s. An example is the flow in zero electric field and a uniform oblique magnetic field (at low magnetic Reynolds number) where the process is defined by specifying df_x/df_y (which equals $-B_y/B_x$) and $H = \text{const}$.

An important member of this family of processes is that which occurs as the structure of a shock in which the magnetic diffusivity is dominant, as considered by Ludford (1959), Bleviss (1959) and Germain (1959). Here we resurrect Maxwell's equations and take **E** as zero. Since the conductivity is finite the process does not belong to the family of flows with **v** and **B** parallel, already discussed. In particular the extrema of entropy, etc., occur when $v_x = a$, the ordinary sound speed, not the fast or slow ones. Thus a is the critical velocity for determining whether or not there is a shock-within-a-shock, in which the other diffusivities operate. Here the process is defined by taking $H = \text{const.}$ and by relating f_x and f_y via the parameter B_y through the equations

$$f_x + B_y^2/2\mu = \text{const.}, \quad f_y - B_x B_y/\mu = \text{const.}$$

It is not proposed to discuss this process further here as we are not primarily concerned with shock structure.

4. Shock transitions

Ever since the Rankine–Hugoniot relations were generalized to include magnetogasdynamic effects by de Hoffman & Teller (1950), the nature of their solutions has been studied by many authors, notably Lüst (1953) and Friedrichs (1954). The results of these and other writers are discussed at the end of this section.

More recently, Germain (1959) has investigated the properties of possible shock transitions. His work is very close to the work reported here in many respects. He too considers an arbitrary gas obeying Weyl's conditions, and also uses the generalized Rayleigh line to establish a classification of shocks by relating the velocity normal to the shock to the slow, fast and Alfvén wave speeds. However, his proof that all shocks must be compressive involves two further loci, one a generalization of the Hugoniot curve, also used by Friedrichs & Kranzer (1958) and Iordanskii (1958), the other a complicated locus somewhat comparable to the (F_x, H) process mentioned earlier. The use of this locus leads him to postulate an extra, unnecessary restriction on the gas properties.

In this paper it is shown how nearly all the results follow simply from the properties of the generalized Rayleigh line. For completeness we start from first principles, taking the x-axis normal to the plane of the shock, i.e. in the direction of one-dimensional variation, with the shock stationary in the co-ordinate system. Maxwell's equations, $\operatorname{div}\mathbf{B} = 0$ and $\operatorname{curl}\mathbf{E} = 0$, then indicate that B_x, E_y and E_z are constant. Since B_x is non-zero we can choose axes moving in the y- and z-directions so as to make E_y and E_z vanish. The shock layer separates two uniform regions devoid of current, since $\operatorname{curl}\mathbf{B} = 0$ in them. Thus Ohm's law indicates that $(\mathbf{v}\times\mathbf{B})_y$ and $(\mathbf{v}\times\mathbf{B})_z$ vanish outside the shock, and $v_z/B_z = v_x/B_x = v_y/B_y$. The shock layer contains a current sheet perpendicular to and responsible for the discontinuity in $\mathbf{B}$ across the shock. We choose the z-axis parallel to this current sheet so that $B_{z1} = B_{z2} = B_z$, say, if we use the suffices 1 and 2 to denote the two sides of the shock. In the shock the fluid suffers a net magnetic force perpendicular to the current sheet. Thus z-momentum is conserved and $v_{z1} = v_{z2} = v_z$, say. Hence $v_z/v_{x1} = B_z/B_x = v_z/v_{x2}$, and *either* (i) $v_{x1} = v_{x2} = v_x$, say, *or* (ii) $v_z = B_z = 0$, two distinct cases.

4.1. *Case* (i). *The Alfvén shock* ($v_{x1} = v_{x2} = v_x$)

The equation of continuity,

$$G_1 = G_2, \quad \text{where} \quad G = \rho v_x, \tag{16}$$

here indicates that $\rho_1 = \rho_2 = \rho$, say. The y-momentum equation is

$$F_{y1} = F_{y2}, \quad \text{where} \quad F_y = Gv_y - B_xB_y/\mu, \tag{17}$$

which here leads to

$$\rho v_x(v_{y1} - v_{y2}) = B_x^2(v_{y1} - v_{y2})/\mu v_x \quad \text{since} \quad v_{y1}/B_{y1} = v_x/B_x = v_{y2}/B_{y2}.$$

It follows that $v_x = \pm B_x/(\mu\rho)^{\frac{1}{2}}$ if we reject the trivial case $v_{y1} = v_{y2}$. The wave is seen to be an Alfvén shock, also called a transverse or symmetrical shock by some. The energy equation is

$$H_1 = H_2, \quad \text{where} \quad H = h + \tfrac{1}{2}v^2 \quad (v^2 = v_x^2 + v_y^2), \tag{18}$$

since $\mathbf{E}\,.\,\mathbf{j}$ is zero everywhere. For the Alfvén shock this gives

$$h_1 + B_{1y}^2/2\mu\rho = h_2 + B_{2y}^2/2\mu\rho.$$

The x-momentum equation is

$$F_{x1} = F_{x2}, \quad \text{where} \quad F_x = p + Gv_x + B_y^2/2\mu, \tag{19}$$

which here yields $p_1 + B_{1y}^2/2\mu = p_2 + B_{2y}^2/2\mu$. We see that $u_1 = u_2$, where u is the internal energy $(h - p/\rho)$, and that the thermodynamic state, uniquely defined by u and ρ, is unchanged by the shock. It follows that $s_1 = s_2$ and $|\mathbf{B}_1| = |\mathbf{B}_2|$. The transverse field component simply rotates arbitrarily without changing in magnitude. Alfvén shocks in which it rotates through 180° (i.e. $B_z = 0$) also belong to Case (ii).

4.2. *Case* (ii). *Two-dimensional shocks* ($B_z = 0$)

Here the initial and final fields lie in a plane perpendicular to the shock. The array of solutions to the conservation equations (16) to (19) together with

$$B_x = (B_y v_x / v_y)_{1 \text{ or } 2} \tag{20}$$

is much more complicated than in Case (i). We shall approach the problem by exploiting the fact that the states on each side of the shock lie on a Rayleigh line, a locus defined by keeping B_x, G, F_x and F_y constant, subject to condition (20). The Rayleigh line is most simply specified in terms of p and τ (the specific volume $1/\rho$). The resulting relation is

$$F_x = p + G^2\tau + F_y^2 B_x^2 / 2\mu G^4 (\tau - \tau_0)^2, \tag{21}$$

where $\tau_0 = B_x^2/\mu G^2 = \text{const}$. It is instructive to consider the family of Rayleigh lines characterized by fixed values of F_x, B_x, G and τ_0 and a series of values of $|F_y|$. These obviously take the form illustrated in figure 3, as Germain (1959) has

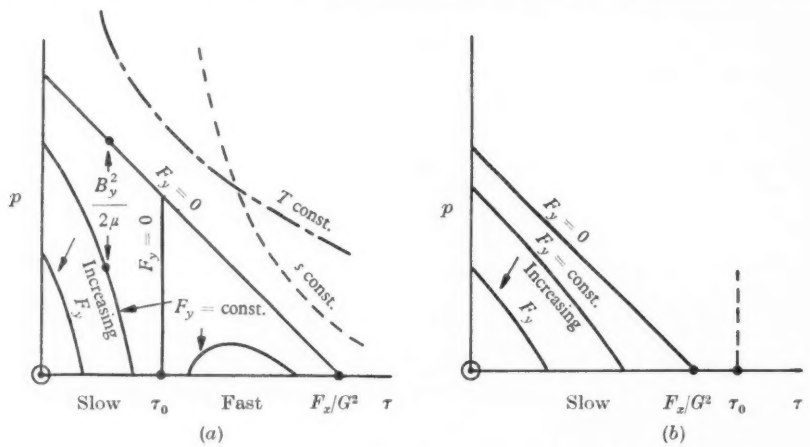

FIGURE 3. Rayleigh lines for given (G, B_x, F_x) and various F_y on the p-τ plane. (*a*) $F_x > B_x^2/\mu$, (*b*) $F_x < B_x^2/\mu$.

remarked. The condition for the occurrence of two branches (figure 3*a*) is $F_x > B_x^2/\mu$. The branches are labelled fast and slow according as $v_x >$ or $< b_x$, where $b_x = B_x/(\mu\rho)^{\frac{1}{2}}$, the longitudinal Alfvén speed. In fact $v_x^2/b_x^2 = \tau/\tau_0$. Also

$$B_y(\tau - \tau_0) = F_y B_x / G^2 \quad \text{and} \quad v_y(\tau - \tau_0) = \tau F_y / G. \tag{22}$$

Hence the line $F_y = 0$ consists of two straight lines, the ordinary Rayleigh line $F_x = p + G^2\tau$, ($B_y = 0$), and the part of the vertical line $\tau = \tau_0$ that lies below it (since $B_y^2/2\mu$ is positive). In physical terms the latter could represent a kind of Alfvén wave in which changes are brought about by heat exchange or heat release. As $|F_y|$ increases from zero in figure 3*a*, the fast branch disappears when $F_y^2 \geqslant 8\mu(F_x - B_x^2/\mu)^3/27B_x^2$ and the slow branch disappears when $F_y^2 \geqslant 2B_x^2 F_x/\mu$.

The fast disappears first if $4B_x^2/\mu > F_x$, and vice versa. These inequalities should be regarded as limitations on the shock states possible for given values of F_x, F_y and B_x.

Figure 3 also displays the dependence of B_y on τ along a Rayleigh line since the vertical intercept between that line and the ordinary Rayleigh line equals $B_y^2/2\mu$. For a given value of F_y, B_y and v_y take different signs in the slow and fast regions, because of (22).

A vital fact about Rayleigh lines is that along them $T\,ds = dH$. This is easily verified from (16) to (20) using $T\,ds = dh - dp/\rho$. We are interested in states on Rayleigh lines having the same values of H so as to be mutually accessible via shocks and having increasing entropy as one proceeds downstream. This leads us to follow the standard procedure of considering the lines on the T-s diagram.

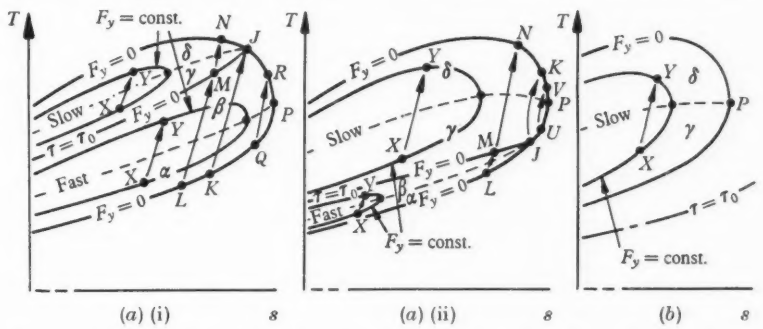

FIGURE 4. Rayleigh lines for given (G, B_x, F_x) and various F_y on the T-s plane. (*a*) $F_x > B_x^2/\mu$, (i) $\tau^* > \tau_0$, (ii) $\tau^* < \tau_0$. (*b*) $F_x < B_x^2/\mu$.

Since derivatives such as $(\partial p/\partial \tau)_s$, $(\partial p/\partial \tau)_T$, $(\partial p/\partial s)_\tau$, etc., have been assumed constant in sign, the p-τ and T-s diagrams are very simply related topologically. Since also $(\partial^2 p/\partial \tau^2)_s$, $(\partial^2 p/\partial \tau^2)_T$ are taken positive, Rayleigh lines and lines of constant s or T have opposite curvature in the p-τ diagram, and points on Rayleigh lines where s or T are stationary are clearly *maxima* of s or T. Moreover, only one point of each kind occurs on each (slow or fast) branch of a Rayleigh line. It follows that the lines for given (F_x, B_x, G) must be disposed as shown in figure 4. More rigorous proofs of the properties of the Rayleigh line are available in § 3.

The line $F_y = 0$ consists of the familiar ordinary Rayleigh line, with its entropy maximum at P where $v_x = a$ and $\tau = \tau^*$, say, plus part of the constant volume line $\tau = \tau_0$. The distinction between (*a*) (i) and (*a*) (ii) lies in the relative positions of P and the point J where $v_x = b_x$ and $\tau = \tau_0$. For case (*a*) (i) we need $\tau^* > \tau_0$. This is a condition on F_x, B_x and G. To be more specific one needs more facts about the gas; if it is a perfect gas then the condition for (*a*) (i) is $F_x > (\gamma+1)B_x^2/\gamma\mu$.

As $|F_y|$ increases from zero the branches move downwards and leftwards in figure 4 and finally disappear in accordance with the inequalities already discussed. Note that figures 3 and 4 are independent of the sign of F_y, since F_y appears squared in (21).

4.2.1. *Fast and slow shocks*

Since $T\,ds = dH$ along Rayleigh lines, to a point such as X on each branch there corresponds another point Y on the same branch having the same value of H and placed more or less as shown in figure 4 to satisfy the condition $\int_X^Y T\,ds = 0$. Such pairs of points satisfy the conservation relations for a shock. Moreover, X, the point of lower entropy (and lower density in view of figure 3) must be upstream. Thus shocks of this type, which we shall call slow or fast, depending on which branch they belong to, must be compressive and longitudinally decelerative. From (22) it follows that $|B_y|$ and $|v_y|$ increase across fast shocks and decrease across slow shocks. Across both types B_y and v_y do not change sign. We observe that B_y varies in the same way as in the slow and fast compressive simple waves discussed in § 2.

As we increase H, and X moves rightwards along its branch of a Rayleigh line, X and Y finally coincide at the entropy maximum, also a maximum of H. In this limit the shock becomes a weak sound wave across which F_x, F_y, H and s are conserved and at which v_x equals either c_f, the fast, or c_s, the slow sound speed given by the well-known equation

$$c^4 - c^2(a^2+b^2) + a^2 b_x^2 \equiv (c^2 - c_s^2)(c^2 - c_f^2) = 0. \tag{23}$$

The dotted lines in figure 4 are the loci of these sonic points as F_y varies, which together with the line $\tau = \tau_0$ divide the ordinary Rayleigh loop into four zones α, β, γ, δ (two in figure 4*b*). From (21) and $ds/d\rho = (\partial s/\partial p)_\rho\,(dp/d\rho - a^2)$, or otherwise, it follows that along a Rayleigh line,

$$\frac{ds}{d\rho} = \left(\frac{\partial s}{\partial p}\right)_\rho \frac{(v_x^2 - c_s^2)(v_x^2 - c_f^2)}{(v_x^2 - b_x^2)},$$

in which c_s, c_f and b_x are *local* values. Note that $c_f^2 \geqslant b_x^2 \geqslant c_s^2$ and $(\partial s/\partial p)_\rho$ is positive. It is evident from figures 3 and 4 that $ds/d\rho$ is positive in regions α and γ, negative in β and δ, while $(v_x^2 - b_x^2)$ is positive in α and β, negative in γ and δ. Since $b_x^2 \geqslant c_s^2$, $(v_x^2 - c_s^2)$ is also positive in α and therefore $(v_x^2 - c_f^2)$ is positive there too. In this fashion we may readily establish the following inequalities that characterize states lying in the four zones:

$$\left.\begin{aligned} &(\alpha) \quad v_x > c_f, \\ &(\beta) \quad c_f > v_x > b_x, \\ &(\gamma) \quad b_x > v_x > c_s, \\ &(\delta) \quad c_s > v_x, \end{aligned}\right\} \tag{24}$$

if we take all these velocities as positive.

In particular we observe that the normal velocity v_x in slow and fast shocks jumps from supersonic to subsonic relative to the slow and fast sound speeds, but stays respectively below or above the Alfvén speed.

4.2.2. *Switch-on, switch-off, Alfvén and ordinary shocks*

The case $F_y = 0$ deserves closer scrutiny, since here the upper arm of the fast branch and lower arm of the slow branch have coalesced. Typical fast shocks now appear in figure 4 as LM or QR and typical slow shocks as MN or UV. The shock LN also satisfies the conservation and entropy conditions. Shocks QR, UV and LN are all ordinary shocks since the end points all lie on the ordinary Rayleigh line where $B_y = 0$ and B_x is ineffectual.

At M, $v_x = b_x$ and $B_y \neq 0$. Thus LM is what Friedrichs & Kranzer (1958) call a switch-on shock, while MN is the switch-off shock. They are extreme cases of fast and slow shocks, respectively. On the side where the field is oblique the velocity equals the Alfvén velocity; on the side where the field is normal to the shock, c_f = the greater of a and b_x, c_s = the lesser, and (24) indicate that upstream of a switch-on shock $v_x >$ both a and b_x, while downstream of a switch-off shock $v_x <$ both a and b_x.

The point M represents two states, differing only in the sign of B_y and v_y. This point therefore represents an Alfvén shock (in the case $B_z = 0$) in which B_y and v_y reverse but the thermodynamic state (T, s) is unchanged.

Switch-on and off shocks are not possible for all values of F_x, G, B_x and H, even granted that $F_x > B_x^2/\mu$, to permit the $\tau = \tau_0$ branch. Given values of F_x, G and B_x fix the point J in figure 4. Switch-on or off shocks will obviously be possible only for smaller values of H than its value at J. In other words, a switch-on shock is not possible starting from a state from which an ordinary shock leads to a state at which $v_x > b_x$, i.e. starting from points to the right of K in figure 4 (a)(i), K being the other point having the same H as J. Equally it is not possible to jump to points to the right of K in figure 4 (a)(ii) via switch-off shocks.

As H increases to its limit for switch-on shocks, the related switch-off shock weakens to vanishing point, and vice versa (e.g. M and $N \to J$ as $L \to K$). These limits on switch-on and off shocks are expressible in many ways. Bleviss (1959) in effect gives them as upper and lower limits on B_x for a given upstream state, L say, where $B_y = 0$. Then B_x and τ_0 must be such that J lies between L and N.

4.2.3. *Intermediate shocks*

We now consider shocks which join points lying on *different* branches of a Rayleigh line, in which therefore B_y, v_y and $(v_x^2 - b_x^2)$ change sign. Following Germain (1959) we call these intermediate shocks. Provided F_x, F_y and B_x satisfy the conditions for two branches to exist, there will be two pairs of states lying on the two different branches and having the same value of H, provided H is less than the lesser of the two maxima of H for given G, B_x, F_x and F_y, which may lie on either the slow or the fast branch. That there can be up to four states mutually accessible via shocks was observed by Ludford (1959) in the case of a perfect gas. We shall number these four states, 1, 2, 3 and 4 in order of increasing density, 1 and 2 being fast, 3 and 4 being slow. The fast shock 12 and slow shock 34 have already been discussed. There will also be four intermediate ones which travel in a direction to be determined from the entropy condition.

The four states, 1, 2, 3 and 4 lie respectively in the regions α, β, γ and δ and the inequalities (24) apply to them.

Consider the two states 2 and 3 on the two arms closest to the $\tau = \tau_0$ line. Suppose $s_2 \geqslant s_3$, as shown in figure 5. Consider the isentropics through 2 and 3 which cut the $F_y = 0$ Rayleigh line in W and Z. Figure 5 shows the two possibilities. From (16) to (20), with G, B_x, F_x and s constant, we find that

$$\partial H/\partial\rho = (v_x^2 - c_s^2)(v_x^2 - c_f^2)/\rho b_x^2,$$

which is negative along $2W$ and $Z3$, in the β and γ zones. Along $2W$ and $Z3$, ρ increases monotonically since $(\partial T/\partial\rho)_s$ is positive. Thus H decreases along

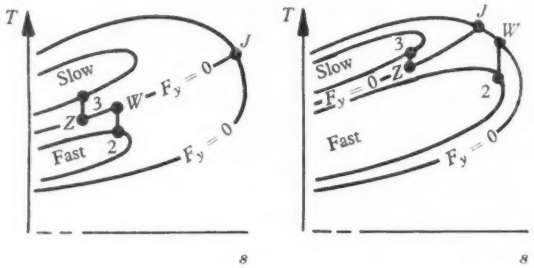

FIGURE 5

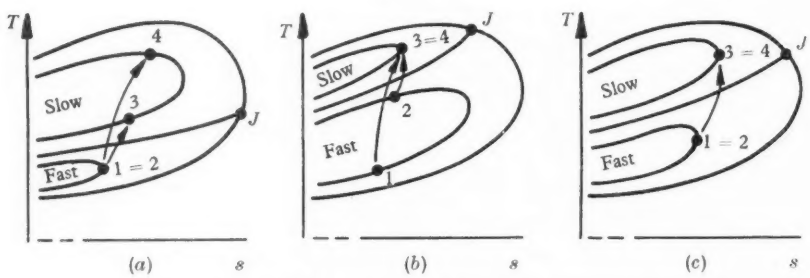

FIGURE 6. Rayleigh lines on the T-s plane, showing shocks that are (*a*) sonic ahead, (*b*) sonic behind and (*c*) sonic ahead and behind.

$2W$ and $Z3$, as it does along WZ since $T\,ds = dH$. We conclude, wrongly, that $H_2 > H_3$. Inevitably, then, $s_2 < s_3$. In fact the states are numbered in order of increasing entropy, and we conclude that all six shocks joining them must involve increases of density and hence of pressure, since $(\partial p/\partial\rho)_s$ and $(\partial p/\partial s)_\rho$ are both positive and non-zero, except at extreme states, such as those for a perfect gas where T, a^2 and p all tend to zero. (For a perfect gas we have $(\partial p/\partial s)_\rho = (\gamma - 1)\,p/R$.) Moreover, except at such states, we see that h also increases across shocks since $dh = T\,ds + \tau\,dp$, and hence that the kinetic energy $\frac{1}{2}(v_x^2 + v_y^2)$ decreases, H being constant.

In all intermediate shocks, upstream the velocity is above the local Alfvén velocity, downstream it is below it. The four types 13, 14, 23 and 24 are distinguished by the inequalities (24) applied appropriately upstream and downstream.

Intermediate shocks may be sonic ahead or behind; this occurs when H equals the lesser maximum of H for given values of G, B_x, F_x and F_y, and is illustrated in figure 6. If G, B_x, F_x and F_y are suitably matched, the two maxima of H are equal and the strangest case of all, sonic ahead and behind, can occur (figure 6*c*). If H is increased beyond the lesser of the two maxima for given G, B_x, F_x and F_y, intermediate shocks no longer occur.

The Alfvén shock is the limit of 23 shocks as $F_y \to 0$. Similarly 13, 14 and 24 shocks in this limit become switch-on, ordinary and switch-off shocks, respectively.

4.2.4. *Strong shocks*

Questions so far avoided are whether H has lower limits in addition to upper limits on a Rayleigh line, whether H can be so low that members of the set of states 1, 2, 3, 4 disappear and whether all parts of a Rayleigh line are accessible via shocks. In ordinary gasdynamics the high density end of the Rayleigh line is not accessible from shocks, since for very strong shocks having infinite pressure ratio the density ratio is finite.

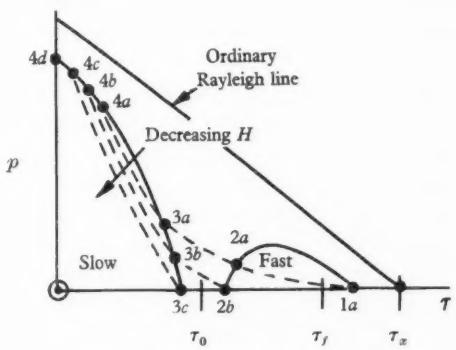

FIGURE 7. Rayleigh line on the p-τ plane showing strong shocks. $\tau_0 = B_x^2/\mu G^2$, $\tau_x = F_x/G^2$, $\tau_f = \frac{1}{3}(\tau_0 + 2\tau_x)$.

Figure 7 shows a two-branched Rayleigh line, cutting the p and τ axes in the points 1*a*, 2*b*, 3*c* and 4*d*. It may be shown that, whatever the behaviour of the gas, the kinetic energy $\frac{1}{2}(v_x^2 + v_y^2)$ is successively less at these four points in the above order. The proof of this simple result is to be found in the appendix. To make progress we must plausibly assume that at these states at very low p (or τ at 4*d*) the enthalpies h may be taken as equal. This is valid, for instance, if the gas approaches the perfect gas state there. It implies that the stagnation enthalpy H is successively less at the four points in order, so that at the point 2*a*, at which H has the *same* value as at 1*a*, H has a higher value than at 2*b* and so 2*a* lies off the zero pressure axis. [N.B. $dH/d\tau$ and dH/dp are finite at 2*b* in view of table 1 provided $T(\partial s/\partial p)_\rho$ is finite there. This is certainly true for a perfect gas, for which $T(\partial s/\partial p)_\rho = \tau/(\gamma - 1)$.] The shock 1*a*2*a* is a fast *strong* shock with an infinite pressure ratio but a finite density ratio. In a similar way, we can deduce the occurrence of the five other strong shocks 1*a*3*a*, 1*a*4*a*, 2*b*3*b*, 2*b*4*b*, 3*c*4*c*. In figure 7 the dotted lines loosely connect points at which H is the same.

Of course it is possible that the lines of higher H may not intersect the slow branch at all and some of the six strong shocks may be missing. If the Rayleigh line has only one branch, only one strong shock occurs. All the strong shocks have a finite density ratio.

Several parts of the Rayleigh line are inaccessible to shocks. No shock can lead to the arcs $2a2b$, $3b3c$ or $4c4d$, though shocks can start from the first two of these.

Finally, we remark that, for a given Rayleigh line specified by (G, B_x, F_x, F_y), as H is lowered the states 1, 2, 3 and 4 will disappear in that order as the pressure at each state falls to zero in turn. In other words, members of the family of six shocks characterized by given values of (G, B_x, F_x, F_y, H) may be missing because H is too low, just as they may be missing because H is too high and for other reasons already discussed.

4.3. *Comparison with previous work on shocks*

Our simple classification of shocks into six types obviously needs reconciling with previous classifications. Germain's (1959) work has already been mentioned. Friedrichs's earlier work (1954) had only limited circulation, but one gathers he classified shocks as fast, Alfvén and slow, and omitted intermediate shocks altogether. An anomaly appears in Friedrichs & Kranzer's later paper (1958), however, where it is wrongly stated that B_y may reverse in slow shocks for which $v_x \leqslant b_x$ on both sides.

Several other authors, including Helfer (1953), Lüst (1955) and Bazer & Ericson (1959), have performed extensive numerical explorations of the shocks that occur for the case of a perfect gas with $\gamma = \frac{5}{3}$. The parameters they choose to specify their shocks, though they may be convenient for computation, are awkward for classifying the shocks, chiefly owing to the fact that upstream and downstream conditions are not treated symmetrically. One might argue in their favour that one usually knows conditions upstream of a shock, but even this is debatable. Usually the obliquity of a shock is *not* known. Here the work of Cabannes (1959) is perhaps more realistic, since he takes flow deflexion angle as a known quantity instead.

Helfer recognized the *three* classes of shocks, fast, slow and intermediate, but did not distinguish the four types of intermediate shock. He presents his numerical results without much comment. Lüst's results are discussed later.

Bazer & Ericson chose as basic parameters to specify a shock the upstream values of $(a/b)^2$, $\tan^{-1}(B_y/B_x)$ and $|\Delta B_y|/B$, which they denote by s_0, θ_0 and h, respectively. Δ denotes change across the shock. They classify shocks into fast shocks in which B_y increases and 'slow' shocks in which B_y decreases *and may reverse*. We add the inverted commas to distinguish true slow shocks from 'slow' shocks, which also include the four kinds of intermediate shocks. They further subdivide their fast and 'slow' shocks into two types, depending on whether the shock is uniquely or doubly defined by h, for given values of s_0 and θ_0. This is a purely mathematical distinction, depending on the fickle behaviour of the variable h, although for 'slow' shocks it does distinguish between shocks in which $|B_y|$ increases or decreases, as is discussed later.

It is not difficult to locate the five different sorts of 'slow' shocks on Bazer & Ericson's graphs. Figure 8 shows a typical specimen, a rough and augmented version of the curves of v_x/b_x (upstream of shock) against h for $s_0 = \frac{1}{16}$ and $\theta_0 = 20°$ and 60°, taken from their figure 7. Bazer & Ericson themselves point out that at A and F the shock degenerates to a slow sound wave and to an Alfvén shock, respectively. They also point out that D, the maximum of v_x/b_x (upstream) for given values of s_0 and θ_0, occurs when the flow is slow-sonic, downstream.

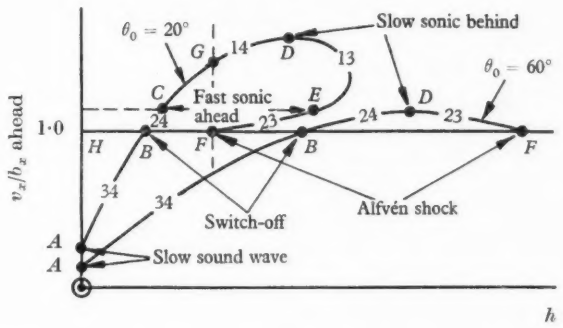

FIGURE 8. Approximate reproduction of Bazer and Ericson's graph. (N.B. h is $|\Delta B_y|/B$, not enthalpy.)

Another critical point on the curves is where $v_x = b_x$ (upstream) at B. Here we have the switch-off shock, where $h = \sin\theta_0$, so that $B_y = 0$ downstream. $HB = BF$. Finally, we have points where the flow is fast-sonic upstream. At such points, (23) gives

$$(v_x/b_x)^2_{\text{upstream}} = [(1+s_0) + \{(1+s_0)^2 - 4s_0\cos^2\theta_0\}^{\frac{1}{2}}]/2\cos^2\theta_0.$$

These points, C and E, are readily located on the $\theta_0 = 20°$ curve at the value $v_x/b_x = 1{\cdot}07$, but $\theta_0 = 60°$ is too large for them to occur. Here then is a more significant division of Bazer & Ericson's curves for 'slow' shocks into two types, depending on whether or not there occur these fast-sonic points. This division does not coincide with Bazer & Ericson's division even for a perfect gas.

The critical points A to F separate the five types of 'slow' shock in figure 8. Starting from the slow sound wave at A we traverse a region of pure slow shocks 34 before these change to intermediates of type 24 as the upstream state crosses the $v = b, \tau = \tau_0$ line at the switch-off shock B, and so-on, until the Alfvén shock F is reached.

As θ_0 tends to zero, the arc AD tends to the axis $h = 0$ representing ordinary shocks, EF vanishes and DE becomes the switch-on shock curve shown by Bazer & Ericson. Fast and slow shock régimes are connected to intermediate régimes via switch-on and switch-off shocks, respectively.

For each suitable value of s_0 there will be a value of θ_0 for which C, D and E coincide. This triple point then represents those freak intermediate shocks which are fast-sonic upstream and slow-sonic downstream.

Another interesting feature of Bazer & Ericson's curves is that they show when $|B_y|$ increases in intermediate shocks. This occurs on the part of the curve to the right of FG in figure 8. This question was also considered by Polovin & Liubarskii (1958), whose condition $B_x^2 < \mu v_{x1}^2 \rho_1(\rho_1+\rho_2)/2\rho_2$ in our notation is more simply written $\tau_0 < \bar{\tau}$ (bar denotes mean value between two sides of shock).

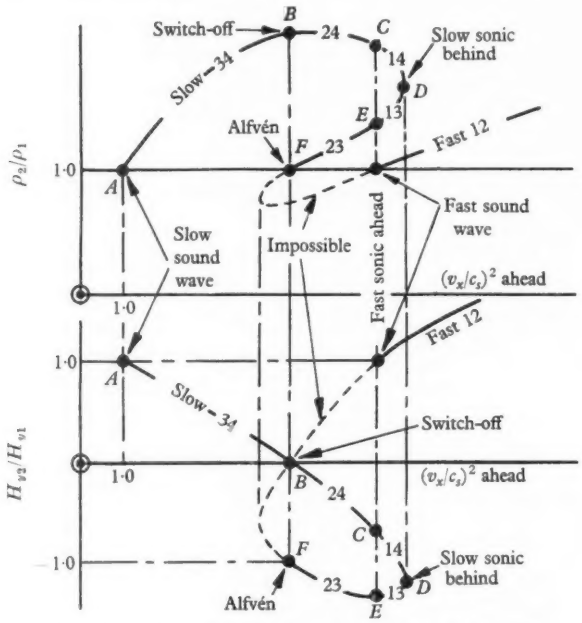

FIGURE 9. Approximate reproduction of Lüst's graphs.

which follows easily from (22). We observe that there exist shocks (G) besides Alfvén shocks (F) in which the magnetic field intensity is unchanged. Such shocks have various simple properties, including

$$\bar{\tau} = \tau_0, \quad \Delta p + G^2 \Delta\tau = 0 \quad \text{and} \quad \Delta h + (B^2/2\mu)\,\Delta\tau = 0.$$

Bazer & Ericson's graphs do not show the strong shocks considered in § 4.2.4, for which s_0 tends to zero. The only strong shocks they do show are *ordinary* strong shocks which occur as a case of fast shocks as a and b tend to zero, s_0 being finite and non-zero.

Lüst's (1955) graphs are similar to those of Bazer & Ericson. Figure 9 shows approximate specimens taken from Lüst's figures 5 and 6. The curves again correspond to constant values of s_0 and θ_0. Indeed the lower figure is almost the same as our figure 8, because $(v_x/b_x)^2 \propto (v_x/c_s)^2$ and $h \propto 1 - H_{y2}/H_{y1}$ for given values of s_0 and θ_0. The various regions on Lüst's curves are readily identifiable. In the example illustrated the intermediate branch enters the 13 and 14 regions by going fast-sonic ahead at the same value of $(v_x/c_s)^2$ as that at which the *fast* branch begins. Lüst's curves show how the fast and intermediate branches are

connected via the impossible region, which infringes the Second Law. This part of the curve would be significant, however, if we were to interchange upstream and downstream conditions.

Bazer & Ericson remark that if the values of s_0 and θ_0 are fixed, Δs and v_x/b_x (upstream) are stationary when the normal velocity is sonic downstream. This identifies the point D in figures 8 and 9. This result is a general one, independent of the perfect gas assumption, as may be seen from the following argument.

To fix s_0 and θ_0, let us specify the upstream thermodynamic state and field strength and orientation completely, leaving the velocity free to vary. If suffix 1 denotes upstream, then we find that, as the upstream condition varies,

$$dF_x = 2v_{x1}dG, \quad dF_y = 2v_{y1}dG, \quad dH = (v_{x1}^2+v_{y1}^2)\,dG/G.$$

Generalizing (11) to permit variation of the spatially uniform parameter G gives

$$v_x dF_x + v_y dF_y + GT\,ds - G\,dH = (v_x^2+v_y^2)\,dG,$$

which may be applied to the downstream state (2), which has the same values of F_x, F_y, H and G as does (1). Hence

$$GT_2 ds_2 = \{(v_{x1}-v_{x2})^2+(v_{y1}-v_{y2})^2\}\,dG,$$

which is equivalent to Bazer & Ericson's equation (78). Hence if ds_2 vanishes so do dG, dF_x, dF_y and dH if the states 1 and 2 are different. But

$$\frac{dH}{d\rho_2} = \left(\frac{\partial H}{\partial \rho_2}\right)_{GF_y s_2} + \left(\frac{\partial H}{\partial s_2}\right)_{\rho_2 GF_y}\frac{ds_2}{d\rho_2} + \left(\frac{\partial H}{\partial G}\right)_{\rho_2 s_2 F_y}\frac{dG}{d\rho_2} + \left(\frac{\partial H}{\partial F_y}\right)_{\rho_2 s_2 G}\frac{dF_y}{d\rho_2}$$

and

$$\left(\frac{\partial H}{\partial s_2}\right)_{\rho_2 GF_y}, \quad \left(\frac{\partial H}{\partial G}\right)_{\rho_2 s_2 F_y} \quad \text{and} \quad \left(\frac{\partial H}{\partial F_y}\right)_{\rho_2 s_2 G}$$

are easily shown to be finite if $\tau_2 \neq \tau_0$. Thus, when s_2 and G are stationary we have

$$\left(\frac{\partial H}{\partial \rho_2}\right)_{GF_y s_2} = 0,$$

which, by table 1, implies that state 2 is sonic, provided $\tau_2 \neq \tau_0$. Moreover, since s_1, ρ_1 and b_1 are fixed, Δs and $(v_x/b_x)_1$ are indeed stationary in this case.

4.4. *Conclusion*

It is apparent that the generalized Rayleigh line offers many advantages for the study of magnetogasdynamic shocks, without the use of the perfect gas assumption. From it, we easily demonstrate the facts that the shocks must be compressive and that there are up to four states mutually accessible via six kinds of shocks, these four states being distinguished by the magnitude of the normal velocity in relation to the three local velocities, the two sound speeds and the Alfvén speed. It is easy to see how the six kinds of shock are connected with one another via the degenerate special cases of sonic states, Alfvén shocks, switch-on, switch-off and ordinary shocks. Not least of the advantages of the

Rayleigh line is its utility as a visual aid to remembering the multiplicity of cases which occur!

In this paper the questions of shock structure, shock stability and the ability of dissipative processes to permit the shocks to occur have been ignored. The most exhaustive discussion of shock structure is that of Germain (1959). Probably not all the shocks are possible; Alfvén *shocks*, as distinct from Alfvén *simple waves* (so broad that dissipation may be neglected) involve the absurdity of zero entropy change in the face of high spatial gradients, and one suspects that the closely related 23 shocks also fail because the entropy change is too small.

It is a pleasure to record my debt to M. D. Cowley for many stimulating discussions.

Appendix: Proof that the kinetic energy is successively less at the points 1*a*, 2*b*, 3*c* and 4*d* in figure 7

At 4*d* v_x and v_y both vanish and so we need consider 4*d* no further.

At 1*a*, 2*b* and 3*c*, τ is given by the cubic

$$E \equiv (\tau-\tau_x)(\tau-\tau_0)^2+\tau_0\tau_y^2/2 = 0, \tag{25}$$

derived from (21), where $\tau_x = F_x/G^2$, $\tau_y = F_y/G^2$. The kinetic energy

$$\tfrac{1}{2}(v_x^2+v_y^2) = \tfrac{1}{2}G^2\tau^2\{1+2(\tau_x-\tau)/\tau_0\},$$

in which we have used (25) to eliminate τ_y or F_y. We are thus essentially interested in the quantity $K = \tau^2\{1+2(\tau_x-\tau)/\tau_0\}$. Now

$$\begin{aligned}(\tau_x-\tau_0)K &= (\tau_x-\tau_0)K+(1+2\tau_x/\tau_0)E\\ &\equiv 3\tau^3-3\tau^2(\tau_0+2\tau_x)+\tau(\tau_0+2\tau_x)^2+(\tau_0+2\tau_x)(\tau_y^2/2-\tau_0\tau_x).\end{aligned}$$

This cubic form has been arranged to increase monotonically with τ. Its derivative is positive and only falls to zero at the value $\tau_f = \frac{1}{3}(\tau_0+2\tau_x)$, which always lies between 1*a* and 2*b*, and in fact is the value of τ at which 1*a* and 2*b* finally coincide when the fast branch falls below the τ axis as F_y increases. Since $\tau_x > \tau_0$ here, K therefore increases monotonically with τ at the three points 3*c*, 2*b* and 1*a* and our proof is complete.

REFERENCES

Akhiezer, A. J. *et al.* 1958 *J.E.T.P.* **35**, 731.

Bazer, J. & Ericson, W. B. 1959 *Astro. J.* **129**, 758.

Bleviss, Z. O. 1959 *Heat Transfer and Fluid Mechanics Inst., Calif.* 27.

Cabannes, H. 1959 *Rech. aéro.* **71**, 3.

Friedrichs, K. O. 1954 *Los Alamos Rep.* LAMS-2105.

Friedrichs, K. O. & Kranzer, H. 1958 *N.Y.U. Inst. of Math. Sci. Rep.* NYO-6486.

Germain, P. 1959 *O.N.E.R.A. Publ.*, no. 97.

Helfer, H. L. 1953 *Astro. J.* **117**, 177.

de Hoffman, F. & Teller, E. 1950 *Phys. Rev.* **80**, 692.

IORDANSKII, S. V. 1958 *C.R. Acad. Sci. U.R.S.S.* **121**, 610.
KULIKOVSKY, A. G. 1958 *C.R. Acad. Sci. U.R.S.S.* **121**, 987.
LIUBARSKII, G. I. & POLOVIN, R. V. 1958 *J.E.T.P.* **35**, 509.
LUDFORD, G. S. S. 1959 *J. Fluid Mech.* **5**, 67.
LÜST, R. 1953 *Z. Naturf.* **8***a*, 277.
LÜST, R. 1955 *Z. Naturf.* **10***a*, 125.
POLOVIN, R. V. & LIUBARSKII, G. I. 1958 *J.E.T.P.* **35**, 510.
SHERCLIFF, J. A. 1958 *J. Fluid Mech.* **3**, 645.
SHERCLIFF, J. A. 1960 *Rev. Mod. Phys.* appearing shortly.
WEYL, H. 1949 *Commun. Pure Appl. Math.* **2**, 103.

Finite tidal waves propagated without change of shape

By F. K. BALL
C.S.I.R.O. Division of Meteorological Physics, Aspendale, Victoria, Australia

(Received 11 June 1960)

Coriolis terms are introduced into the equations governing the motion of a finite tidal wave. Various types of solution are found, all of which travel without change of shape and some which are periodic with sharp crests and broad troughs. The classical result that such waves cannot be propagated without change of shape is therefore untrue in these circumstances.

1. Introduction

The shallow water theory in its lowest approximation (i.e. tidal theory) has been applied with advantage not only to the study of long gravitational waves and tides but also to many problems of hydraulic engineering, particularly in connexion with flow in open channels. More recently applications of this type of theory have been made in meteorology (e.g. Abdullah 1949; Tepper 1950; Freeman 1951; Ball 1956, 1960), and it is certain that the usefulness of the theory in this context has not yet been adequately explored.

In tidal theory one makes the basic assumption that the vertical accelerations are sufficiently small for the vertical pressure gradient to be regarded as hydrostatic. This implies that the horizontal pressure gradient is determined solely by the inclination of the free surface. These assumptions are appropriate when the depth is small compared with some other significant length, such as for example the radius of curvature of the free surface. Now it is well known that under such conditions finite waves cannot be propagated without change of shape (e.g. see Lamb 1932, p. 278). It will be shown here that when Coriolis terms are introduced into the equations of motion and an additional force assumed so that geostrophic equilibrium can prevail, the resulting system has finite solutions which *are* propagated without change of shape; furthermore some of these solutions are periodic and represent an oscillation about geostrophic equilibrium.

In geophysical applications an additional force is acting when the fluid flows on sloping ground or when it flows as a layer beneath a lighter fluid. In the former case the force is provided by gravity and geostrophic flow is parallel to the surface contours; in the latter case the force is provided by the (horizontal) pressure gradient in the upper fluid and geostrophic flow is parallel to the isobars. Both types of flow occur, for example, on the Antarctic Ice Cap where there is frequently a layer of very cold air in contact with the ice. This cold air flows under the combined influence of gravity and the superimposed pressure gradient, gravity usually being dominant when the slope of the ice exceeds about 2×10^{-3}.

2. Basic equations

We will assume that there are two liquid layers with densities ρ_0 and ρ_1 ($\rho_0 < \rho_1$) and that the interface is at a height H above the base of the lower layer, which in turn is at a height Z above some fixed datum. The horizontal pressure gradient in the lower layer is then given by the sum of the superimposed pressure gradient in the upper layer and the gradient resulting from the slope of the interface. Thus $\nabla_1 p_1 = \nabla_1 p_0 + (\rho_1 - \rho_0) g \nabla_1 (H+Z)$ where ∇_1 denotes the horizontal gradient and the equations governing the motion of the lower layer can be written

$$\frac{\partial H}{\partial t} + \frac{\partial}{\partial X}(HU) + \frac{\partial}{\partial Y}(HV) = 0, \tag{1}$$

$$\frac{DU}{Dt} = -\frac{1}{\rho_1}\frac{\partial p_0}{\partial X} - g^* \frac{\partial}{\partial X}(H+Z) + fV, \tag{2}$$

$$\frac{DV}{Dt} = -\frac{1}{\rho_1}\frac{\partial p_0}{\partial Y} - g^* \frac{\partial}{\partial Y}(H+Z) - fU, \tag{3}$$

where g^* is the modified gravitational acceleration, $(\rho_1 - \rho_0) g/\rho_1$, and f is the Coriolis parameter. Capital letters are here used to denote some of the variables, small letters being reserved for the corresponding dimensionless quantities introduced below. We now assume further that $\nabla_1 (p_0/\rho_1 + g^* Z)$ is constant (this expression represents the additional force mentioned in the introduction), and consequently the equations have a solution (geostrophic equilibrium) given by

$$U_g = -\frac{1}{f}\frac{\partial}{\partial Y}\left(\frac{p_0}{\rho_1} + g^* Z\right), \tag{4}$$

$$V_g = \frac{1}{f}\frac{\partial}{\partial X}\left(\frac{p_0}{\rho_1} + g^* Z\right), \tag{5}$$

where the equilibrium depth $H = H_g$ is constant.

We wish to investigate simple solutions of equations (2) and (3) which represent disturbances propagated without change of shape and with constant velocity c in the X-direction under the influence of a constant external force of arbitrary direction. This force is represented for convenience by the geostrophic flow U_g, V_g which it would induce. We also assume that a disturbance has negligible variation in the Y-direction, and thus $\partial H/\partial Y$, $\partial U/\partial Y$ and $\partial V/\partial Y$ are all equivalent to zero, and $\partial/\partial t$ is equivalent to $-c\partial/\partial X$. The equations then take the form

$$H(U-c) = Q, \tag{6}$$

$$Q\frac{dU}{dX} = -Hg^*\frac{dH}{dX} + Hf(V - V_g), \tag{7}$$

$$Q\frac{dV}{dX} = Hf(U_g - U), \tag{8}$$

where Q is a constant of integration representing physically the volume flow of the lower liquid relative to the moving system.

If we eliminate H from equations (7) and (8) by using equation (6), and make the substitutions $u = (U-c)/U_c$, $v = (V-V_g)/U_c$, $x = Xf/U_c$ and $\alpha = (U_g-c)/U_c$, where U_c is the 'critical speed' of mathematical hydraulics given by $U_c^3 = Qg^*$, then the equations have the dimensionless form

$$u\frac{du}{dx}(1-u^{-3}) = v, \tag{9}$$

$$u\frac{dv}{dx} = \alpha - u, \tag{10}$$

with the equilibrium (geostrophic) solution $v = 0, u = \alpha$. The direction of increasing X (and also x) has been so chosen that $U-c > 0$; whence, since $H > 0$, we have $Q > 0$ and $u > 0$.

The form of the solution of equations (9) and (10) depends on the value of the parameter α and the boundary condition (e.g. the condition that the solution passes through a particular point in the (u, v)-plane, the origin of x being immaterial). In the following sections all possible types of solution will be considered and the conditions under which periodic solutions can occur will be investigated in detail.

3. Solution types

The easiest way to determine the types of solution that can arise involves consideration of the 'phase portrait', i.e. solution curves in the (u, v)-plane (i.e. the 'phase plane'). To determine the form of the phase portraits we note the following facts. If we change the sign of both v and x, the form of the equations is unchanged; thus the phase portrait is symmetrical about the u-axis. The lines $u = 0$, $u = 1$, $u = \alpha$ and $v = 0$ divide the phase plane into regions within each of which du/dx and dv/dx have constant sign; furthermore on each of these lines one or other of dv/dx and du/dx is either zero or infinite. Making use of these facts it is a simple matter to sketch the phase portraits as in figure 1, the upper half plane $u > 0$ being the part of interest. There are three basically different patterns according as $\alpha > 1$, $1 > \alpha > 0$ or $0 > \alpha$. The arrows give the direction of increasing x.

The closed curves in figure 1 (*a*) correspond to the periodic solutions in which our main interest lies. These solutions are clearly periodic, for if one of these closed curves is followed in an anticlockwise direction then x continuously increases whereas u and v alternate regularly between their extreme values. On the other hand the closed curves in figures 1 (*b*) and 1 (*c*) do *not* correspond to *simple* periodic solutions since the direction of increasing x changes where the curves cross the line $u = 1$. The solutions corresponding to these curves form a series of closed loops in the (u, x)-plane. Furthermore it is certain that these solutions (and all others that cross the line $u = 1$ with a reversal of the direction of increasing x) are physically invalid in the neighbourhood of $u = 1$, not only because vertical accelerations are likely to be important there but also because the solution 'turns back' in a way which is physically inconsistent with our assumptions.

The lowest group of curves in figures 1 (*a*) and 1 (*b*) correspond to a moving trough with maximum u (minimum H) and a change in sign of v. Because of the superimposed pressure distribution the minimum of H does not necessarily coincide with minimum pressure. We do not propose to discuss this type of solution here.

The only solution which is admissible over its whole range, apart from the periodic type and the trough type mentioned above, is the singular solution, in the form of a closed loop in the phase plane, indicated by the heavier line in

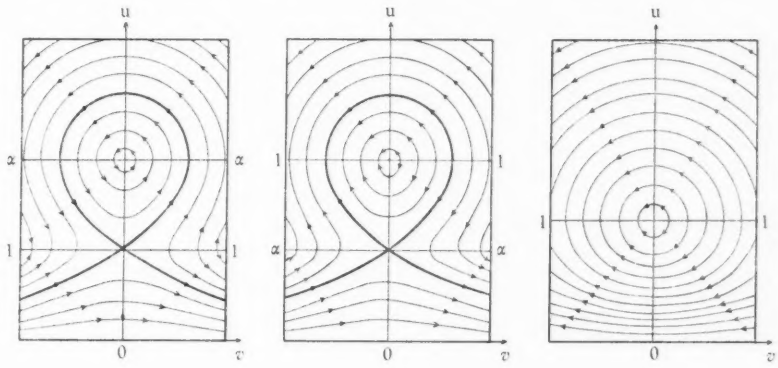

FIGURE 1. Possible phase portraits: (*a*) $\alpha > 1$; (*b*) $1 > \alpha > 0$; (*c*) $0 > \alpha$.

figure 1 (*a*). This solution is unique in that it crosses the line $u = 1$ without du/dx becoming infinite. It is also important because it forms the boundary of the periodic region, and the extreme values of u and v which occur on the loop give the upper and lower bounds of u and v which are possible in a periodic solution.

4. The periodic solutions

Equations (9) and (10) can readily be integrated once to a form which gives the analytic expression for the phase portrait, viz. by multiplying equation (9) by $u-\alpha$ and equation (10) by v, adding and integrating to give

$$\frac{1}{2}\left[v^2+(u-\alpha)^2-\alpha\left(\frac{u-\alpha}{\alpha u}\right)^2\right] = E. \tag{11}$$

The constant of integration E is a measure of the energy of the motion regarded as a disturbance of the geostrophic flow $v = 0$, $u = \alpha$. The extreme values for a periodic solution are $E = 0$ corresponding to geostrophic equilibrium and $E = (\alpha-1)^3/2\alpha$ corresponding to the singular solution passing through the point $v = 0$, $u = 1$. The conditions for a simple periodic solution are therefore $\alpha > 1$, $u > 1$ and

$$\left[v^2+(u-\alpha)^2-\alpha\left(\frac{u-\alpha}{\alpha u}\right)^2\right] < \frac{(\alpha-1)^3}{\alpha}.$$

The extreme values of v occur when $u = \alpha$, and the maximum possible amplitude of v for a simple periodic solution is given by

$$|v| = \left[\frac{(\alpha-1)^3}{\alpha}\right]^{\frac{1}{2}};$$

similarly the extreme values of u occur when v is zero, whence u lies in the range

$$1 < u < (\alpha-1) + [\alpha(\alpha-1)+1]^{\frac{1}{2}}.$$

When the amplitude of the oscillation is small the solution curve in the phase plane is a small ellipse centred on the point $(0, \alpha)$. A simple analytic solution can readily be found by linearizing the equations (9) and (10). The result is

$$u - \alpha = A\cos\frac{2\pi x}{\lambda},$$

$$v = -A\left(\frac{\alpha^3-1}{\alpha^3}\right)^{\frac{1}{2}}\sin\frac{2\pi x}{\lambda}, \tag{12}$$

where the wavelength λ is given by

$$\lambda = 2\pi\left(\frac{\alpha^3-1}{\alpha}\right)^{\frac{1}{2}}. \tag{13}$$

An analytic solution can also be found in the other extreme when

$$E = (\alpha-1)^3/2\alpha$$

and the wave has maximum possible amplitude. We then have from equation (11)

$$v^2 = \left(\frac{u-1}{u}\right)^2[\alpha + 2u(\alpha-1) - u^2],$$

whence from equation (9)

$$\frac{du}{dx} = \frac{u[\alpha+2u(\alpha-1)-u^2]^{\frac{1}{2}}}{u^2+u+1}.$$

Therefore

$$x = \int_1^u \frac{(s^2+s+1)\,ds}{s[\alpha+2s(\alpha-1)-s^2]^{\frac{1}{2}}},$$

where x is the distance from the wave crest (minimum u). Furthermore

$$\int \frac{(s^2+s+1)\,ds}{s[\alpha+2s(\alpha-1)-s^2]^{\frac{1}{2}}} = -\left\{\alpha\cos^{-1}\left(\frac{s-\alpha-1}{\beta}\right)\right.$$
$$\left. + \alpha^{-\frac{1}{2}}\ln\left|\frac{[\alpha(\alpha+2s(\alpha-1)-s^2)]^{\frac{1}{2}}+\alpha+s(\alpha-1)}{s}\right| + [\alpha+2s(\alpha-1)-s^2]^{\frac{1}{2}}\right\},$$

where $\beta^2 = \alpha(\alpha-1)+1$. Therefore the wavelength is given by

$$\lambda = 2\int_1^{\beta+\alpha-1} \frac{(s^2+s+1)\,ds}{s[\alpha+2s(\alpha-1)-s^2]^{\frac{1}{2}}}$$
$$= 2\left\{\alpha\cos^{-1}\left(\frac{2-\alpha}{\beta}\right) + \alpha^{-\frac{1}{2}}\ln\left|\frac{\{3\alpha(\alpha-1)\}^{\frac{1}{2}}+2\alpha-1}{\beta}\right| + \{3(\alpha-1)\}^{\frac{1}{2}}\right\}.$$

A graph of this function, representing the dependence of the maximum possible wavelength on α, is shown in figure 2 together with a graph of the corresponding

function for waves of infinitesimal amplitude (equation (13)). When α is large we have $\lambda \simeq 2\pi\alpha$ for both infinitesimal and maximum amplitude. It appears therefore that there is little change in wavelength with variation in amplitude.

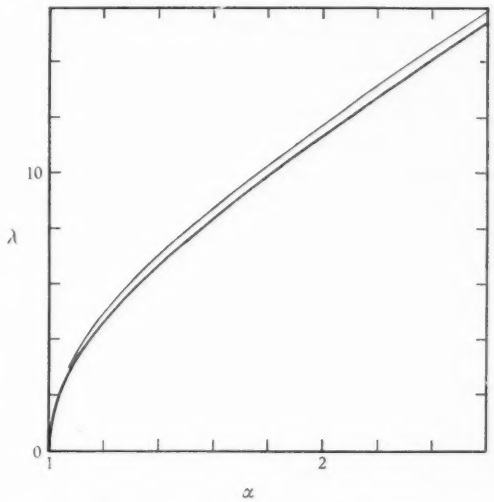

FIGURE 2. Wavelength as a function of α. Upper curve: infinitesimal wave. Lower curve: wave of maximum amplitude.

To express the actual wavelength L for the infinitesimal wave in terms of the physical variables, we note that

$$L = \frac{\lambda U_c}{f} = \frac{2\pi}{f}\left[(U_g - c)^2 - \frac{Qg^*}{U_g - c}\right]^{\frac{1}{2}}.$$

The equilibrium depth is given by $H_g = Q/(U_g - c)$, whence

$$L = \frac{2\pi}{f}\left[(U_g - c)^2 - H_g g^*\right]^{\frac{1}{2}}. \tag{14}$$

When the wavelength is small this reduces to the usual expression for the velocity of tidal waves.

More detailed investigation reveals that the waves have the following properties. The wave of infinitesimal amplitude is harmonic in form. As the amplitude increases the wavelength decreases slightly, the troughs become broad and shallow and the crests narrow and sharp. The cross wave component changes rapidly from one extreme to another on the passage of a sharp crest. At maximum amplitude the wave crests become pointed, the points becoming so sharp for large values of α that the waves are almost cusped. Some of these properties are illustrated in figure 3. For completeness an 'inadmissible' periodic solution, corresponding to a closed curve in figure 1 (*b*), is illustrated in figure 4. As mentioned in § 3, this and other solutions are physically invalid in the neighbourhood of $u = 1$ (this does not, however, imply that the other parts of these solutions are necessarily invalid).

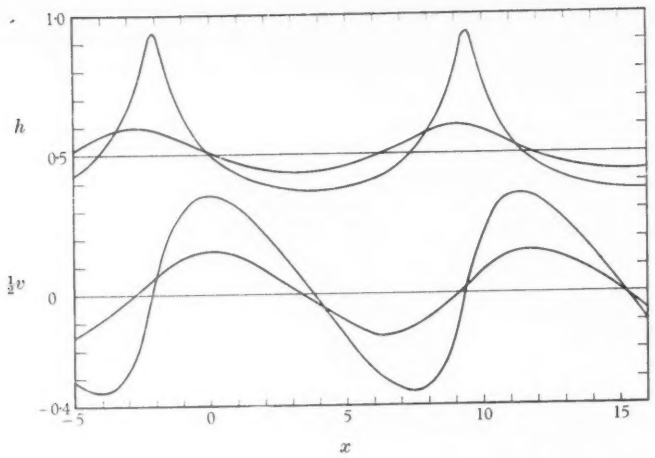

FIGURE 3. Typical wave forms; $\alpha = 2$. Upper curves: profiles of h $(= u^{-1})$ for large and small amplitude; lower curves: corresponding profiles of $\frac{1}{2}v$.

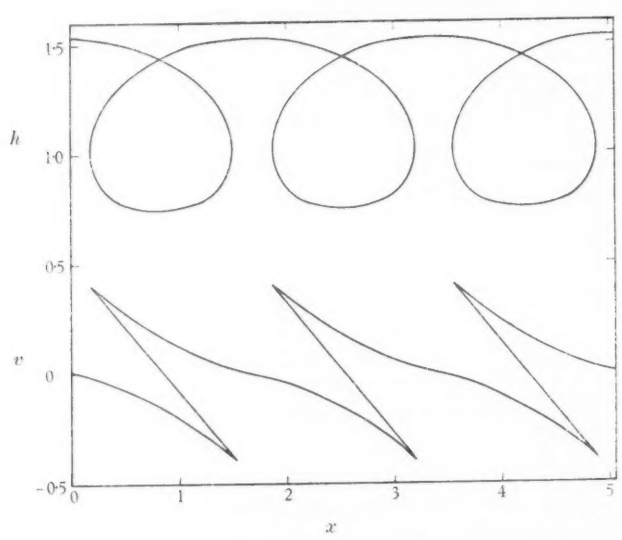

FIGURE 4. An 'inadmissible' periodic solution; $\alpha = 0{\cdot}5$. Upper curve: profile of h $(= u^{-1})$; lower curve: profile of v.

REFERENCES

ABDULLAH, A. J. 1949 *J. Met.* **6**, 86.

BALL, F. K. 1956 *Aus. J. Phys.* **9**, 373.

BALL, F. K. 1960 *Quart. J. Roy. Met. Soc.* **86**, 51.

FREEMAN, J. C. 1951 Compendium of Meteorology, *Amer. Met. Soc.*, p. 421.

LAMB, H. 1932 *Hydrodynamics*, 6th ed. Cambridge University Press.

TEPPER, M. 1950 *J. Met.* **7**, 21.

Effects of a flexible boundary on hydrodynamic stability

By T. BROOKE BENJAMIN

Department of Engineering, University of Cambridge

(Received 22 September 1960)

The theoretical study presented in this paper was inspired by the recent report (Krämer 1960) of experiments showing that considerable reductions in the drag of an underwater solid body were achieved by covering it with a skin of flexible material; apparently this effect was due to the boundary layer being stabilized in the presence of the skin, so that transition to a turbulent condition of flow was prevented or at least delayed. The stability problem for flow past a flexible boundary is here formulated in a general way which allows a full exploration of the possibility of a stabilizing effect without the need to assign specific properties to the flexible medium; the collective properties of possible boundaries are represented by a 'response coefficient' α (a sort of 'effective compliance') measuring the deflexion of the surface under a travelling sinusoidal distribution of pressure.

A remarkably simple analytical connexion is established between the present general problem and the corresponding stability problem for the boundary layer on a rigid plane wall, and hence many details of the existing theory of hydrodynamic stability are immediately useful. However, the presence of the flexible boundary admits possible modes of instability additional to those which already exist when the boundary is rigid, and clearly every mode must be considered with regard to practical measures for stabilization—that is to say, it might be useless to inhibit one mode by a device which lets in another. What is believed to be an essentially complete interpretation of the over-all possibilities is deduced on recognizing three more or less distinct forms of instability. The first comprises waves resembling the unstable waves which can arise in the presence of a rigid boundary, but now being modified by the effects of flexibility. These waves tend to be stabilized when the boundary has a compliant response to them, which means the respective wave velocity has to be less than the velocity of *free* surface waves on the boundary; but it is found that the effect of internal friction in the flexible medium is actually *de*stabilizing. The second form of instability is essentially a resonance effect and comprises waves travelling at very nearly the velocity of free surface waves. These waves can only be excited when the latter velocity falls below the free-stream velocity; they are scarcely affected by the viscosity of the fluid since the 'wall friction layer' is largely cancelled, so that damping due to the medium itself becomes the only stabilizing factor. The third form is akin to Kelvin–Helmholtz instability.

This interpretation of the theoretical results seems to point to the essential factors in the operation of a flexible skin as a stabilizing device, and accordingly in the concluding section of the paper two alternative sets of criteria are proposed

each of which would provide a logical basis for designing such a device. The principle of the first alternative explains the success of Kramer's invention, but the second appears equally promising and the relative advantages of the two can really be proved only by further experiment.

1. Introduction

The recently reported experiments by Krämer (1960*a*, *b*) have evidently aroused wide interest in the possible uses of coatings of elastic material as a practical means of preventing transition to turbulence in laminar boundary layers. His important pioneering papers presented evidence that the device invented by him had brought about considerable reductions in the drag of underwater bodies, and following the publication of his original idea there has naturally been speculation regarding other applications of this method of stabilization. The purpose of the present paper is to examine this idea theoretically, attempting to reveal the general practical possibilities rather than to establish complete solutions applicable to specific stabilizing devices. The problem is treated by use of the Tollmien–Schlichting type of stability theory, and the discovery is made that the minimum Reynolds number for the existence of neutral wave disturbances is in various circumstances increased by flexibility of the boundary. This is encouraging from a practical point of view, because in its more familiar applications, the perturbation theory of boundary-layer stability has been well-confirmed experimentally.

At first sight the present problem appears vastly more complicated than the corresponding one for a rigid boundary, which itself is by no means easy; but a way is found to adapt the results of previous theories fairly readily, so that solutions can be found without very much additional labour. The main difficulty intrinsic to all stability problems of the present kind is to solve the hydrodynamical equations to an adequate degree of approximation; but there is no need to tackle this anew since our problem admits use of the 'Tietjens function' and other functions depending on the general solution of the Orr–Sommerfeld equations which have been calculated previously. The analysis in fact leads to an equation which, except for a simple additional term, is the same as the central result of Lin's modified formulation (1945, 1955) of the Tollmien–Schlichting theory for parallel flows with rigid boundaries. As in this previous case, the complete class of neutral stability conditions is represented by this equation; in the present case, however, its interpretation is rather more difficult.

The proposed method of stabilization may generally require close specification to insure a useful result, since its application is liable to have the contrary effect of destabilizing the flow. The extra mobility introduced when a flow boundary is made flexible creates the possibility of modes of instability additional to those which may already exist when the boundary is rigid, and there is one such type of instability whose importance in present respects can at once be recognized. This takes the form of waves progressing in the flow direction at very nearly the same speed as free surface waves in the flexible medium, the waves being amplified by the action of the flow which supplies sufficient energy to counterbalance

internal dissipation. The mechanism of generation of surface waves in this way has been studied at length by Miles (1957) and Brooke Benjamin (1959: hereafter this paper will be referred to as I). As formulated in the following pages, the stability analysis covers this type of waves as well as a type that can be considered to comprise Tollmien–Schlichting waves modified by the influence of the flexible boundary. The two types are not really distinct analytically, but the physical problem is most readily understood by considering them separately. (Two such distinct classes of waves were recognized by Lock (1954) in his treatment of the stability problem—which is closely related to the present one—for a boundary layer at the interface between an air stream and deep water; he called them respectively 'water waves' and 'air waves'. The theoretical results presented in his paper are very complicated, and are insufficient to indicate a general physical interpretation of the effects of the water surface on stability.) A third type, which will be called 'Kelvin–Helmholtz' instability in view of its analogy in the classical problem of discontinuous fluid motions, has also to be recognized as a possibility.

The analysis will be made on the usual lines of stability theories for parallel flows, and many of the familiar details will be taken for granted. We generally take dimensionless variables according to the usual scheme (Schlichting 1955, p. 316), but we change without comment to dimensional forms whenever this is helpful and the new meaning is clear. The case of boundary layers with positive (adverse) pressure gradient will not be covered explicitly; this case is within the scope of the theory, and the general conclusions derived here would appear to apply to it, but it presents complications which can well be left for later study. The essential effects to be brought to light are demonstrated adequately with reference to boundary layers with negative or zero pressure gradient, for which the velocity profile has no inflexion. Most of the analysis is concerned with neutral disturbances which are simple-harmonic in time and in the co-ordinate x parallel to the primary flow velocity $U(y)$; that is, all velocity and stress perturbations have the common factor $\exp\{ik(c-ct)\}$, where the wave-number k and wave-velocity c are real. The justification for confining attention to two-dimensional disturbances will be considered briefly in §5.

As a preliminary to the main analysis in §3, an outline of the Tollmien–Schlichting theory is given in §2. The results recalled in §2 are all quite well known (e.g. see Schlichting 1955, ch. 16, or Lin 1955), but it is a great advantage to have a short account of them here for easy reference in the later parts of the paper.

2. The Tollmien–Schlichting theory of boundary-layer stability

The essential points of this theory are to be adapted directly to the present problem, and its physical basis is specially worth reconsidering here. The theory recognizes that, for the large Reynolds numbers at which neutral small disturbances become possible, the effects of viscosity are confined to two 'friction layers' whose thickness is very much smaller than that of the whole boundary layer. The first adjoins the wall and its thickness is $O(kR)^{-\frac{1}{2}}$. The second surrounds the critical point $y = y_c$ at which $U = c$, and this layer is rather more diffuse than

the first, its thickness being $O(kR)^{-\frac{1}{3}}$. A vital step in the theory is the assertion that an adequate approximation to the solution of the Orr–Sommerfeld equation can be found in the form

$$\phi(y)+f(y), \tag{2.1}$$

where $\phi(y)$ is the solution of the inviscid version of the equation, and $f(y)$ is a rapidly varying solution which can be taken to be insignificant outside the wall layer: $f(y)$ is approximated as the solution of another simplified version of the equation derived from the facts that $f''/f = O(kR) \gg U''/c$ and $\gg k^2$. The condition to be satisfied by the solution at the outer edge of the boundary layer is taken to be a condition on ϕ alone; thus,

$$\phi'/\phi \to -k \quad \text{for} \quad U \to U_0. \tag{2.2}$$

The effects of viscosity over the inner friction layer are not explicitly represented in this approximate solution, and the solution is therefore invalid in this region. However, the theory demonstrates that (2.1) will be a uniformly valid approximation on either side of the inner friction layer, provided that in $y < y_c$ the inviscid solution ϕ takes on a certain feature which is left unresolved by the inviscid equation. The critical point is a singular point of this equation, and consequently ϕ' has a logarithmic singularity at $y = y_c$. In passing through $y = y_c$, therefore, ambiguity arises as to which branch of the logarithm to take. Tollmien showed how the choice is determined from the complete Orr–Sommerfeld equation; he investigated an approximate solution which tends to ϕ for $y > y_c + O(kR)^{-\frac{1}{3}}$ but which remains valid in the immediate region of $y = y_c$, and so indicates the appropriate form of ϕ for $y < y_c - O(kR)^{-\frac{1}{3}}$. When the approximation (2.1) is adjusted according to the principle established by Tollmien and substituted in the boundary conditions at the wall $y = 0$, relations between the parameters k, R, c can be found which describe the conditions of neutral stability.

The conditions of zero normal and tangential velocity at the wall require that

$$\left.\begin{aligned} \phi_w + f_w &= 0, \\ \text{and} \qquad \phi'_w + f'_w &= 0, \end{aligned}\right\} \tag{2.3}$$

where the subscript denotes values for $y = 0$. Hence

$$\frac{f_w}{f'_w} = \frac{\phi_w}{\phi'_w}. \tag{2.4}$$

Now, f_w/f'_w can be found from the simplified equation describing the effects of viscosity in the wall layer, and the only characteristic of the boundary-layer profile on which it depends is the initial gradient U'_w. When equation (2.4) is multiplied by $-U'_w/c$, the quantity given on the left-hand side is found to be a function of $z = (kRU'_w)^{\frac{1}{3}} c/U'_w$ alone; and the right-hand side, being independent of R, is a function of k and c only. Thus the equation can be expressed as

$$F(z) = E(k, c). \tag{2.5}$$

The 'Tietjens function' $F(z)$ has been extensively tabulated; and since it is independent of the form of the velocity profile, it is universally applicable to

stability problems of the present kind. The function $E(k, c)$ depends on the overall velocity profile, and the calculation of this function is the most difficult part of the practical task of finding neutral-stability curves. Later in this paper use is made of an approximate expression for $E(k, c)$, such as was used originally by Tollmien and Schlichting to estimate this function for the Blasius velocity profile on a flat plate at zero incidence. More accurate calculations have been made by Lin (1945, 1955), Holstein (1950), Shen (1954) and other writers, and their results are suitable for adaptation to our problem; but the expression we shall consider has the advantage of simplicity, and seems adequate for the purpose of this exploratory study.

For details of the calculation of neutral-stability curves by the original method, we may refer to Schlichting's book (1955, pp. 327–329). The imaginary parts of F and E are plotted against their real parts on the same graph, the curves being determined parametrically by z, k and c. From the points of intersection of the curves, one obtains sets of values of z, k, c representing conditions of neutral stability. Elimination of c from z then gives the co-ordinates of the neutral-stability curve in the (R, k)-plane.

This outline of the theory omits the various refinements due to Lin and others which have led to improved estimates of the neutral-stability curves. For instance, the Tietjens function can be applied in a more exacting way than at present (see Lin 1955, pp. 40, 80), although the simple definition is reasonably adequate for most cases of interest—more specifically, for cases where the critical point is close to the boundary, so that the approximations $U'_w \doteqdot U'_c\ (\equiv U'(y_c))$, $y_c \doteqdot c/U'_w$ are fairly good. However, the main improvements that have been made on the original calculations of Tollmien and Schlichting are due to better estimates of the function $E(k, c)$, and the status of this function in the modern theories remains the same as in the original theory. The important thing to note in this connexion is that although we shall introduce here some rather crude approximations taken from the Tollmien–Schlichting theory, the analysis of the flexible-boundary problem is set in a form such that the way is clear to take advantage of the best available results if the need for precise data should arise.

One small detail of post-Schlichting theories needs to be noted. This is a modification of the formula (2.5) which was introduced by Lin (see Lin 1955, p. 40). If one defines

$$\mathscr{F}(z) = \frac{1}{1-F(z)}, \quad u+iv = \frac{1}{1-E},$$

(2.5) can be put in the form

$$\mathscr{F}(z) = u+iv. \tag{2.6}$$

This alternative form has the practical advantage that successive approximations to $u+iv$ can be expressed much more conveniently than the equivalent approximations to E. It turns out that v varies only slightly with k (see Lin 1955, bottom of p. 40), and this fact is found to be highly significant in the present problem.

The physical ideas underlying the theory, particularly with regard to the two friction layers, provide a useful insight into the analytical results derived later; and although the points in question are fairly well known, they deserve to be

reconsidered here as a preliminary to our physical interpretation of the effects of a flexible boundary. It is a remarkable fact, first realized clearly by Prandtl many years ago, that viscosity is responsible for the instability of laminar boundary layers in the absence of adverse pressure gradient. For fluids without viscosity, two theorems due to Rayleigh prove that a parallel flow whose velocity profile has no inflexion is stable; and so, if for a real fluid such a flow is to be unstable at all, viscosity must be capable of a destabilizing action in addition to its expected damping effect on small disturbances. Prandtl (1935) showed that the required destabilizing effect is generated by the wall friction layer. When the primary flow (at large yet finite R) is given a wavy disturbance, this layer of intense vorticity occurs because the tangential velocity component of the disturbance has to be brought to zero right at the wall. The vorticity distribution in the layer is such as to displace the effectively inviscid flow outside it in a manner quite unlike that which would happen if viscosity were entirely absent and the edge of the flow were governed by a kinematical condition alone. The velocity components u, v of the disturbance just outside the wall layer are thereby given a difference in phase such that the average Reynolds stress $-\rho\overline{uv}$ is positive. This means that energy is converted from the basic flow into the disturbance, at a rate $-\rho\overline{uv}U'\delta y$ per unit length in each layer δy; and when the energy supply is sufficient to balance viscous dissipation, a neutral disturbance can occur. It is a simple matter to show that this Reynolds stress is given by

$$\tau = \tfrac{1}{2}\rho k\mathscr{I}(\phi^*\phi') = -\tfrac{1}{2}\rho k\mathscr{I}(\phi\phi'^*),$$

where the asterisk denotes complex conjugates and $\mathscr{I}$ the imaginary part.

As a slight variation on Prandtl's argument, we observe from (2.4) that the phase relation between ϕ and ϕ' right at the wall is determined by properties of the viscous solution f. But whereas f becomes insignificant outside the wall layer, the values of ϕ and ϕ' for a considerable distance beyond the layer are very approximately the same as their values at the wall. Hence, putting $\phi_w = (f_w/f'_w)\,\phi'_w$, we conclude that a close approximation to the Reynolds stress outside the wall layer is

$$\tau = -\tfrac{1}{2}\rho k\,|\phi'_w|^2\,\mathscr{I}(f_w/f'_w) = \tfrac{1}{2}\rho k(c/U'_w)|\phi'_w|^2\,\mathscr{I}\{F(z)\}. \tag{2.7}$$

The imaginary part of the Tietjens function is positive for all relevant values of z (z being necessarily positive for waves travelling in the flow direction), except for small values ($< 2{\cdot}3$) at which the critical point is brought so close to the wall that the two friction layers overlap and the present assumption of an intermediate inviscid region breaks down. Thus, the Reynolds stress is shown to be positive, as it must be for a neutral disturbance to be maintained against the dissipative action of viscosity.

The theory of the inviscid equation shows that $\mathscr{I}(\phi^*\phi')$ is constant throughout any range of y not including the critical point; but on opposite sides of the critical point the constant can have different values. The boundary condition (2.2) requires that ϕ is in phase with $-\phi'$ at the outer edge of the boundary-layer profile, which means that the Reynolds stress is zero there and hence, because of the property noted in the last sentence, it must be zero everywhere beyond the inner friction layer. The phase difference necessary for the positive Reynolds

stress in the region between the two friction layers is therefore acquired entirely at the critical point, this effect being of course just another interpretation of the matter discussed in the second paragraph of this section.

Tollmien was the first to establish an explicit relation between the Reynolds stress and conditions at the critical point (see Lin 1955, p. 54). His result, applicable to the neutral case, is

$$\tau = -\pi\rho k\,|\phi_c|^2\,U_c''/U_c'. \tag{2.8}$$

This formula confirms that τ can be positive, since the critical point obviously can occur where the profile curvature U_c'' is negative.

3. Theory for a flexible boundary

Consider first the boundary condition to be satisfied at $y = 0$ if the boundary is flexible, though still solid, and a wave travelling at velocity c is superposed on it. The equation of the deformed boundary may be written

$$y = a\,e^{ik(x-ct)}$$

with the amplitude a considered to be in general a complex quantity. If this wave is generated by the action of the flow alone, as we shall presently suppose, all velocity and stress perturbations in the fluid are proportional to a; however, it is important not to express these perturbations with a as a common factor, because the mathematical problem has to be formulated in such a way that the Tollmien–Schlichting problem is recovered by letting $a \to 0$. For the wavy boundary, the kinematical and non-slipping conditions on the fluid velocity components take the following form (cf. I, p. 169), where the subscript w again denotes values at $y = 0$:

$$\left.\begin{aligned} \phi_w + f_w &= ca, \\ \phi_w' + f_w' &= -U_w' a. \end{aligned}\right\} \tag{3.1}$$

These are the exact boundary conditions according to linearized theory, the only restriction on their validity being that $|a|$ should be very much smaller than the wavelength, so that $k\,|a| \ll 1$. Condition (2.2) applies as before at the outer edge of the boundary layer, which means that ϕ_w/ϕ_w' is exactly the same function of k and c that occurs in the Tollmien–Schlichting analysis.

We now assume that the wave on the boundary arises in response to a pressure fluctuation developed in the fluid. The effect of the accompanying shear-stress fluctuation can be neglected, since this stress is extremely small in comparison with the pressure (see I, § 7). Expressing the surface pressure distribution by

$$p_s = \rho P_s e^{ik(x-ct)},$$

we can represent the response of the flexible medium by the equation

$$a = \alpha P_s/U_w' c, \tag{3.2}$$

which defines a parameter $\alpha/U_w' c$ dependent only on the properties of the medium and on k and c. The case of a rigid boundary is represented by $\alpha \to 0$. (The factor $1/U_w' c$ is included in this definition merely for convenience later.)

A very good approximation to P_s can be obtained in terms of ϕ_w and ϕ'_w by using the fact, demonstrated in I, that the pressure varies to a quite insignificant extent across the wall friction layer. The result is (cf. I, §3)

$$P_s = k^2 \int_0^\infty (U-c)\,\phi\,dy = U'_w \phi_w + c\phi'_w. \tag{3.3}$$

By use of (3.2) and (3.3) the boundary conditions (3.1) can now be arranged to give

$$\left.\begin{aligned}(1-\alpha)\,\phi_w - \frac{\alpha c}{U'_w}\,\phi'_w + f_w = 0,\\ (1+\alpha)\,\phi'_w + \frac{\alpha U'_w}{c}\,\phi_w + f'_w = 0.\end{aligned}\right\}$$

Hence, introducing the functions $F(z)$ and $E(k,c)$ defined in §2, we obtain directly

$$\begin{aligned}F(z) &= \frac{E+\alpha(1-E)}{1+\alpha(1-E)}\\ &= E_1(k,c), \quad \text{say.}\end{aligned} \tag{3.4}$$

This result has the same standing as the Tollmien–Schlichting formula (2.5), and clearly reduces to it when $\alpha \to 0$, i.e. when the boundary is made rigid. When the properties of the flexible medium are specified, α can be found as a function of k and c; and so, just as with (2.5), the right-hand side of (3.4) is calculable as a function of k and c only, while the left-hand side is again a function of z alone. Neutral-stability curves can therefore be found by the same graphical method as before.

A more convenient way of treating the problem appears, however, when F and E are expressed in terms of the functions $\mathscr{F}$ and $u+iv$ used in Lin's formula (2.6). Equation (3.4) then gives

$$\mathscr{F}(z) = u + iv + \alpha. \tag{3.5}$$

Thus, a remarkably simple analytical connexion is established between the present case and the case of a rigid wall. Nevertheless, it does not follow that the *complete* solution of our problem is provided merely by a simple transformation of the neutral-stability curves for a rigid wall, because the additional term α entering Lin's formula cannot be prescribed physically other than as a function of k and c, without restriction on the range of these parameters, and so the equation may admit solutions quite unrelated to those for $\alpha = 0$. In particular, we must allow the possibility of neutral waves of the kind studied by Miles (1957) and in I, which are largely independent of viscosity.

Three aspects of the above result will be considered under separate headings as follows. It may be helpful to note in advance that this division of material coincides roughly with our coverage of the expected three classes of waves, but there is necessarily some overlapping.

Non-dissipative flexible media

In this case α is real, being positive or negative accordingly as the wave velocity c is greater or less than the velocity of free waves on the boundary (see below). We first consider a property of the transformation on the right-hand side of

(3.4) which is discovered when the values of E_r and E_i calculated by Schlichting for the Blasius profile are substituted; we refer to the plot of E_i *vs* E_r given in his book (1955, p. 328). For α real, it appears that a plot of the real and imaginary parts of our function $E_1(k, c)$ describes exactly the same lines $c = \text{const.}$ as the plot of E_i *vs* E_r. In other words, the complex value of E_1 is given everywhere as the value of E for the same c but some different value of k; thus $E_1(k, c) = E(k_0, c)$, say. This property is unexpected; but the reason for it is soon found when the nature of the approximations in Schlichting's calculation is examined, and the property is seen to be only an approximate one.

As in many existing stability calculations, Schlichting's estimate of E was essentially a first-order approximation for small k. It was equivalent to the following approximation to $u+iv$ noted by Lin (1955, p. 86):

$$u+iv = 1+U'_w c\int_0^1 \frac{dy}{(U-c)^2}+\frac{U'_w c}{k(1-c)^2}. \tag{3.6}$$

The path of integration extends from the wall to the outer edge of the boundary layer ($y = 1$ since the boundary-layer thickness is implied to be the unit of length), and is indented *under* the singularity of the integrand at $U(y_c) = c$ on the real axis of y. Hence, by use of the calculus of residues, (3.6) gives

$$u = 1+U'_w c\mathscr{P}\int_0^1 \frac{dy}{(U-c)^2}+\frac{U'_w c}{k(1-c)^2}, \tag{3.7}$$

$$v = -\pi c U''_c/U'^2_c, \tag{3.8}$$

where $\mathscr{P}$ denotes the principal value of the integral. According to this approximation, v is independent of k. It follows that if z, k_0, c is a set of values which satisfies (3.5) when $\alpha = 0$, then the equation is also satisfied, for $\alpha \neq 0$ and real, with the same z and c but with a k such that $u(k, c)+\alpha = u(k_0, c)$. That is,

$$\frac{U'_w c}{(1-c)^2}\left\{\frac{1}{k}-\frac{1}{k_0}\right\}+\alpha = 0. \tag{3.9}$$

At this point it would clearly be an advantage to redefine α without the normalizing factor $U'_w c$ introduced in (3.2), and hence cancel this factor from (3.9). As an alternative we define a 'stiffness coefficient' for the flexible medium, writing

$$\beta = -\frac{P_s}{k\alpha} = -\frac{U'_w c}{k\alpha}. \tag{3.10}$$

An important advantage of this definition is that, anticipating considerations made below regarding the possible properties of the flexible medium, we recognize that the functional dependence of β on k and c always follows the form $\{c_0^2(k)-c^2\}F(k)$; and for a non-dispersive frictionless medium (see § 4), we have always $\beta = Ak\{c_0^2-c^2\}$, where A and c_0 are constants independent of k. In terms of β, (3.9) gives immediately

$$k = k_0\left\{1-\frac{(1-c)^2}{\beta}\right\}. \tag{3.11}$$

This simple result provides us readily with a complete description of the effect of a non-dissipative flexible boundary on the stability of Tollmien–Schlichting

waves. The conclusions to be based on this result are, of course, only approximate; but they would appear to be fairly reliable since more accurate estimates of v show it to vary only very slightly with k, which is the crucial property in present respects.

To fix ideas, let us reconsider Schlichting's graph of the imaginary versus the real parts of $F(z)$ and $E(k, c)$ for the Blasius profile. It has been established just above that we can use this graph—or any similar ones for other profiles—exactly as it stands, if the lines k = const. are now interpreted as k_0 = const. Therefore, from each point of intersection of the F and E curves, we get a set of values of

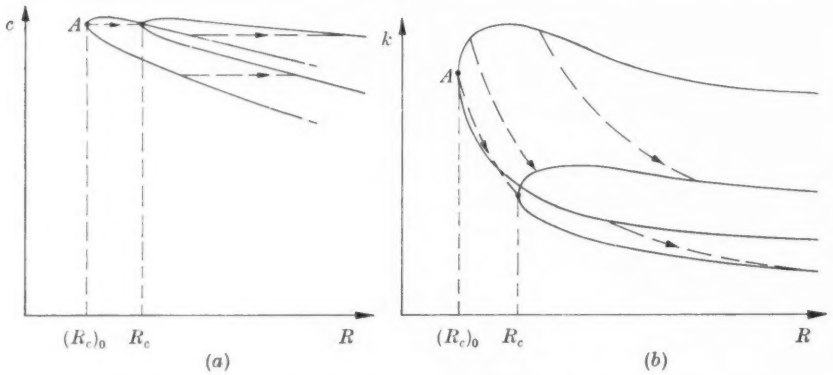

FIGURE 1. Displacements of curves of neutral stability due to a compliant non-dissipative boundary ($\alpha_r < 0$, $\alpha_i = 0$).

z, k_0, c which is the same set of values specifying neutrally stable conditions in the case of a rigid boundary. But, from the definition of z, the product kR must be the same for each given pair of values of z and c; thus kR for a flexible boundary is the same as $k_0 R_0$, where R_0 is the Reynolds number deduced from the same point of the graph in the rigid case. This means simply that the neutral curve c *vs* R will be displaced from the corresponding curve for a rigid boundary (see Schlichting 1955, p. 329) in the manner indicated in figure 1*a*: to the right if $\alpha < 0$ (i.e. $\beta > 0$) so that according to (3.11) $k_0 > k$, and to the left if $\alpha > 0$ so that $k_0 < k$. Points on the neutral curve k *vs* R will be displaced along the hyperbolae $kR = k_0 R_0$ as indicated in figure 1*b*: downward if $\alpha < 0$, and upward if $\alpha > 0$.

It is clearly possible that in a practical example $\alpha(k, c)$ changes sign within the relevant range of k and c, so that different parts of the neutral curves are displaced in opposite directions. When this possibility is examined with regard to general properties of flexible media, an important new feature of the problem appears. In fact, according to the present theory for α real, the flow is destabilized down to indefinitely small Reynolds numbers when α can change its sign at any c within the range of Tollmien–Schlichting waves, and further study shows this to be true when α changes sign at any positive $c < 1$. The reason is as follows.

Whatever the actual nature of the non-dissipative mechanical system forming a boundary to the flow, it will have the property that, in the absence of the flow,

simple-harmonic surface waves are transmitted at a certain velocity c_0—which depends on k if the system is 'dispersive'. This assertion implies no more than that the system has both inertia and stiffness. Now, to have $\alpha < 0$, which means that an applied surface pressure is in opposite phase to the wave formed on the boundary in response to it, the velocity c has to be less than c_0 for the respective k, because the stiffness of the system is then the predominant factor in determining the response (cf. the example treated in §4). If the pressure is to be in phase with the wave so that $\alpha > 0$, we must have $c > c_0$ because the inertia of the system is then the predominant factor. In fact, as has already been noted, it turns out generally that for a fixed k the effective stiffness β is proportional to $c_0^2 - c^2$. This result bears out the already fairly obvious conclusion that, if c approaches c_0, there is a resonance effect and the response of the system becomes unbounded in the limit. It follows that if equation (3.5) admits a solution with $(c - c_0) \to 0^+$ for any k, the neutral curve will have a loop extending to the region $R \to 0$.

Thus, if an effectively frictionless flexible device were to be used for stabilization, one essential requirement appears to be that its characteristic surface-wave velocity $c_0(k)$ should not be less than the greatest velocity of neutral Tollmien–Schlichting waves, which for the Blasius profile is about 0·42 times the free-stream velocity.

Consider now point A of figure 1*a* and 1*b* which gives the critical Reynolds number—i.e. the minimum value for which a neutral disturbance is possible—for a rigid boundary. Assuming that this point is transformed approximately to a corresponding extreme point on the neutral curve given by a real negative α, which is true if α does not vary too rapidly with k and c, we have

$$R_c = \frac{k_0}{k}(R_c)_0, \tag{3.12}$$

where $(R_c)_0$ is the original critical value, k_0 is the corresponding wave-number, and $k\,(< k_0)$ is the solution of

$$k = k_0\left\{1 - \frac{(1-c_1)^2}{\beta(k, c_1)}\right\}, \tag{3.13}$$

which is equation (3.11) with the velocity c_1 of the optimum Tollmien–Schlichting wave substituted. (For the Blasius profile, we have $c_1 \doteqdot 0{\cdot}41$.) By means of similar relationships, other points (k, R) on the neutral curve could be derived from the co-ordinates of the original curve. From these results it is clearly a simple matter to estimate the critical Reynolds number when $\beta(k, c)$ is specified for a particular flexible device.

According to these results, an obvious requirement for a large stabilizing effect is that β should be small for small k. Although for a non-dispersive medium (see §4), β is proportional to k, this idealized case is an unhelpful example in present respects since (3.13) has no meaningful solution; furthermore, it can be seen from the discussion of Kelvin–Helmholtz instability a few paragraphs below that if this property were specified to hold down to indefinitely small k, this second form of instability would appear to be inevitable if $c_0 < 1$, which seems unrealistic. However, for any real flexible medium the coefficient β is bound to

become large at finite wavelengths λ, since for indefinitely great length scales it is impossible to keep the ratio P_s/a decreasing as rapidly as $1/\lambda$; in fact, the practical extreme is that P_s/a tends to a constant (i.e. a uniform compressibility). In practice, therefore, β will have a certain minimum, and for effective stabilization this should evidently be made to occur at a reasonably small k, preferably rather smaller than the typical k_0 of Tollmien–Schlichting waves. We now assume this to be the case, and since the actual extent of stabilization then depends on the magnitude of the minimum rather than on the particular k, we can usefully write $\beta(k, c) = \beta_m(c)$ in the theory and ignore the variations of β with k in so far as they fix the solutions of (3.11) or (3.13).

The interpretation of (3.13) presents certain difficulties which are to be discussed below in connexion with Kelvin–Helmholtz instability, and it will appear that stabilization to indefinitely high Reynolds number, which (3.13) indicates to be a possibility, may not in fact be realizable. However, we can recognize a wide range of conditions where there is a considerable stabilizing effect on Tollmien–Schlichting waves while at the same time the possibility of other forms of instability is ruled out. For example, suppose that the minimum stiffness under static loading ($c = 0$) is $\beta_m(0) = 1$, and also $c_0 = 1^+$. Kelvin–Helmholtz instability cannot occur under these conditions (see equation (3.17) below). Since

$$\beta_m(c) = \beta_m(0)\left\{1 - \frac{c^2}{c_0^2}\right\},$$

we get from (3.13), for $c_1 = 0{\cdot}41$,

$$\frac{k}{k_0} = 1 - \frac{(0{\cdot}59)^2}{1 - (0{\cdot}41)^2} \doteqdot 0{\cdot}58.$$

Hence, according to (3.12), the critical Reynolds number is increased by approximately 72 %, which implies that the distance from the leading edge at which instability first occurs is increased by a factor $(1{\cdot}72)^2 \doteqdot 3{\cdot}0$.

It remains to consider whether other types of neutral wave are possible, such perhaps as to specify the limit of an additional mode of instability in circumstances where Tollmien-Schlichting waves are damped. The case where $c \doteqdot c_0$ has obviously not yet been properly covered; for even if c_0 is made greater than the velocity of any Tollmien–Schlichting wave, so that the apparently disastrous effect on stability described above is avoided, waves with speeds near c_0 may still be possible.

The other outstanding case is as follows.

Kelvin–Helmholtz instability

Equations (3.12) and (3.13) indicate that the optimum Tollmien–Schlichting wave would be stabilized to extremely high Reynolds number if $\beta_m(c_1) \to (1 - c_1^2)$, and similar results apply to waves with other values of c. This interpretation must be treated with caution, however, because values of β which are of the order of unity imply that the surface stiffness is of the same order of magnitude as the dynamic pressure of the free stream, and in such circumstances the Kelvin–Helmholtz type of instability (see Lamb 1932, §§232, 268) becomes an important

possibility. This mechanism of instability is largely independent of viscosity, and theoretical treatments of it (see particularly Miles 1959) generally assume an inviscid fluid; the leading result of the theory as regards the flow properties were in fact justified in the paper I as asymptotic limits at infinite Reynolds number. This does not, of course, mean that this type of instability occurs only at very large Reynolds number; to the contrary, the fact that it can happen in the absence of viscosity implies that when the physical situation is such as to be more than marginally unstable at infinite Reynolds number, the instability will still be manifested at quite low Reynolds numbers since a large viscous effect is necessary to overcome the destabilizing factor.

The present analysis is inappropriate to account directly for Kelvin–Helmholtz instability, but a slight reformulation of ideas is enough to explain it. At very large Reynolds number the pressure on a wave is very nearly of opposite phase to the surface displacement, although there remains a small component proportional to k which is in phase with the wave slope (I, §7); provided k is small enough for the latter component to be insignificant, a neutral wave is therefore possible when the negative in-phase pressure just balances the stiffness forces in the flexible medium, which tend to cancel the wave. Hence, using a result derived in I (equation (7.34)), we deduce the condition for a neutral wave to be

$$\beta(k,c) = \frac{P_s}{ka} = \int_0^\infty (U-c)^2 e^{-ky}\, d(ky). \tag{3.14}$$

If k is very small, $U = 1$ over most of the range in which $\exp(-ky)$ is significant, so that (3.14) gives very approximately

$$\beta(k,c) = (1-c)^2. \tag{3.15}$$

Thus we have an interpretation of the result indicated by (3.11) or (3.13) that a neutral wave exists at infinite Reynolds number when (3.15) is satisfied.

Considering the minimum value of β, we have

$$\beta_m(c) = \beta_m(0)\left\{1 - \frac{c^2}{c_0^2}\right\}, \tag{3.16}$$

which is a result that has already been noted, and on substitution of this into (3.15) a quadratic equation for c is obtained. Kelvin–Helmholtz instability is indicated by this equation having complex conjugate roots (cf. Lamb, §232). The instability condition is found to be

$$\beta_m(0) < 1 - c_0^2 \quad (c_0 < 1), \tag{3.17}$$

and the velocity of the wave which first becomes unstable is $c = c_0^2$.

We shall not pursue this topic further since for present purposes it seems enough to note (3.17) as a practical test for this type of instability. Nevertheless, the connexion between the present results and the asymptotic results for Tollmien–Schlichting waves is a matter of great theoretical interest, and certainly it needs further study if our general problem is to be fully resolved.

Dissipative flexible media

In this case α has a negative imaginary part which, as will be verified later, is a measure of the work that must be done by the pressure on the disturbed boundary in order to maintain a neutral wave.

For a given z, equation (3.5) shows v to be greater by an amount $-\alpha_i$ than its value in the case of a rigid boundary. But, according to the approximation (3.8), v is a function of c alone that increases with increasing c over all values relevant to Tollmien–Schlichting waves. For $\alpha_i < 0$, therefore, wave velocities are greater than the velocities of the respective neutral waves for a rigid boundary. It turns out also that the values of k have to be slightly large, for the increased values of c, in order to satisfy the real part of (3.5) for a given z.

When z is fixed, R is proportional to $k^{-1}c^{-3}$, and hence we see that a negative imaginary part of α tends strongly to shift the neutral stability curves everywhere towards lower Reynolds numbers. If $-\alpha_i$ is large enough, it may even cancel the stabilizing effect of a negative α_r. This general conclusion is confirmed when one applies the transformation (3.4) with complex α to Schlichting's results for E.

It is thus established that dissipation in the flexible medium has a *destabilizing* effect in relation to Tollmien–Schlichting waves. This result is surprising at first sight, but its physical explanation is readily forthcoming when Prandtl's and Tollmien's interpretations of the mechanism of instability—as recalled in § 2—are applied in the present context. We shall return to this matter presently.

We consider next the class of waves on the boundary whose velocity of propagation is determined mainly by the properties of the flexible medium; i.e. these are essentially 'free' waves with c very nearly equal to c_0. Unlike the cases previously considered, the essential physical factor now is that the over-all stiffness of the boundary is quite high (e.g. for static loading, $\beta(k, 0) \gg 1$), and the response to the flow depends primarily on the resonance effect at $c \doteq c_0$. Thus the Kelvin–Helmholtz type of instability is altogether ruled out, since the effect of the negative in-phase pressure will displace c only very slightly below c_0.

As regards the interpretation of (3.5) in this case, the outstanding fact is that the equation represents essentially a balance between $u + iv$ and α, owing to the fact that α_r is now extremely sensitive to the value of c. Thus the effects of viscosity as represented by the function $\mathscr{F}(z)$ ceases to have a critical influence on the conditions for a neutral wave, and to represent typical neutral conditions this function can well be ignored. (Of course, if we specified k, R and $c \doteq c_0$ to be typical of Tollmien–Schlichting waves, this function has the same sort of magnitude as previously considered; but the important thing now is that the question of whether the wave is stable or unstable under such conditions depends critically on factors other than viscosity, and so these conditions are not representative of neutral waves.) We therefore take the neutral conditions to be given typically by $u = -\alpha_r, v = -\alpha_i$, which are equivalent to

$$E_r = 1 + \left(\frac{1}{\alpha}\right)_r, \tag{3.18}$$

$$E_i = \left(\frac{1}{\alpha}\right)_i. \tag{3.19}$$

Now, although these two equations have an unfamiliar form, a little study shows that they reproduce essentially the problem treated by Miles (1957) and further investigated in I. Miles derived a theory of water-wave formation by wind on the assumptions that (i) the water-wave velocity is independent of the air flow, (ii) the conditions for a neutral wave may be decided very critically by approximate energy considerations, i.e. an expression for the energy transfer from the air flow is put equal to an expression for the rate of viscous dissipation in the water, and (iii) the effects of viscosity in the air are negligible, except in so far as they determine the phase change across the 'critical layer' at which $U = c$ (see §2). It is now seen that a similar theory would account for waves of the present sort.

The first fact to be observed from (3.18) and (3.19) is that $E = -U'_w\phi_w/c\phi'_w \doteqdot 1$ very nearly, which means simply that the boundary conditions (3.1) are satisfied by ϕ alone, i.e. there is no wall friction layer. This would be the natural starting point if the present special case were to be treated individually in a way such as Miles used. Actually the non-slipping boundary condition cannot be applied rigorously to an inviscid flow; but, as was discussed in I, this condition is satisfied automatically if one applies the modified kinematical condition introduced by Miles—i.e. $\phi \to (c-U)a$ for $y \to 0$, which means physically that streamlines close to the boundary must follow the wave contour as well as the bounding streamline itself. The fact that the latter condition is only approximate allows the small difference $(1/\alpha)$ from the result $E = 1$ which would follow if both the kinematical and non-slipping boundary conditions were applied rigorously to the inviscid solution. The essential scheme of Miles's theory is to find ϕ from the approximate boundary condition and then estimate E_i, as needed in (3.19), from properties of ϕ accumulated over the whole flow.

The term $(1/\alpha_r)$ in (3.18) is evidently of little consequence. It merely implies that the wave velocity is not quite c_0, since the in-phase negative pressure on the wave makes a slight reduction in the over-all stiffness of the system as experienced by the wave.

The crucial relation with regard to stability conditions is (3.19). This can be shown to correspond exactly to Miles's criterion that the energy supply to a neutral wave on the boundary balances the rate of energy absorption. Thus we recognize that the stability of waves of the present sort depends critically on the internal damping of the flexible medium. Instability can always be prevented by making the damping large enough, although we know that damping has a contrary effect on the mode of instability examined previously. Note that these waves can only be excited when c_0 is less than the free-stream velocity, since only then is E_i (or v) positive; i.e. a positive Reynolds stress is developed by a wave only when there is a critical point at which $U(y_c) = c \doteqdot c_0 < 1$.

As a final comment on the analysis, in particular to interpret the remarkable difference in the effects of damping noted just above, we note that the imaginary part of (3.5) is a precise representation of the energy balance maintained by a neutral wave; thus we have

$$v - |\alpha_i| - \mathscr{F}_i(z) = 0, \tag{3.20}$$

where the three terms represent the relative magnitudes of, respectively, the

rate of energy conversion from the primary flow by Reynolds stress, the work done on the boundary by the surface pressure distribution, and the rate of dissipation by viscosity. [It is fairly easy to check this result. For instance, the rate of energy conversion τc may be estimated by Tollmien's formula (2.8); and hence by use of the approximations $\phi_c = \phi_w + (c/U'_w)\,\phi'_w$ and $U'_c = U'_w$, it may be identified with the approximation (3.8) for v; again a precise identification with v may be established by taking the formula (2.7) for τ and using the boundary conditions. The second term in (3.20) is readily established from the fact that the average work done on the boundary is $-\overline{p_s \partial\eta/\partial t}$, where η is the displacement.]

For the surface waves that were studied last, the relative energy supply v is essentially fixed since c is nearly equal to c_0 which is a property of the flexible medium. Thus we see that internal damping, as represented by $|\alpha_i|$ can take over the role that viscosity would have in stabilizing a neutral wave. For the modified Tollmien–Schlichting waves, on the other hand, the over-all stiffness must be so small in order to have any effect that c is not fixed by the properties of the medium. Thus an increase in internal damping is readily accommodated by an increase in v (i.e. the flow is permitted to develop additional Reynolds stress); and from our knowledge of the structure of the wall friction layer (i.e. its dependence on the special combination of parameters in z), we see that for an increased c the Reynolds number has to be reduced in order to make the relative viscous dissipation sufficient to restore the energy balance for a neutral wave.

4. The flexible medium

It has been seen that a requirement for any useful stabilizing device is that it comprises a *dispersive* medium for the transmission of surface waves. The precise analysis of such devices is liable to be fairly complicated, and it is not proposed to consider any example here. The case of a non-dispersive medium is very straightforward, however, and the following simple treatment is included to illustrate the meaning of the response coefficient α. Two instances of non-dispersive media, i.e. media in which free waves are propagated at a velocity independent of wavelength, are (i) a flexible inextensible sheet under longitudinal tension and (ii) a deep layer of uniform elastic material, the surface waves in this case being 'Rayleigh waves' (Love 1927, §214).

Consider a small displacement $y = \eta(x,t)$ of the plane surface bounding the medium. In the absence of dissipative forces, the dynamical equation satisfied by η is the wave equation

$$T\frac{\partial^2\eta}{\partial x^2} - m\frac{\partial^2\eta}{\partial t^2} = 0. \tag{4.1}$$

Here T is a constant 'stiffness coefficient' for the surface, and m is the effective mass per unit area of the surface. In the case of a flexible sheet, T is simply the tension per unit span and m the actual mass per unit area; but these constants have corresponding, though perhaps less immediate, interpretations in all examples of the class considered. The velocity $\pm c_0$ of free waves is therefore given by

$$c_0^2 = T/m. \tag{4.2}$$

When the waves are subject to linear damping, their equation takes the modified form

$$c_0^2 \frac{\partial^2 \eta}{\partial x^2} - \frac{\partial^2 \eta}{\partial t^2} - \kappa \frac{\partial \eta}{\partial t} = 0, \tag{4.3}$$

where κ is a damping coefficient, being necessarily real and positive. (The medium is now dispersive, but only very slightly so if κ/kc_0 is small; for example, non-periodic waves are propagated with little change of form though with over-all attenuation.)

Now, (4.1) and (4.3) are in effect equations relating the normal force per unit area developed on the surface $y = 0$ to the inertial reaction of the medium exerted across this surface. And so, if an external pressure $p_s(x, t)$ is applied on this surface, the equation governing the response of the medium clearly is

$$p_s = m\left(c_0^2 \frac{\partial^2 \eta}{\partial x^2} - \frac{\partial^2 \eta}{\partial t^2} - \kappa \frac{\partial \eta}{\partial t}\right). \tag{4.4}$$

For applied pressure $p_s = \rho P_s e^{ik(x-ct)}$

producing a deflexion $\eta = a\, e^{ik(x-ct)}$,

equation (4.4) shows that

$$\rho P_s = m\{(c^2 - c_0^2)\, k^2 + i\kappa kc\}\, a. \tag{4.5}$$

Hence, for the surface compliance a/P_s, we get

$$\frac{a}{P_s} = \frac{\rho}{m}\left\{\frac{(c^2 - c_0^2)\, k^2 - i\kappa kc}{|(c^2 - c_0^2)\, k^2 + i\kappa kc|^2}\right\}, \tag{4.6}$$

and α is the dimensionless coefficient obtained on multiplying this by cU'_w. An electrical analogue of this result is the 'effective capacity' of a series LCR circuit; the pressure P_s is analogous to an applied voltage alternating at frequency kc, and the displacement a is analogous to the resulting charge on the condenser.

Two points illustrated by this result may be noted. For the real part of α to be negative, which was shown in § 3 to promote stabilization, we must have $c_0^2 > c^2$; i.e. the velocity of free waves in the medium must exceed the velocity of the relevant flow disturbances. This criterion for a negative α_r in fact applies generally, whether or not c_0 depends on k, and its physical basis is obvious. (It is perhaps already perfectly clear from the analogy noted above.) Consider the wave which travels over the surface of the medium in response to a simple-harmonic pressure distribution with a certain k and c. If $c^2 < c_0^2$, the frequency $|kc|$ of the forced vibrations at a fixed point of the surface is less than the frequency $|kc_0|$ at which an undamped free simple-harmonic motion can occur, and at which therefore the inertial forces generated in the motion exactly balance the restoring forces due to the stiffness of the medium. Thus, the stiffness forces will predominate when $c^2 < c_0^2$, so that the surface will respond to the applied pressure in the same direction as it would to a static load. Equation (4.6) also confirms that for positive c the imaginary part of α is negative when the medium is dissipative, i.e. when energy is absorbed from the agency responsible for the moving pressure distribution.

5. Conclusion

The theoretical results derived in §3 serve at least to point out the essential factors in the operation of a flexible boundary as a stabilizing device, and so they may be useful as a guide for further experimental development of Krämer's idea (1960*a*, *b*). It must be emphasized, however, that the present theory only concerns stability with respect to very small disturbances to which the principle of linear superposition can be applied. Nothing has been learnt about the influence of a flexible boundary on flow disturbances which are not small, although in relation to the practical problem this matter may be just as important as the one studied here. That is to say, it remains in question whether a flexible boundary might inhibit the development of the concentrated turbulent spots which are often the first manifestation of instability in laminar boundary layers when the flow has a high level of 'background' turbulence.

The stability analysis dealt only with long-crested waves travelling in the direction of flow, yet 'three-dimensional' waves travelling obliquely to the flow are obviously a physical possibility. For parallel flows with rigid boundaries, it is well known that consideration of two-dimensional waves is sufficient to solve the stability problem since Squire's theorem (Lin 1955, §3.1) shows these waves to have the greatest tendency to instability. The same theorem applies to our problem also, though the conclusions to be drawn from it are not quite as definite as in the previous case. If the response of the boundary is assumed to be independent of the wave direction, as it well might be in practice, then the stability problem for an oblique wave is the same as that for a wave in the flow direction at a lower flow velocity; this follows from the fact that an oblique wave depends on the primary flow only in respect of its component in the direction of propagation of the wave. As regards the modified Tollmien–Schlichting waves and the Kelvin–Helmholtz waves which have been considered, the present two-dimensional theory would appear therefore to account adequately for the practical stability conditions. This may not always be so, however, as regards surface waves whose velocity in any direction of approximation is approximately c_0, for a situation is conceivable in which a reduction in the effective free-stream velocity (i.e. by taking the resolved component in an oblique direction) would tend to destabilize such waves by putting the critical point in a more favourable part of the velocity profile. Nevertheless, this possibility does appear rather exceptional, and though we need to make some slight reservation on its account we can fairly confidently propose that the two-dimensional theory essentially covers the practical problem.

Our conclusions regarding the two main classes of waves—i.e. modified Tollmien–Schlichting waves, say Class A, and surface waves, say Class B—suggest two possible approaches to the design of practical measures for boundary-layer stabilization. The first is to specify the flexible medium with a fairly high over-all stiffness but such that, at values of k for the 'most dangerous' Tollmien–Schlichting waves, the velocity $c_0(k)$ coincides with the Tollmien-Schlichting wave velocity. Hence the response of the boundary will have a totally disruptive effect on the Tollmien-Schlichting mechanism of instability, the wall friction

layer being effectively removed. In other words, Class A is turned into Class B, and the role of stabilization is taken over wholly by the internal damping of the flexible medium. The damping should be just large enough to prevent Class B waves from developing, and its amount is liable to be fairly critical; too much inhibits Class B instability yet tends to 'let in' Class A again, and might even result in an over-all destabilization because of its effect on Class A waves at velocities somewhat different from c_0; on the other hand, too little damping would have the disastrous effect of allowing the excitation of Class B waves, which would happen at Reynolds numbers less than the critical value for a rigid boundary since the damping action of viscosity is largely cancelled for Class B waves. It is probably important that $c_0(k)$ should be made nearly equal to—or perhaps just slightly greater than—the Tollmien–Schlichting wave velocity near the minimum of R on the neutral-stability curve for a rigid wall (e.g. for Blasius flow, $c = 0{\cdot}41U_0$ for $k = 0{\cdot}34/\delta^*$); this seems the first step to insure that the critical Reynolds number is raised to some extent by the present means. At higher Reynolds numbers the value of c and k for the Tollmien–Schlichting wave of greatest amplification steadily decrease, c being very roughly proportional to k, and it would seem that this relationship between c and k should be followed as closely and as far as possible in order to obtain maximum stabilization. If the stabilizing device were a layer of uniform visco-elastic solid material, for example, its thickness would have to be considerably less than a wavelength for c to vary with k as much as is required. A practical possibility is that such a layer might be 'tuned' to the Tollmien–Schlichting waves over a considerable range of Reynolds number (i.e. over a considerable length of the boundary layer) by varying its thickness.

The present method of design seems at first sight somewhat unpromising since its success apparently depends rather critically on the choice of properties for the flexible medium, and it may be expected to serve only for a very limited range of the free-stream velocity. However, the success of Krämer's experiments appears to be attributable to the particular mechanism of stabilization described here, and indeed a rough version of the general specifications explained above was established empirically by him. For instance, the flexible coatings used in his experiments were designed in such a way that our $c_0(k)$ would match the Tollmien–Schlichting wave velocity at the average Reynolds number of the coated area [in his paper (1960*b*) he tentatively assumes the boundary-layer waves to be equivalent in their effect on the boundary to standing pressure waves, and he specifies that the product $F\lambda$, where F is the frequency of resonance of the coating for a wavelength λ, should equal the representative velocity of the boundary-layer waves; the wavelength cancels from his design formula because his assumptions regarding the properties of the coating make it in effect non-dispersive]. His experimental results also showed that there is an optimum amount of damping in relation to stabilizing effect.

As the second possible method, the flexible medium might be designed with fairly low over-all stiffness but such that c_0 is large enough to avoid the possibility of Class B instability entirely. Stabilization of Class A waves is then effected by the compliant response of the boundary, i.e. as the result of a negative real α.

As the essential physical mechanism of stabilization in this case, the wall friction layer is modified so as to render Class A waves incapable of developing sufficient Reynolds stress to overcome viscous dissipation; in other words, there is a cancellation of the destabilizing effect of viscosity for which Prandtl's explanation was recalled in §2. If this method is used, an important requirement is that damping in the medium should be small, because it has been seen in §3 that damping provides an alternative means for the development of Reynolds stress by Class A waves and is therefore a destabilizing factor.

Roughly speaking, this second method requires an elastic medium which is both soft (to have a large response to surface pressures) and also light (to keep c_0 fairly high despite the first property), and which at the same time suffers little internal friction. The stiffness of the boundary may possibly need to be kept above a certain margin, however, so that the Kelvin–Helmholtz type of instability is avoided, and this factor may limit the ultimate scope of the method; this point deserves further study.

To obtain a useful stabilizing effect by the second method, it seems likely that the elastic constants of the medium (rigidity modulus, etc.) would have to be of about the same order of magnitude as the dynamic pressure $\frac{1}{2}\rho U_0^2$ of the free stream, and so the method might prove impracticable for low-speed applications because effective materials would be too fragile (though, of course, sufficiently enlarged clear compliances might possibly be obtained by use of cellular structures like Krämer's device). On the other hand, there may well be suitable materials for use at high speeds, and it is such applications that appear to offer the most exciting possibilities for this new means of boundary-layer stabilization.

REFERENCES

Brooke Benjamin, T. 1959 Shearing flow over a wavy boundary. *J. Fluid Mech.* **6**, 161.

Holstein, H. 1950 Über die äussere und innere Reibungsschicht bei Störungen laminar Strömungen. *Z. angew. Math. Mech.* **30**, 25.

Krämer, M. O. 1960*a* *Reader's Forum, J. Aero/Space Sci.* **27**, 68.

Krämer, M. O. 1960*b* Boundary layer stabilization by distributed damping. *J. Amer. Soc. Nav. Engrs*, **72**, 25.

Lamb, H. 1932 *Hydrodynamics*, 6th ed. Cambridge University Press.

Lin, C. C. 1945 On the stability of two-dimensional parallel flows, Parts I, II and III. *Quart. Appl. Math.* **3**, 117, 218, 277.

Lin, C. C. 1955 *The Theory of Hydrodynamic Stability.* Cambridge University Press.

Lock, R. C. 1954 Hydrodynamic stability of the flow in the laminar boundary layer between parallel streams. *Proc. Camb. Phil. Soc.* **50**, 105.

Love, A. E. H. 1927 *The Mathematical Theory of Elasticity*, 4th ed. Cambridge University Press.

Miles, J. W. 1957 On the generation of surface waves by shear flows. *J. Fluid Mech.* **3**, 185.

Miles, J. W. 1959 On the generation of surface waves by shear flow. Part 3. Kelvin–Helmholtz instability. *J. Fluid Mech.* **6**, 583.

Prandtl, L. 1935 *The Mechanics of Viscous Fluids.* Article in *Aerodynamic Theory* (ed. W. F. Durand), Vol. **3**. Berlin: Springer.

Schlichting, H. 1955 *Boundary Layer Theory.* London: Pergamon.

Shen, S. F. 1954 Calculated amplified oscillations in plane Poiseuille and Blasius flows. *J. Aero. Sci.* **21**, 62.

Kinematic formulation of rotational gas flow

By M. VINOKUR

Lockheed Aircraft Corporation, Missiles and Space Division, Sunnyvale, California

(Received 12 May 1960)

It is shown that for the steady isoenergetic rotational flow of an ideal gas, both the specific enthalpy and the speed of sound can be expressed as functions of the velocity. As a result, it is possible to formulate the equations of motion so that the velocity is the only dependent variable. For a gas whose enthalpy and sound speed are functionally related, the results are a generalization of those for a perfect gas. If the enthalpy and sound speed are independent variables, the new formulation leads to a single vector equation whose solution completely determines the flow.

1. Introduction

The steady flow of an ideal gas is governed by equations expressing the conservation of mass, momentum, and energy, supplemented by an appropriate equation of state. The dependent variables that are introduced can be classed into two groups. One consists of the kinematic variables, which are the components of the vector velocity. The other group contains the thermodynamic variables such as the pressure, density, entropy, etc. If the flow is irrotational, all these variables are expressible in terms of one new variable, the velocity potential. The problem is then reduced to the study of a single non-linear partial differential equation in one unknown. This reduction is in general not possible for a rotational flow. In that case, one may still be able to eliminate the thermodynamic variables, so that the equations contain only the vector velocity as an unknown. Such equations will be said to constitute the kinematic formulation of the flow. Although this new formulation may not make it easier to solve a given problem, it can be used to study flows by means of inverse methods.

The kinematic formulation of rotational flow was first obtained by Crocco (1937) for the special case of isoenergetic flow of a perfect gas in the absence of external forces. The results were extended by Prim (1952) to non-isoenergetic (but still adiabatic) flows of a more general gas obeying the power-law equation of state

$$\rho = p^k S(s), \tag{1.1}$$

where ρ, p, and s are the density, pressure, and specific entropy. $S(s)$ is an arbitrary function of s and k is a constant. Prim also showed that all the thermodynamic variables except the pressure can be eliminated for an even more general gas obeying the product equation of state

$$\rho = P(p)\,S(s), \tag{1.2}$$

where $P(p)$ is an arbitrary function of p. These results have also been extended to diabatic flows (Gustafson & Krzywoblocki 1957).

For any real gas, there are temperature ranges in which internal modes of energy are excited. As long as the excitation process is fast enough to maintain local thermodynamic equilibrium in the flow, the gas can still be treated as an ideal gas, but with a more involved equation of state. For example, the excitation of rotational and vibrational modes of a polyatomic gas (without dissociation) can be represented by the equation of state of a thermally perfect gas. (This is a gas that still obeys the law $p = \rho RT$ with R constant, but whose specific heats are functions of temperature.) A gas that is partially dissociated or ionized will in general have no simple equation of state. All the work on the kinematic formulation of rotational flow referred to above does not apply to any of these cases; even the thermally perfect gas law satisfies neither (1.1) nor (1.2). The question naturally arises as to whether a kinematic formulation can be constructed to include these cases. Current interest in this question is motivated by the prevalence of very high speed flows that give rise to high temperatures in strongly rotational stagnation regions.

The purpose of this paper is to show that at least for isoenergetic flows the question can be answered affirmatively. A surprising result of the investigation is that the flow of a gas obeying a perfectly arbitrary equation of state (such as a partially dissociated or ionized gas) possesses certain simple properties that are not present in a perfect or thermally perfect gas. Although external forces are neglected in the analysis, the results can easily be generalized to include them. In order to introduce the ideas in a simple manner, the case of incompressible flow will be discussed first.

2. Kinematic formulation of incompressible flow

The equations governing an incompressible flow are

$$\operatorname{div} \mathbf{V} = 0, \tag{2.1}$$

$$-(1/\rho)\operatorname{grad} p = \mathbf{V}.\operatorname{grad}\mathbf{V} = \operatorname{curl}\mathbf{V}\times\mathbf{V} + \tfrac{1}{2}\operatorname{grad}\mathbf{V}^2, \tag{2.2}$$

where $\mathbf{V}$ is the vector velocity. From (2.2) it follows that

$$\mathbf{V}.\operatorname{grad}(p + \tfrac{1}{2}\rho\mathbf{V}^2) = 0. \tag{2.3}$$

If all the streamlines pass through a region where $p + \frac{1}{2}\rho\mathbf{V}^2$ is constant (such as uniform flow), it follows from (2.3) that

$$p + \tfrac{1}{2}\rho\mathbf{V}^2 = p_0, \tag{2.4}$$

where p_0 is the stagnation pressure, which is a constant for the whole flow. If the gradient of (2.4) is substituted into (2.2), one obtains†

$$\operatorname{curl}\mathbf{V} = 0, \tag{2.5}$$

i.e. the flow is irrotational. Equations (2.1) and (2.5) constitute the kinematic formulation of an irrotational incompressible flow. By introducing a velocity

† Equations (2.5) and (3.8) should actually be replaced by the less stringent condition for a Beltrami flow, namely $\mathbf{V}\times\operatorname{curl}\mathbf{V} = 0$. This does not affect the argument for a kinematic formulation. In most problems of interest, such as planar or axisymmetric flow, a Beltrami flow is also irrotational.

potential, determination of the velocity field is reduced to the solution of Laplace's equation. Once the velocity is known, the pressure is immediately obtained from (2.4).

In the general case where (2.4) and (2.5) do not hold, the pressure can still be eliminated by taking the curl of (2.2), resulting in

$$\operatorname{curl}(\mathbf{V} \times \operatorname{curl} \mathbf{V}) = 0. \tag{2.6}$$

Equations (2.1) and (2.6) constitute the kinematic formulation of a rotational incompressible flow. Equation (2.6) can be considered a compatibility relation which picks out those solutions of the continuity equation that are also dynamically possible. Once the velocity field is determined, the pressure can be obtained by integration from (2.2).

In comparing the formulations of rotational and irrotational flows, one notes that the former is more involved in two respects. The equations describing the velocity field are of higher order, and also non-linear. In addition, determination of the pressure requires an integration, instead of a simple arithmetical operation.

3. Kinematic formulation of compressible flow

3.1. *Irrotational flow*

The equations governing a compressible adiabatic flow are

$$\operatorname{div}(\rho \mathbf{V}) = 0, \tag{3.1}$$

$$-(1/\rho)\operatorname{grad} p = \mathbf{V}.\operatorname{grad}\mathbf{V} = \operatorname{curl}\mathbf{V} \times \mathbf{V} + \tfrac{1}{2}\operatorname{grad}\mathbf{V}^2, \tag{3.2}$$

$$\mathbf{V}.\operatorname{grad} s = 0. \tag{3.3}$$

Using the thermodynamic relation

$$\rho = \left(\frac{\partial p}{\partial h}\right)_s, \tag{3.4}$$

where h is the specific enthalpy, (3.2) and (3.3) can be combined to yield

$$\mathbf{V}.\operatorname{grad}(h + \tfrac{1}{2}\mathbf{V}^2) = 0. \tag{3.5}$$

In the following analysis, it will be assumed that all the streamlines pass through a region where both s and $h + \frac{1}{2}\mathbf{V}^2$ are constant (such as uniform flow). If the fact that the quantity $h + \frac{1}{2}\mathbf{V}^2$ is unchanged at a shock discontinuity is used, it follows from (3.5) that

$$h + \tfrac{1}{2}\mathbf{V}^2 = h_0, \tag{3.6}$$

where h_0 is the stagnation enthalpy, which is a constant for the whole flow. Equation (3.6) is the condition for an isoenergetic flow.

In the absence of shock waves, (3.3) leads to the additional condition

$$s = s_0, \tag{3.7}$$

i.e. the flow is isentropic. When (3.2), (3.4), and (3.6) are used, it immediately follows that

$$\operatorname{curl}\mathbf{V} = 0. \tag{3.8}$$

Therefore an isentropic isoenergetic flow is also irrotational. In order to complete the kinematic formulation of such a flow, it is necessary to eliminate the density

from the continuity equation. Since the entropy is given, the density and pressure can be expressed as functions of the enthalpy for a given gas. In other words, the functions

$$\rho = g_1(h; s_0), \tag{3.9}$$

and

$$p = g_2(h; s_0) \tag{3.10}$$

are known once the entropy and gas are specified. Substitution of (3.6) and (3.9) into (3.1) yields

$$\operatorname{div}\left[g_1(h_0 - \tfrac{1}{2}\mathbf{V}^2; s_0)\,\mathbf{V}\right] = 0. \tag{3.11}$$

Equations (3.8) and (3.11) constitute the kinematic formulation of the irrotational flow of an arbitrary gas. The introduction of a velocity potential results in a non-linear partial differential equation in one unknown. With the velocity determined, the pressure is then obtained from (3.10).

3.2. *General considerations for rotational flow*

It was seen above that the kinematic formulation of a compressible irrotational flow differs from the incompressible case only in that one of the equations is non-linear. The essential feature that the problem can be solved completely using a kinematic description has been preserved. In each case, the knowledge of the velocity field is all that is required, since the thermodynamic variables are then found by simple substitution.

If one now turns to the general case where (3.7) and (3.8) do not hold, one finds the situation more complicated. Equation (3.6) expresses the enthalpy as a function of the velocity, but the variables one must eliminate from (3.1) and (3.2) are the density and the pressure. The elimination of the pressure by taking the curl of the momentum equation as it stands is not possible. It would therefore be desirable to relate some other thermodynamic variable to the velocity.

Fortunately, such a relationship does exist. Equation (3.1) can be written

$$\mathbf{V}.\operatorname{grad}\rho = -\rho \operatorname{div}\mathbf{V}, \tag{3.12}$$

while from (3.2) it follows that

$$\mathbf{V}.\operatorname{grad}p = -\tfrac{1}{2}\rho\,\mathbf{V}.\operatorname{grad}\mathbf{V}^2. \tag{3.13}$$

Using (3.3), one then obtains

$$\left(\frac{\partial p}{\partial \rho}\right)_s = \frac{\mathbf{V}.\operatorname{grad}\mathbf{V}^2}{2\operatorname{div}\mathbf{V}}. \tag{3.14}$$

Here $(\partial p/\partial \rho)_s$ is, of course, equal to the square of the speed of sound in the gas. The significant results for the steady, compressible adiabatic flow of an ideal gas may therefore be summarized as follows.

A knowledge of the kinematics of the flow (i.e. the velocity field) also determines the speed of sound at every point. If the flow is isoenergetic, it also determines the specific enthalpy at every point.

The second result is well known, since it follows immediately from the definition of isoenergetic flow. However, the first result, which comes from (3.14), has not been fully appreciated. It is this equation that actually provides the key for the kinematic formulation of the flow of an arbitrary gas. In order to proceed further, one must distinguish between two types of gas laws—one in which h and $(\partial p/\partial \rho)_s$ are functionally dependent, and the other in which they are independent

variables. Each will lead to a different kinematic formulation. Of course, there exist flows in which both cases are found in different regions of the flow. In such an event, a different formulation must be used in the two regions. These two cases will be examined in the following sections.

3.3 *Rotational flow:* $(\partial p/\partial \rho)_s = f(h)$

In this section, it will be assumed that the speed of sound is functionally related to the specific enthalpy; i.e.

$$\left(\frac{\partial p}{\partial \rho}\right)_s = f(h). \tag{3.15}$$

With the aid of (3.4) it can be easily shown that the density must satisfy the relation

$$\rho = H(h)\,S(s), \tag{3.16}$$

where

$$H(h) = \exp\left[\int \frac{dh}{f(h)}\right]. \tag{3.17}$$

When (3.3), (3.6) and (3.16) are used, (3.1) may be rewritten as

$$\operatorname{div}\left[H(h_0 - \tfrac{1}{2}\mathbf{V}^2)\,\mathbf{V}\right] = 0. \tag{3.18}$$

The pressure law is obtained by integrating (3.4), using (3.16). Its general form is

$$p = A(h)\,S(s) + c(s), \tag{3.19}$$

where

$$A(h) = \int H(h)\,dh, \tag{3.20}$$

and $c(s)$ is an arbitrary function of s which is not proportional to $S(s)$. In order to determine $c(s)$, one can use the boundary condition that

$$p(\rho = 0) = 0. \tag{3.21}$$

This relation follows from the first and second laws of thermodynamics, written in the form

$$T\,ds = dh - \frac{1}{\rho}\,dp, \tag{3.22}$$

where T is the absolute temperature. As long as T remains bounded when $\rho \to 0$, (3.22) requires that $dp \to 0$ also. Therefore $p = \text{const.}$ when $\rho = 0$, and since in this formulation, the pressure is defined only within an additive constant, the constant may be chosen equal to zero. An alternative proof depends on the relation between the specific enthalpy and the specific internal energy u, namely

$$h = u + p/\rho. \tag{3.23}$$

Equation (3.21) then follows immediately if one imposes the condition that the enthalpy and internal energy remain bounded as $\rho \to 0$.

If the range of validity of (3.15) includes the value of $h = a$ for which $H(a) = 0$, it follows from (3.16), (3.19), and (3.21) that $c(s) = 0$ and $A(a) = 0$. On the other hand, if (3.15) does not hold for $h = a$, then the laws of thermodynamics alone cannot determine $c(s)$. In order to eliminate the pressure from the momentum equation, it will be necessary to set

$$c(s) = 0. \tag{3.24}$$

Thus, if (3.15) is not valid at $h = a$, then (3.24) must be considered an additional assumption for the gas law.

Equations (3.16), (3.19), and (3.24) can be combined to yield

$$\rho = pB(h), \tag{3.25}$$

where

$$B(h) = \frac{H(h)}{A(h)} = \frac{\exp\left[\int \frac{dh}{f(h)}\right]}{\int \exp\left[\int \frac{dh}{f(h)}\right] dh}. \tag{3.26}$$

Substitution of (3.6) and (3.25) into (3.2) results in

$$B(h_0 - \tfrac{1}{2}\mathbf{V}^2)\,\mathbf{V}.\,\mathrm{grad}\,\mathbf{V} + \mathrm{grad}\,(\ln p) = 0. \tag{3.27}$$

The curl of (3.27) then gives the final form

$$\mathrm{curl}\,[B(h_0 - \tfrac{1}{2}\mathbf{V}^2)\,\mathbf{V} \times \mathrm{curl}\,\mathbf{V}] = 0. \tag{3.28}$$

Equations (3.18) and (3.28) constitute the kinematic formulation of the rotational flow of a gas that obeys (3.15) (and is also subject to condition (3.24), if necessary). If $\mathbf{V}^2 \ll 2h_0$, the equations reduce to (2.1) and (2.6), which are the corresponding expressions for an incompressible flow. It is seen that the compressible formulation differs chiefly in that the continuity equation is now also non-linear. With the velocity known, the pressure is obtained by integrating (3.27). The enthalpy, density, and entropy are then found by substitution from (3.6), (3.25), and (3.16). The temperature can be evaluated by using the following formula, derived from (3.19), (3.22), and (3.24):

$$p = -\rho T S(s)/S'(s). \tag{3.29}$$

A special case of interest is the thermally perfect gas law, $p = \rho RT$. From (3.25) and (3.29), it follows that

$$S(s) = \exp(-s/R); \quad B(h) = \frac{1}{RT}. \tag{3.30}$$

If the gas is also calorically perfect, it can be readily shown that

$$f(h) = (\gamma - 1)\,h, \tag{3.31}$$

where γ is the ratio of specific heats. Equations (3.18), (3.27), and (3.28) then become

$$\mathrm{div}\,[(h_0 - \tfrac{1}{2}\mathbf{V}^2)^{1/(\gamma-1)}\,\mathbf{V}] = 0, \tag{3.32}$$

$$\mathbf{V}.\,\mathrm{grad}\,\mathbf{V} + \frac{\gamma - 1}{\gamma}\,(h_0 - \tfrac{1}{2}\mathbf{V}^2)\,\mathrm{grad}\,(\ln p) = 0, \tag{3.33}$$

$$\mathrm{curl}\left[\frac{\mathbf{V} \times \mathrm{curl}\,\mathbf{V}}{(h_0 - \frac{1}{2}\mathbf{V}^2)}\right] = 0. \tag{3.34}$$

This set of equations for a perfect gas was first derived by Crocco (1937).

3.4. *Rotational flow: $(\partial p/\partial \rho)_s$ and h are independent variables*

The flow of a gas whose sound speed and enthalpy are independent variables will now be considered. Once such a gas is specified, the density and pressure are in principle known functions of these two variables; i.e.

$$\rho = F_1\left[h, \left(\frac{\partial p}{\partial \rho}\right)_s\right], \tag{3.35}$$

$$p = F_2\left[h, \left(\frac{\partial p}{\partial \rho}\right)_s\right]. \tag{3.36}$$

If (3.6), (3.14), (3.35), and (3.36) are substituted into (3.2), one obtains

$$F_1\left[(h_0-\tfrac{1}{2}\mathbf{V}^2), \frac{\mathbf{V}\cdot\operatorname{grad}\mathbf{V}^2}{2\operatorname{div}\mathbf{V}}\right]\mathbf{V}\cdot\operatorname{grad}\mathbf{V}+\operatorname{grad}F_2\left[(h_0-\tfrac{1}{2}\mathbf{V}^2), \frac{\mathbf{V}\cdot\operatorname{grad}\mathbf{V}^2}{2\operatorname{div}\mathbf{V}}\right]=0. \tag{3.37}$$

Equation (3.37) represents the kinematic formulation of the rotational flow of a gas whose sound speed and enthalpy are independent variables. Since (3.14), which is a combination of the continuity and momentum equations, was used in deriving (3.37), no additional equation is required. A velocity field which is a solution of (3.37) satisfies all the conservation laws governing the flow. The thermodynamic state of the gas is then obtained directly from (3.6), (3.14), (3.35), and (3.36). It is important to note that no additional problem needs to be solved to determine the dynamical variables. This is in contrast with the situation that exists not only for the flow of a gas in which $(\partial p/\partial\rho)_s = f(h)$, but even for an incompressible flow. In both these cases, the velocity field given by the kinematic equations does not automatically determine the dynamical variables, but a further vectorial integration is required. In this respect, the rotational flow of a perfectly arbitrary gas possesses a simplicity which is not present in a more specialized fluid. This is due to the fact that the kinematics of the flow brings with it knowledge concerning two thermodynamic variables. For a general gas, the knowledge is sufficient to determine the complete dynamics of the problem. But a gas that in this sense is degenerate already possesses some of this knowledge and therefore does not extract from the kinematics all the information that it needs. Consequently, the kinematic formulation of the flow of such a gas requires one more equation, and the determination of the dynamics requires an additional integration. Inasmuch as it completely uncouples the kinematics and the dynamics, the rotational flow of an arbitrary gas may even be said to resemble an irrotational flow.

For any given gas, (3.37) can be specialized further, since the functions F_1 and F_2 are not independent. They can be indirectly related through the equation

$$\left(\frac{\partial p}{\partial\rho}\right)_s^{-1} = \frac{1}{\rho}\left(\frac{\partial\rho}{\partial h}\right)_p + \left(\frac{\partial\rho}{\partial p}\right)_h, \tag{3.38}$$

which follows directly from (3.4). To illustrate, two simple types of gas laws will be considered. The first is

$$\rho = bp + G(h), \tag{3.39}$$

where b is a constant and $G(h)$ is an arbitrary function of h. Substituting (3.39) into (3.38), and solving for p, one obtains the expression for F_2:

$$F_2\left[h, \left(\frac{\partial p}{\partial\rho}\right)_s\right] = -\frac{1}{b}\left[\frac{G'(h)}{b-\left(\dfrac{\partial p}{\partial\rho}\right)_s^{-1}} + G(h)\right], \tag{3.40}$$

while F_1 becomes

$$F_1\left[h, \left(\frac{\partial p}{\partial\rho}\right)_s\right] = bF_2\left[h, \left(\frac{\partial p}{\partial\rho}\right)_s\right] + G(h) = \frac{-G'(h)}{b-\left(\dfrac{\partial p}{\partial\rho}\right)_s^{-1}}. \tag{3.41}$$

As a second example, let $w(p)$ be a function whose inverse can be written explicitly. Define

$$W(p) = \int w(p)\,dp. \tag{3.42}$$

Then if

$$\rho = \frac{W(p)}{G(h)}, \tag{3.43}$$

it follows from (3.38) that

$$w(p) = \frac{G(h)}{\left(\frac{\partial p}{\partial \rho}\right)_s} + G'(h), \tag{3.44}$$

and consequently

$$F_2\left[h, \left(\frac{\partial p}{\partial \rho}\right)_s\right] = w^{-1}\left[\frac{G(h)}{\left(\frac{\partial p}{\partial \rho}\right)_s} + G'(h)\right], \tag{3.45}$$

while

$$F_1\left[h, \left(\frac{\partial p}{\partial \rho}\right)_s\right] = \frac{W(F_2)}{G(h)}. \tag{3.46}$$

A special case of (3.43) is the relation

$$h = h_1 + \nu \frac{p}{\rho^n}, \tag{3.47}$$

where h_1, ν and n are constants. Equation (3.47) has been suggested (Wohlwill 1957) as giving a good approximation to the equation of state of partially dissociated air in the subsonic region behind a detached shock wave. If (1.2) is integrated using (3.4) (and the arbitrary function of s that is introduced is set equal to zero), one obtains

$$\rho h = P(p) \int \frac{dp}{P(p)}. \tag{3.48}$$

Thus, (1.2) is also seen to be a special case of (3.43).

4. Discussion of results

The main results of this investigation are embodied in (3.18), (3.28), and (3.37). Taken together, these equations give a kinematic representation of the rotational flow of any gas (except one obeying (3.19) with $c(s) \equiv 0$). The complete formulation of a flow problem requires the specification of boundary conditions. These pose no difficulty since they can also be expressed kinematically, as is shown below.

It has been implicitly assumed in this analysis that the stagnation enthalpy h_0 is a known quantity. This is certainly the case if one of the conditions of the problem is uniform flow at infinity. At any rate, the specification of h_0 is one of the boundary conditions. There are two types of boundary conditions involving geometric surfaces. One is a solid boundary, at which the normal component of velocity must be zero. The other is a surface of discontinuity, such as a shock wave. Here the tangential momentum equation leads to the condition that there is no jump in tangential velocity. The continuity and normal momentum equations combined lead to a relation involving the normal velocity and the quantity

p/ρ on each side of the shock wave. But from (3.6), (3.14), (3.25), (3.35), and (3.36), it follows that no matter which type of gas exists on either side, p/ρ can be expressed as a function of the velocity. Therefore, the shock boundary conditions can also be expressed in kinematic form.

A few remarks should be made concerning the application of the two types of gas laws to an actual gas. At pressures normally encountered in flow problems, any gas is well approximated by an at least thermally perfect gas law up to the temperatures where dissociation or ionization become non-negligible. The formulation of §3.3 applies in this case. Another region of applicability is for a polyatomic gas which dissociates completely before it starts to ionize. In this temperature region, such a gas becomes monatomic and again behaves like a perfect gas. Both are examples of gases that obey (3.15) and also (3.24). On the basis of the behaviour of known gases, it seems doubtful that (3.15) can hold without at the same time (3.24) being true.

The general gas law described in §3.4 should apply to all other gases. This includes a gas at such high pressures that cohesive forces and the finite volume of molecules force departures from the perfect gas law. A wider range of applicability is for a gas that is partially dissociated or ionized. A difficulty in practice is that explicit forms of (3.35), and (3.36) will usually not exist. For limited regions of the flow, special forms of the gas law such as (3.39) or (3.43) which do give rise to explicit expressions for F_1 and F_2 may be found useful.

It might be instructive as an illustration to consider the uniform flow of a polyatomic gas past a blunt-nosed body over a wide range of speeds. At very low speeds, the flow is incompressible and irrotational and is governed by equations (2.2) and (2.5). The problem is linear, and the kinematics and dynamics are completely uncoupled. As the speed increases, and compressibility can no longer be neglected, (2.2) has to be replaced by (3.11). This introduces a non-linearity, but the dynamics and kinematics are still uncoupled. As the critical Mach number is exceeded, shocks begin to form, and behind them the flow becomes rotational. When the uniform flow becomes supersonic, a detached shock wave forms ahead of the body, and the entire flow between the body and the shock wave is rotational. The gas initially will behave like a perfect gas, and will be described by (3.32) and (3.34). Not only have both equations become non-linear, but the integration of (3.33) is now required to determine the pressure, once the velocity is known. At still higher speeds the temperature in the nose region becomes high enough to excite vibration. The gas departs from a perfect gas, and the more general (3.18) and (3.28) must be used. As the uniform flow becomes hypersonic the gas in the nose region starts to dissociate. The flow is now described completely by (3.37), and the dynamics and kinematics are uncoupled again. If the gas dissociates completely before it begins to ionize, increasing the velocity even further will result in a flow near the nose that is again described by (3.32) and (3.34).

The above example shows that the various types of rotational gas flows considered in this paper can easily occur in practice. There is a question whether the kinematic formulation of such flows can actually be useful in their solution. To answer this, one must first consider simpler problems. These include the

simplification of the equations for two-dimensional (planar or axisymmetric) flows, and the search for solutions that have simple kinematic properties by using inverse methods. Much of this work has already been done for the case of a perfect gas law (Prim 1952). The extension of some of these results to the more general types of gas laws considered here will be reported in a future publication.

REFERENCES

Crocco, L. 1937 Eine neue Stromfunction für die Erforschung der Bewegung der Gase mit Rotation. *Z. angew. Math. Mech.* **17**, 1–7.

Gustafson, W. A. & v. Krzywoblocki, M. Z. 1957 On multiplicity theorems and an exact solution in diabatic flow. *Acta Phys. Austriaca* **11**, 131–46, 294–320.

Prim, R. C. 3rd 1952 Steady rotational flow of ideal gases. *J. Rat. Mech. Anal.* **1**, 425–97.

Wohlwill, H. E. 1957 The stream function equation for a high-temperature gas in axisymmetric rotational flow. *Space Technology Laboratories, Inc., Rep. no.* GM-TN-0165-00100.

The flow due to a two-dimensional jet issuing parallel to a flat plate

By R. A. SAWYER

Engineering Department, Cambridge University

(Received 17 May 1960)

An experiment has been performed to determine the cavity pressure and cavity length for the flow under a curved two-dimensional turbulent jet discharging parallel to a flat plate at some distance from the surface. The measurements agree quite closely with the predictions of a simple analysis of the flow when a value is assigned to the spread parameter for the curved jet which is somewhat different from that for the plane jet.

Detailed pressure and velocity measurements show that the rate of growth of the curved jet is in fact closely similar to that of the plane jet. This suggests that the adjustment of the spread parameter should be regarded simply as a convenient device for taking into account the quantitative errors of the assumptions made in the analysis.

1. Introduction

This work was undertaken to give some experimental backing to a simple model proposed by Dodds (1960) for the flow resulting from a two-dimensional jet issuing parallel to a flat plate. Recently it has come to the author's notice that a similar experiment has been performed by Bourque (1959). However, the two sets of results appear to be complementary rather than duplicative in that they cover somewhat different ranges of the relevant variables.

The essential feature of the flow is the entrainment of fluid by the turbulent jet, which enables a stable flow pattern to be attained by the following mechanism. The entrainment of fluid near to the plate causes a pressure difference across the jet, curving the jet towards the plate. The jet divides on striking the plate, a proportion of the volume flow being reversed into the cavity. The final configuration is that in which the mean volume flow entrained from the cavity by the inner edge of the jet is balanced by the mean volume flow fed back into the cavity at the attachment point of the jet to the plate.

This flow is typical of cavity flows, other examples of which are to be found in connexion with separation bubbles, sudden expansions in pipes and channels, the flow over spoilers, the wakes of bluff bodies at certain Reynolds numbers, and so on.

It is well recognized (for example, see Townsend 1956) that the mechanism of entrainment is intimately connected with the growth of turbulent shear flows, and it is possible to use entrainment properties in the setting up of mean flow equations for such flows. For example, it is possible to construct an entrainment

relation for the turbulent boundary layer under the assumption that the entrainment properties at a particular boundary-layer station are a function of the shape of the velocity profile there as given, say, by the shape parameter $H = \delta^*/\theta$ (in the notation of Ludwieg & Tillman 1951). A detailed experiment could be performed to relate an entrainment parameter to H and R_0 which, with the Ludwieg–Tillman (1951) relations connecting C_f, R_θ and H, would furnish an approximate method for the calculation of turbulent boundary layers through the momentum and entrainment equations. This idea has been put forward by Head (1958).

Implicit in such arguments is the assumption that the turbulent structure of a shear layer, or that part of the turbulent structure which affects the mechanism of entrainment, is a function of an over-all shape parameter. In the case of a plane turbulent jet or other free turbulent shear layer, it is expected that the entrainment properties will be completely dependent on profile shape, because of a lack of solid boundaries. Turbulent shear flows may be considered to consist of a body of wholly turbulent fluid separated from the non-turbulent fluid by a clearly defined surface (the 'laminar superlayer' introduced by Corrsin & Kistler (1954) of an irregular and fluctuating character. The process of entrainment may be taken to be the advancing of this bounding surface into the non-turbulent fluid. Townsend indicates that the position of the bounding surface of the turbulent fluid is almost wholly due to the large eddy structure of the flow, which is the structure responsible for the value of the shape parameter H of the velocity profile.

The entrainment properties of a curved two-dimensional turbulent jet are expected to differ from those of the corresponding plane jet, momentum transport arguments indicating a reduced entrainment along the inner edge and an enhanced entrainment along the outer edge. For consider the transport of a small parcel of fluid from a region of higher velocity to a region of lower velocity nearer to the outside edge of the jet. If this parcel of fluid arrives with some excess velocity over its surroundings, it is now subjected to a greater centrifugal force than its surroundings. But its surroundings are subjected to centrifugal forces and pressure forces which just balance in the mean. Thus it is expected that the parcel of fluid will experience a total force tending to move it further outwards, which implies a more vigorous mixing than that which occurs with no curvature. A reverse argument holds for the mixing at the inner edge.

Dodds has put forward a simple model of the cavity flows of a curved two-dimensional reattaching jet, in which plausible assumptions regarding the division of the jet at reattachment lead to expressions relating the cavity pressure and cavity length to the jet momentum per unit jet width and the geometry of the boundaries. These expressions involve a spread parameter connected with the entrainment properties of the inner edge of the jet. The experiment has been performed to ascertain the correctness of Dodds's predictions and to find the value of the spread parameter.

2. Notation

h distance of slot centre-line from plate;
h_0 height of equivalent control volume used in reversed flow pressure recovery calculation;
J jet momentum/unit span;
J_2 momentum/unit span of reversed flow;
J_3 momentum/unit span of flow downstream of reattachment;
$K = 1{\cdot}825/\sigma$;
l cavity length, or distance of reattachment point from step;
p static pressure;
p_a static pressure far downstream;
p_s an average static pressure inside the cavity;
Δp pressure difference across jet;
Δp_2 pressure recovery of reversed flow;
Q quantity flow/unit span in jet;
Q_2 quantity flow/unit span in initial reversed flow;
R radius of curvature of jet;
t thickness of jet at exit;
$T = \tanh \eta_R$;
T_1 value of T at X_1;
u mean velocity;
U_0 reference velocity;
$U_{\max}$ maximum velocity of jet profile;
x, y co-ordinates parallel and perpendicular to plate ($x = 0$ at step, $y = 0$ at plate);
X, Y co-ordinates along and perpendicular to jet centre-line ($X = X_0$ at slot, $Y = 0$ on jet centre line);
X_1 value of X where jet inner edge would touch plate;
δ_1 thickness of jet at X_1;
δ_2, δ_3 thicknesses of initial reversed flow and initial downstream flow at the reattachment point;
μ viscosity;
ψ streamline parameter ($\psi = 0$ on reattaching streamline);
ρ density;
σ spread parameter ($= 7{\cdot}67$ for plane jet);
θ angle between jet centre-line at X_1 and plate;
$\eta = \sigma Y/X$, non-dimensional jet profile co-ordinate;
η_R value of η on reattaching streamline.

The notation is further explained by figure 1.

3. Dimensional analysis

The significant variables of the problem are the step-height h, the slot thickness t, a velocity U_0 representative of the jet velocity at the slot and the fluid properties μ and ρ. If these quantities are specified, the physical features of the flow are determined.

Dimensional considerations then show that the cavity length and the pressure difference across the jet may be expressed as follows:

$$\frac{l}{h} = f_1\left(\frac{h}{t}, \frac{\rho U_0 t}{\mu}\right),$$

where U_0 is given by $J = \rho U_0^2 t$, the jet momentum/unit span, and

$$\frac{p_s - p_a}{\frac{1}{2}\rho U_0^2} = f_2\left(\frac{h}{t}, \frac{\rho U_0 t}{\mu}\right).$$

In particular, if the jet is thin (h/t large) and fully turbulent ($\rho U_0 t/\mu$ large), it is expected that

$$\frac{\Delta p}{J/h} = -\frac{(p_s - p_a)h}{\rho U_0^2 t}$$

should be nearly independent of $\rho U_0 t/\mu$ (or $\sqrt{(J\rho t)}/\mu$) and substantially independent of h/t.

Similarly, l/h is expected to be nearly independent of jet Reynolds number and to vary little with h/t for large h/t.

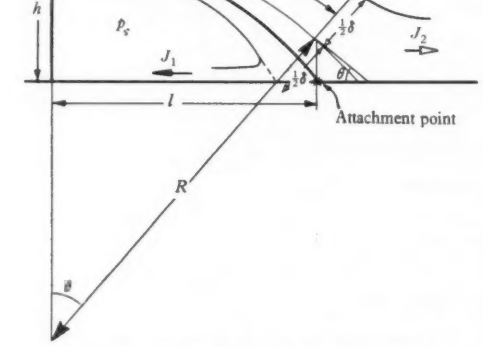

FIGURE 1. Notation used in the analysis.

4. An approximate analysis for the case of a thin fully developed turbulent jet

The analysis runs as follows. The curvature of the jet is expressed as the ratio of the pressure difference across the jet to the jet momentum. Knowing the geometry of the jet centre-line, assumptions regarding the jet velocity profile and rate of spread (as measured by a spread parameter σ) lead to an expression for the amount of air entrained by the jet along its inner edge, which is taken to be the volume flow fed back into the cavity at reattachment. Thus the division of volume flow of the jet at reattachment is known. Assumptions of velocity profile shapes of the initial reversed flow and the initial attached downstream flow, with the aid of a momentum balance equation at the reattachment point,

then give the division of momentum flow at reattachment. But the division of momentum at reattachment implies the geometry of the jet. Thus the chain of reasoning is complete and a solution can be found. The analysis is set out in detail below.

Assume that the velocity profile of the jet is similar to that of a two-dimensional plane jet, so that the profile is given approximately by the equation

$$\frac{u}{U_{\max}} = \operatorname{sech}^2 \eta,$$

where $\eta = \sigma Y/X$ (Görtler 1942), and where X, Y are co-ordinates measuring distances along and perpendicular to the jet centre-line. Note that $X = 0$ does not coincide with the position of the slot.

The value of the free constant σ for the case of the plane jet was found experimentally by Reichardt (1942) to be 7·67. It is expected that the value of σ relevant to entrainment along the inner edge of the curved jet will be somewhat higher than this due to suppression of turbulent mixing as a consequence of curvature.

The jet momentum per unit span is given by

$$J = \tfrac{4}{3}\rho U_{\max}^2 \frac{X}{\sigma},$$

and the volume flow per unit span is given by

$$Q = 2U_{\max} \frac{X}{\sigma}.$$

Thus
$$Q = \sqrt{\left(\frac{3JX}{\sigma\rho}\right)} \quad \text{and} \quad U_{\max} = \sqrt{\left(\frac{3\sigma J}{4\rho X}\right)}. \tag{1}$$

It is assumed that there is a constant pressure p_s in the cavity, so that there is a constant pressure difference $\Delta p = (p_a - p_s)$ acting across the jet. If the jet is thin, the centre-line of the jet lies approximately on an arc of a circle of radius R, where

$$\Delta p = \frac{J}{R}. \tag{2}$$

In the absence of any precise guide, the station $X = X_1$, which is representative of the state of the jet near the reattachment point, is taken to be that at which the inner edge of the jet as given by $u/U_{\max} = 0{\cdot}1$ would first strike the plate, i.e. in such a position that, in the absence of reattachment-point effects, the jet centre-line continues to lie along the circle of radius R and the jet continues to grow at its normal rate, the locus $u/U_{\max} = 0{\cdot}1$ intersects the line of the plate.

Then the thickness δ_1 of the jet at $X = X_1$ is given by

$$\frac{\delta_1}{2X_1} = \frac{1}{\sigma}\tanh^{-1}\sqrt{(0{\cdot}9)}$$

$$= \frac{1{\cdot}825}{\sigma} = K, \quad \text{say.} \tag{3}$$

Geometrically it is seen that

$$X_1 - X_0 = R\theta, \tag{4}$$

where θ is the angle between the jet centre-line at station $X = X_1$ and the plate, and where $X = X_0$ corresponds to the slot. We also have

$$h = R(1-\cos\theta)+\tfrac{1}{2}\delta_1\cos\theta, \tag{5}$$

and for ease of computation take

$$l = R\sin\theta. \tag{6}$$

The mass flow between the jet centre-line and the reattaching streamline (the streamline springing from the inner edge of the slot) is constant and equal to $\frac{1}{2}\sqrt{(Jtp)}$, assuming a uniform velocity profile across the slot.

Thus the reattaching streamline is given by

$$\begin{aligned}\tfrac{1}{2}\sqrt{(Jtp)} &= \rho\sqrt{\left(\frac{3J\sigma}{4\rho X}\right)}\frac{X}{\sigma}\int_0^{\eta_R}\operatorname{sech}^2\eta\,d\eta \\ &= \sqrt{\left(\frac{3\rho JX}{4\sigma}\right)}T,\end{aligned}$$

where $T = \tanh\eta_R$ corresponds to the value of η at the reattaching streamline, i.e.

$$\frac{1}{T^2} = \frac{3X}{\sigma t}. \tag{7}$$

In particular, we have

$$X_0 = \frac{\sigma t}{3}, \tag{8}$$

$$\frac{X_0}{X_1} = T_1^2. \tag{9}$$

Equations (1) to (9) give

$$\frac{h}{t} = \frac{\sigma}{3\theta}\left(\frac{1-T_1^2}{T_1^2}\right)\left(1-\cos\theta+\frac{K\theta\cos\theta}{1-T_1^2}\right), \tag{10}$$

$$\frac{l}{h} = \frac{\sin\theta}{\{1-\cos\theta+K\theta\cos\theta/(1-T_1^2)\}}, \tag{11}$$

$$\frac{\Delta p}{J/h} = \{1-\cos\theta+K\theta\cos\theta/(1-T_1^2)\}. \tag{12}$$

To relate T_1 to θ, consider the momentum balance at the reattachment point. Dodds supposes that the initial reversed flow and initial downstream flow have velocity profiles similar to that of half a Görtler jet profile with maximum velocities $U_{\max_1}\sin\theta$ and $U_{\max_1}$, respectively. The factor $\sin\theta$ is arbitrary, being chosen to satisfy the conditions for $\theta = 0, \frac{1}{2}\pi$. Any reasonably well-behaved function $f(\theta)$ such that $f(\theta) = 0$, $f(\frac{1}{2}\pi) = 1$ would be equally acceptable. $U_{\max_1}$ is the velocity maximum of the free-jet profile at $X = X_1$.

If δ_2, δ_3 are the thicknesses of half-jet profiles, the equations of continuity and momentum in the x-direction at the reattachment point give

$$\delta_1 = \delta_2\sin\theta+\delta_3,$$

$$\delta_1\cos\theta = -\delta_2\sin^2\theta+\delta_3,$$

if pressure differences are neglected near the attachment point, so that

$$\frac{\delta_2}{\delta_1} = \frac{1}{\sin\theta}\left(\frac{1-\cos\theta}{1+\sin\theta}\right).$$

Thus the reversed volume flow is

$$U_{\max_1}\sin\theta\frac{\delta_2}{\sigma K}\int_0^\infty \operatorname{sech}^2\eta\,d\eta = U_{\max_1}\frac{\delta_1}{\sigma K}\left(\frac{1-\cos\theta}{1+\sin\theta}\right)$$
$$= \sqrt{\left(\frac{3\sigma J}{4\rho X_1}\right)}\frac{\delta_1}{\sigma K}\left(\frac{1-\cos\theta}{1+\sin\theta}\right),$$

from (1). But this is equal to

$$\tfrac{1}{2}(Q_1-Q_0) = \frac{1}{2}\left\{\sqrt{\left(\frac{3JX_1}{\sigma\rho}\right)}-\sqrt{\left(\frac{3JX_0}{\sigma\rho}\right)}\right\}.$$

Hence

$$\frac{\delta_1}{KX_1}\left(\frac{1-\cos\theta}{1+\sin\theta}\right) = 1-\sqrt{\frac{X_0}{X_1}},$$

or

$$T_1 = 1-2\left(\frac{1-\cos\theta}{1+\sin\theta}\right). \tag{13}$$

Bourque (1959) has obtained a different relation between T_1 and θ by the following reasoning. Assume that at the attachment point the jet flow divides in such a manner that the profiles of the initial reversed flow and initial flow downstream of the attachment point are similar to the parts of the free-jet profile at $X = X_1$ below and above the reattaching streamline, at least in so far as over-all volume flow and momentum are concerned.

Then the momentum per unit span of the jet below the reattaching streamline is

$$J_2 = \int_{T_1}^1 \rho U_{\max_1}^2\frac{X_1}{\sigma}(1-T^2)\,dT$$
$$= \tfrac{3}{4}J(\tfrac{2}{3}-T_1+\tfrac{1}{3}T_1^3).$$

The momentum per unit span of the jet above the reattaching streamline is

$$J_3 = \int_{-1}^{T_1}\rho U_{\max_1}^2\frac{X_1}{\sigma}(1-T^2)\,dT$$
$$= \tfrac{3}{4}J(\tfrac{2}{3}+T_1-\tfrac{1}{3}T_1^3).$$

If pressure differences near the attachment point are neglected, the momentum balance at the attachment point gives

$$J\cos\theta = J_3-J_2,$$

so that

$$\cos\theta = \tfrac{3}{2}T_1-\tfrac{1}{2}T_1^3. \tag{14}$$

Relation (14) is likely to be more accurate than relation (13), and accordingly the experimental results have been compared with the predictions given by equations (10), (11), (12) and (14).

5. Experimental arrangement

The experimental arrangement is shown in figure 2. The top of the tank was bolted down through a rectangular spacer, one side of which formed the lower surface of the slot and the step on the plate. Three step heights were used, namely $\frac{1}{2}$, 1 and 2 in. The upper surface of the slot was attached to the top of the

tank by horizontal bolts through slotted holes so that the width of the slot was variable between zero and $\frac{1}{4}$ in. The combination of step heights and slot widths covered a large range of h/t.

A fine-mesh gauze was placed across the pipe from the blower at the entry to the tank so as to smooth the flow from the blower.

Vertical end-plates isolating 12 in. of the slot flow were fixed to the plate to preserve two-dimensional conditions as far as possible, in particular to remove spanwise flow into the low-pressure cavity. It was found that the flow was substantially two-dimensional (see below).

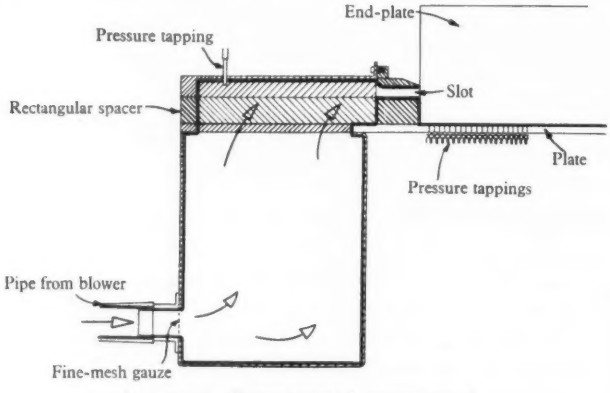

FIGURE 2. Experimental arrangement.

The static pressure distribution on the plate was measured by means of surface pressure tappings at intervals of 0·2 in. Static pressures and total pressures were measured by means of static and Pitot tubes fixed to a vertical traverse gear sliding on a spanwise horizontal bar which moved on streamwise horizontal rails. The jet momentum was found from Pitot and static traverses across the slot. All pressure readings were referred to a pressure tapping in the top of the tank.

Tests of two-dimensionality

Velocity traverses across the slot showed that the maximum velocity at the slot was constant across the slot length to 1 %. The surface streamlines on the plate and end-plates were made visible by applying a suspension of titanium dioxide in penetrating oil to these surfaces which had been painted matt black. Figure 3 (plate 1) shows that the streamlines on the end plates are not at all similar to the mean streamlines in figure 4, and that the reattachment distance varies somewhat along the width of the plate. The photographs indicate that there is a secondary flow close to the end-plates which feeds air from outside into the cavity. Thus there is not an exact balance between the quantity of air entrained by the jet from the cavity and the quantity of reversed flow at reattachment. Near the centre of the slot length, however, it is estimated that this lack of balance is negligible and that the flow corresponds very nearly to two-dimensional conditions.

Pressure readings and measurements of reattachment distance

Detailed measurements of mean velocities and reattachment position were carried out for the slot width and step height giving the case $h/t = 5{\cdot}62$.

Because of the end effects described above, it was not possible to use static pressure tappings in an end-plate to give a reliable static pressure map of the cavity. Apart from the pressures measured by means of tappings in the horizontal plate, all static pressures were measured by a standard static tube aligned

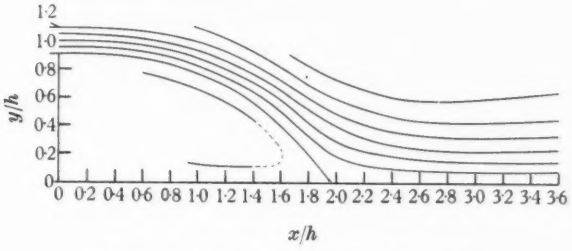

FIGURE 4. Streamlines for case $h/t = 5{\cdot}62$.

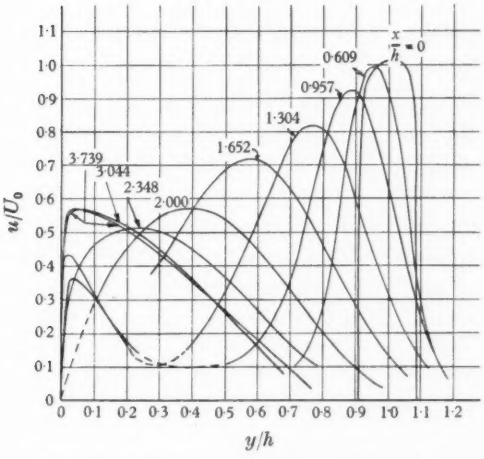

FIGURE 5. Velocity profiles for case $h/t = 5{\cdot}62$.

with the direction of local streamlines. Because of the sensitivity of flattened Pitot tubes in regions of strong turbulence to the fluctuations of flow direction all total pressures (other than those of the reversed flow regions), were measured by a round thin-wall Pitot tube of diameter 0·040 in. aligned with the mean flow direction. This Pitot tube was insensitive to yaw to $\frac{1}{2}\%$ of dynamic pressure over the range $\pm 15°$. Total pressures in the reversed flow near to the plate, i.e. in those reversed flow regions in which the fluctuations of flow direction were suppressed by the proximity of the plate, were measured with a flattened Pitot tube of 0·010 in. over-all thickness.

The technique used was to make transverses with the tubes at various angles, selecting those which gave stationary values of static pressure and Pitot pressure with respect to alignment angle at the point considered. The velocity profiles obtained (figure 5), together with approximate flow directions, gave a mean streamline picture from which more accurate flow directions were found. Using these new flow directions a more accurate streamline picture was calculated, and so on. As a check on the final streamline plot (figure 4) obtained by repeating the above procedure three times, it was seen that the position of reattachment calculated from the integrated velocity profiles corresponded very closely (l/h accurate to 1 %) to that found by surface-Pitot traverses and to that indicated by the visualization technique. The surface-Pitot traverses were made with identical flattened Pitots, one facing forward and one reversed. The results are presented in table 1. The reattachment point was taken as that point at which the

x/h	$\frac{P-p_a}{\frac{1}{2}\rho U_0^2}$, forward Pitot	$\frac{P-p_a}{\frac{1}{2}\rho U_0^2}$, reversed Pitot
1·826	0·540	0·415
1·913	0·585	0·550
2·000	0·600	0·625

TABLE 1. Attachment point determined by surface Pitots. For case $h/t = 5{\cdot}62$.

two Pitots gave the same reading. It was found that the position of reattachment coincided with the position of maximum pressure on the horizontal plate. This position of maximum pressure was taken as the reattachment position in all other cases.

In calculating the velocity profiles from Pitot and static traverses the Young & Maas (1936) correction to Pitot measurements was applied. Even in the case of extreme velocity gradients encountered at the slot itself, the Young & Maas correction applied to the 0·040 in. Pitot gave profile widths accurate to 0·001 in. as measured by slot width. One particular profile at the slot obtained in this way was checked against that measured with a flattened boundary-layer Pitot of 0·010 in. over-all thickness and the two were found to be almost identical.

6. Comparison of experimental results with the analysis

The values of $\Delta p/(J/h)$ and l/h obtained for various h/t are given in table 2, and the results found by Bourque in the range of h/t considered are given for comparison in table 3. In figures 6 and 7 these results are compared with corresponding theoretical curves for $\sigma = 5$, 10, 15 and 20. It is interesting to see that the dual-jet flow measurements of Miller & Comings (1960) give values of $\Delta p/(J/h)$ and l/h which agree quite well with the results presented here.

As mentioned previously, the position of reattachment was taken to be the position of maximum pressure on the plate. Figure 8 shows the distribution of pressure on the plate. It is seen that for large h/t the pressure is far from uniform through the cavity. However, figure 9 shows that the pressure along the plate

follows quite closely the static pressure under the jet, and the value of Δp chosen was the (negative) mean of the pressure on the plate over the range of x/h between zero and 0·95 times its value at $p - p_a = 0$.

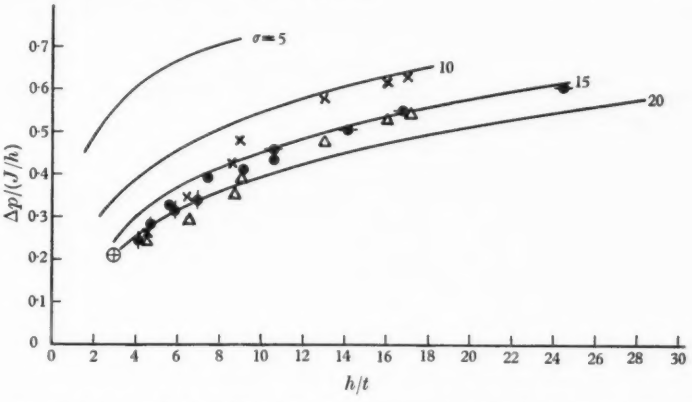

FIGURE 6. Variation of $\Delta p/(J/h)$ with h/t compared with Dodds–Bourque analysis. ⊕, Miller & Comings dual-jet flow; ⧫, ½ in. step; ●, 1 in. step; ●–, 2 in. step; ×, Bourque's results (using pressure minimum on plate to define Δp); △, Bourque's results (recalculated to correspond to average Δp and corrected J).

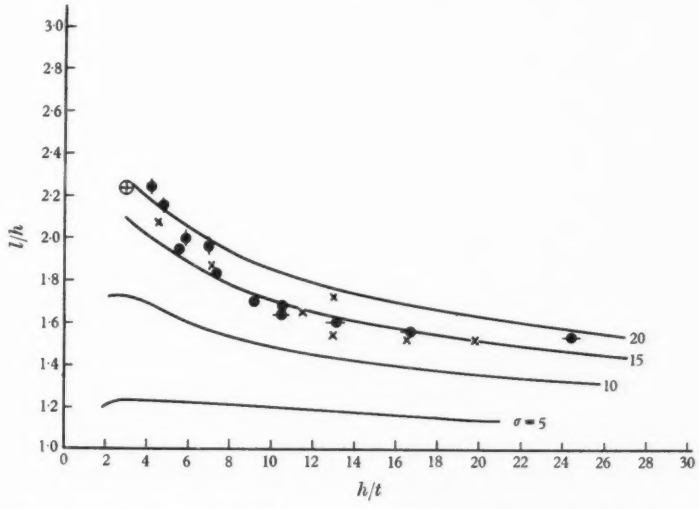

FIGURE 7. Variation of l/h with h/t compared with the analysis. ⧫, ½ in. step; ●, 1 in. step; ●–, 2 in. step; ×, Borque's results; ⊕, Miller & Comings dual-jet flow.

It is seen that Bourque's results giving the variation of l/h with h/t agree very well with those obtained by the author. However, there is considerable systematic discrepancy between the sets of results for the variation of $\Delta p/(J/h)$ with h/t.

Bourque uses a very short entry length to the jet exit in order to obtain a square-edged initial jet profile and computes the jet momentum J from the

measured pressure in the chamber just before the contraction to the slot under the assumption that the dynamic pressure of the jet is that given by the chamber pressure. However, Bourque also presents measurements of the initial jet profiles which show that the velocity is far from uniform across the slot width.

For comparison, the values of $\Delta p/(J/h)$ measured by Bourque and computed using the minimum static pressure on one plate in his definition of Δp and the chamber pressure to define J, have been recalculated using the definitions of Δp and J used in this experiment.

	h/t	l/h	$\Delta p/(J/h)$
$\frac{1}{2}$ in. step	4·15	2·25	0·244
	4·81	2·15	0·279
	5·92	2·00	0·318
	6·99	1·97	0·342
1 in. step	5·62	1·96	0·327
	7·35	1·83	0·394
	9·13	1·70	0·412
	10·64	1·68	0·439
2 in. step	10·65	1·65	0·459
	14·06	1·60	0·508
	16·74	1·57	0·556
	24·40	1·54	0·606

TABLE 2. Experimental results.

h/t	$\Delta p/(J/h)$*	h/t	l/h
4·5	0·27	4·5	2·07
6·5	0·35	7·1	1·87
8·7	0·43	11·5	1·65
9·0	0·48	13·0	1·54
13	0·58	13·0	1·72
16	0·62	16·5	1·52
17	0·61	19·8	1·52

* Note that Bourque takes pressure minimum on plate to define Δp.

TABLE 3. Bourque's results.

In this connexion it should be noted that while in the present experiment the jet Reynolds number $\sqrt{(J\rho t)}/\mu$ was almost constant for all readings at about $9{\cdot}5 \times 10^4$, Bourque's experiment was conducted at much lower Reynolds numbers between $0{\cdot}8 \times 10^4$ and $1{\cdot}5 \times 10^4$.

Figures 6 and 7 show that $\Delta p/(J/h)$ and l/h are quite closely defined functions of h/t following roughly the curves given by the analysis for $\sigma = 15$.

7. Discussion of detailed velocity and pressure measurements

Velocity profiles across sections at right angles to the jet have been calculated for the stations $x/h = 0{\cdot}609$ and $x/h = 1{\cdot}304$ (referring to the position of the velocity maximum of the profile) for the case $h/t = 5{\cdot}62$, by a direct application

of the assumption that the local growth of the jet is that of the free jet with spread parameter $\sigma = 15$ to the measured velocity profiles at $x/h = 0{\cdot}609$ and $x/h = 1{\cdot}304$. These profiles are shown in figure 10. The method of calculation is set out in an appendix.

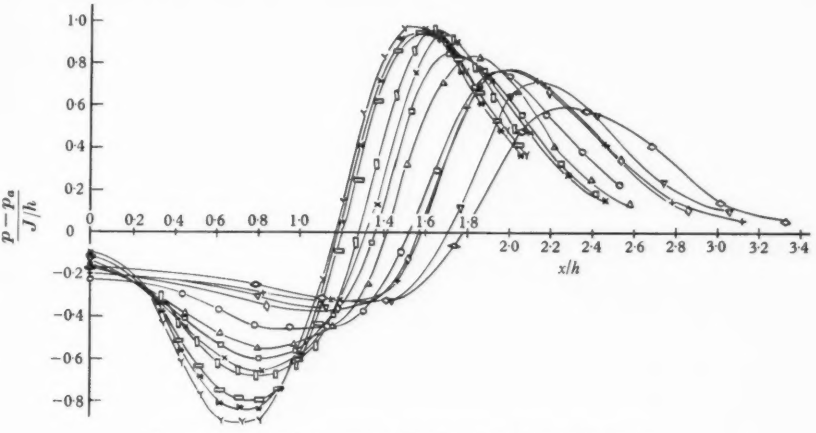

FIGURE 8. Static pressure distribution along the plate.

Symbol	h/t	Symbol	h/t
◇	4·15	□	9·13
▽	4·81	×	10·64
+	5·92	▯	10·65
◇	6·99	▭	14·06
○	5·62	*	16·74
△	7·35	Y	24·40

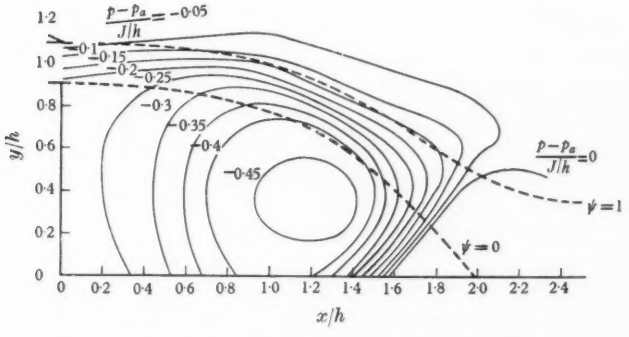

FIGURE 9. Static pressure contours for case $h/t = 5{\cdot}62$.

In the calculation it is necessary to assume a value of J, the jet momentum. It is found on integrating the calculated profiles that the values of the profile momentum are substantially larger than that at the slot exit, due to different static pressures at the various stations. The calculation has therefore been repeated using these new values of momentum at the relevant stations and the new

calculated profiles taken to be sufficiently close approximations to reality (they are almost identical with those originally found).

By comparing the values of jet momentum at the stations $x/h = 0{\cdot}609$, $1{\cdot}304$ with that measured at the jet exit, it is possible to obtain a check on the consistency of the Pitot and static tube measurements. It is found that the computed values of momentum agree to within 2%. This is of the same order as the uncertainty which exists regarding the use of Pitot and static tubes in highly fluctuating turbulent flows.

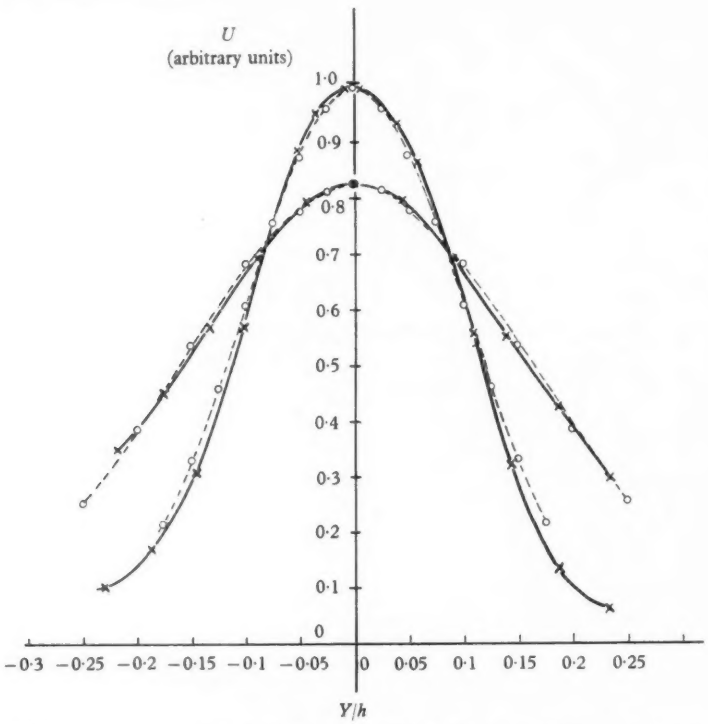

FIGURE 10. Jet profiles at $x/h = 0{\cdot}609$, $1{\cdot}304$ calculated from Pitot-static traverses by application of free-jet analysis with $\sigma = 15$. —×—, calculated profiles; --○--, plane jet profiles fitted to calculated profiles at U_{max} and $\frac{1}{2}U_{max}$.

In figure 10 the calculated jet profiles have been compared with the plane-jet profile as measured by Förthmann (1934) which has been matched at the values of $\overline{Y}/h$ corresponding to U_{max} and $\frac{1}{2}U_{max}$. There is quite close agreement between the curves. The profile at $x/h = 0{\cdot}609$ is somewhat flattened near $\overline{Y}/h$ for U_{max} but this is to be expected, for this station is only some 3·4 slot widths downstream of the jet exit. There is no indication of one-sidedness of the profiles expected from considerations of jet curvature.

It is possible to calculate an approximate value of σ, the spread parameter of the jet between these two profiles. Direct measurement of profile half-width

gives $\sigma = 9{\cdot}8$. Calculation based on velocity maxima gives $\sigma = 10{\cdot}3$ assuming $J/\rho U_0^2 h = 0{\cdot}191$, $\sigma = 11{\cdot}1$ assuming $J/\rho U_0^2 h = 0{\cdot}177$, $\sigma = 11{\cdot}9$ assuming $J/\rho U_0^2 h = 0{\cdot}165$ (i.e. that measured at the jet exit). Inasmuch as σ measures jet spread, a value in the region $\sigma = 10$ would be most realistic. It is noted that even taking the value of jet momentum to be that measured at the jet exit, the spread parameter is somewhat smaller than the value giving best agreement with the analysis. However, a reduced entrainment along the inner edge and an enhanced entrainment along the outer edge of the curved jet is expected to give a total spread parameter in the region of 10.

The analysis gives the volume of reversed flow:

$$\frac{Q_2}{U_0 h} = \frac{1-T_1}{2T_1}\sqrt{\left(\frac{J}{\rho U_0^2 h}\right)}\Big/\sqrt{\left(\frac{h}{l}\right)},$$

where $\cos\theta = \frac{3}{2}T_1 - \frac{1}{2}T_1^3$ and θ is the angle at which the jet strikes the plate. For $h/t = 5{\cdot}62$, $\sigma = 15$ and $J/\rho U_0^2 h = 0{\cdot}165$, $\theta = 43°$ and $Q_2/U_0 h = 0{\cdot}067$. Now the measured values are $\theta = 43°$ and $Q_2/U_0 h = 0{\cdot}068$, and so there is very good agreement in this case.

The reversed flow momentum J_2 is equal to $\frac{1}{2}J(1-\cos\theta)$ giving $J_2/J = 0{\cdot}135$ for $\theta = 43°$. The reversed flow momentum at $x/h = 1{\cdot}304$ is given by

$$J_2/\rho U_0^2 h = 0{\cdot}021,$$

at $x/h = 0{\cdot}957$ is $J_2/\rho U_0^2 h = 0{\cdot}018$

by integration of velocity profiles, so that at $x/h = 1{\cdot}304$ and $0{\cdot}957$, $J_2/J = 0{\cdot}127$ and $0{\cdot}109$. Again there is good agreement with the analysis.

The pressure recovery experienced by the reversed flow is given by $\Delta p_2/(J/h) = 0{\cdot}23$ from figure 8. This corresponds to the case of a jet with momentum J_2 entering a rectangular control volume through one end, losing this momentum entirely in a pressure rise and diffusing sideways out of the control volume. The pressure difference Δp_2 across the control volume is given by $h_0 \Delta p_2 = J_2$, so that $h_0/h = (J_2/J)\,\Delta p/(J/h)$. If $\Delta p_2/(J/h) = 0{\cdot}23$, $J_2/J = 0{\cdot}132$ then $h_0/h = 0{\cdot}57$. This is of the order expected, for if a control volume is constructed which is bounded by the plate, the step, the station $x/h = 1{\cdot}2$, and the locus of points at which the component of mean velocity parallel to the plate is zero, integrating the pressure round the control volume gives the loss of momentum in the x-direction. The shape of such a control volume is expected to be a function of the shape of the cavity. Values of h_0/h have been calculated as follows. For each measurement a mean value of σ from figures 6 and 7 is obtained, which with the known value of h/t gives the value of θ relevant to the analysis. Writing $J_2/J = \frac{1}{2}(1-\cos\theta)$ and using the experimental results of pressure recovery gives h_0/h from the above relation. In figure 11 h_0/h is plotted against θ. It is seen that the points lie on a reasonably well-defined curve for larger values of θ (i.e. for larger h/t). With this information it is possible to predict the back pressure on the step by the analysis.

Table 4 gives values of total pressure at stations on the reattaching streamline and on the locus of positions at which the velocity of the y-wise profiles is a maximum. It is interesting to see that the values of streamline number ψ for the positions of U_{max} on the y-wise profiles are very near to $0{\cdot}5$ for a considerable

distance along the curved jet. The effect of non-uniformity of the jet profile at the slot is very quickly lost, and any expectation of a clearly defined upwards trend of $\psi_{U_{\max}}$ with x/h which, in the absence of one-sided profiles, would perhaps reflect different mixing rates on the two sides of the jet, has not been fulfilled. Figure 8 shows that the maximum pressure on the plate $(p-p_a)/(J/h) = 0{\cdot}77$ is

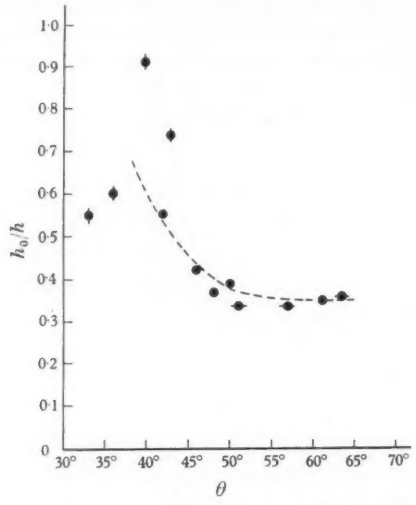

FIGURE 11. Pressure recovery parameter. ♦, ½ in. step; ●, 1 in. step; ●—●, 2 in. step.

x/h	$(y/h)_{\psi=0}$	$\left(\frac{\frac{1}{2}\rho u^2}{J/h}\right)_{\psi=0}$	$\left(\frac{P-p_a}{J/h}\right)_{\psi=0}$
0·609	0·870	1·41	1·13
0·957	0·780	1·35	0·975
1·304	0·620	1·08	0·67
1·652	0·355	0·725	0·46

x/h	$(y/h)_{U_{\max}}$	$\frac{\frac{1}{2}\rho U_{\max}^2}{J/h}$	$\left(\frac{P-p_a}{J/h}\right)_{U_{\max}}$	$\psi_{U_{\max}}$
0·609	0·955	3·11	2·92	0·47
0·957	0·885	2·92	2·62	0·47
1·304	0·760	2·58	2·29	0·50
1·652	0·575	2·26	2·03	0·63

TABLE 4. Total pressures on reattaching streamline and locus of velocity maximum of y-wise profiles. For case $h/t = 5{\cdot}62$.

much higher than that obtained by extrapolating the total pressure on the reattaching streamline, but is very much lower than that obtained by extrapolating the total pressure on the maximum velocity locus. This can be explained by considering the effect of a highly fluctuating flow near the reattachment point; the high-velocity parcels of fluid give a correspondingly larger contribution to the wall pressure than the lower-velocity parcels. Streamlines depend on mean squared velocity.

8. Conclusions

The variations of $\Delta p/(J/h)$ and l/h with h/t found experimentally agree quite closely with those predicted by the Dodds analysis (as amended by Bourque) in that they are consistent with a choice of spread parameter σ which is substantially constant at the value 15 over the range of $h/t > 6$. The relevant value of σ is somewhat larger than this for h/t in the region of 4.

Detailed flow measurements for the case $h/t = 5{\cdot}62$ show that $\sigma = 15$ gives reasonably accurate prediction of initial reversed volume flow and reversed flow momentum.

The value of σ for which the analysis is in best agreement with the results is not in fact the true value of the spread parameter for the curved jet, and the discrepancy between the two values is a measure of the collective errors in the various assumptions made in the analysis, so that the choice of $\sigma = 15$ is now to be regarded as the fixing of a convenient empirical constant in order that the analysis may be applied to give reasonably accurate predictions of cavity length and cavity pressure. In this connexion it is noted that any change in the rate of entrainment along the inner and outer edges of the jet due to curvature effects as predicted by momentum transport considerations, would not necessarily be accompanied by a change in the rate of growth of the jet as a whole. Since the velocity profiles across the curved jet were found to be very like those of a plane jet, a difference in the rate of entrainment on the two sides of the jet would imply that the locus of velocity maximum is not a streamline. The measurements of velocity and pressure are not of sufficient accuracy to detect this effect and further experiments are being carried out to investigate the effect of curvature on entrainment properties.

The author wishes to thank Dr M. R. Head for his advice and encouragement, and also Mr H. Bridgeman who constructed the apparatus.

REFERENCES

Bourque, C. 1959 M.Sc. Thesis. University of Laval. Also *Aero. Quart.* **11**, 201.

Corrsin, S. & Kistler, A. L. 1954 The free-stream boundaries of turbulent flows. *NACA Tech. Note* 3133.

Dodds, J. I. 1960 Ph.D. Thesis. Cambridge University.

Förthmann, E. 1934 Über turbulente Strahlausbreitung. *Ingen.-Arch.* **5**, 42. Also *NACA Tech. Note* 789.

Görtler, H. 1942. Berechnung von Aufgaben der Freien Turbulenz auf Grund eines neuen Näherungsansatzes. *Z. angew. Math. Mech.* **22**, 244.

Head, M. R. 1958 Entrainment in the turbulent boundary layer. *A.R.C. Report* no. 20,338.

Ludwieg, H. & Tillman, W. 1951 Investigations of the wall-shearing stress in turbulent boundary layers. *NACA Tech. Mem.* 1285.

Miller, D. R. & Comings, E. W. 1960 *J. Fluid Mech.* **7**, 237.

Reichardt, H. 1942 Gesetzmässigkeiten der freien Turbulenz. *VDI-Forschungsheft*, p. 414.

Townsend, A. A. 1956 *The Structure of Turbulent Shear Flow.* Cambridge University Press.

Young, A. D. & Maas, J. N. 1936. The behaviour of a Pitot tube in a transverse total-pressure gradient. *A.R.C. Rep. & Mem.* no. 1770.

Appendix

Calculation of jet profiles from profiles in the y-direction

The notation is shown in figure 12. The velocity at $\bar{y}$ is that corresponding to $(X, Y) = (\bar{X} - \bar{y}\sin\phi, \bar{y}\cos\phi)$, i.e. to

$$\bar{\eta} = \frac{\sigma\bar{y}\cos\phi}{\bar{X} - \bar{y}\sin\phi}, \quad X = \bar{X} - \bar{y}\sin\phi.$$

Hence
$$\frac{(u)_{\bar{y}}}{(U_{\max})_{\bar{X}-\bar{y}\sin\phi}} = \operatorname{sech}^2\bar{\eta} = \left(\frac{u}{U_{\max}}\right)_{X,\,Y}, \tag{1}$$

which defines $\bar{Y}$ to be the Y-co-ordinate of the required profile corresponding to $\bar{\eta}$, and so corresponding to $\bar{y}$ of the measured profile. Therefore

$$\frac{\sigma\bar{y}\cos\phi}{\bar{X} - \bar{y}\sin\phi} = \bar{\eta} = \frac{\sigma\bar{Y}}{\bar{X}},$$

and hence
$$\bar{Y} = \bar{y}\cos\phi\,\frac{\bar{X}}{\bar{X} - \bar{y}\sin\phi}. \tag{2}$$

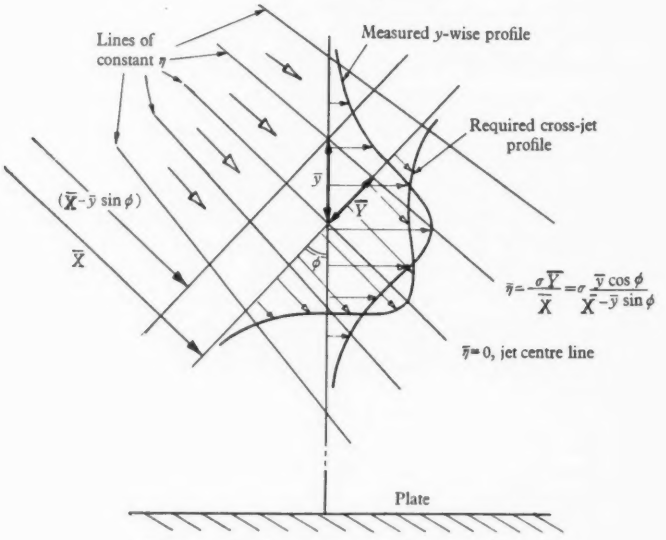

FIGURE 12. Notation used in appendix.

Now from (1), $$\left(\frac{u}{U_0}\right)_{X,\,Y} = \left(\frac{u}{U_0}\right)_{\bar{X}-\bar{y}\sin\phi,\,\bar{y}\cos\phi} \frac{(U_{\max})_{\bar{X}}}{(U_{\max})_{\bar{X}-\bar{y}\sin\phi}},$$

and so
$$\left(\frac{u}{U_0}\right)_{X,\,Y} = \left(\frac{u}{U_0}\right)_{\bar{X}-\bar{y}\sin\phi,\,\bar{y}\cos\phi} \sqrt{\left(\frac{\bar{X} - \bar{y}\sin\phi}{\bar{X}}\right)}, \tag{3}$$

for free-jet analysis gives
$$J = \tfrac{4}{3}\rho U_{\max}^2 \frac{X}{\sigma}.$$

Now
$$\frac{\bar{X}}{h} = \tfrac{3}{4}\sigma\left(\frac{J}{\rho U_0^2 h}\right)\left(\frac{U_0}{U_{\max}}\right)_{\bar{X}}^2. \tag{4}$$

Equations (2) to (4) then give the required profile. Intitially $J/\rho U_0^2 h = 0{\cdot}165$, as measured at the jet exit.

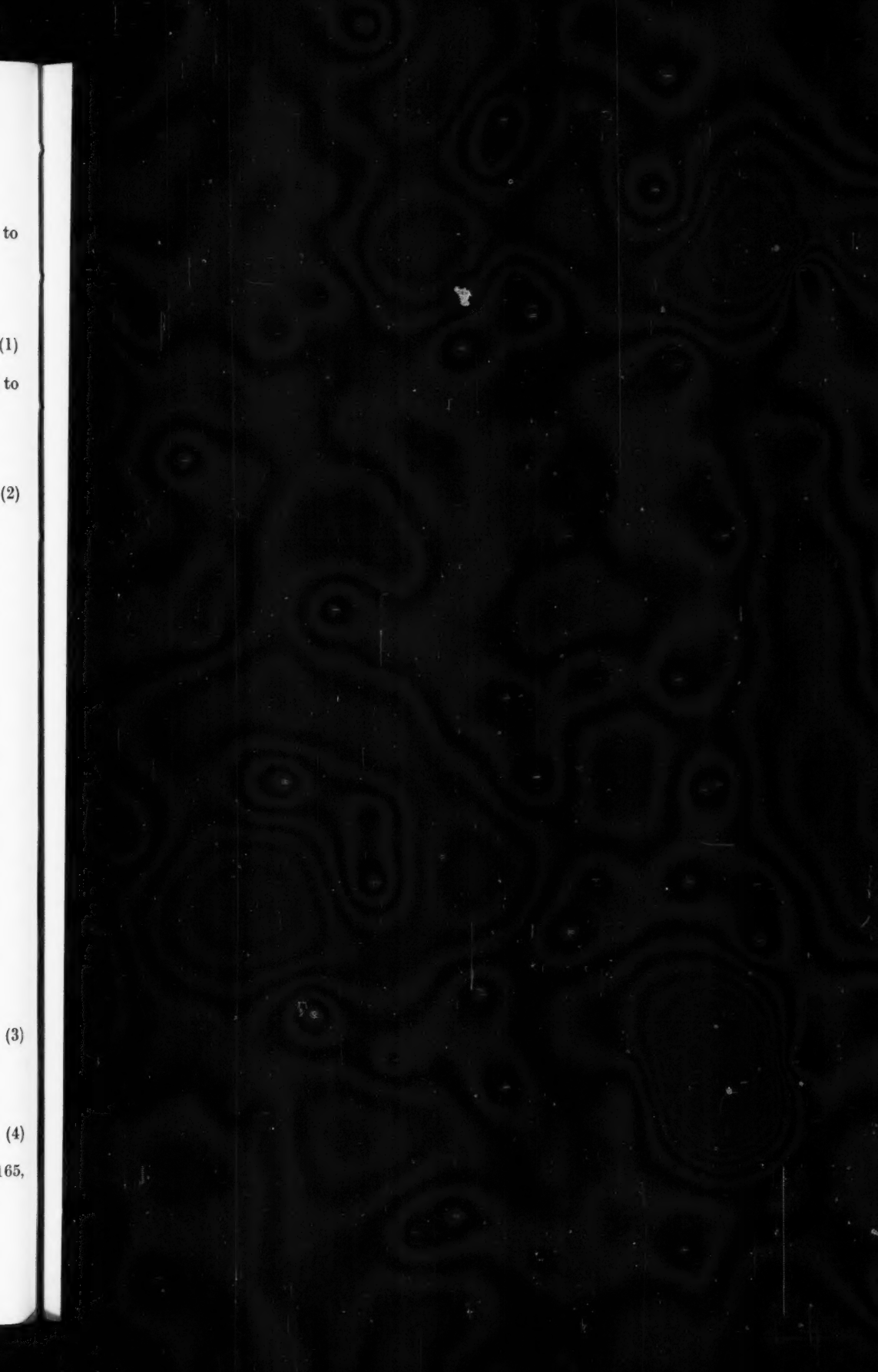

(*a*)

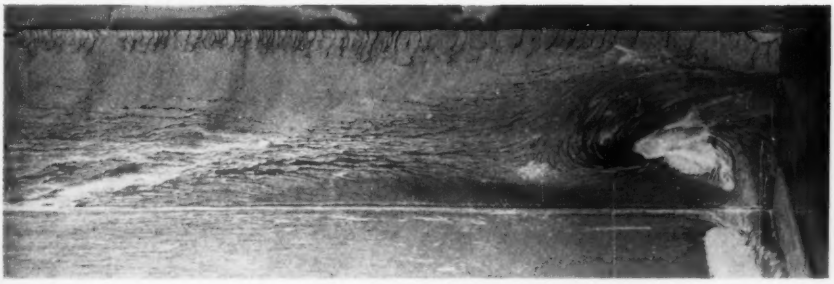

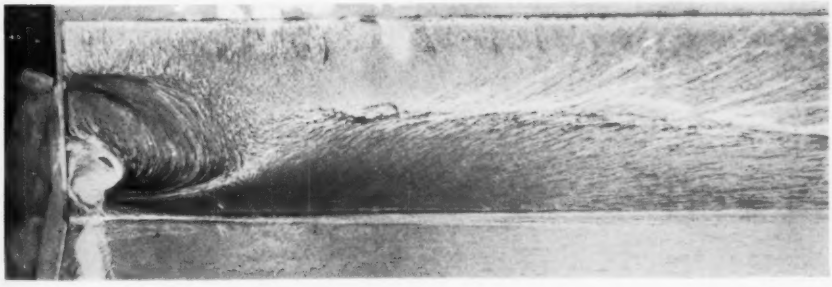

(*b*)

FIGURE 3 (plate 1). Flow visualization of surface streamlines.
(*a*) Base plate; (*b*) end-plates.

The method of images in shear flow

By M. B. GLAUERT

Department of Mathematics, University of Manchester

(Received 20 May 1960)

The method of images is used to determine the flow perturbation caused by a small point source of fluid in a stream containing a vortex sheet, a number of vortex sheets, or a continuous two-dimensional distribution of vorticity. Calculations are carried out for a variety of such shear flows, to illustrate the range of applicability of the method.

The image source distribution provides an alternative approach to that given by Lighthill for calculating small disturbances to a parallel shear flow, and suggests a simple physical picture by which to interpret the complicated effects associated with the distortion and stretching of vortex lines.

1. Introduction

Much attention has recently been paid to the problem of calculating the effect of disturbances to a non-uniform stream of fluid containing vorticity. The flow is assumed to be steady and incompressible and viscous effects are neglected. The purely two-dimensional case is relatively simple, since the vortex lines remain straight and unstretched, but for three-dimensional disturbances the distortion of the vortex lines creates problems of an entirely different order of difficulty, even if the undisturbed stream is two-dimensional.

One approach has been to consider that the vorticity is small, and that its effect may be represented as a 'secondary flow' produced by the convection of the vorticity by the 'primary flow', that which would occur if stream vorticity were absent. Earlier work on these lines has been extended by Lighthill (1956, 1957*a*, *b*) by making use of the concept of the 'drift' of material fluid surfaces, discussed by Darwin (1953).

A second approach is to study small three-dimensional disturbances to a two-dimensional parallel stream or shear layer, without making any assumption that the stream vorticity is small. Lighthill (1957*c*) has examined the fundamental disturbance solution, that due to a small point source, and has shown that an equation for the velocity perturbation may be obtained by taking the Hankel transform of the Orr–Sommerfeld equation which governs small inviscid disturbances to the shear flow. The effects of more complicated small disturbances may be found by suitably differentiating and superposing such fundamental solutions. A basic assumption is that the source causes only a small proportionate change in velocity, and consequently the method cannot be applied for shear layers in which the stream velocity falls to zero at any finite point. Lighthill gives a very full account of the background to the problem, and obtains a great

deal of valuable information about the solutions of his equation in various cases. In particular he shows that difficulties as to the nature of secondary flow solutions can be resolved by matching the secondary flow at large distance from an obstacle to the form of the small-disturbance solution at small distance.

This paper describes an alternative theory to Lighthill's for deriving the perturbation due to a small source. The shear layer is replaced by a number of layers of uniform flow, separated by vortex sheets. It is shown that the effect of the vortex sheets can be represented by a series of image sources, and that when the number of sheets tends to infinity and their spacing tends to zero a continuous image source distribution is obtained, applicable to the continuous shear layer. The restrictions on the validity of the equations are precisely the same as in Lighthill's approach, and the majority of the chief deductions of each method of analysis can be obtained by the other, in complete accord with one another in all cases.

However, the development of this alternative theory justifies itself on a number of grounds. Each of the theories may serve to stimulate development in the other, and there are important results on each side which have not yet been proved by means of the rival theory. In addition, the image system is helpful in indicating a simple physical model of the flow in a disturbed shear layer. It is not easy to visualize in detail the effect of the stretching and bending of vortex lines, and meditating on the image source distribution may lead to a better understanding of phenomena for which untutored physical intuition provides no clear guide.

2. Single vortex sheet

Consider an unbounded volume of homogeneous incompressible fluid such that, with Cartesian co-ordinates (x, y, z), the fluid in $y > 0$ (the upper region) has uniform velocity U_1 in the x-direction and in $y < 0$ (the lower region) has uniform velocity U_0 in the same direction. Thus $y = 0$ is a vortex sheet of strength $U_1 - U_0$. Suppose that there is a three-dimensional point source of fluid of small strength M at the point O in the lower region, at a distance h from the interface. Let us try to find the effect of this source by use of the method of images.

We postulate that the flow perturbation in the lower fluid is that due to M itself together with a source m_i (i for image) at O_1, the mirror image of O in the interface $y = 0$, and that the perturbation in the upper fluid is that due to a source m_t (t for transmitted) at O. There can of course be no source at O_1 for the flow in the upper region, since there is no actual singularity at this point. This representation will be legitimate only if the necessary conditions at the interface can be satisfied by a suitable choice of the values of m_i and m_t. These conditions are that the pressure shall be continuous, and that continuity shall be satisfied, which requires that the displacement of the interface in the y-direction be the same in the two regions.

Let the perturbation velocity at (x, y, z) be (u, v, w) and suppose that the source M is so small that on the interface squares and products of u, v and w may be neglected. Then by Bernoulli's equation the first of our conditions requires that over the interface, for equal increments of pressure in the two regions, $U_0 u_0 = U_1 u_1$,

where the suffixes 0 and 1 indicate the lower and upper regions respectively. For small disturbances this condition may be applied on $y = 0$, the undisturbed interface, and it is satisfied by our image source distribution provided that

$$U_0(M + m_i) = U_1 m_t. \tag{2.1}$$

At a fixed position the displacement of a streamline due to a small source is inversely proportional to the stream velocity, and hence our second condition is satisfied if

$$\frac{M - m_i}{U_0} = \frac{m_t}{U_1}. \tag{2.2}$$

An alternative method of obtaining (2.2) is to interpret the continuity condition as requiring that the flow directions in the upper and lower fluids shall be compatible at the interface, and so v/U must be continuous.

From equations (2.1) and (2.2) we obtain

$$m_i = \left(\frac{U_1^2 - U_0^2}{U_1^2 + U_0^2}\right) M, \quad m_t = \left(\frac{2U_1 U_0}{U_1^2 + U_0^2}\right) M. \tag{2.3}$$

Certain special forms of these expressions are of interest. For a free surface at $y = 0$, $U_1 = 0$ and we have

$$m_i = -M, \quad m_t = 0. \tag{2.4}$$

This is a familiar result, used in the theory of wind-tunnel interference. The case of a solid boundary at $y = 0$ is obtained by putting $U_1 = \infty$, since the upper fluid then has infinite momentum and so no displacement of the interface can occur. We then have

$$m_i = M, \quad m_t = 0. \tag{2.5}$$

This value of m_i is well known from the elementary theory of the method of images, and is valid no matter how large the value of M.

An immediate practical application of the type of analysis we have been using concerns the effect at large distance of a small point source M at the origin in a shear layer of limited width. Suppose that the stream velocity varies from U_{-1} to U_1, the stream velocity at the level of the source being U_0. For numerically large values of y the shear layer may be treated as a single vortex sheet. Above the layer the flow perturbation is that due to a source m_1, and below the layer that due to a source m_{-1}, each source being at the origin. As in (2.1), pressure continuity along the vortex sheet requires

$$m_1 U_1 = m_{-1} U_{-1}. \tag{2.6}$$

The fluid from the source flows downstream to form a tube of cross-sectional area M/U_0, and displaces the surrounding stream surfaces outwards by this amount. Equating this to the displacements in the upper and lower fluids due to the effective sources, we have

$$\frac{M}{U_0} = \frac{m_1}{2U_1} + \frac{m_{-1}}{2U_{-1}}, \tag{2.7}$$

since in each case only half the flux from the source enters the appropriate region. This equation takes the place of (2.2). From equations (2.6) and (2.7) we obtain

$$m_1 = \frac{2U_1 U_{-1}^2}{U_0(U_1^2 + U_{-1}^2)} M, \quad m_{-1} = \frac{2U_1^2 U_{-1}}{U_0(U_1^2 + U_{-1}^2)} M. \tag{2.8}$$

By use of his Hankel transform method, Lighthill (1957*c*) obtained the same result, though with greater labour, and he also found the effective displacements of the sources m_1 and m_{-1} from the plane $y = 0$. The present analysis, which was briefly mentioned by Lighthill, has no obvious extension which would enable these displacements to be calculated.

3. Multiple vortex sheets

We now consider a flow in which there are a number of vortex sheets in planes $y =$ constant, separating layers in each of which there is a uniform stream in the x-direction. By taking the vortex sheets to be sufficiently numerous and closely spaced we shall then be able to deduce results applicable to a shear flow, with continuously varying velocity.

Assume that the vortex sheets are spaced at equal intervals δ and that the perturbing source M, at $y = 0$, is at a point midway between two of the sheets. Let U_r be the stream velocity in the rth layer, with centre at $y = r\delta$. In this rth layer, we shall seek to represent the flow perturbation as that due to a set of image sources $m_{r,s}$, $s = 0, \pm 1, \pm 2, \ldots$, where s indicates the layer in the centre of which the image is located, all the images being on the line in the y-direction through the source M.

The conditions which must be satisfied at the interface between the rth and $(r+1)$th layers are that the pressure perturbation and the interface deflexion shall be consistent on the two sides, precisely as for equations (2.1) and (2.2). Furthermore, since sources at different distances produce effects which vary in different manners over the interface, the set of sources at each particular distance must satisfy the conditions separately. Thus for the sources at a distance $(k-\frac{1}{2})\delta$ from the interface we require

$$U_r(m_{r,r+k} + m_{r,r-k+1}) = U_{r+1}(m_{r+1,r+k} + m_{r+1,r-k+1}), \tag{3.1}$$

$$\frac{1}{U_r}(m_{r,r+k} - m_{r,r-k+1}) = \frac{1}{U_{r+1}}(m_{r+1,r+k} - m_{r+1,r-k+1}). \tag{3.2}$$

Eliminating $m_{r+1,r-k+1}$ and $m_{r,r+k}$, respectively, we may replace (3.1) and (3.2) by the equivalent pair of equations

$$(U_{r+1}{}^2 + U_r{}^2)\, m_{r,r+k} = (U_{r+1}{}^2 - U_r{}^2)\, m_{r,r-k+1} + 2U_{r+1}U_r m_{r+1,r+k}, \tag{3.3}$$

$$(U_{r+1}{}^2 + U_r{}^2)\, m_{r+1,r-k+1} = 2U_{r+1}U_r m_{r,r-k+1} - (U_{r+1}{}^2 - U_r{}^2)\, m_{r+1,r+k}. \tag{3.4}$$

In addition, from the known presence or absence of sources in the layers themselves,

$$m_{0,0} = M, \quad \text{and} \quad m_{r,r} = 0 \quad (r \neq 0). \tag{3.5}$$

Equation (3.5) gives the terms of the array $m_{r,s}$ on the principal diagonal, and in equations (3.3) and (3.4) the terms on the right are $(k-1)$ steps from the principal diagonal while the terms on the left are k steps away. Hence the calculation of the terms $m_{r,s}$ may be carried stage-by-stage away from the principal diagonal, by taking successively $k = 1, 2, 3, \ldots$.

It is possible to obtain a relation between four neighbouring image sources

by elimination between (3.3) and the forms of equations (3.3) and (3.4) with r replaced by $r-1$ and k by $k-1$. The result is

$$\frac{2U_rU_{r-1}}{U_r^2-U_{r-1}^2}m_{r-1,s-1}+\frac{2U_{r+1}U_r}{U_{r+1}^2-U_r^2}m_{r+1,s+1}=\frac{U_r^2+U_{r-1}^2}{U_r^2-U_{r-1}^2}m_{r,s-1}+\frac{U_{r+1}^2+U_r^2}{U_{r+1}^2-U_r^2}m_{r,s+1}. \tag{3.6}$$

This equation may also be used to calculate successively the sources $m_{r,s}$.

Certain general points are worth attention. As is readily proved from (3.3) and (3.4) by induction over k, $m_{r,s}$ depends only on the terms on the principal diagonal between $m_{u,u}$ and $m_{v,v}$ inclusive, where $u, v = r \pm |r-s|$; indeed it is a linear combination of these terms. It follows from (3.5) that

$$m_{r,s}=0 \quad \text{for} \quad |r-s|<r. \tag{3.7}$$

Thus for the flow in any layer there are no image sources nearer than the source M itself. An immediate consequence of (3.3) and (3.4) is that if $U_r = U_{r+1}$, then $m_{r,s} = m_{r+1,s}$, and hence as expected the image pattern is the same in the two layers. Near the principal diagonal non-zero images occur only for small values of r, and their strengths depend on the distribution of stream velocity near M itself. It is interesting to compare this with one of Lighthill's main deductions; that when expanded in powers of distance from the source the first-order perturbation is just the source flow itself, and the second-order perturbation depends only on the velocity and shear at $y = 0$.

4. Continuous velocity distribution

For a flow in which the stream velocity U in the x-direction is a continuously varying function of y, equations for the image source distribution representing the effects of a small source M at the origin may be deduced from the analysis of the last section, by taking the layer thickness δ to be small, and replacing U_r and $m_{r,s}$ by $U(y)$ and $m(y,s)$. Thus at the point (x,y,z) the perturbation to the flow is determined by a source distribution along the y-axis, of strength per unit length $m(y,s)$ at $(0,s,0)$.

In equations (3.3) and (3.4) we replace $U_{r+1}-U_r$ by $U'\delta$, where the dash denotes differentiation, and ignore δ^2. Each equation leads to

$$\frac{\partial m}{\partial y}(y,s)+\frac{U'}{U}m(y,2y-s)=0. \tag{4.1}$$

To obtain an equation for $m(y,s)$ alone, replace s by $2y-s$ in (4.1), giving

$$\frac{\partial m}{\partial y}(y,2y-s)+\frac{U'}{U}m(y,s)=0. \tag{4.2}$$

Here the first term is to be interpreted as the value of $(\partial/\partial y)\,m(y,s)$ at the point $(y,2y-s)$ in the ys-plane. Differentiation of (4.1) with respect to y and s respectively gives

$$\frac{\partial^2 m}{\partial y^2}(y,s)+\left(\frac{U''}{U}-\frac{U'^2}{U^2}\right)m(y,2y-s)+\frac{U'}{U}\frac{\partial m}{\partial y}(y,2y-s)+2\frac{U'}{U}\frac{\partial m}{\partial s}(y,2y-s)=0, \tag{4.3}$$

$$\frac{\partial^2 m}{\partial y\,\partial s}(y,s)-\frac{U'}{U}\frac{\partial m}{\partial s}(y,2y-s)=0, \tag{4.4}$$

and substitution in (4.3) from equations (4.1), (4.2) and (4.4) leads to the required equation for $m(y, s)$

$$\frac{\partial^2 m}{\partial y^2} + 2\frac{\partial^2 m}{\partial y \partial s} + \left(\frac{U'}{U} - \frac{U''}{U'}\right)\frac{\partial m}{\partial y} - \frac{U'^2}{U^2} m = 0. \tag{4.5}$$

This is the fundamental equation for the source function. It may also be deduced directly from (3.6). We are interested in solutions for which $m = 0$ on the line $y = s$, except for a singular source M at $y = 0$, i.e.

$$\lim_{\epsilon \to 0} \int_{-\epsilon}^{\epsilon} m(0, s)\, ds = M, \quad \text{or} \quad m(0, s) = M\delta(s). \tag{4.6}$$

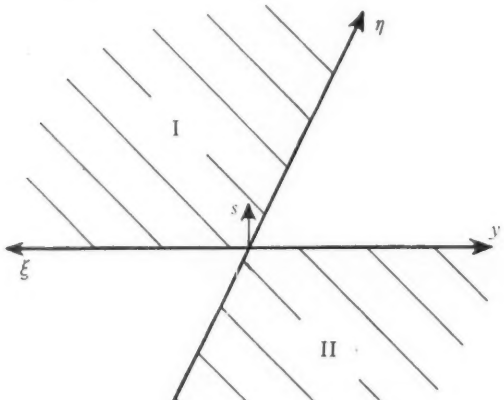

FIGURE 1. The regions I and II in the ys-plane in which the image source distribution $m(y, s)$ is non-zero.

Equation (4.5) is a hyperbolic equation, with characteristics $s - 2y =$ constant and $s =$ constant, and we may conveniently introduce characteristic variables

$$\xi = s - 2y, \quad \eta = s. \tag{4.7}$$

The effects of the source M are therefore confined to the two regions I ($\xi > 0$, $\eta > 0$) and II ($\xi < 0$, $\eta < 0$), as shown in figure 1. This is as was to be anticipated from (3.7). The equation (4.5) may be solved separately for the two regions, though the solutions are connected by (4.1), which relates conditions at a point in I to conditions at a point in II.

As regards the boundary conditions which apply along the boundaries $\xi = 0$ and $\eta = 0$, it is clear from (4.1) with $s = 0$ and (4.6) that there is a singular source of constant strength $M\delta(s)$ along the whole of the y-axis, since m is finite on the line $s - 2y = 0$. Consider next (4.1) with s constant, equal to $2y_1 > 0$, and integrate with respect to y over a short interval including $y = y_1$. Since $m = 0$ for $y > y_1$, the left-hand side gives $-m(y_1, 2y_1)$. The right-hand side gives

$$\lim_{\epsilon \to 0} \frac{U'}{U}(y_1) \int_{-\epsilon}^{\epsilon} m(y_1, 2\theta)\, d\theta = \tfrac{1}{2} M \frac{U'}{U}(y_1).$$

The required boundary condition at $\xi = 0$ in I is therefore

$$m(y, 2y) = \tfrac{1}{2}M\frac{U'}{U}(y) \quad (\eta > 0). \tag{4.8}$$

A similar calculation shows that the corresponding boundary condition at $\xi = 0$ in II is

$$m(y, 2y) = -\tfrac{1}{2}M\frac{U'}{U}(y) \quad (\eta < 0). \tag{4.9}$$

The boundary conditions at $\eta = 0$ are now given by a further application of (4.1). In I, $y < 0$ on $s = 0$ and hence we have

$$\frac{\partial m}{\partial y}(y, 0) = \tfrac{1}{2}M\left\{\frac{U'}{U}(y)\right\}^2 \quad (\xi > 0), \tag{4.10}$$

on making use of (4.9), as is appropriate since the point $(y, 2y)$ is in II. The corresponding condition at $\eta = 0$ in II is

$$\frac{\partial m}{\partial y}(y, 0) = -\tfrac{1}{2}M\left\{\frac{U'}{U}(y)\right\}^2 \quad (\xi < 0). \tag{4.11}$$

These conditions (4.8)–(4.11) are sufficient for the complete solution of (4.5). To be precise, they should be interpreted as giving the limiting values as the boundary is approached from within the region in question, since m is discontinuous or singular on the boundary. It is easy to write down integrated forms of (4.10) and (4.11) which give $m(y, 0)$ directly, since $m(0, 0)$ is known from equations (4.8) and (4.9), but the forms given are usually the most convenient.

Before proceeding further we must refer to an important point in regard to the velocity field which corresponds to the source distribution. For uniform flow with velocity discontinuities, as considered in §3, the perturbation velocity presents no difficulties, being merely that due to the set of image sources appropriate for the particular layer. But for a continuously varying stream the velocity field due to the source distribution $m(y, s)$, $-\infty < s < \infty$, is not the whole perturbation velocity. The stream surface at (x, y, z) has been displaced a distance d, say, in the y-direction from its undisturbed position, and in consequence the stream velocity at (x, y, z) is that at $(x, y-d, z)$ in the undisturbed flow. Thus there is an additional perturbation velocity in the x-direction of amount $u_c = -dU'$, since d is small for a weak source. Now we may write

$$d = \int_{-\infty}^{x} \frac{v}{U}\,dx, \tag{4.12}$$

since the perturbation is small and hence

$$u_c = -\frac{U'}{U}\int_{-\infty}^{x} v\,dx, \quad \frac{\partial u_c}{\partial x} = -\frac{U'}{U}v. \tag{4.13}$$

The velocity given by (4.13) makes a contribution to the continuity equation

$$\frac{\partial u}{\partial x} + \frac{\partial v}{\partial y} + \frac{\partial w}{\partial z} = 0, \tag{4.14}$$

which must be satisfied everywhere except at the origin. This at first looks unpromising, but it is soon apparent that the velocity field due to the image sources themselves does *not* satisfy (4.14). The flow due to a fixed set of sources would of course do so, and the displacements which determine $\partial u/\partial x$ and $\partial w/\partial z$ do not involve any change in the source distribution. But a displacement in the y-direction does cause the image system $m(y, s)$ to alter, and so $\partial v/\partial y$ contains an extra, unbalanced, term. We can show that this term is precisely that needed to cancel the contribution from (4.13).

Due to the image sources, the velocity in the y-direction at (x, y, z) is

$$v = \int_{-\infty}^{\infty} m(y, s) \frac{y-s}{4\pi\rho^3} ds, \tag{4.15}$$

where ρ is the distance between the points $(0, s, 0)$ and (x, y, z). The unbalanced term in $\partial v/\partial y$ is that due to the variation of $m(y, s)$, namely

$$\begin{aligned} \int_{-\infty}^{\infty} \frac{\partial m}{\partial y}(y, s) \frac{y-s}{4\pi\rho^3} ds &= -\frac{U'}{U} \int_{-\infty}^{\infty} m(y, 2y-s) \frac{y-s}{4\pi\rho^3} ds \\ &= \frac{U'}{U} \int_{-\infty}^{\infty} m(y, s_1) \frac{y-s_1}{4\pi\rho_1{}^3} ds_1 \\ &= \frac{U'}{U} v \end{aligned} \tag{4.16}$$

by (4.1), where $s_1 = 2y - s$ and ρ_1 is the distance between $(0, s_1, 0)$ and (x, y, z). This is the required result, and confirms the consistency of our equations.

It may be remarked that all our analysis may be applied immediately to the simpler problem of a purely two-dimensional disturbed flow. If the point source M at the origin is replaced by a line source of strength M per unit length along the z-axis, the strength of the image source distribution $m(y, s)$ has precisely the same form as for the three-dimensional flow with the same stream velocity $U(y)$, since all the conditions used in deriving the equations for $m(y, s)$ are unchanged. The velocity field is of course different, since the velocity due to each source element falls off like the inverse first power instead of the inverse square of the distance from the source.

A further point of interest concerns the nature of the fluid emitted from the source. In the discrete-layer model of the shear flow described in § 3, the fluid from the source emerges into a layer of uniform stream velocity, and naturally is itself irrotational. The source is not affected by the limiting process in which the layers become increasingly narrow and numerous, and so in the continuous-velocity flow the source fluid is still irrotational. In two-dimensional perturbed flow with constant verticity ω_0, this is not always assumed to be the case. It is then often convenient to write down a solution for the velocity field which has vorticity ω_0 everywhere, including the regions occupied by fluid which has emerged from a source. Such solutions are therefore not immediately comparable with the results of the present theory.

In this paper we shall make no further reference to the case of purely two-dimensional disturbed flow. The calculation of the corresponding velocity field presents no new difficulties.

5. Special solutions

Further progress can be made only with more definite assumptions about the form of the stream velocity distribution $U(y)$. We shall here concentrate chiefly on simple shear flow, for which $U = a(y+y_0)$, but first we shall briefly investigate what other velocity distributions are tractable.

First, we may note that (4.5) is unchanged if $U(y)$ is replaced by $U^*(y) = 1/U(y)$, and hence the same general solution $m(y, s)$ is applicable. The boundary conditions (4.8) and (4.9) change sign, but not conditions (4.10) and (4.11), and so the particular solution required will be different.

The form of (4.5) is simplified in three cases. These are when the coefficient of m is zero, when the coefficient of $\partial m/\partial y$ is zero, and when the equation can be immediately integrated with respect to y. We shall examine each of these in turn, and shall find that the special cases considered by Lighthill (1957*c*) will all be included.

The term $(U'^2/U^2)\,m$ in (4.5) is small compared with the other terms when the relative velocity change through the sheer layer is small. If this term is neglected (4.5) becomes

$$\left(\frac{\partial}{\partial y}+2\frac{\partial}{\partial s}\right)\log\left(\frac{U}{U'}\frac{\partial m}{\partial y}\right) = 2\frac{\partial}{\partial \eta}\log\left(\frac{U}{U'}\frac{\partial m}{\partial y}\right) = 0, \tag{5.1}$$

on introducing the characteristic variables (4.7). Hence

$$\frac{\partial m}{\partial y} = \frac{U'}{U}F(\xi) = \frac{U'}{U}F(s-2y), \tag{5.2}$$

where $F(\xi)$ is an arbitrary function. In region I, (4.10) shows that

$$F(-2y) = \tfrac{1}{2}M\frac{U'}{U}(y).$$

Equation (5.2) can now be integrated with respect to y to give

$$m = G(s)+\tfrac{1}{2}M\int_{\frac{1}{2}s}^{y}\frac{U'}{U}(t)\frac{U'}{U}(t-\tfrac{1}{2}s)\,dt. \tag{5.3}$$

From (4.8) the arbitrary function $G(s)$ satisfies

$$G(2y) = \tfrac{1}{2}M\frac{U'}{U}(y).$$

The solution for region I is therefore

$$m = \tfrac{1}{2}M\frac{U'}{U}(\tfrac{1}{2}s)-\tfrac{1}{2}M\int_{y}^{\frac{1}{2}s}\frac{U'}{U}(t)\frac{U'}{U}(t-\tfrac{1}{2}s)\,dt. \tag{5.4}$$

In region II, the boundary conditions (4.9) and (4.11) show that the required expression for m is that of (5.4), with the sign changed.

The solution may be improved by using (5.4) to approximate to the neglected term in (4.5). The integration to find the extra contribution to m is quite straight-

forward, and the boundary conditions have already been satisfied exactly. The result for region I is

$$\frac{2m}{M} = \frac{U'}{U}(\tfrac{1}{2}s) - \int_y^{\frac{1}{2}s} \frac{U'}{U}(t)\frac{U'}{U}(t-\tfrac{1}{2}s)\,dt - \int_y^{\frac{1}{2}s} \frac{U'}{U}(u)\,du \int_0^{\frac{1}{2}s} \frac{U'}{U}(t+u-\tfrac{1}{2}s)\frac{U'}{U}(t)\,dt$$
$$+ \int_y^{\frac{1}{2}s} \frac{U'}{U}(v)\,dv \int_0^{\frac{1}{2}s} \frac{U'}{U}(u+v-\tfrac{1}{2}s)\,du \int_{u+v-\frac{1}{2}s}^{u} \frac{U'}{U}(t)\frac{U'}{U}(t-u)\,dt. \quad (5.5)$$

In region II the sign is changed. The process of successive approximation may be repeated as often as required.

Lighthill (1957*c*) considered a shear layer with what he called 'small velocity spread', and obtained the equivalent of the first term of (5.5) in the form $m = \frac{1}{2}MU'(\frac{1}{2}s)/U(0)$. A direct application of the formulae of §2 leads to this result, and indeed also to the fuller result (5.5), and is of interest as indicating the physical significance of the successive terms in the solution.

Suppose that the shear layer is replaced by N layers of uniform flow, each of thickness δ, separated by vortex sheets each of strength $O(\epsilon)\,U$, where ϵ is small. From (2.3) the transmitted source at one of the vortex sheets is $M\{1+O(\epsilon^2)\}$, and hence from the source at the origin to the observation point (x, y, z) the transmitted source is changed to $M\{1+O(N\epsilon^2)\}$. The shear layer may be considered to be the limiting case where $\delta \to 0$, $N \to \infty$ and $\epsilon \to 0$, the total velocity change of magnitude $O(N\epsilon)\,U$ remaining fixed. The source M is therefore transmitted unaltered. From (2.3) the image source m_i due to a velocity discontinuity $k\epsilon U$ passing through $(0, l, 0)$, where $l > y > 0$, is $m_i = M\{k\epsilon + O(\epsilon^2)\}$. These images sources m_i are spaced at intervals 2δ along the y-axis, and so the source density at $(0, 2l, 0)$ is approximately $Mk\epsilon/2\delta$. Now as $\delta \to 0$, $k\epsilon/\delta \to (U'/U)\,(l)$, and hence the sources m_i combine to form the distribution $m(y, s) = \frac{1}{2}M(U'/U)\,(\frac{1}{2}s)$, $s > 2y$, exactly as given by the first term of (5.5). For $0 < l < y$ there is no image source m_i and for $l < 0$ there is agreement in region II, as is seen most easily by reversing the direction of the y-axis.

The primary images m_i which are appropriate at $(0, t, 0)$ will have secondary images in the vortex sheet passing through this point, provided that they are on the same side of the sheet as the observation point (x, y, z). The total strength of the primary images is $O(N\epsilon)\,M$, and hence the set of secondary images in the N discontinuities has total strength $O(N^2\epsilon^2)\,M$. If the relative velocity spread across the layer is small, $N\epsilon$ is small, and only the primary images are of importance. This is in accord with Lighthill's result. The source density due to the secondary images may be shown to agree with the second term of (5.5), by an extension of the analysis given above. That the velocity discontinuities are appropriately situated is seen by constructing diagrams as shown in figure 2, considering the image sources to be due to reflexions in the vortex sheets. Further diagrams and calculations check that the later terms of (5.5) correctly represent the effects of third- and fourth-order images. The physical interpretation of the terms in the series solution (5.5) is thus well established.

If the velocity is uniform outside the range $-a < y < b$, the primary images are clearly confined to the interval $-2a < s < 2b$, and the secondary images are

confined to $-2(a+b) < s < 2(a+b)$, for otherwise the corresponding integrand in (5.5) is nowhere non-zero. In each case there are no sources in the range $|s-y| < y$. Similarly, the third-order images are confined to

$$-4a-2b < s < 2a+4b,$$

and the fourth order to $-4(a+b) < s < 4(a+b)$. These results are also readily deduced from diagrams like those of figure 2.

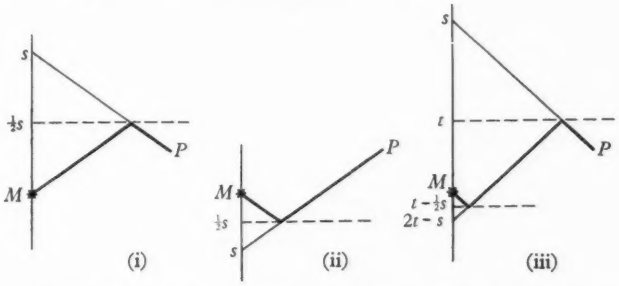

FIGURE 2. Illustrations of the location of primary and secondary images of the point source M at the origin, as observed at $P(x, y, z)$: (i) a primary image with $s > 2y > 0$; (ii) a primary image with $s < 0$; (iii) a secondary image. ———, paths of reflexion; – – – –, vortex sheets at which reflexion takes place.

In the second case we are to examine, the coefficient of $\partial m/\partial y$ in (4.5) is zero. This occurs when $U'/U = U''/U'$, i.e. when $U = a\,e^{\lambda y}$, where a and λ are constants. This case proved easy to solve by Lighthill's method. Equation (4.5) reduces to

$$\frac{\partial^2 m}{\partial y^2} + 2\frac{\partial^2 m}{\partial y\,\partial s} - \lambda^2 m = 0, \tag{5.6}$$

which in terms of the variables (ξ, η) of (4.7) becomes

$$4\frac{\partial^2 m}{\partial \xi\,\partial \eta} + \lambda^2 m = 0. \tag{5.7}$$

The boundary conditions (4.8) and (4.10) in region I give

$$m(0,\eta) = \tfrac{1}{2}M\lambda, \quad m(\xi,0) = \tfrac{1}{2}M\lambda(1-\tfrac{1}{2}\lambda\xi). \tag{5.8}$$

The required solution of (5.7) is readily deduced from the form of solution given by Courant & Hilbert (1937, ch. v, § 4.3). It is

$$\begin{aligned}\frac{2m}{M\lambda} &= J_0(\lambda\xi^{\frac{1}{2}}\eta^{\frac{1}{2}}) - \xi^{\frac{1}{2}}\eta^{-\frac{1}{2}}J_1(\lambda\xi^{\frac{1}{2}}\eta^{\frac{1}{2}}) \\ &= J_0\{\lambda(s-2y)^{\frac{1}{2}}\,y^{\frac{1}{2}}\} - (s-2y)^{\frac{1}{2}}\,s^{-\frac{1}{2}}J_1\{\lambda(s-2y)^{\frac{1}{2}}\,s^{\frac{1}{2}}\}.\end{aligned} \tag{5.9}$$

For region II the boundary conditions (5.8) have their signs changed, and remembering that ξ and η are negative the solution is seen to be

$$\begin{aligned}\frac{2m}{M\lambda} &= -J_0\{\lambda(-\xi)^{\frac{1}{2}}(-\eta)^{\frac{1}{2}}\} - (-\xi)^{\frac{1}{2}}(-\eta)^{-\frac{1}{2}}J_1\{\lambda(-\xi)^{\frac{1}{2}}(-\eta)^{\frac{1}{2}}\} \\ &= -J_0\{\lambda(2y-s)^{\frac{1}{2}}(-s)^{\frac{1}{2}}\} - (2y-s)^{\frac{1}{2}}(-s)^{-\frac{1}{2}}J_1\{\lambda(2y-s)^{\frac{1}{2}}(-s)^{\frac{1}{2}}\}.\end{aligned} \tag{5.10}$$

The velocity distribution corresponding to this source distribution may be worked out by precisely the same techniques as those employed in §6, and the author has confirmed that the formulae given by Lighthill (1957*c*) are obtained, on making use of standard integral relations between Bessel functions.

The third special case is that in which (4.5) is immediately integrable with respect to y. For this to be possible

$$\frac{d}{dy}\left(\frac{U'}{U}-\frac{U''}{U'}\right)=-\frac{U'^2}{U^2},$$

and hence

$$\frac{U''}{U}+\frac{U''^2}{U'^2}-\frac{U'''}{U'}=0. \tag{5.11}$$

This is satisfied if $U''=0$, which is simple shear flow $U=a(y+y_0)$. If $U''\neq 0$, (5.11) multiplied by U'/U'' may be integrated to give

$$\log(UU'/U'')=\text{constant}. \tag{5.12}$$

A further integration gives

$$U'=c+dU^2, \tag{5.13}$$

where c and d are constants. The integral of this equation takes one of the forms $U=a(y+y_0)$, $a/(y+y_0)$, $a\tan b(y+y_0)$, $a\tanh b(y+y_0)$, $a\coth b(y+y_0)$. For all these velocity distributions the integration of (4.5) proceeds in a manner closely analagous to that for simple shear flow, to be treated in §6. It may be verified that for the stream $U=a\tanh b(y+y_0)$ the solution in region I is

$$m=Mb\frac{\sinh b(2y-s+y_0)}{\sinh by_0\sinh 2b(y+y_0)}, \tag{5.14}$$

in region II the sign being reversed. By suitable modifications of the constants a and b the solutions for the other streams listed above may now be written down.

It may be argued that some of these velocity distributions are unrealistic, in view of the occurrence of points at which the velocity changes sign or becomes infinite. However, it is possible to consider that a form of velocity distribution holds only over a limited range of y, as will be seen in §7.

6. Simple shear flow

For simple shear flow, $U=a(y+y_0)$ and equation (4.5) becomes

$$\frac{\partial^2 m}{\partial y^2}+2\frac{\partial^2 m}{\partial y\,\partial s}+\frac{1}{y+y_0}\frac{\partial m}{\partial y}-\frac{1}{(y+y_0)^2}m=0. \tag{6.1}$$

This may be integrated immediately with respect to y to give

$$\frac{\partial m}{\partial y}+2\frac{\partial m}{\partial s}+\frac{m}{y+y_0}=G(s). \tag{6.2}$$

In terms of the variable (ξ,η) of (4.7) this may be written in the form

$$2\frac{\partial}{\partial\eta}\{m(y+y_0)\}=(y+y_0)\,G(s). \tag{6.3}$$

The boundary conditions (4.8) and (4.10) in region I are

$$m(y, 2y) = m(0, \eta) = \frac{\frac{1}{2}M}{y+y_0}, \tag{6.4}$$

$$\frac{\partial m}{\partial y}(y, 0) = \frac{\partial m}{\partial y}(\xi, 0) = \frac{\frac{1}{2}M}{(y+y_0)^2}, \tag{6.5}$$

and by applying (6.4) to equation (6.3) on the line $\xi = 0$ we see that $G(s) = 0$. We can therefore integrate (6.3) with respect to η to obtain

$$m(y+y_0) = F(\xi) = F(s-2y). \tag{6.6}$$

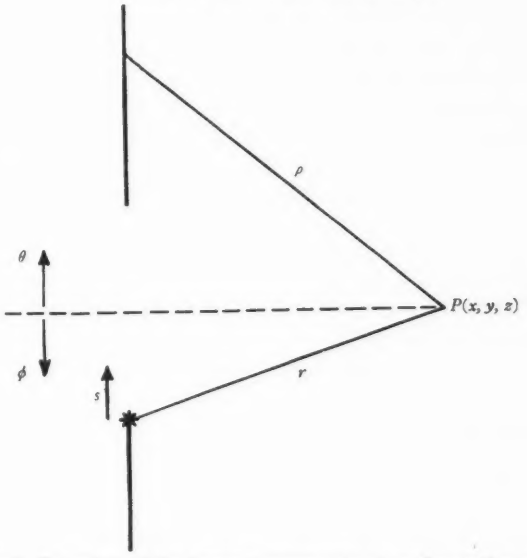

FIGURE 3. Location of the image sources $m(y, s)$, and notation used in calculating the velocity components.

On the line $s = 0$, (6.5) gives

$$m(y, 0) = \frac{M}{y_0} - \frac{M}{2(y+y_0)} = \frac{M(2y+y_0)}{2y_0(y+y_0)} \tag{6.7}$$

since, from (6.4), $m(0, 0) = \frac{1}{2}M/y_0$. Hence from (6.6)

$$m = \frac{M(2y-s+y_0)}{2y_0(y+y_0)}. \tag{6.8}$$

In region II the sign is changed in equations (6.4) and (6.5), and hence

$$m = -\frac{M(2y-s+y_0)}{2y_0(y+y_0)}. \tag{6.9}$$

Note that (6.8) is equal to the limiting value of (5.14) as $b \to 0$.

Consider now the velocity perturbation at the point $P(x, y, z)$ due to a source M at the origin. The image source strength $m(y, s)$ at $(0, s, 0)$ is given by (6.8) and (6.9). For $y > 0$ the situation is as shown in figure 3. It is convenient to introduce

co-ordinates θ and ϕ as shown, to describe the positions of the image sources in regions I and II respectively. Thus

$$\theta = s - y, \quad \phi = y - s. \tag{6.10}$$

In terms of these, equations (6.8) and (6.9) become

$$\left.\begin{aligned} \frac{2y_0 m}{M} &= 1 - \frac{\theta}{y+y_0} \quad (\theta > y), \\ \frac{2y_0 m}{M} &= -1 - \frac{\phi}{y+y_0} \quad (\phi > y). \end{aligned}\right\} \tag{6.11}$$

Pairs of points at which θ and ϕ are equal are symmetrically situated with respect to P, and hence the sources corresponding to the terms 1 and -1 in (6.11) have no net effect on u and w, and equal effects on v. Similarly, the other terms of (6.11) have no net effect on v, but equal effects on u and w.

The contribution to v from the source distribution (6.11) is

$$v_s = -\frac{M}{y_0}\int_y^\infty \frac{\theta}{4\pi\rho^3}\,d\theta = \frac{M}{4\pi y_0}\left[\frac{1}{\rho}\right]_y^\infty = -\frac{M}{4\pi y_0 r}, \tag{6.12}$$

where $\rho = (x^2+\theta^2+z^2)^{\frac{1}{2}}$ is the distance of the image source from P, and $r = (x^2+y^2+z^2)^{\frac{1}{2}}$. There is also the velocity due to the source M itself, giving $v_M = My/(4\pi r^3)$. The total y-component of the perturbation velocity is therefore

$$v = v_M + v_s = \frac{M}{4\pi}\left(\frac{y}{r^3} - \frac{1}{y_0 r}\right). \tag{6.13}$$

Similarly the x-component due to the source distribution is

$$u_s = -\frac{M}{y_0(y+y_0)}\int_y^\infty \theta\,\frac{x}{4\pi\rho^3}\,d\theta = -\frac{Mx}{4\pi y_0(y+y_0)r}, \tag{6.14}$$

the integral being of the same form as that occurring above, and $u_M = Mx/(4\pi r^3)$. We have also to include the convective component u_c as given by (4.13). This equation shows that

$$\frac{\partial u_c}{\partial x} = -\frac{v}{y+y_0} = -\frac{M}{4\pi(y+y_0)}\left(\frac{y}{r^3} - \frac{1}{y_0 r}\right),$$

and hence

$$u_c = -\frac{M}{4\pi(y+y_0)}\left\{\frac{xy}{(y^2+z^2)\,r} - \frac{1}{y_0}\log(r+x) + f(y,z)\right\}. \tag{6.15}$$

The arbitrary function $f(y,z)$ presents difficulties, since $\log(r+x)$ becomes logarithmically infinite at $x = \pm\infty$. If we require u_c to be zero at $x = 0$, then we should write $f(y,z) = (1/2y_0)\log(y^2+z^2)$, and

$$\begin{aligned} u &= u_M + u_s + u_c \\ &= \frac{M}{4\pi}\left\{\frac{x}{r^3} - \frac{x}{y_0(y+y_0)\,r} - \frac{xy}{(y+y_0)\,(y^2+z^2)\,r} + \frac{1}{2y_0(y+y_0)}\log\frac{r+x}{r-x}\right\}. \end{aligned} \tag{6.16}$$

Finally, w has precisely the same form as u, except that no convective term is present, and so

$$w = \frac{M}{4\pi}\left\{\frac{z}{r^3} - \frac{z}{y_0(y+y_0)\,r}\right\}. \tag{6.17}$$

These velocity components are in accord with those given by Lighthill (1957*c*). Although they have been derived only for $y > 0$, a consideration of the effect of reversing the direction of the y-axis shows that the formulae all hold unchanged for $y < 0$.

Lighthill described the infinity in u as 'an extremely discouraging feature'. The author's view is rather more optimistic. The occurrence of the infinity emphasizes the artificial nature of the assumption that the uniform shear extends indefinitely in all directions. In practice there are always constraining boundaries to limit the drift of streamlines. For that is what causes the trouble in (6.16). The displacement d in the y-direction of streamlines between $x = 0$ and $x = \pm\infty$, as given by (4.12), is logarithmically infinite. This is nothing peculiar to shear layers; the same is true for the flow with circulation past a cylinder. But it does indicate that in any attempt to make measurements of the Pitot-tube displacement effect the nature of the boundaries to the shear flow, however distant, has a vital influence. In some cases (6.16) could probably be used quite effectively by taking given undisturbed conditions to be attained not at $x = -\infty$ but at some plausible position $x = -x_0$. If the shear flow terminates at planes $y =$ constant, the modified image source distribution may be determined as shown below.

A more serious objection to placing reliance on the solution obtained in this section is that the stream velocity falls to zero at $y = -y_0$. This invalidates the basic assumption on which the whole method of analysis is based, starting from equations (2.1) and (2.2). Indeed we have no real reason to suppose that our solution is reliable *anywhere*, since the true source distribution $m(y, s)$, if one exists, might well obey conditions at $y = -y_0$ which are quite different from those obeyed by the solutions (6.8) and (6.9).

7. Bounded shear flows

In flows occurring in practice it will happen only rarely that the velocity distribution $U(y)$ in the undisturbed shear layer can be considered to have the same simple analytic form for all y. Either the flow will be terminated by solid or free boundaries, or the velocity will become uniform outside a certain range of values of y. The analysis given in this paper can be extended to determine the image source distribution for streams in which the form $U(y)$ changes abruptly at some value $y = -y_1$, the expressions for $U(y)$ in both the regions $y > -y_1$ and $y < -y_1$ being ones for which solutions have been found. A discontinuity in $U(y)$ at $y = -y_1$ is permissible.

For simplicity we shall here examine in detail only the stream consisting of simple shear flow $U = a(y + y_0)$ in the region $y > -y_1$ and uniform flow $U = U_0$ in $y < -y_1$. There is then a velocity discontinuity $U_1 - U_0$ at $y = -y_1$, where $U_1 = a(y_0 - y_1)$.

The regions of the ys-plane in which $m(y, s)$ has to be determined are shown in figure 4. In A and A^* the source distributions are given by equations (6.8) and (6.9), since the hyperbolic nature of (6.1) shows that the effects of the change at $y = -y_1$ cannot extend beyond the lines $2y - s + 2y_1 = 0$ and $s + 2y_1 = 0$. From (4.1), m is independent of y for $y < -y_1$, since U is constant, and in

particular $m = 0$ in C^*. The relations which hold across the line $y = -y_1$ are now given by equations (3.3) and (3.4) as

$$(U_1^2 + U_0^2)\, m(-y_1, s)_C = 2U_1 U_0 m(-y_1, s)_B, \tag{7.1}$$

$$m(-y_1, 2y - s)_{B^*} = \alpha m(-y_1, s)_B, \tag{7.2}$$

where $\alpha = (U_0^2 - U_1^2)/(U_0^2 + U_1^2)$. We also see from (3.4) or (2.3) that there is a concentrated source $\alpha M \delta(s + 2y_1)$ for $y > -y_1$ and hence, as for (4.8) and (6.4), m has a discontinuity $\frac{1}{2}\alpha M(y + y_0)$ on passing from A to B across the line $2y - s + 2y_1 = 0$.

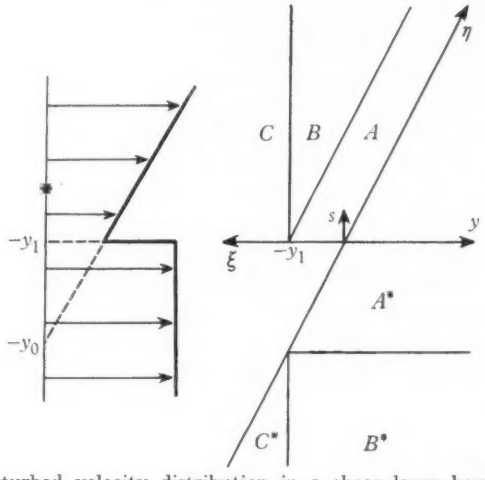

FIGURE 4. Undisturbed velocity distribution in a shear layer bounded at $y = -y_1$, and the regions of the ys-plane in which $m(y, s)$ has to be determined.

We require a more general solution of (6.3) than the form (6.8). If in (6.3) we for convenience replace the arbitrary function $G(s)$ by $4G''(s)$ the equation becomes

$$\frac{\partial}{\partial \eta}\{m(y + y_0)\} = (\eta - \xi + 2y_0)\, G''(\eta), \tag{7.3}$$

which gives on integration

$$m(y + y_0) = (\eta - \xi + 2y_0)\, G'(\eta) - G(\eta) + F(\xi). \tag{7.4}$$

Reverting to the variables (y, s) we obtain as the general solution of (6.3)

$$m = \frac{F(s - 2y)}{y + y_0} + \frac{2(y + y_0)\, G'(s) - G(s)}{y + y_0}. \tag{7.5}$$

The solution (6.8) is given by $F = \frac{1}{2}M(2y - s + y_0)/y_0$, $G = 0$ and also by $F = 0$, $G = \frac{1}{2}M(s + y_0)/y_0$. The first of these forms of solution may be said to be propagated in the η-direction (along lines ξ = constant) and the second in the ξ-direction (along lines η = constant). It is a useful fact that either form is appropriate for unlimited simple shear flow.

In the present problem the solution in region A may be taken to be in the η-direction, and consequently the same must be true in B, so that there

$$m = \frac{F(s-2y)}{y+y_0}. \tag{7.6}$$

The boundary condition (7.2) combined with (4.1) gives

$$\frac{\partial m}{\partial y}(-y_1, s) = -\frac{\alpha}{y_0-y_1} m(-y_1, s), \tag{7.7}$$

and on substituting the form (7.6) we obtain at once

$$F = F_0 \exp\left[\frac{(1-\alpha)(2y-s)}{2(y_0-y_1)}\right] \tag{7.8}$$

provided that $\alpha \neq 1$. The discontinuity of m on $2y-s+2y_1 = 0$, as found above, enables the constant F_0 to be determined and gives us the final result for region B

$$m = \frac{M\{(\alpha+1)y_0-2y_1\}}{2y_0(y+y_0)} \exp\left[\frac{(1-\alpha)(2y-s+2y_1)}{2(y_0-y_1)}\right]. \tag{7.9}$$

Equation (4.2) now shows that in B^*

$$m = \frac{M\{(\alpha+1)y_0-2y_1\}\{(\alpha-1)y+\alpha y_0-y_1\}}{2y_0(y_0-y_1)(y+y_0)} \exp\left[\frac{(1-\alpha)(s+2y_1)}{2(y_0-y_1)}\right]. \tag{7.10}$$

When $\alpha = 1$, (7.8) is replaced by $F = F_0$ and we obtain

$$m = \frac{M(y_0-y_1)}{y_0(y+y_0)} \tag{7.11}$$

in both B and B^*, as would be given by putting $\alpha = 1$ in equations (7.9) and (7.10). In region C equations (7.1) and (7.9), and the condition that m is independent of y, show that

$$m = \frac{2U_1U_0}{U_1^2+U_0^2} \frac{M\{(\alpha+1)y_0-2y_1\}}{2y_0(y_0-y_1)} \exp\left[\frac{(\alpha-1)s}{2(y_0-y_1)}\right], \tag{7.12}$$

and from (2.3) there is in addition a concentrated source

$$\frac{2U_1U_0}{U_1^2+U_0^2} M\delta(s)$$

for $y < -y_1$.

When $\alpha = 1$, $U_0 = \infty$. Such a stream could not be deflected by any finite pressure force, so the solution applies for a solid wall at $y = -y_1$. Other cases of practical interest are $\alpha = 0$, corresponding to no discontinuity of stream velocity at $y = -y_1$ but merely a change from uniform shear to constant velocity, and $\alpha = -1$, for which the fluid in the region $y < -y_1$ is at rest. Since $-1 \leqslant \alpha \leqslant 1$ the image source strength in both B and B^* decreases exponentially with distance from the origin (except when $\alpha = 1$), provided that $y_0 > y_1$, i.e. provided that there is no plane of zero stream velocity in the physical flow. If $y_0 < y_1$ the sources increase exponentially with distance, which again emphasizes the unreality of solutions for streams in which the velocity passes through zero.

The calculation of the velocity fields corresponding to these source distributions is a straightforward extension of that for an unbounded simple shear flow, although unless $\alpha = 1$ the results cannot be expressed in terms of elementary functions. For $\alpha = 1$, with a solid wall at $y = -y_1$, the image source distribution in terms of the co-ordinates θ and ϕ of (6.10) is given by

$$\frac{2y_0 m}{M} = \begin{cases} 2\dfrac{y_0 - y_1}{y - y_0} & (\theta > y + 2y_1), \\ 1 - \dfrac{\theta}{y + y_0} & (y + 2y_1 > \theta > y), \\ -1 - \dfrac{\phi}{y + y_0} & (y + 2y_1 > \phi > y), \\ 2\dfrac{y_0 - y_1}{y + y_0} & (\phi > y + 2y_1). \end{cases} \tag{7.13}$$

The integrations to find the velocity components are so similar to those of §6 that it will be sufficient to quote the results.

$$u = \frac{M}{4\pi(y+y_0)}\left\{x(y+y_0)\left(\frac{1}{r^3}+\frac{1}{r_1^3}\right)+\frac{x}{y_0}\left(\frac{1}{r_1}-\frac{1}{r}\right)+\frac{2(y_0-y_1)x}{u_0 r_1(r_1+y+2y_1)}\right.$$
$$\left.-\left[\frac{y}{r(r-x)}+\frac{y+2y_1}{r_1(r_1-x)}+\frac{1}{y_0}\log\frac{r-x}{r_1-x}\right]\right\}, \tag{7.14}$$

$$v = \frac{M}{4\pi}\left\{\frac{y}{r^3}+\frac{y+2y_1}{r_1^3}+\frac{1}{y_0}\left(\frac{1}{r_1}-\frac{1}{r}\right)\right\}, \tag{7.15}$$

$$w = \frac{M}{4\pi(y+y_0)}\left\{z(y+y_0)\left(\frac{1}{r^3}+\frac{1}{r_1^3}\right)+\frac{z}{y_0}\left(\frac{1}{r_1}-\frac{1}{r}\right)+\frac{2(y_0-y_1)z}{y_0 r_1(r_1+y+2y_1)}\right\}, \tag{7.16}$$

where $r_1 = \{x^2 + (y+2y_1)^2 + z^2\}^{\frac{1}{2}}$ is the distance from P to the concentrated image source M at $s = -2y_1$. The term in u enclosed in square brackets represents the convective component u_c, and the arbitrary function of y and z appearing in it has been chosen so that $u_c \to 0$ as $x \to -\infty$. The difficulty in this respect for an unlimited shear layer no longer arises, for any value of α.

The value (u_w, v_w, w_w) of the perturbation velocity at the wall is found by putting $y = -y_1$, $r_1 = r = (x^2 + y_1^2 + z^2)^{\frac{1}{2}}$ in equations (7.14), (7.15) and (7.16). The result is

$$v_w = 0, \quad \frac{u_w}{x} = \frac{w_w}{z} = \frac{M}{2\pi}\left\{\frac{1}{r^3}+\frac{1}{y_0 r(r+y_1)}\right\}. \tag{7.17}$$

8. Shear flow in a channel

When the shear flow is bounded both above and below, at $y = y_2$ and at $y = -y_1$, an infinite series of regions in the ys-plane has to be considered, corresponding to multiple reflexions in the boundaries. The regions are periodic in the s-direction with period $2(y_1 + y_2)$, as illustrated in figure 5. For simple shear flow $U = a(y + y_0)$ with solid boundaries at $y = y_2$ and $y = -y_1$ the image source distributions in A and B are given by equations (6.8) and (7.11). The source

distribution in C may also be deduced from (7.11) by reversing the direction of the y-axis and replacing y_0 by $-y_0$ and y_1 by y_2. We find that in C

$$m = -\frac{M(y_0+y_2)}{y_0(y+y_0)}, \tag{8.1}$$

and we also see that there is concentrated source $M\delta(s-2y_2)$ for $y < y_2$. Since the solution in the whole region made up of A, B, C and D must be expressible in the form (7.5), and so is the sum of solutions propagated in the ξ- and η-directions,

$$m_A + m_D = m_B + m_C, \tag{8.2}$$

which shows that in D

$$m = -\frac{M(2y-s+2y_1+2y_2+y_0)}{2y_0(y+y_0)}. \tag{8.3}$$

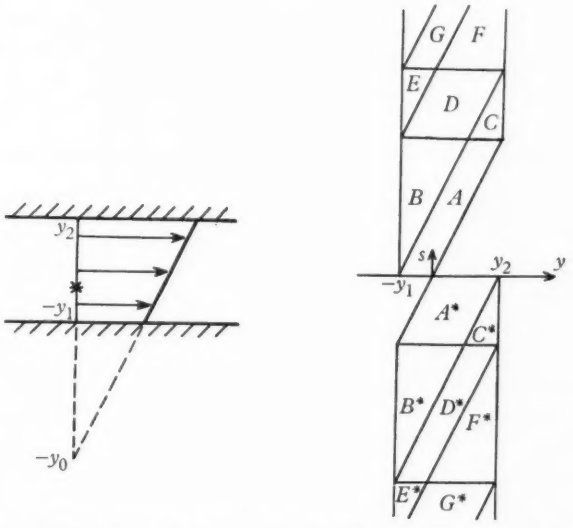

FIGURE 5. Undisturbed velocity distribution in a shear layer bounded at $y = -y_1$ and at $y = y_2$, and the regions of the ys-plane in which $m(y, s)$ has to be determined.

The regions D and A^* are seen from figure 5 to be geometrically identical, and furthermore a comparison of equations (6.9) and (8.3) shows that the source strengths at corresponding points are equal, since the point (y, s) in D corresponds to the point $(y, s-2y_1-2y_2)$ in A^*. Since conditions in D completely determine the source distribution in more distant regions it is clear that m is periodic in the s-direction, with period $2(y_1+y_2)$; in particular $m = 0$ in regions E, F, E^* and F^*. This is not true if the boundaries at $y = -y_1$ and $y = y_2$ are not solid, for then the source strengths in B and C vary exponentially with s, as shown by equations (7.9) and (7.10).

The evaluation of the velocity components corresponding to the periodic source distribution is aided by a formula derived by Olver (1949) and Reuter

(1949) which expresses the potential of an infinite row of point sources as a series of Bessel functions. The formula states that if $h(n) = \{x^2 + (y-n)^2\}^{-\frac{1}{2}}$, then

$$\sum_{-\infty}^{\infty} h(n) = \sum_{t=1}^{\infty} K_0(2\pi t x)\cos(2\pi t y) + \text{constant}. \tag{8.4}$$

Since $K_0(z) \sim (\pi/2z)\,e^{-z}$ as $z \to \infty$, the series converges rapidly unless x is very small. This formula and its derivatives with respect to x and y lead to the following results:

$$v = \frac{M}{\pi y_0(y_1+y_2)} \sum_{t=1}^{\infty} K_0\left(\frac{\pi t(x^2+z^2)^{\frac{1}{2}}}{y_1+y_2}\right)\left(\frac{\pi t y_0}{y_1+y_2}\cos\frac{\pi t y_1}{y_1+y_2} - \sin\frac{\pi t y_1}{y_1+y_2}\right)\sin\frac{\pi t(y+y_1)}{y_1+y_2}, \tag{8.5}$$

$$\begin{aligned}\frac{u-u_c}{x} = \frac{w}{z} = \frac{M}{\pi y_0(y_1+y_2)(y+y_0)(x^2+z^2)^{\frac{1}{2}}}\Bigg\{&\frac{(y_0-y_1)(y_0+y_2)}{2(x^2+z^2)^{\frac{1}{2}}} \\ &+ \sum_{t=1}^{\infty} K_1\left(\frac{\pi t(x^2+z^2)^{\frac{1}{2}}}{y_1+y_2}\right)\left(\frac{\pi t y_0}{y_1+y_2}\cos\frac{\pi t y_1}{y_1+y_2} - \sin\frac{\pi t y_1}{y_1+y_2}\right) \\ &\times\left((y+y_0)\cos\frac{\pi t(y+y_1)}{y_1+y_2} - \frac{y_1+y_2}{\pi t}\sin\frac{\pi t(y_2+y_1)}{y_1+y_2}\right)\Bigg\}.\end{aligned} \tag{8.6}$$

To these velocity components must be added the convective velocity component u_c, given by (4.13), which requires numerical integration.

At values of $(x^2+z^2)^{\frac{1}{2}}$ which are not large enough for the expansions to converge satisfactorily, the velocity components due to the nearest regions in the ys-plane may be calculated directly, and the source distribution in more distant regions may be replaced by a smoothed-out source of constant strength in the s-direction.

The bounded shear flows treated in this paper are only samples of the many types which may be successfully studied by use of the method of images. The techniques developed here and simple extensions of them lead to useful quantitative results in many other cases of interest, but the number of possible configurations is so large that there seems little point in attempting to compile a comprehensive list of solutions.

REFERENCES

Courant, R. & Hilbert, D. 1937 *Methoden der mathematischen Physik*, II. Berlin: Springer.

Darwin, C. G. 1953 *Proc. Camb. Phil. Soc.* **49**, 342.

Lighthill, M. J. 1956 *J. Fluid Mech.* **1**, 31.

Lighthill, M. J. 1957*a* *J. Fluid Mech.* **2**, 311.

Lighthill, M. J. 1957*b* *J. Fluid Mech.* **2**, 493.

Lighthill, M. J. 1957*c* *J. Fluid Mech.* **3**, 113.

Olver, F. W. J. 1949 *Quart. J. Mech. Appl. Math.* **2**, 452.

Reuter, G. E. H. 1949 *Quart. J. Mech. Appl. Math.* **2**, 457.

ries

8.4)

ery
ing

$_1$),
$_2$
8.5)

8.6)

ent

erge
ane
ons
ion.
any
The
an-
con-
le a

rlin:

Stability of a conducting rotating fluid of variable density

By S. P. TALWAR

Physics Department, Delhi University, Delhi, India

(Received 29 June 1960)

The Rayleigh instability of an incompressible, infinitely conducting, inviscid fluid of variable density is investigated under the influence of an horizontal magnetic field and coriolis forces. After establishing the equations of the problem when both the density and the magnetic field vary with distance in the upward direction, two special cases of density distribution are studied in detail. Both the magnetic field and coriolis forces are found to have a stabilizing influence on the configuration and further it is concluded that they may bring about stability in the configuration when it is thoroughly unstable without them.

1. Introduction

The problem of the hydromagnetic stability of conducting fluid of variable density is of considerable importance in astrophysics (e.g. in theories of sunspot magnetic fields, heating of solar corona, stability of the stellar atmospheres in magnetic field) and has been investigated in recent years by some workers (Hide 1955; Ferraro & Plumpton 1958). Talwar (1959) investigated the influence of a magnetic field on the character of the equilibrium of two superposed highly conducting fluids and of a stratified layer of highly conducting fluid. It was shown that the magnetic field has a stabilizing influence on the configuration and helps in bringing about stability in a configuration when it is thoroughly unstable without a field. However, in many astrophysical and geophysical problems, coriolis forces also play an important role and their effect may at least be as important as those of electromagnetic forces. Keeping this in mind, we investigate in the present paper the effect of a magnetic field on the equilibrium of an inviscid, incompressible, infinitely conducting *rotating* fluid of variable density. The density stratification may be supposed to be due to a change in composition. In §2 we shall establish the general equations of the problem, assuming that there is a variation of both density and the horizontal magnetic field with respect to distance in the upward direction alone. For simplicity, the fluid is assumed to be incompressible, inviscid, and of infinite electrical conductivity, so that the magnetic field assumed is effectively 'frozen' in the fluid. However, in a more realistic situation one should study the problem including the effects of viscosity, compressibility, and finite conductivity, and it is hoped to include them in a later communication.

Earlier, Lord Rayleigh (1883) initiated the study of the hydrodynamic stability of a fluid of variable density. Having developed the equations for a horizontally stratified, non-rotating, inviscid, incompressible fluid, he discussed

two special density variations corresponding to (*a*) two superposed fluids and (*b*) a continuously stratified fluid. Bjerknes, Bjerknes, Solberg & Bergeron (1933) extended Rayleigh's treatment for superposed fluids to include the effect of rotation. Further the investigation was extended by Chandrasekhar (1955) and Hide (1956) to include viscosity in the non-magnetic case without and with rotation, respectively.

2. Equations of the problem

Take axis $Oxyz$ such that Oz is vertical. Suppose that there exists a horizontal magnetic field (stratified upwards) along the x-direction in the fluid which is further assumed to have a variable density in the upward direction. Let the configuration rotate uniformly with an angular velocity Ω about the z-axis.

The equation of motion appropriate to the problem under consideration is,

$$\rho\frac{\partial\mathbf{u}}{\partial t}+\rho(\mathbf{u}.\nabla)\,\mathbf{u}-2\rho(\mathbf{u}\times\boldsymbol{\Omega})=-\nabla p+\mathbf{g}\rho+\frac{\mu}{4\pi}[(\nabla\times\mathbf{H})\times\mathbf{H}], \tag{1}$$

where $\mathbf{u}, \mathbf{H}$ denote the velocity and the magnetic field vectors and p, ρ, g respectively denote the pressure, density at a point and the acceleration due to gravity with component $-g$ in the z-direction (or g may denote the net acceleration downward in case there is an additional imposed acceleration over and above the usual gravitational acceleration). μ is the permeability of the medium.

The equation of continuity of matter is

$$\frac{\partial\rho}{\partial t}+\nabla.(\rho\mathbf{u})=0. \tag{2}$$

Since the fluid is heterogenous and incompressible and the diffusion effects are ignored, the density of an element does not alter as the element moves about; (2) then reduces to

$$\nabla.\mathbf{u}=0. \tag{3}$$

For a perfectly conducting fluid which is also incompressible we have

$$\frac{\partial\mathbf{H}}{\partial t}+(\mathbf{u}.\nabla)\,\mathbf{H}=(\mathbf{H}.\nabla)\,\mathbf{u}. \tag{4}$$

Finally we have the equation

$$\nabla.\mathbf{H}=0. \tag{5}$$

In order to investigate the stability of the static equilibrium configuration characterized by $\mathbf{u}=0$, let us consider the effect of a small velocity field disturbance $\mathbf{u}$, with components u, v, w in x-, y- and z-directions, respectively. We write,

$$\left.\begin{aligned}\rho&=\rho_0(z)+\delta\rho(x,y,z,t),\\ p&=p_0(z)+\delta p(x,y,z,t),\\ \mathbf{H}&=\mathbf{H}_0(z)+\mathbf{h}(x,y,z,t),\end{aligned}\right\} \tag{6}$$

where $\delta\rho$, δp, and $\mathbf{h}$ are perturbations of the first order of smallness so that powers higher than the first and their mutual products can be ignored. Hence the

equations for the first-order disturbance components, with an undisturbed horizontal field in the x-direction, can be written as

$$\rho_0 \frac{\partial u}{\partial t} - 2\rho_0 v\Omega = -\frac{\partial \delta p}{\partial x} + \frac{\mu}{4\pi} h_z \frac{dH_0}{dz}, \tag{7}$$

$$\rho_0 \frac{\partial v}{\partial t} + 2\rho_0 u\Omega = -\frac{\partial \delta p}{\partial y} + \frac{\mu}{4\pi} H_0 \left(\frac{\partial h_y}{\partial x} - \frac{\partial h_x}{\partial y} \right), \tag{8}$$

$$\rho_0 \frac{\partial w}{\partial t} = -\frac{\partial \delta p}{\partial z} - g\delta\rho - \frac{\mu}{4\pi} H_0 \left(\frac{\partial h_x}{\partial z} - \frac{\partial h_z}{\partial x} \right) - \frac{\mu}{4\pi} h_x \frac{dH_0}{dz}, \tag{9}$$

$$\frac{\partial u}{\partial x} + \frac{\partial v}{\partial y} + \frac{\partial w}{\partial z} = 0, \tag{10}$$

$$\frac{\partial \delta\rho}{\partial t} + w \frac{d\rho_0}{dz} = 0, \tag{11}$$

$$\frac{\partial h_x}{\partial t} = H_0 \frac{\partial u}{\partial x} - w \frac{dH_0}{dz}, \tag{12}$$

$$\frac{\partial h_y}{\partial t} = H_0 \frac{\partial v}{\partial x}, \tag{13}$$

$$\frac{\partial h_z}{\partial t} = H_0 \frac{\partial w}{\partial x}, \tag{14}$$

and

$$\frac{\partial h_x}{\partial x} + \frac{\partial h_y}{\partial y} + \frac{\partial h_z}{\partial z} = 0. \tag{15}$$

Suppose, as usual in problems of this kind, that the components of the disturbance vary with x, y, z, t as

$$(\text{some function of } z) . \exp (ik_x x + ik_y y + nt),$$

where k_x and k_y are the horizontal wave-numbers of the harmonic disturbance. On substituting in the above equations (7)–(15) we get

$$n\rho_0 u - 2\rho_0 v\Omega = -ik_x \delta p + (\mu/4\pi) h_z DH_0, \tag{16}$$

$$n\rho_0 v + 2\rho_0 u\Omega = -ik_y \delta p + (\mu H_0/4\pi)(ik_x h_y - ik_y h_x), \tag{17}$$

$$n\rho_0 w = -D\delta p - g\delta\rho - (\mu/4\pi) H_0 [Dh_z - ik_x h_z + h_x (DH_0/H_0)], \tag{18}$$

$$ik_x u + ik_y v + Dw = 0, \tag{19}$$

$$n\delta\rho + wD\rho_0 = 0, \tag{20}$$

$$nh_x = H_0 ik_x u - wDH_0, \tag{21}$$

$$nh_y = H_0 ik_x v, \tag{22}$$

$$nh_z = H_0 ik_z w, \tag{23}$$

and

$$ik_x h_x + ik_y h_y + Dh_z = 0, \tag{24}$$

where D stands for d/dz.

We now eliminate some of the variables and derive an equation for, say, the component w of velocity perturbation vector. Multiply (16), (17) by ik_x and ik_y, respectively, and add, to get, on making use of (19),

$$-n\rho_0 Dw - 2\rho_0 \Omega (ik_x v - ik_y u) - \frac{\mu}{4\pi} ik_x h_z DH_0 \tag{25}$$

$$-\frac{\mu}{4\pi} H_0 ik_y [ik_x h_y - ik_y h_x] = k^2 \delta p, \tag{26}$$

where $k^2 = k_x^2 + k_y^2$. Eliminate δp from equations (25) and (18) (after having eliminated $\delta\rho$ by using equation (20)) by operating the former by D and multiplying the latter by k^2 and adding. In this way we get

$$-nD(\rho_0 Dw) - 2\Omega D[\rho_0(ik_x v - ik_y u)] - \frac{\mu}{4\pi} ik_x D(h_z DH_0) - \frac{\mu}{4\pi} ik_y D[H_0(ik_x h_y - ik_y h_x)] + n\rho_0 k^2 w + \frac{\mu H_0}{4\pi} k^2 \times \left[Dh_x - ik_x h_z + h_x \frac{DH_0}{H_0}\right] - \frac{gk^2}{n} wD\rho_0 = 0. \quad (27)$$

If for a moment, we assume $H = 0$ and write the equation for w, we obtain,

$$\left[\rho_0 nk^2 - \frac{gk^2}{n} D\rho_0\right] w - nD(\rho_0 Dw) = 2\Omega D(\rho_0 \zeta). \quad (28)$$

where we have written,

$$\zeta = ik_x v - ik_y u. \quad (29)$$

In equation (27), the terms involving the magnetic field reduce to (after some simplications employing equation (24))

$$\frac{\mu}{4\pi} ik_x[H_0(D^2 - k^2) h_z - h_z D^2 H_0]. \quad (30)$$

On making use of (23) we get the magnetic terms, after some simplifications, as,

$$-\frac{\mu}{4\pi n} k_x^2[H_0^2(D^2 - k^2) w + 2H_0 DwDH_0]. \quad (31)$$

Thus the complete equation (27) for w can be written as,

$$\left[\rho_0 nk^2 - \frac{gk^2}{n} D\rho_0\right] w - nD(\rho_0 Dw) - \frac{\mu k_x^2}{4\pi n}[H_0^2(D^2 - k^2) w + 2H_0 DH_0 Dw] = 2\Omega D(\rho_0 \zeta). \quad (32)$$

Now eliminate δp from equations (16) and (17) by multiplying the former by $-ik_y$ and latter by ik_x and adding. We get

$$n\rho_0[ik_x v - ik_y u] + 2\rho_0 \Omega[ik_y v + ik_x u] - (\mu/4\pi)[ik_x H_0(ik_x h_y - ik_y h_x) - ik_y DH_0 . h_z] = 0. \quad (33)$$

Thus the equation determining ζ becomes,

$$\zeta = \frac{2\rho_0 \Omega Dw}{\left[n\rho_0 + \frac{\mu H_0^2}{4\pi n} k_x^2\right]}. \quad (34)$$

On eliminating ζ in equations (32) and (34), we get the equation for w as

$$(D^2 - k^2) u \left[1 + \frac{\mu H_0^2}{4\pi\rho_0} \frac{k_x^2}{n^2}\right]^3 + \frac{4\Omega^2}{n^2} D^2 w \left[1 + \frac{\mu H_0^2}{4\pi\rho_0} \frac{k_x^2}{n^2}\right] + \frac{D\rho_0}{\rho_0}\left[\left(Dw + \frac{gk^2}{n^2} w\right)\left(1 + \frac{\mu H_0^2}{4\pi\rho_0} \frac{k_x^2}{n^2}\right)^2 + \frac{4\Omega^2}{n^2} Dw\left(1 + \frac{\mu H_0^2}{2\pi\rho_0} \frac{k_x^2}{n^2}\right)\right] + \frac{\mu k_x^2}{2\pi n^2 \rho_0} H_0 DH_0 Dw\left[\left(1 + \frac{\mu H_0^2}{4\pi\rho_0} \frac{k_x^2}{n^2}\right)^2 - \frac{4\Omega^2}{n^2}\right] = 0. \quad (35)$$

In §§ 3 and 4 we shall be studying two special cases, namely, the hydromagnetic stability of (i) a continuously stratified layer of fluid, and (ii) a configuration of two superposed fluids, respectively.

3. Hydromagnetic stability of a continuously stratified fluid of finite depth

Here we shall consider the special case in which an inviscid, infinitely conducting layer of fluid is confined between two rigid horizontal boundaries at $z = 0$, and $z = l$, and there is present a horizontal magnetic field in the x-direction. We assume that the density is stratified according to the law

$$\begin{aligned} \rho_0(z) &= \rho_1 e^{\beta z}, \quad 0 \leqslant z \leqslant l, \\ &= 0 \quad \text{elsewhere}, \end{aligned} \tag{36}$$

where ρ_1, and β are constants.

We further assume, for reasons of simplification in analysis, that the permanent horizontal magnetic field is also stratified in the upward direction in such a way that the local hydromagnetic wave velocity is constant throughout the fluid, which means that H_0^2/ρ_0 is constant throughout the fluid or

$$H_0^2(z) = H_1^2 e^{\beta z}. \tag{37}$$

With equations (36) and (37), the equation (35) becomes

$$\begin{aligned} D^2 w\left[\left(1+\frac{k_x^2 V^2}{n^2}\right)^2+\frac{4\Omega^2}{n^2}\right]+\beta Dw\left[\left(1+\frac{k_x^2 V^2}{n^2}\right)^2+\frac{4\Omega^2}{n^2}\right] \\ +w\left(1+\frac{k_x^2 V^2}{n^2}\right)\left[g\beta\frac{k^2}{n^2}-k^2\left(1+\frac{k_x^2 V^2}{n^2}\right)\right]=0, \end{aligned} \tag{38}$$

where we have written $V^2 = \mu H_1^2/4\pi\rho_1$.

We shall now discuss some special cases before coming back to the general case.

(*a*) *Non-rotating configuration*

If we suppose that the configuration is non-rotating, equation (38) simplifies to

$$D^2 w+\beta Dw+wk^2\frac{\left[\frac{g\beta}{n^2}-\left(1+\frac{k_x^2 V^2}{n^2}\right)\right]}{\left[1+\frac{k_x^2 V^2}{n^2}\right]}=0. \tag{39}$$

This particular case of zero rotation has been treated before (Talwar 1959, hereafter called paper I) and the equation determining n is

$$n^2 = \frac{4k^2 l^2 g\beta}{4(k^2 l^2+\alpha^2\pi^2)+\beta^2 l^2}-k_x^2 V^2, \tag{40}$$

where α is an integer. The equation (40) clearly manifests the stabilizing influence of horizontal magnetic field. Harmonic disturbances (when $\beta < 0$) give rise to horizontal waves propagated with phase velocity given by

$$U_{p,k} = \left[V_k^2-\frac{g\beta l^2}{k^2 l^2+\alpha^2\pi^2}\right]^{\frac{1}{2}}, \tag{41}$$

which is greater than the Alfvén velocity V_k in the direction $\mathbf{k}$ when $\beta < 0$. Here $|\beta l| \ll 1$, which means that the total density change in the fluid between $z = 0$ and $z = l$ is much less than the average density. The group velocity $U_{g,k}$ is written as,

$$U_{g,k} = \frac{[V_k^2(k^2l^2+\alpha^2\pi^2)^2 - g\beta l^2\alpha^2\pi^2]}{[V_k^2(k^2l^2+\alpha^2\pi^2) - g\beta l^2]^{\frac{1}{2}}\,(k^2l^2+\alpha^2\pi^2)^{\frac{3}{2}}}, \tag{42}$$

which is less than the phase velocity for $\beta < 0$. The equations (40) and (41) suggest that whereas under gravity alone there is complete instability for $\beta > 0$, there is no instability, in our present context, for wavelengths smaller than a certain critical value λ_* given by the following equation

$$k_* = \frac{2\pi}{\lambda_*} = \left[\frac{g\beta}{V_k^2} - \frac{\alpha^2\pi^2}{l^2}\right]^{\frac{1}{2}}. \tag{43}$$

Again (43) shows that the critical field necessary for complete stability (corresponding to the lowest value of the parameter α, namely unity) is given by

$$V_k^2 = g\beta l^2/\pi^2. \tag{44}$$

Further, since $n = 0$ at $k = 0$ and also at $k = k_*$, there should be a mode of maximum instability for an intermediate value of k given by

$$k_m = \left[\frac{(g\beta)^{\frac{1}{2}}\,\alpha\pi}{V_k l} - \frac{\alpha^2\pi^2}{l^2}\right]^{\frac{1}{2}} \tag{45}$$

and the growth rate, n_m, of this mode is

$$n_m = \frac{k_m^2 l V_k}{\alpha\pi}. \tag{46}$$

For $k = k_*$ the wave velocity vanishes and the group velocity becomes infinitely large. It is interesting to note that whereas the wave velocity is more than the group velocity for $\beta < 0$ (ordinarily stable configuration), the group velocity becomes more than the wave velocity in the presence of a horizontal magnetic field for the case $\beta > 0$ (when the configuration is thoroughly unstable without magnetic field) in the region of wavelength 0 to λ_*. Thus we conclude, in our present context, that, for waves which travel with speed less than the Alfvén wave velocity, the group velocity is greater than the phase velocity, while for those with speeds greater than the Alfvén velocity the group velocity is less than the wave velocity.

(*b*) *Rotating configuration without magnetic field*

If the medium is field-free, and is partaking in a uniform rotation about the z-axis then the expression for n can be derived to be (when $|\beta l| \ll 1$),

$$n^2 = \frac{g\beta k^2l^2 - 4\Omega^2\alpha^2\pi^2}{k^2l^2+\alpha^2\pi^2}. \tag{47}$$

This equation shows that the coriolis force has a stabilizing influence on the configuration. For $\beta < 0$, the expressions for the phase and group velocities can be easily worked out. The equation (47) also suggests that even when $\beta > 0$ (when

under pure gravity the configuration is thoroughly unstable) we may have stability provided

$$\Omega^2 > \frac{g\beta k^2 l^2}{4\alpha^2\pi^2}. \tag{48}$$

Thus for a given positive value of β, and for a given angular speed, (48) defines a critical value k^* of wave-number, namely $(4\Omega^2\alpha^2\pi^2/g\beta l^2)^{\frac{1}{2}}$. For disturbances with wave-numbers less than this critical, the configuration will be stable and will be unstable only for values of the wave-number greater than this. Thus, as in the corresponding case of magnetic field, we find that rotation has a stabilizing effect. There are, however, a few points of difference in the nature of stabilizing role of magnetic field and rotation. Coriolis force has greater stabilizing effect for large wavelength, whereas magnetic field stabilizes smaller wavelengths to a greater extent. Again there exists a critical magnetic field given by equation (44) which can remove instability altogether (for all k), but it seems that no finite amount of rotation can achieve that result. Also there does not seem to exist a maximum of the growth-rate of any mode at finite wavelength in the presence of rotation, although there does (*vide* equation 45) in the case of magnetic field. The maximum growth-rate occurs, in this case of zero magnetic field, at $k_m = \infty$ and is given by $n_m = (g\beta)^{\frac{1}{2}}$. The coriolis forces do not act on motion parallel to the axis of rotation, and the result that $k_m = \infty$ independently of rotation is associated with the fact that there is no horizontal motion when $k_m = \infty$.

(c) *Simultaneous presence of rotation and magnetic field*

If m_1, m_2 are the roots of the equation (38), then

$$m_1 + m_2 = -\beta \tag{49}$$

and $$m_1 m_2 = k^2\left[\frac{g\beta}{n^2} - \left(1 + \frac{k_x^2 V^2}{n^2}\right)\right]\left[1 + \frac{k_x^2 V^2}{n^2}\right]\left[\left(1 + \frac{k_x^2 V^2}{n^2}\right)^2 + \frac{4\Omega^2}{n^2}\right]^{-1},$$

and the general solution of the equation (38) is

$$w(z) = A\, e^{m_1 z} + B\, e^{m_2 z}, \tag{50}$$

where A, B are constants to be determined from the boundary conditions. Since the fluid is bounded by rigid planes at $z = 0$, and $z = l$,

$$w = 0 \quad \text{at} \quad z = 0, \quad \text{which gives} \quad B = -A \tag{51}$$

and $$w = 0 \quad \text{at} \quad z = l, \quad \text{which gives} \quad e^{(m_1 - m_2)l} = 1, \tag{52}$$

whence $$(m_1 - m_2)\, l = 2\alpha i\pi, \tag{53}$$

α being an integer. Thus equation (50) may be rewritten as,

$$w(z) = A' e^{-\frac{1}{2}\beta z} \sin\frac{\alpha\pi z}{l}. \tag{54}$$

The equation for n for different values of the parameter α can then be worked out to be

$$n^4 + n^2\left[2k^2 V_k^2 + \frac{4\Omega^2 E - g\beta}{1+E}\right] + \left[k^4 V_k^4 - \frac{g\beta k^2 V_k^2}{1+E}\right] = 0, \tag{55}$$

where we have written E for $(4\alpha^2\pi^2+\beta^2l^2)/4k^2l^2$ for convenience, and V_k denotes the component of Alfvén velocity in the direction of wave-number **k**. The two roots for n^2 of this equation are both real and negative for $\beta<0$ and also when β is positive but less than $(1+E).(k^2V_k^2/g)$. Thus we can conclude that a configuration of stratified fluid under the joint influence of a horizontal magnetic field and the coriolis force will be stable not only when the density is decreasing function of the vertical distance but even when $\beta>0$ and less than $[(1+E)\,k^2V_k^2]/g$. The configuration will therefore be unstable only when $\beta>[(1+E)\,k^2V_k^2]/g$,

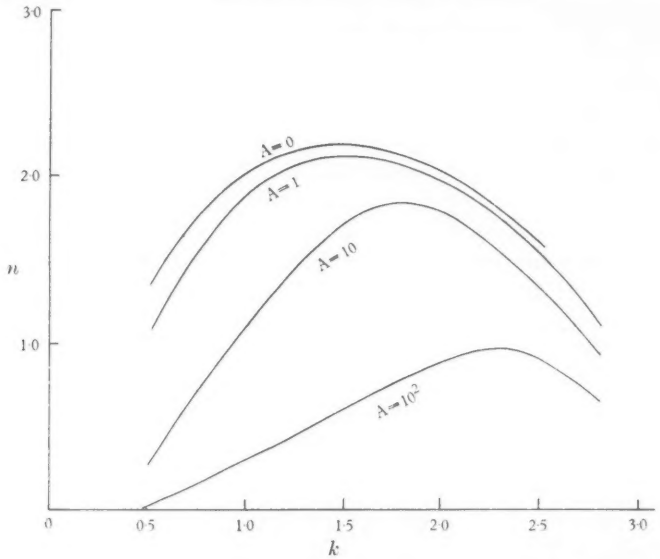

FIGURE 1. Illustrates the inhibiting influence of rotation in the unstable case of a continuously stratified fluid with horizontal magnetic field. The growth-rate n (measured with the unit $\pi V_k/l\,\mathrm{sec}^{-1}$) is plotted as a function of wave-number **k** (measured with the unit $\pi/l\,\mathrm{cm}^{-1}$) for $B\ (=g\beta l^2/\pi^2V_k^2)=10$ and for several values of $A\ (=4\Omega^2l^2/\pi^2V_k^2)$.

since then one of the two roots of the above equation becomes positive. When the configuration is stable, harmonic disturbance leads to propagation of horizontal waves with velocity given by the following expression:

$$U_{p_{1,2}}^2=\left[V_k^2+\frac{4\Omega^2\alpha^2\pi^2/k^2-g\beta l^2}{2(\alpha^2\pi^2+k^2l^2)}\right]\mp\left[\left\{\frac{4\Omega^2\alpha^2\pi^2/k^2-g\beta l^2}{2(\alpha^2\pi^2+k^2l^2)}\right\}^2+4V_k^2\frac{\Omega^2}{k^2}\frac{\alpha^2\pi^2}{(\alpha^2\pi^2+k^2l^2)}\right]^{\frac{1}{2}}. \tag{56}$$

We may also write this expression as

$$U_{p_{1,2}}^2-V_k^2=\frac{4\Omega^2\alpha^2\pi^2/k^2-g\beta l^2}{2(\alpha^2\pi^2+k^2l^2)}\left[1\mp\left\{1+\frac{16\Omega^2\alpha^2\pi^2V_k^2(k^2l^2+\alpha^2\pi^2)}{k^2[4\Omega^2(\alpha^2\pi^2/k^2)-g\beta l^2]^2}\right\}^{\frac{1}{2}}\right]. \tag{57}$$

We find therefore that simultaneous presence of rotation and field produces a stabilizing effect; as we have already seen, that rotation and magnetic field individually also have a stabilizing influence.

In the unstable case ($\beta > [(1+E)\,k^2 V_k^2]/g$) we are interested in the real positive root of equation (55). Let us measure k and n in units of $(\pi/l)\,\mathrm{cm}^{-1}$ and $(\pi V_k/l)\,\mathrm{sec}^{-1}$, respectively, so that the equation (55) can be rewritten in the form

$$n^4 + n^2\left[2k^2 + \frac{A\alpha^2 - Bk^2}{k^2+\alpha^2}\right] + k^4\left[1 - \frac{B}{k^2+\alpha^2}\right] = 0, \tag{58}$$

where

$$A = 4\Omega^2\alpha^2/\pi^2 V_k^2 \quad \text{and} \quad B = \frac{g\beta l^2}{\pi^2 V_k^2} \tag{59}$$

are pure numbers.

The calculation of the positive root of the above equation has been carried out for $B = 10$ and for several values of A for the case $\alpha = 1$, and the results are presented graphically in figure 1. Curves of n against k for $B = 10$ and $A = 0, 1, 10, 10^2$ are given. These curves clearly show (i) that for a given k, n decreases with increase in A, (ii) that n_m, the maximum growth-rate, also decreases with increase of A, and (iii) that k_m, the wave-number for the mode of maximum instability increases with increasing A. The parameter A being a measure of the relative dynamical importance of the coriolis forces with the magnetic forces, we can conclude that, for a given B, the effect of increase in rotation is to increase the time taken for the system to depart from equilibrium and to decrease the wavelength of the mode of maximum instability.

4. Hydromagnetic stability of two superposed rotating fluids

In this section we shall investigate the effect of a uniform horizontal magnetic field on the equilibrium of two uniform, inviscid, infinitely conducting, superposed *rotating* fluids. The fluids will be taken to have uniform densities ρ_1 (for lower fluid) and ρ_2 (for upper fluid) and will be assumed to rotate uniformly about the z-axis.

In this particular case equation (35) reduces to

$$\left[n + \frac{\mu H^2}{4\pi\rho}\frac{k_x^2}{n}\right](D^2 - k^2)\,w + 4\Omega^2 D^2 w = 0, \tag{60}$$

since we have assumed $D\rho = 0$ and $DH = 0$.

The equation is true for either fluid. Hence we can write

$$w_1 = A_1 e^{m_1 z} + B_1 e^{-m_1 z} \quad (z < 0), \tag{61}$$

$$w_2 = A_2 e^{-m_2 z} + B_2 e^{m_2 z} \quad (z > 0). \tag{62}$$

The boundary conditions to be satisfied are as follows. (i) The velocity should vanish at $z = -\infty$ (for lower fluid) and at $z = +\infty$ (for upper fluid). (ii) The normal component of velocity should be continuous at the interface, i.e. to our approximation $w(z)$ is continuous at $z = 0$. (iii) The pressure should be continuous across the interface, which means that

$$\delta p_1 - \delta p_2 + g(\rho_2 - \rho_1)\,\xi + \frac{\mu H}{4\pi}[(h_x)_1 - (h_x)_2] = 0, \tag{63}$$

where the subscripts 1, 2 stand for the lower ($z < 0$) and upper fluids ($z > 0$), respectively. Here ξ denotes the displacement of the interface given by w/n.

On applying the boundary conditions (i) and (ii), we find that equations (61) and (62) become

$$w_1 = A\,e^{m_1 z} \quad (z < 0), \qquad w_2 = A\,e^{-m_2 z} \quad (z > 0), \tag{64}$$

since $A_1 = A_2 = A$.

On making use of the equations (21)–(23), (25) and (34) and simplifying, we find that the equation (63) gives the following equation for n:

$$gk(\rho_2 - \rho_1) = \rho_1[(n^2 + k^2 V_{k_1}^2)^2 + 4\Omega^2 n^2]^{\frac{1}{2}} + \rho_2[(n^2 + k^2 V_{k_2}^2)^2 + 4\Omega^2 n^2]^{\frac{1}{2}}. \tag{65}$$

This equation reduces to Rayleigh's result, namely $n^2 = gk(\rho_2 - \rho_1)/(\rho_1 + \rho_2)$, when both the coriolis force and the magnetic field are absent. The above equation is an 8th-degree equation in n, and is too difficult to be discussed without making some simplifications. Let us therefore investigate some simple special cases before we come back to the general case when both rotation and the magnetic field are present simultaneously.

(i) Non-rotating superposed fluids with magnetic field ($\Omega = 0$, $H \neq 0$):

The equation for n is

$$n^2 = gk\frac{\rho_2 - \rho_1}{\rho_1 + \rho_2} - \frac{\mu H_k^2}{2\pi}\frac{k^2}{\rho_1 + \rho_2}; \tag{66}$$

this case has been thoroughly discussed in paper I.

(ii) Rotating superposed fluids with zero magnetic field ($\Omega \neq 0$, $H = 0$). This is a purely hydrodynamic case originally solved by Bjerknes *et al.* (1933), and the expression for n is easily seen to be (cf. Hide 1956)

$$n^2\left(1 + \frac{4\Omega^2}{n^2}\right)^{\frac{1}{2}} = gk\alpha, \quad \text{where} \quad \alpha = \frac{\rho_2 - \rho_1}{\rho_1 + \rho_2}$$

or alternatively,

$$n^2 = gk\alpha[(1 + x^2)^{\frac{1}{2}} - x], \quad \text{where} \quad x = 2\Omega^2/gk\alpha. \tag{67}$$

When $\rho_2 > \rho_1$, α and x are both positive and the configuration is unstable as in the non-rotating case, but the effect of increase in rotation is to decrease the positive value of n for a definite positive α.

Alternatively, when $\rho_2 < \rho_1$, the situation is thoroughly stable, as is also the case with zero rotation, and the effect of rotation is to increase the stability of the configuration since it makes n^2 more negative.

(iii) Homogeneous fluid under the joint influence of rotation and field ($\rho_1 = \rho_2 = \rho$).

For a single fluid carrying a uniform horizontal magnetic field and rotating uniformly about the vertical axis, the equation for n is

$$n^4 + n^2(4\Omega^2 + 2k^2 V_k^2) + V_k^4 k^4 = 0, \tag{68}$$

which gives

$$n_{1,2}^2 = -(2\Omega^2 + k^2 V_k^2) + 2\Omega(\Omega^2 + k^2 V_k^2)^{\frac{1}{2}}; \tag{69}$$

the two roots are always negative thus showing stability. Harmonic disturbances lead to the propagation of two stable modes of waves with phase velocities given by

$$U_{p_{1,2}} = V_k[x \pm (1 + x^2)^{\frac{1}{2}}], \tag{70}$$

where x is written for Ω/kV_k. Thus we find that the effect of coriolis force is to split an Alfvén wave into two waves travelling with different wave-speeds, one greater and one less than the Alfvén velocity. A similar result for a different orientation of field and rotation axes was obtained by Lehnert (1954). The group velocities for the two modes can be easily evaluated and are found to be

$$U_{g_{1,2}} = \frac{U_{p_{1,2}}}{(1+x^2)^{\frac{1}{2}}\,[(1+x^2)^{\frac{1}{2}} \pm x]} = \frac{V_k}{(1+x^2)^{\frac{1}{2}}}, \tag{71}$$

wherefrom it follows that for both modes the group velocity is less than the Alfvén velocity. Also it follows from the above expressions (70), (71) that for the mode for which the phase velocity is more than the Alfvén velocity, the corresponding group velocity is less than the phase velocity, but for the other mode for which the phase velocity is less than the Alfvén velocity, the corresponding group velocity is more than the phase velocity.

(iv) Instability in superposed fluids under joint influence of rotation and field. Putting $\rho_2/\rho_1 = \gamma$, we can rewrite equation (65) as

$$gk(\gamma-1) = [(n^2+k^2V_{k_1}^2)^2+4\Omega^2n^2]^{\frac{1}{2}} + \gamma[\{n^2+k^2(V_{k_1}^2/\gamma)\}^2+4\Omega^2n^2]^{\frac{1}{2}}. \tag{72}$$

As the equation cannot be easily discussed without simplifications, let us be satisfied with the investigation of the characteristics of the mode of maximum instability (when $\rho_2 > \rho_1$) under two conditions, namely, the 'high' and 'low' rotation cases. Because there is no fixed length scale in the system, we require that the coriolis force exceeds or is less than the other forces operating, that is, that

$$\Omega \gtrless n_m, \quad \text{and} \quad \Omega \gtrless k_m V_{k_1}$$

according as we are dealing with 'high' or 'low' rotation.

(*a*) *Instability in the 'low rotation' case*

In this case the magnetic field influences the motion much more than the coriolis force. The solution in the limiting case of zero rotation has already been given (paper I) as

$$n_m^2 = \frac{\gamma-1}{2(\gamma+1)}gk_m, \quad \text{and} \quad k_m = \frac{(\gamma-1)g}{4V_{k_1}^2}. \tag{73}$$

We expect that introduction of low rotation should not lead to results very different from the results quoted above for $\Omega = 0$. Under the assumptions $n_m > \Omega$ and $k_m V_{k_1} > \Omega$, we get the following characteristic equation for n

$$n^2(\gamma+1) = [g(\gamma-1)k - 2k^2V_{k_1}^2]\left[1-\frac{2\Omega^2}{k^2V_{k_1}^2}\frac{1+\gamma^2}{1+\gamma}\right]. \tag{74}$$

On differentiating this expression with respect to k, and putting $dn/dk = 0$, we find that for the mode of maximum instability

$$k_m \approx \frac{g(\gamma-1)}{4V_{k_1}^2}\left(1+\frac{2\Omega^2}{k_m^2V_{k_1}^2}\frac{1+\gamma^2}{1+\gamma}\right), \tag{75a}$$

and

$$n_m^2 \simeq \frac{g(\gamma-1)}{2(\gamma+1)}k_m\left[1-\frac{4\Omega^2}{k_m^2V_{k_1}^2}\frac{1+\gamma^2}{1+\gamma}\right]$$

$$= (n_m^2)_0\left[1-\frac{2\Omega^2}{k_m^2V_k^2}\frac{1+\gamma^2}{1+\gamma}\right], \tag{75b}$$

where $(n_m)_0$ represents the growth rate of the mode of maximum instability for zero rotation as given by (73) above. The value of k_m occurring on the right sides of the above expressions may, to the first order of approximation, be taken to refer to the zero rotation case. Thus we see that the presence of slow rotation in superposed fluids permeated by a horizontal field decreases the growth rate of the mode of maximum instability and, at the same time, increases the wave-number of this mode.

(*b*) *Instability in the high rotation case*

When the magnetic field is zero, it easily follows that, under the assumption $n^2 < \Omega^2$,

$$n = \frac{gk(\gamma-1)}{2\Omega(\gamma+1)}, \tag{76}$$

to the first approximation. Thus the mode of maximum instability, under pure rotation of a configuration of inviscid superposed fluids, is characterized by $n_m = \infty$ and $k_m = \infty$. We are interested in investigating the influence of the introduction of a small magnetic field on this configuration. It is easily seen that with the assumptions $\Omega > n_m$ and $\Omega \gg k_m V_{k_1}$, the characteristic equation for n becomes

$$n\left[1 + \frac{k^2 V_{k_1}^2}{2\Omega^2(\gamma+1)} + \frac{n^2}{8\Omega^2}\right] = \frac{gk(\gamma-1)}{2\Omega(\gamma+1)}, \tag{77}$$

which to the first order of approximation yields the following results for the mode of maximum instability:

$$k_m^2 = [2\Omega^2(\gamma+1)]/V_{k_1}^2, \quad n_m^2 = \frac{g^2(\gamma-1)^2}{8V_{k_1}^2(\gamma+1)}. \tag{78}$$

These equations show that the effect of introduction of low magnetic field in a rotating configuration of two superposed fluids of zero viscosity is to decrease both the wave-number and the growth-rate of the mode of maximum instability.

REFERENCES

Bjerknes, V., Bjerknes, J., Solberg, H. & Bergeron, T. 1933 *Physikalische Hydrodynamik*. Berlin: Springer.

Chandrasekhar, S. 1955 *Proc. Camb. Phil. Soc.* **51**, 162.

Ferraro, V. C. A. & Plumpton, C. 1958 *Astrophys. J.* **127**, 459.

Hide, R. 1955 *Proc. Roy. Soc.* A, **233**, 376.

Hide, R. 1956 *Quart. J. Mech. Appl. Math.* **9**, 35.

Lehnert, B. 1954 *Astrophys. J.* **119**, 647.

Rayleigh, Lord 1883 *Proc. Lond. Math. Soc.* **14**, 170 (also *Scientific Papers* **2**, 200).

Talwar, S. P. 1959 *Z. Astrophys.* **47**, 161.

An example of steady laminar flow at large Reynolds number

By IAN PROUDMAN
Department of Applied Mathematics and Theoretical Physics,
University of Cambridge

(Received 22 July 1960)

The purpose of this note is to describe a particular class of steady fluid flows, for which the techniques of classical hydrodynamics and boundary-layer theory determine uniquely the asymptotic flow for large Reynolds number for each of a continuously varied set of boundary conditions. The flows involve viscous layers in the interior of the flow domain, as well as boundary layers, and the investigation is unusual in that the position and structure of all the viscous layers are determined uniquely. The note is intended to be an illustration of the principles that lead to this determination, not a source of information of practical value.

The flows take place in a two-dimensional channel with porous walls through which fluid is uniformly injected or extracted. When fluid is extracted through both walls there are boundary layers on both walls and the flow outside these layers is irrotational. When fluid is extracted through one wall and injected through the other, there is a boundary layer only on the former wall and the inviscid rotational flow outside this layer satisfies the no-slip condition on the other wall. When fluid is injected through both walls there are no boundary layers, but there is a viscous layer in the interior of the channel, across which the second derivative of the tangential velocity is discontinuous, and the position of this layer is determined by the requirement that the inviscid rotational flows on either side of it must satisfy the no-slip conditions on the walls.

1. Introduction

One of the central problems of hydrodynamics which remains substantially unsolved is how to determine the steady flow of a viscous incompressible fluid when the Reynolds number is large. The difficulty cannot fairly be said to be due to the largeness of the Reynolds number. Into the problem as a whole, this largeness introduces a substantial simplification, without which the hopelessly intractable equations of general viscous flow would govern the motion. The point is more that the largeness of the Reynolds number also introduces, as a by-product, a peculiar difficulty which has not been resolved.

The simplification is that the asymptotic flow pattern for very large Reynolds numbers is divided into a number of regions, in the interior of which the relatively simple laws of inviscid dynamics are valid. Moreover, near the bounding surfaces of these regions, where the space gradients of the flow variables are large

where $(n_m)_0$ represents the growth rate of the mode of maximum instability for zero rotation as given by (73) above. The value of k_m occurring on the right sides of the above expressions may, to the first order of approximation, be taken to refer to the zero rotation case. Thus we see that the presence of slow rotation in superposed fluids permeated by a horizontal field decreases the growth rate of the mode of maximum instability and, at the same time, increases the wave-number of this mode.

(*b*) *Instability in the high rotation case*

When the magnetic field is zero, it easily follows that, under the assumption $n^2 < \Omega^2$,

$$n = \frac{gk(\gamma-1)}{2\Omega(\gamma+1)}, \tag{76}$$

to the first approximation. Thus the mode of maximum instability, under pure rotation of a configuration of inviscid superposed fluids, is characterized by $n_m = \infty$ and $k_m = \infty$. We are interested in investigating the influence of the introduction of a small magnetic field on this configuration. It is easily seen that with the assumptions $\Omega > n_m$ and $\Omega \gg k_m V_{k_1}$, the characteristic equation for n becomes

$$n\left[1 + \frac{k^2 V_{k_1}^2}{2\Omega^2(\gamma+1)} + \frac{n^2}{8\Omega^2}\right] = \frac{gk(\gamma-1)}{2\Omega(\gamma+1)}, \tag{77}$$

which to the first order of approximation yields the following results for the mode of maximum instability:

$$k_m^2 = [2\Omega^2(\gamma+1)]/V_{k_1}^2, \quad n_m^2 = \frac{g^2(\gamma-1)^2}{8V_{k_1}^2(\gamma+1)}. \tag{78}$$

These equations show that the effect of introduction of low magnetic field in a rotating configuration of two superposed fluids of zero viscosity is to decrease both the wave-number and the growth-rate of the mode of maximum instability.

REFERENCES

Bjerknes, V., Bjerknes, J., Solberg, H. & Bergeron, T. 1933 *Physikalische Hydrodynamik*. Berlin: Springer.

Chandrasekhar, S. 1955 *Proc. Camb. Phil. Soc.* **51**, 162.

Ferraro, V. C. A. & Plumpton, C. 1958 *Astrophys. J.* **127**, 459.

Hide, R. 1955 *Proc. Roy. Soc.* A, **233**, 376.

Hide, R. 1956 *Quart. J. Mech. Appl. Math.* **9**, 35.

Lehnert, B. 1954 *Astrophys. J.* **119**, 647.

Rayleigh, Lord 1883 *Proc. Lond. Math. Soc.* **14**, 170 (also *Scientific Papers* **2**, 200).

Talwar, S. P. 1959 *Z. Astrophys.* **47**, 161.

An example of steady laminar flow at large Reynolds number

By IAN PROUDMAN
Department of Applied Mathematics and Theoretical Physics, University of Cambridge

(Received 22 July 1960)

The purpose of this note is to describe a particular class of steady fluid flows, for which the techniques of classical hydrodynamics and boundary-layer theory determine uniquely the asymptotic flow for large Reynolds number for each of a continuously varied set of boundary conditions. The flows involve viscous layers in the interior of the flow domain, as well as boundary layers, and the investigation is unusual in that the position and structure of all the viscous layers are determined uniquely. The note is intended to be an illustration of the principles that lead to this determination, not a source of information of practical value.

The flows take place in a two-dimensional channel with porous walls through which fluid is uniformly injected or extracted. When fluid is extracted through both walls there are boundary layers on both walls and the flow outside these layers is irrotational. When fluid is extracted through one wall and injected through the other, there is a boundary layer only on the former wall and the inviscid rotational flow outside this layer satisfies the no-slip condition on the other wall. When fluid is injected through both walls there are no boundary layers, but there is a viscous layer in the interior of the channel, across which the second derivative of the tangential velocity is discontinuous, and the position of this layer is determined by the requirement that the inviscid rotational flows on either side of it must satisfy the no-slip conditions on the walls.

1. Introduction

One of the central problems of hydrodynamics which remains substantially unsolved is how to determine the steady flow of a viscous incompressible fluid when the Reynolds number is large. The difficulty cannot fairly be said to be due to the largeness of the Reynolds number. Into the problem as a whole, this largeness introduces a substantial simplification, without which the hopelessly intractable equations of general viscous flow would govern the motion. The point is more that the largeness of the Reynolds number also introduces, as a by-product, a peculiar difficulty which has not been resolved.

The simplification is that the asymptotic flow pattern for very large Reynolds numbers is divided into a number of regions, in the interior of which the relatively simple laws of inviscid dynamics are valid. Moreover, near the bounding surfaces of these regions, where the space gradients of the flow variables are large

and viscosity is important, the dynamics again takes a relatively simple form: that involved in boundary-layer theory. These is no proof of these results; but they are, with good reason, commonly accepted and are here taken as the starting-point.

The peculiar difficulty of determining such a flow is that the position of the viscous layers in the flow field is *a priori* unknown. If all the layers were attached to the rigid boundaries of the flow, forming conventional boundary layers, the problem would be relatively easy. This is rarely the case, however; there are usually internal viscous layers, and owing to the non-linearity of the governing equations the position of these layers depends upon the details of the particular solution that is relevant to the problem in hand. An important example of such layers is provided by the phenomenon of flow separation (boundary-layer separation), and it is a sobering thought that, despite the fifty or so years that the techniques of boundary-layer theory have been at our disposal, so little progress has been made with the problem that even such a bulk characteristic as the dependence of drag coefficient on (large) Reynolds number is still a matter of pure conjecture.

Unfortunately, the work described in this note is far too special to be of much, if any, value as a contribution to the general problem described above. But it is an example, I think the first, of a non-linear boundary-value problem of viscous flow theory in which the positions of all the viscous layers, both boundary layers and internal layers, can be deduced unambiguously by the established techniques of boundary-layer theory. As such, the reader may find it interesting and perhaps useful for didactic purposes.

2. Description of the flow

The flow to be studied takes place in a two-dimensional channel bounded by the plane porous walls $y = \pm h$. Through these walls fluid is injected or extracted with constant and uniform velocity V_1 at $y = -h$ and V_2 at $y = +h$. Both of these velocities may have either sign (counted positive in the positive y-direction), and the object is to find the steady laminar flow induced by all possible combinations of V_1 and V_2 consistent with the Reynolds number being large. In this context the Reynolds number is that formed from h, the kinematic viscosity ν, and the greater of the absolute magnitudes of V_1 and V_2.*

Flows of this type seem first to have been studied by Berman (1953) who noticed that the boundary conditions and equations of motion may all be satisfied by assuming that the component of velocity v normal to the walls is independent of x, the co-ordinate measured along the length of the channel. By continuity, the component of velocity u parallel to the walls is then given by

$$u(x, \eta) = -\frac{x}{h} v'(\eta) + u_0(\eta),$$

where the prime denotes differentiation with respect to the non-dimensional variable $\eta = y/h$, and u_0 is an arbitrary function. For such a flow, the equation

* In all viscous flows in long and narrow regions it is the Reynolds number based on the cross flow that is the dynamically significant parameter, because this determines the departure from unidirectional flow in which the acceleration is zero.

of motion normal to the walls may be integrated immediately to give the kinematic pressure p:

$$p = \frac{\nu}{h}v' - \tfrac{1}{2}v^2 + P(x),$$

where $P(x)$ is an arbitrary function of integration. Substitution of this result in the other equation of motion then yields the required constraints on the velocity field. Thus we have

$$-\frac{v'}{h}\left(-\frac{xv'}{h}+u_0\right)+v\left(-\frac{xv''}{h^2}+\frac{u_0}{h}\right) = -\frac{dP}{dx}+\nu\left(-\frac{xv'''}{h^3}+\frac{u_0''}{h^2}\right),$$

so that

$$P(x) = \tfrac{1}{2}k\frac{x^2}{h^2}+l\frac{x}{h}+m,$$

where k, l, m, are constants. By a suitable choice of origin of x we may take $l = 0$ (provided $k \neq 0$), and the equations for the velocity field are then

$$\left.\begin{aligned} vv''-v'^2-\frac{\nu}{h}v''' &= k,\\ vu_0'-v'u_0-\frac{\nu}{h}u_0'' &= 0. \end{aligned}\right\} \tag{1}$$

The boundary conditions for these equations are

$$v(-1) = V_1, \quad v(1) = V_2, \tag{2}$$

$$v'(-1) = 0, \quad v'(1) = 0, \tag{3}$$

and, if the walls are at rest,

$$u_0(-1) = 0, \quad u_0(1) = 0.$$

Whether or not it is proper to regard this last pair as no-slip conditions, or even their validity, depends to some extent on the nature of the porous material. However, for the purpose in hand, which is really an exercise in boundary-layer theory, the no-slip interpretation seems justified and we take the solution for u_0 to be $u_0 \equiv 0$. (The possibility of eigensolutions has not been examined, largely because the principal problem, that of determining v, is independent of u_0.) The same ambiguity does not arise in connexion with the boundary conditions (3). Here we are merely asserting that there is some condition on the tangential component of velocity at the wall and that it is independent of x. For brevity we again refer to it as a no-slip condition.

The four boundary conditions (2) and (3) determine the constant k and the three constants of integration in the solutions of (1). The problem is thus to find the asymptotic form of these solutions as $\nu \to 0$ for fixed values of V_1 and V_2.

3. Principles for determining the asymptotic solution

3.1. *Possible positions of the viscous layers*

In steady flow, internal viscous layers must obviously coincide with stream surfaces of the asymptotic flow for large Reynolds numbers. The essence of the matter is that there is no mechanism to hold a layer steadily in position against

the convective effect of a normal velocity component (unless, of course, the layer is supported by a porous boundary, in which case it is not internal). Also, in view of the geometrical similarity of the flow under consideration at different values of x, the viscous layers must coincide with the co-ordinate surfaces $y =$ constant. The condition that these two kinds of surfaces should coincide is that $v = 0$, and it is in this sense that the positions of the internal layers depend on particular solutions of (1), that is, on the boundary conditions.

We thus start with the idea that, as $\nu \to 0$ for fixed values of V_1 and V_2, the asymptotic solution of (1) is such that the flow is divided into a number of cells which are bounded by either the walls or the planes $v = 0$. In the interior of these cells the solution satisfies the inviscid form of (1). Near the bounding planes the solution may, but does not necessarily, have a viscous structure. At this stage of the argument the flow may consist of any number of cells, and the next step in reducing the number of possibilities is to find the general inviscid solution for v in each of them.

3.2. *The general inviscid solution*

A first integral of the inviscid form of (1), namely

$$vv'' - v'^2 = k, \tag{4}$$

is

$$v'^2 = Av^2 - k, \tag{5}$$

where A is a constant. Then, depending on the signs of A and k, the following possibilities arise:

(i) $k < 0$:

$$A < 0, \quad v = (k/A)^{\frac{1}{2}} \sin\{(-A)^{\frac{1}{2}}\eta + \epsilon\}; \tag{6}$$

$$A = 0, \quad v = (-k)^{\frac{1}{2}}\eta + \epsilon; \tag{7}$$

$$A > 0, \quad v = (-k/A)^{\frac{1}{2}} \sinh\{A^{\frac{1}{2}}\eta + \epsilon\}. \tag{8}$$

(ii) $k = 0$, $A \geqslant 0$:

$$v = \exp\{A^{\frac{1}{2}}\eta + \epsilon\}. \tag{9}$$

(iii) $k > 0$, $A > 0$:

$$v = (k/A)^{\frac{1}{2}} \cosh\{A^{\frac{1}{2}}\eta + \epsilon\}. \tag{10}$$

In each case, ϵ is the second arbitrary constant of integration.

It should be noticed that (9) and (10) have no zeros, so that these solutions can be relevant only to cases in which there are no internal viscous layers. Similarly, (7) and (8) have only one zero, so that these solutions can refer only to cells which are bounded on at least one side by a porous wall. However, (6) has more than one zero, and it is the existence of this solution that continues to make possible, at least at this stage of the argument, the idea of a flow divided into any number of cells.

3.3. *Continuity conditions across viscous layers*

The remaining piece of information that may be deduced from the inviscid equations is that v' must have the same value on both sides of an internal viscous layer. This follows immediately from (5). For k is an exact constant in the original viscous problem and therefore takes the same value in each cell of the asymptotic solution. Then, since $v = 0$ at an internal viscous layer, v' must be continuous through such a layer.

Continuity of v' implies continuity of u, which shows that the internal viscous layers are not shear layers, as they usually are in more general laminar flows at large Reynolds numbers. Apparently they have a weaker structure in which there is a rapid transition in a normal derivative of u rather than u itself (which derivative will emerge shortly).

Finally, at a boundary layer, we take only v to be continuous.

3.4. *Necessary positions of the viscous layers*

The first point to be settled by a consideration of viscous mechanics is whether every zero of v in the list of inviscid solutions need give rise to a viscous layer. In the case of the linear solution (7), the answer is clearly that it need not, since this solution is an exact solution of the full differential equation.

For the remaining two functions (6) and (8), the easiest procedure is to differentiate the differential equation (1) twice, which yields

$$vv^{\mathrm{iv}} - v''^2 - \frac{\nu}{h} v^{\mathrm{v}} = 0. \tag{11}$$

Thus we see that v^{v} must vanish at any point where v and v'' vanish simultaneously. In both of the inviscid solutions (6) and (8), v and v'' vanish simultaneously but v^{v} does not vanish at the same point. Hence, there must be viscous layers at the zeros of (6) and (8), in which there is a rapid transition in at least the fifth derivative (and possibly a lower one, the ambiguity arising from the loss of information through differentiation of the differential equation).

We now have the result that v can change sign in the interior of an inviscid cell only if the solution is (7) and that, in this case, the whole flow consists of a single cell.

3.5. *Structure of the boundary layers*

Near a porous boundary through which fluid flows with velocity V, the boundary-layer approximation to (1) is

$$Vv'' - \frac{\nu}{h} v''' = 0, \tag{12}$$

and the solution for v' (the lowest derivative in which there is a rapid variation across the boundary layer) is

$$v' = K(1 - e^{Vh\eta/\nu}), \tag{13}$$

where K is a constant and the boundary is taken (for the moment) to be at $\eta = 0$.

For present purposes, the most important property of (13) is that a boundary layer is possible only if

$$V\eta < 0. \tag{14}$$

This is the well-known and physically obvious result that a boundary layer can exist on a porous boundary if there is extraction of fluid but not if there is injection of fluid. In the latter case, the inviscid solution in the cell nearest to the boundary must be uniformly valid right up to the boundary and must there satisfy the no-slip condition $v' = 0$.

In the extraction case, the no-slip condition on the inviscid solution may be relaxed, in the usual way, and the constant K must then be taken as the value of v' at the boundary, according to the inviscid solution.

It should be added here that, if $V = 0$, the boundary layer takes the known form for two-dimensional stagnation flow and that, again, a steady boundary layer is possible only if the normal velocity near the boundary is directed towards the boundary.

3.6. *Structure of the internal viscous layers*

According to § 3.3, v' must have the same value $(-k)^{\frac{1}{2}}$ on each side of an internal viscous layer. Hence we attempt to determine the structure of the layer by assuming that the function

$$v \sim (-k)^{\frac{1}{2}}\eta \tag{15}$$

(the layer is again taken to be near $\eta = 0$) provides a uniformly valid first approximation to v and its first derivative. Within the layer we therefore set

$$v = (-k)^{\frac{1}{2}}\eta + \bar{v}, \tag{16}$$

and find from (1) that $\bar{v}$ satisfies the equation

$$(-k)^{\frac{1}{2}}\eta\bar{v}'' - 2(-k)^{\frac{1}{2}}\bar{v}' - \frac{\nu}{h}\bar{v}''' = 0. \tag{17}$$

It then follows that, for a full balance between the inertial and viscous terms, the thickness of the layer must be proportional to $\nu^{\frac{1}{2}}$ and that the amplitude of $\bar{v}$ is left arbitrary. This amplitude is of course fixed by the inviscid solutions on either side of the layer. In fact, according to the inviscid solutions (6), (7) and (8), the first approximation to $\bar{v}$ for small values of η is proportional to η^3, with a constant of proportionality independent of ν (and possibly zero). Hence in the outer parts of the layer, where the viscous and inviscid solutions have to be matched, the amplitude of $\bar{v}$ is proportional to $\nu^{\frac{3}{2}}$; and, owing to the linearity of equation (17), this estimate remains valid throughout the whole layer. Thus the layer is such that $\bar{v}'''$ (and hence v''') remains bounded as $\nu \to 0$. The easiest way to determine the essential role of the layer is then to differentiate (17) twice, to the form

$$(-k)^{\frac{1}{2}}\eta\bar{v}^{\mathrm{iv}} - \frac{\nu}{h}\bar{v}^{\mathrm{v}} = 0, \tag{18}$$

and integrate twice to obtain

$$\bar{v}''' = \alpha\int_0^{\xi} \exp\{\tfrac{1}{2}h(-k)^{\frac{1}{2}}\xi^2\}\,d\xi + \beta \quad (\xi = \eta/\nu^{\frac{1}{2}}), \tag{19}$$

where α and β are constants of integration independent of ν.

The most important property of (19) is, once again, the qualitative constraint arising from the irreversibility of the mechanics. Thus a viscous layer is possible only if $(-k)^{\frac{1}{2}}$ is negative. By (15), this implies that

$$v' < 0 \tag{20}$$

and the condition is again that the normal velocity near the layer is directed towards the layer. When the condition is satisfied, the role of the layer may be regarded as smoothing out a discontinuity in v''' at the boundary between two cells of the asymptotic solution, and the constants α and β must be chosen accordingly.

If it should happen that v''' has the same value on both sides of the layer (and this is so for one particular set of boundary conditions), then $\alpha = 0$ and the essential viscous structure of (19) is lost. Moreover, continuity of v''' across the layer implies continuity of the constant A in (5), and so the inviscid solution in one of the contiguous cells must be the analytic continuation of the solution in the other. Thus, were it not for the results of § 3.4, we might expect a viscous layer to be unnecessary. However, we have seen in § 3.4 that this is possible only for the linear solution (7). For the remaining solutions (6) and (8), a repetition of the preceding analysis with the assumption that

$$v \sim (-k)^{\frac{1}{2}}\eta + \tfrac{1}{6}A(-k)^{\frac{1}{2}}\eta^3$$

is uniformly valid yields the result that v^{v} remains bounded throughout the layer as $\nu \to 0$ with a variation given by

$$v^{\mathrm{v}} = A^2 k h \xi^2 - A^2(-k)^{\frac{3}{2}} h^2 \xi \exp\{\tfrac{1}{2}(-k)^{\frac{1}{2}} h\xi^2\} \int_0^{\xi} \xi^2 \exp\{-\tfrac{1}{2}(-k)^{\frac{1}{2}} h\xi^2\}\, d\xi$$

$$\to A^2(-k)^{\frac{1}{2}} \quad \text{as} \quad \xi \to \pm\infty, \tag{21}$$

provided condition (20) is still satisfied. There are no arbitrary constants in this solution, and the viscous structure disappears only if $A = 0$, which corresponds to the linear solution (7). In this last case it is a simple matter to show that a viscous layer is not only unnecessary but impossible.

4. The asymptotic solution for arbitrary V_1 and V_2

We are now in a position to determine uniquely the asymptotic solution as $\nu \to 0$ for all fixed values of V_1 and V_2. For the most part, the arguments that select the number of inviscid cells and the solutions in each of them depend on the particular combination of signs of V_1 and V_2 under consideration. But there is one important result which is common to all possibilities:

$$v \text{ can have at most one zero.} \tag{22}$$

This follows immediately from the principles of § 3. For, if v has more than one zero, the inviscid solution in the cell bounded by two of them must be (6), this being the only solution with more than one zero. From § 3.4 we then have that both zeros must coincide with viscous layers, and finally, from § 3.6 that one of these layers, the one at which $v' > 0$, is impossible. Hence the asymptotic solution consists of at most two cells, and there is at most one internal viscous layer.

The separate cases are considered below.

4.1. *The case* $V_1 > 0, \quad V_2 \geqslant 0$

By (22), $v > 0$ for all η, and the asymptotic solution consists of a single cell. Moreover, on the left-hand boundary (left and right refer to $\eta < 0$ and $\eta > 0$, respectively; see figure 1), there is injection of a fluid and a boundary layer is impossible, by § 3.5. The inviscid solution must therefore satisfy the boundary conditions

$$v(-1) = V_1, \quad v'(-1) = 0, \quad v(1) = V_2. \tag{23}$$

Now the only inviscid solutions with zero derivatives are (6) and (10), and then, depending on the relative magnitudes of V_1 and V_2, the unique solution satisfying (23) is easily found to be

$$V_2 < V_1, \quad v = V_1 \cos\{\tfrac{1}{2}(1+\eta)\cos^{-1}(V_2/V_1)\}; \tag{24}$$

$$V_2 = V_1, \quad v = V_1; \tag{25}$$

$$V_2 > V_1, \quad v = V_1 \cosh\{\tfrac{1}{2}(1+\eta)\cosh^{-1}(V_2/V_1)\}. \tag{26}$$

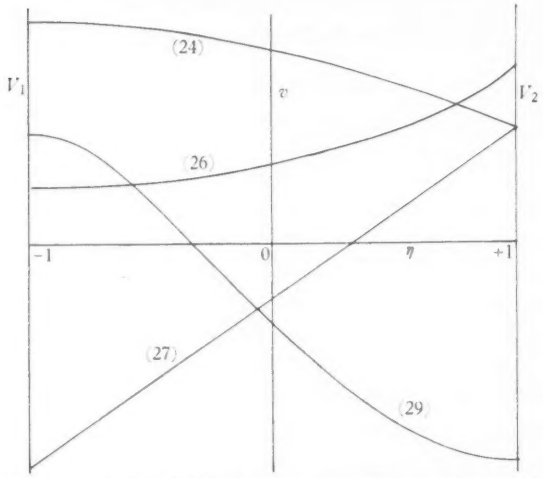

FIGURE 1. The asymptotic solution for v as $\nu \to 0$. The number beside each curve refers to the corresponding equation in the text. The velocity scale is arbitrary.

In (24) the smallest positive values of $\cos^{-1}(V_2/V_1)$ must be taken. In every case there is a conventional 'suction' boundary layer on the right-hand boundary of the type (13).

4.2. *The case* $V_1 < 0, \quad V_2 > 0$

In this case there must be a zero of v at which $v' > 0$. The only possible solution is therefore (7):

$$v = V_1 + \frac{V_2 - V_1}{2h}(1+\eta). \tag{27}$$

On both walls there are suction boundary layers of the type (13).

The solution (27) represents an irrotational flow and is, of course, unique in this respect. That such a flow should develop when fluid is extracted from both boundaries is to be expected; and this provides a more direct method of deriving (27). In fact, Sellars (1955) used essentially the same argument to derive the special case of (27) in which $V_1 = -V_2$.

4.3. *The case* $V_1 = 0, \quad V_2 > 0$

This case represents the transition between those considered in §§ 4.1 and 4.2. It is especially interesting, not only for the physical results themselves but also for the way in which the solution appears as a one-sided limit as $V_1 \to 0$ in the results of §§ 4.1 and 4.2.

Direct consideration of the case $V_1 = 0$ leads to the conclusion that there can be no boundary layer on the left-hand wall. For, if there were, we should have $v'(-1) < 0$ (see the remark at the end of § 3.5), and this would imply the existence of a second zero of v, which is known to be impossible. Thus the inviscid solution in the cell adjacent to the left-hand wall must be uniformly valid up to the wall and must there satisfy the two conditions

$$v(-1) = v'(-1) = 0.$$

The only such solution is

$$v \equiv 0, \quad \eta \neq 1. \tag{28}$$

This solution does not satisfy the right-hand boundary condition, and it seems that there must be a boundary layer on this wall, of a kind much more severe than any considered in § 3: a boundary layer which is responsible for all of the mass flow through the porous wall.

The result (28) may also be obtained as the limit of (26) as $V_1 \to 0$. However, it may not be obtained as the corresponding limit of (27), which refers to negative values of V_1. The reason appears to be the nature of the discontinuity in the left-hand boundary condition on the inviscid solution as V_1 passes through zero: a boundary layer is possible if $V_1 < 0$ but not if $V_1 \geqslant 0$. Thus $V_1 = 0$ should be regarded, so to speak, as the case of no injection, rather than no extraction, and the solution is obtained as the corresponding one-sided limit.

It should be emphasized that (28) means that $v/V_2 \to 0$ for $\eta \neq 1$ as $\nu \to 0$, and gives no indication of the actual velocity distribution in the channel. This failure of the asymptotic analysis to produce more than a qualitative result is due, of course, to the fact that viscosity is everywhere important in this case. If V_2 and h are regarded as the fixed standards of velocity and length from which the large Reynolds number is defined, viscosity is important near the right-hand wall because the length scale is short, and important everywhere else because the velocity is small.

4.4. *The case* $V_1 > 0, \quad V_2 < 0$

When fluid is injected through both boundaries, neither boundary can support a boundary layer and all of the original boundary conditions must be satisfied by the asymptotic inviscid solution. Thus, on grounds of over-determinacy alone (the inviscid equations are of lower order) one would expect an internal viscous layer in this case. That this is so follows immediately from the principles of § 3. The boundary conditions require that there should be a zero of v in the interior of the channel, and the only inviscid solution which has this property and also satisfies the no-slip condition at a wall is (6). The zero therefore coincides with a viscous layer, by § 3.4, and there are two inviscid cells in the asymptotic solution.

The position of the layer follows from the condition that v' must have the same value on both sides. Thus we find:

$$\left.\begin{aligned} v &= V_1 \sin\frac{\pi(\eta_0-\eta)}{2(\eta_0+1)} \quad (\eta < \eta_0), \\ v &= V_2 \sin\frac{\pi(\eta-\eta_0)}{2(1-\eta_0)} \quad (\eta > \eta_0), \end{aligned}\right\} \qquad \eta_0 = \frac{V_1+V_2}{V_1-V_2}. \tag{29}$$

The viscous layer at $\eta = \eta_0$ is of the type (19).

When $V_1 = -V_2$, $\eta_0 = 0$ and the two halves of (29) reduce to the same form. There is then, apparently, a single inviscid solution satisfying all the boundary conditions of the problem, a result which enabled Taylor (1956) and Yuan (1956) to obtain the solution for this special case without considering the possibility of viscous layers. However, this is a very special case. There is still a viscous layer, now at the centre of the channel and of the weaker form (21), and it is a consequence of symmetry that the solution in one inviscid cell is the analytic continuation of the solution in the other, as mentioned in § 3.6.

During part of the period of preparation of this paper, the author was a visitor at the Guggenheim Aeronautical Laboratory of the California Institute of Technology, and he is especially grateful to Professor Paco Lagerstrom and Dr Saul Kaplun for many stimulating discussions about the nature of laminar flow at large Reynolds numbers.

REFERENCES

Berman, A. S. 1953 *J. Appl. Phys.* **24**, 1232.
Sellars, J. R. 1955 *J. Appl. Phys.* **26**, 489.
Taylor, G. I. 1956 *Proc. Roy. Soc.* A, **234**, 456.
Yuan, S. W. 1956 *J. Appl. Phys.* **27**, 267.

On a circular cylinder in a steady wind at transition Reynolds numbers

By JOHN S. HUMPHREYS

AVCO Research and Advanced Development Division, Wilmington, Massachusetts

(Received 13 June 1960)

Some results of an experimental investigation of forces associated with the subsonic flow of air around a circular cylinder in a wind tunnel are presented. The oscillating forces due to the downstream vortex street are studied for Reynolds numbers in the 'critical' range 4×10^4 to 6×10^5. Of particular interest is the observation, at the onset of transition to turbulence, of a spanwise wave or cell pattern near the cylinder surface, which is stabilized in a striking manner by the use of fine threads as a visualization technique.

1. Introduction

The literature on the subject of eddy formation behind cylinders is quite extensive, dating back to Leonard da Vinci. Reviews have been given by Goldstein (1938), Rosenhead (1953), and Birkhoff & Zarantonello (1957), and an extensive one covering work up to 1958 was given by Humphreys (1959). The problem is still of interest because of the sometimes disturbing reaction of circular structures to natural flows, and because it has become possible through modern instrumentation to observe new details, such as the remarkable three-dimensional effects on average force and boundary-layer flow shown here.

A great deal of empirical information is available. The general eddy formation phenomenon (when compressibility effects are negligible) seems to fall into four regions in terms of Reynolds number $Re = \rho U_0 d/\mu$ (where U_0 is the free-stream velocity, d the cylinder diameter, ρ density and μ viscosity), which are not separated by clear boundaries but by transition zones that can, within limits, be altered by individual experimental conditions. These regions can be referred to by the terms symmetric, regular, irregular and supercritical, combining existing terminology. The symmetric range extends from Re about 5 to about 40, and is characterized by a lack of any oscillatory features. In the regular range, with Re between 50 and 140, the vortex motion is laminar and persists for a long distance downstream before being washed out by viscous diffusion.

The irregular region, extending over a wide range of Re from about 300 to 2×10^5 and containing many cases of engineering interest, is different in several respects. The wake contains considerable energy in the form of random turbulent fluctuations, and this can be explained in terms of a transition to turbulence of the free vortex layer that is still laminar as it leaves the cylinder. Due to mixing, the subsequent eddies of the turbulent fluid now die away much faster. Finally, above the 'critical' Re at about 3×10^5, where the C_D sharply drops, the wake is

fundamentally turbulent and no definite vortices are observed. The turbulence originates in the cylinder boundary layer itself before it separates.

As yet the exact details of what occurs in the three transition zones are imperfectly understood. The highest zone, around the critical Re, is perhaps the most interesting in practice,* and new force and flow data are presented here for this region.

2. Force measurements

The apparatus used in the present study is shown schematically in figure 1, and was suspended in and above the test section of the closed circuit one-meter wind tunnel at Harvard University. A polished aluminium cylinder of 6 in.

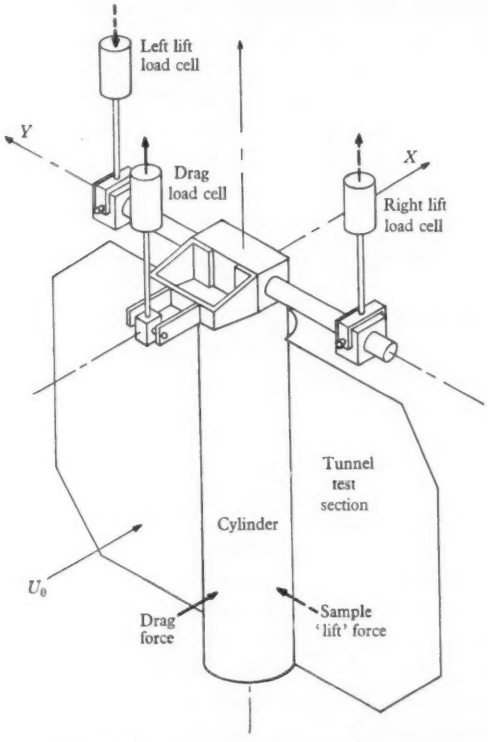

FIGURE 1. Diagram of force measuring system.

diameter was used for all of the results given here. It projected down through the tunnel roof and ended without support less than 0·05 in. off the floor of the test section. The tunnel itself can produce effective free-stream speeds in the test section from about 10 ft./sec to 200 ft./sec, which is still low enough to avoid serious compressibility effects. The force measurement system is built around

* Particularly to designers of large smokestacks, where vibration data at supercritical Reynolds numbers seem much more typical of the irregular region.

three strain-gauge 'load cells', which, when coupled to a high-gain carrier amplifier system, transmit to an oscillograph with very high sensitivity and linearity a record of the axial forces to which they are subjected.

If the wake oscillates regularly with frequency $f = \omega/2\pi$, and L is the cylinder length, then the side (or 'lift') force can be written as $C_K \times (\frac{1}{2}\rho U_0^2 Ld)\sin\omega t$, which defines the 'Karman coefficient' C_K (following Den Hartog 1954). The difference between the outputs of the two 'lift cells' then produces a measure of C_K, while the 'drag cell' output is directly related to the drag coefficient C_D. Calibration was done using static weights on the provisional (and normal) assumption that the phenomenon can be treated as a two-dimensional one, with uniform behaviour along the cylinder span. As described below, this is not in fact the case, so the resulting numbers are only averages over the span, and not simple linear averages at that, since the air forces are actually determined in

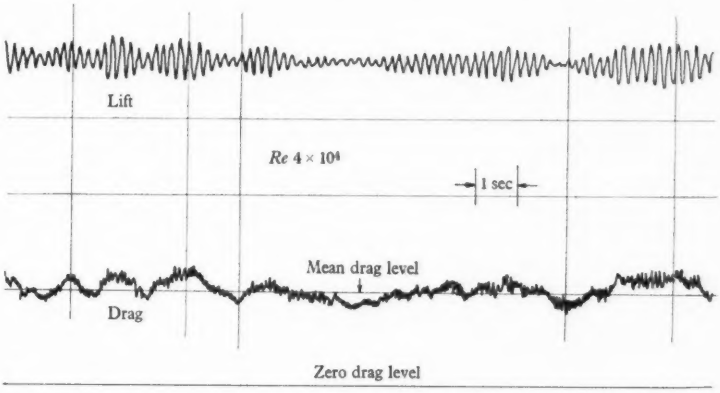

FIGURE 2. Oscillating lift and drag; sample record at subcritical Reynolds number.

terms of the moments that they produce at the support end of the cylinder. The tunnel turbulence level $(\overline{u^2})^{\frac{1}{2}}/U_0$ was found by hot-wire techniques to be close to 1 %, and was not noticeably affected by the presence of the cylinder.

On the hypothesis of a periodic two-dimensional wake, three force components are to be expected: a steady drag due to skin friction and wake underpressure, an oscillating lift at the eddy shedding frequency f due to gradients associated with vortex formation, and a small oscillating drag at frequency $2f$. All three of these quantities were measured by the author, with varying degrees of accuracy, for the range $3 \times 10^4 < Re < 6 \times 10^5$, thus spanning the upper critical Reynolds number region where wake periodicity breaks down. It can immediately be seen, however, from the tracing of a sample record shown in figure 2, that even at distinctly subcritical Re the situation is not as simple as might be hoped. There is superposed on both lift and drag a large-scale random fluctuation, which appears as a modulation of the lift oscillations and as a pronounced change (by as much as 15 %) in the net drag level. The lift modulation, which must be tied to a wake modulation, has been observed before by Roshko (1954), by

Macovsky (1958) and by Fung (1958), but no mention was made of the directly associated and quite significant drag changes. Any given single value, then, for C_D in the region just below critical Re can only be valid as an average over a suitably long period of time, here on the order of 20 sec.

Recognizing this, a mean C_D was determined for each record and is plotted in the usual way in figure 3, with several other curves due to previous workers (see Goldstein 1938 and Delany & Sorenson 1953) for comparison. The exact

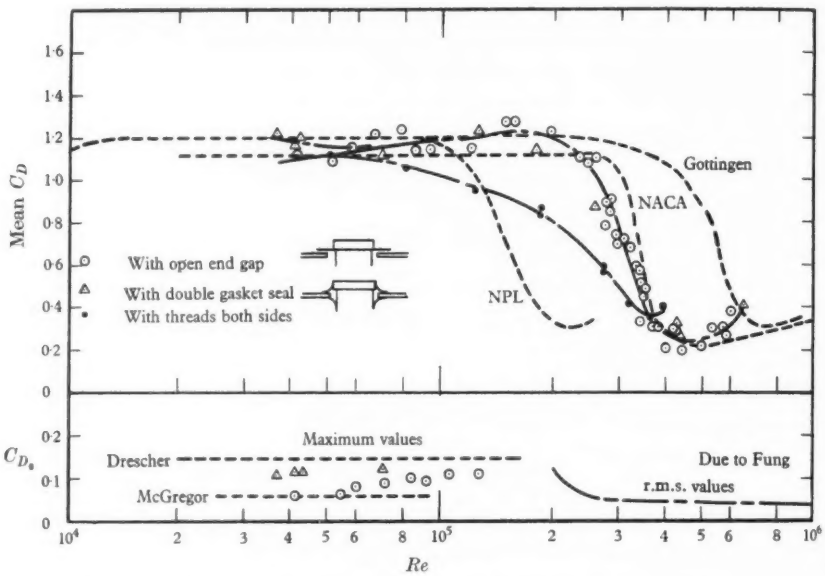

FIGURE 3. Mean and oscillating drag coefficient *vs* Reynolds number.

location of the sudden drop in C_D with increasing Re is understood to be a function of tunnel turbulence level, which determines at what speed the laminar to turbulent transition occurs in the cylinder boundary layer. The sudden narrowing of the wake following this transition provides an explanation for the connexion between drag changes and lift modulation at subcritical Re; both are simply a function of varying wake width. This is exaggerated in a closed tunnel test section (here the model occupies 16 % of the total cross-section area) by wake blockage effects.

A few points are presented in figure 3 for the maximum values of the double-frequency oscillating C_D (or C_{D_0}), but these amplitudes are close to the system noise level for subcritical Re, so accuracy is poor. Moreover, for Re in the critical range and above, this double frequency was close to a structural resonance, and the peak values are not plotted, since their validity would be dubious. Wave analyser studies, not presented here, have confirmed the observations of Fung (1958) that at supercritical Re no discernible peak is present in the frequency spectrum of C_D or C_K at the increased Strouhal numbers ($St = fd/U_0 = 0{\cdot}8$ and

0·4, respectively) that might be expected from reports of earlier hot-wire wake studies (see Goldstein 1938, p. 421, or Delany & Sorenson 1953).

Prior to 1958 there were made some estimates of the side (or 'lift') force, based either on amplitudes of cantilever cylinders vibrating near resonance, where self-excitation is crucial, or on space integrals or pressure distributions measured in various ways; much labour was involved in obtaining these estimates and the resulting points are few. These values of C_K vary from 0·6 (Drescher 1956) to 1·3 (McGregor 1957) for Re between 10^4 and 2×10^5.

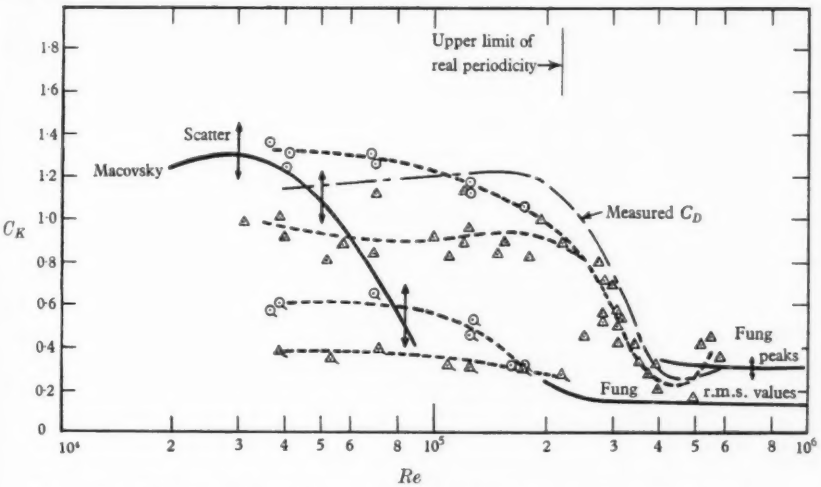

FIGURE 4. Karman lift coefficient *vs* Reynolds number. △ Maximum, ◬ mean, open end gap; ⊙ maximum, ⊙ mean, inside seal.

Some new data concerning the behaviour of the oscillating side force are shown in figure 4, in comparison with recent observations of Macovsky (1958) and Fung (1958), and some comments are required on the origin of these points. With the one exception of Fung (1958), all previously reported data on C_K have been in terms of 'maximum values', the information that is clearly of greatest interest to the smokestack designer, but which is somewhat ambiguous unless an explanation is given of just how this maximum was obtained. It is evident in most cases that this maximum is simply the largest fluctuation observed in the given run, but since random changes are involved here, the length of time of the run is definitely significant. If the result is based on only a few oscillations, as is the case with the earlier calculations based on pressures, then it is doubtful that the result is truly a representative maximum.

In the present case each of the points on figure 4 was computed from records containing (for subcritical Re) at least 500 complete oscillations, the maximum C_K being the largest seen on that record and the mean being the actual average of measured heights of on the order of 500 peaks. It must be mentioned that for Reynolds numbers in and above the critical region the measuring process used was very much more approximate, and even the definition of C_K becomes somewhat obscure, since there is no clearly periodic oscillation on which to

base it. Still, it is not misleading to use the same symbol to refer to one-half of any single maximum peak-to-peak fluctuation, and this is what is given on figure 4. Since the author did not have available a really reliable meter capable of measuring (r.m.s.) averages over long times, no estimates of mean C_K at supercritical Re were made.

End conditions proved to be of unexpected importance. A number of different sealing arrangements were tried for the gap where the cylinder pierces the roof, with striking results of the sort shown in figure 4. Even the small geometry changes involved in replacing the plate by a flexible sponge-rubber collar type of seal (sketched in figure 3) were enough to shift the mean C_K by over 50 %. Since the force is measured in terms of the moment produced at the cylinder support, this effect is even stronger than it appears. Only one conclusion is possible. The change in end geometry must cause flow changes that are not confined to the end, but must affect the entire vortex shedding mechanism along the cylinder. This, in turn, must involve very considerable spanwise pressure gradients, and the whole basis for assuming two-dimensionality is thus thrown into question.

As the Reynolds number approaches the critical region it can be seen from figure 4 that the end effect becomes less and less apparent, which is reasonable since other disturbances become involved and an end disturbance will have relatively less importance. It is also clear from figure 3 that, while C_{D_0} is changed on a scale comparable to C_K, the mean C_D is affected hardly at all (about 5 % at $Re = 4 \times 10^4$). Neither observation lessens the implication that three-dimensional effects are of fundamental importance, and this prompted further investigation into the details of spanwise flow structure.

3. Observations on flow structure

The case of a straight cylinder mounted wall to wall across a symmetric wind tunnel (or water channel) has always been considered to be one of those in which a good argument can be made for eliminating the spanwise dimension. It is generally assumed that distributions in space and time of pressure and velocity measured at any station near the centre will suffice to characterize the entire flow.

There have been several suggestions in recent years that this assumption might not be entirely justified. Roshko (1954) notes a spanwise phase shift, implying periodic structure, in wake hot-wire signals at $Re = 80$, while Etkin, Korbacher & Keefe (1957) are able to explain a consistent discrepancy in acoustic radiation measurements between $Re\, 2 \times 10^4$ and 6×10^4 in terms of spanwise variations with a 'correlation length' of about $8d$. Macovsky (1958) observes large spanwise phase changes and flow components for $10^4 < Re < 10^5$, occurring at random and increasing in importance as Re approaches 10^5. Intuitively it is clear that this must indeed be the case as the transition to turbulent wake flow at critical Re is approached, since turbulence itself is fundamentally three-dimensional.

To visualize the flow character in the wake-forming region near critical Re, the most successful results in the present study were achieved by fastening a set of fine silk threads along the front stagnation line, which were long enough to extend around the surface just past the approximate location of turbulent

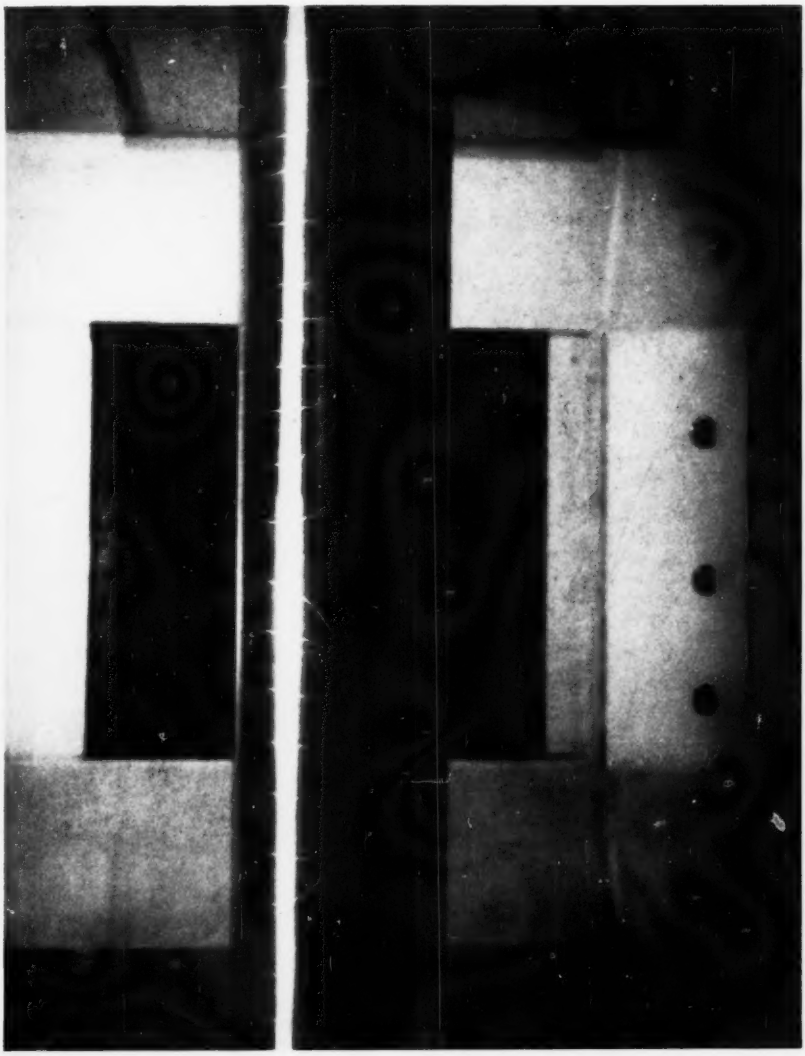

FIGURE 5 (plate 1). Surface thread patterns at critical Reynolds number showing spanwise cell structure.

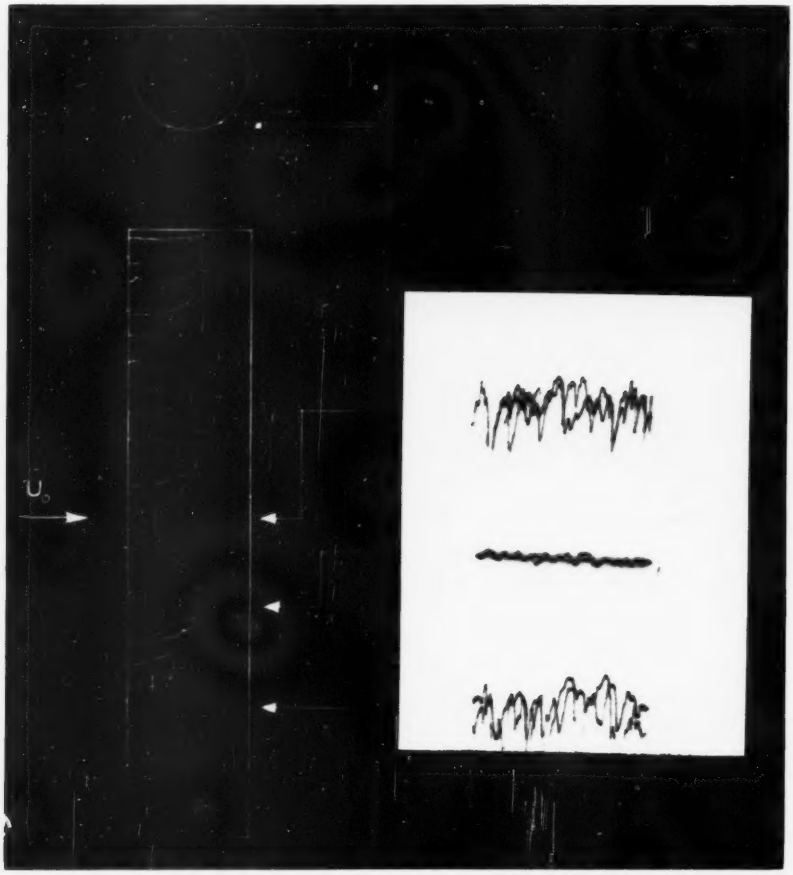

FIGURE 6 (plate 2). Hot-wire records of separated layer at critical Reynolds number, with threads showing spanwise cell structure.

(*a*) Re $2{\cdot}78 \times 10^5$ (*b*) Re $3{\cdot}06 \times 10^5$ (*c*) Re $3{\cdot}29 \times 10^5$ (*d*) with threads

FIGURE 7 (plate 2). Hot-wire correlations of separated layer from bare cylinder at critical Reynolds number; probes positioned as shown in figure 6.

boundary-layer separation (about 130°). For low speeds, the threads merely flap in and out with the wake, showing some spanwise irregularity but nothing that can be easily described or even photographed. When the speed is raised, however, to give a Re of about 10^5 (a point at which a vortex street is still definitely present for the bare cylinder) the remarkable phenomenon shown in figure 5 (plate 1) is observed.

A distinct wave or 'cell' pattern is formed by the threads; a pattern, moreover, which is very stable in time. It just moves slightly up and down, with the boundaries between cells sometimes becoming obscured or the individual cells briefly changing their size; but the central picture remains the same, even on changing end conditions or otherwise perturbing the wake flow. As the speed is increased the cells remain the same size, but the boundaries jump around with greater and greater rapidity, until by $Re\,3 \times 10^5$ they are no longer visible. The pattern is not altered by the presence or absence of threads on the opposite side, or by locating a splitter plate in the wake, which essentially removes the vortex street. Thus the observed periodicity is not tied to wake periodicity.

In fact, at the velocity where the cell pattern first becomes clearly evident, the lift- and drag-force signals show that the oscillating lift has been practically eliminated and the C_D severely reduced, just due to the presence of the threads themselves. It is well known that increased surface roughness lowers the critical Re region in model tests (see Goldstein 1938, p. 432), and this is what seems to occur here, although as shown in figure 3 the effect of threads is really a broadening out of the critical region, rather than a displacement of it. Tests using different sizes of cylinders showed that the characteristic cell size is a function only of the cylinder diameter, and is between $1{\cdot}4d$ and $1{\cdot}7d$ in every case.

It is clear, then, that the cell pattern is associated with a 'critical' flow state, which means with the onset of transition from laminar to turbulent flow in the cylinder boundary layer. The cells then represent an intermediate state, which immediately suggests that perhaps the actual pattern is formed by the alternation of regions of laminar boundary-layer flow (early separation) with regions of turbulent boundary-layer flow (later separation). If this is so, then a hot wire traversed along the cylinder at a point that would be inside a laminar wake but outside a turbulent one should pass alternately through regions of agitated wake flow and smooth outer flow, and indeed it does. As expected, the cell maxima (or points towards which the threads bend) correspond to regions of delayed separation, hence turbulent flow, and it is not surprising to find that the end regions of the cylinder, with presumably greater disturbance levels present (due to wall boundary layers) are always cell maxima. Examples of the hot-wire signals received from a probe 1·2 in. from the surface at 139° from the stagnation point are shown in figure 6 (plate 2), the three positions corresponding to two cell minima and one maximum between.

This method immediately provides a way of answering the basic question whether the same type of cell formation exists at the lower edge of the critical Re region when the threads are removed. The author believes that a positive answer can be made to this question based on evidence that is qualitative in nature. There is no well-defined periodicity, and the cells of turbulence do not sit

boundary-layer separation (about 130°). For low speeds, the threads merely flap in and out with the wake, showing some spanwise irregularity but nothing that can be easily described or even photographed. When the speed is raised, however, to give a Re of about 10^5 (a point at which a vortex street is still definitely present for the bare cylinder) the remarkable phenomenon shown in figure 5 (plate 1) is observed.

A distinct wave or 'cell' pattern is formed by the threads; a pattern, moreover, which is very stable in time. It just moves slightly up and down, with the boundaries between cells sometimes becoming obscured or the individual cells briefly changing their size; but the central picture remains the same, even on changing end conditions or otherwise perturbing the wake flow. As the speed is increased the cells remain the same size, but the boundaries jump around with greater and greater rapidity, until by $Re\,3 \times 10^5$ they are no longer visible. The pattern is not altered by the presence or absence of threads on the opposite side, or by locating a splitter plate in the wake, which essentially removes the vortex street. Thus the observed periodicity is not tied to wake periodicity.

In fact, at the velocity where the cell pattern first becomes clearly evident, the lift- and drag-force signals show that the oscillating lift has been practically eliminated and the C_D severely reduced, just due to the presence of the threads themselves. It is well known that increased surface roughness lowers the critical Re region in model tests (see Goldstein 1938, p. 432), and this is what seems to occur here, although as shown in figure 3 the effect of threads is really a broadening out of the critical region, rather than a displacement of it. Tests using different sizes of cylinders showed that the characteristic cell size is a function only of the cylinder diameter, and is between $1{\cdot}4d$ and $1{\cdot}7d$ in every case.

It is clear, then, that the cell pattern is associated with a 'critical' flow state, which means with the onset of transition from laminar to turbulent flow in the cylinder boundary layer. The cells then represent an intermediate state, which immediately suggests that perhaps the actual pattern is formed by the alternation of regions of laminar boundary-layer flow (early separation) with regions of turbulent boundary-layer flow (later separation). If this is so, then a hot wire traversed along the cylinder at a point that would be inside a laminar wake but outside a turbulent one should pass alternately through regions of agitated wake flow and smooth outer flow, and indeed it does. As expected, the cell maxima (or points towards which the threads bend) correspond to regions of delayed separation, hence turbulent flow, and it is not surprising to find that the end regions of the cylinder, with presumably greater disturbance levels present (due to wall boundary layers) are always cell maxima. Examples of the hot-wire signals received from a probe 1·2 in. from the surface at 139° from the stagnation point are shown in figure 6 (plate 2), the three positions corresponding to two cell minima and one maximum between.

This method immediately provides a way of answering the basic question whether the same type of cell formation exists at the lower edge of the critical Re region when the threads are removed. The author believes that a positive answer can be made to this question based on evidence that is qualitative in nature. There is no well-defined periodicity, and the cells of turbulence do not sit

still, they move about on the surface; but they do appear to exist and to form the basic mechanism by which transition to turbulent boundary-layer flow is actually accomplished across the whole cylinder.

The same two hot wires were used in the same location as above with respect to the cylinder axis, and with a spanwise spacing approximately one half the cell size observed with threads attached. Simultaneous records were taken of the two signals, both on oscillograph paper and in the form of a 'correlation picture' obtained by letting each signal drive one set of plates on an oscilloscope. Four such pictures are shown in figure 7 (plate 2), along with the signal from each probe by itself as a function of time. Each picture is a triple exposure; at the top the signal from one probe for 0·2 sec, in the centre the other probe signal for a different 0·2 sec, and at the bottom a 15 sec correlation figure.

If the two signals were perfectly in phase, the correlation figure would be a straight line, while if they are both random and totally uncorrelated, the figure will be a circular spot with no clearly defined edge. Figure 7 (plate 2) shows three successive tunnel speeds (*a*, *b* and *c*) in the range where transition is partially established, together with a similar picture (*d*) for comparison, with threads on the cylinder and the cell pattern in evidence. The individual traces show periods of quiet flow and periods of large fluctuations succeeding each other fairly rapidly, thus suggesting the existence of moving turbulent cells. The lower figure tells in addition that this occurs quite closely out of phase, i.e. when one probe is experiencing laminar separation behaviour the other probe is (usually) experiencing the quiescent flow characteristic of turbulent separation. Of course, both signals could be small at once without changing the correlation pictures; but if they could also be both large at once, and in a random way, the figures would be much more uniformly filled in without such distinct points as are seen. The change from figure 7*a* to *c* is the sort of uniform transition toward greater dominance of turbulent separation (represented here by small signals) that is to be expected from the force data. On oscillograph records not shown here, it was possible to watch in a clearer way the progression from one hot wire to the other of these cells (or spots) of turbulence, whose motion and growth evidently make up the phenomenon of transition.

With this picture of what is taking place in the cylinder boundary-layer flow, a simple plausible explanation can be given of why cells of a particular size are maintained by the presence of fine threads. For regions where the flow in the boundary layer has become turbulent, the separation point is delayed compared to laminar regions, and there is associated with this a marked change in the surface normal pressure distribution, as is well known (e.g. see Goldstein 1938, p. 422). For stations at angles between 30° and 120° from the front stagnation point, the normal pressure is greater if the boundary layer remains laminar before separation than it is if it becomes turbulent, and it was experimentally confirmed that this is true while the thread cell pattern is present. Along any one generator in this section of the surface at a given time, there exist pressure differences and hence accelerations in the flow, directed from the laminar to the turbulent regions, thus moving the fine threads in the directions seen. But the threads do not have negligible inertia, moreover, they tend to catch on small sur-

face irregularities, the net effect being a 'tripping' of the cross-flow which can trigger the transition to turbulence and preserve the status of the turbulent regions.

The choice of a preferred cell size can be crudely justified by noting that the simplest curve joining the boundaries of a cell without discontinuities or flat spots is a semicircle, and in fact at many times the actual boundary comes close to this shape (see figure 5, plate 1). To fit a semicircle onto the surface between 30° and 120°, where pressure differences exist, requires a spanwise distance of $\frac{1}{2}\pi d$, or $1{\cdot}56d$, which agrees very well with observation.

4. Corrections to velocity and force values

In the determination here of an effective free-stream velocity, corrections have been made for compressibility, contraction losses, solid blockage and wake blockage. Calculations of average force coefficients include a transmissibility correction for the cylinder flexibility, and are based on an effective cylinder length that makes allowance for the wall boundary layers. Known errors in the velocity determination add up to about $\pm 8\,\%$. The data (past and present) as shown graphically does not always indicate these tolerances.

As a result of the large spanwise changes seen here, there might be considerable doubt whether the lift-force modulations seen at lower Reynolds number are really modulations of average force in space instead of time, since net forces are actually read out in terms of support moments. To check this, the structure was modified to measure C_K directly, with results that were not appreciably different from earlier records, implying that the fluctuations in C_K indeed are due to time variation of the whole vortex street flow.

5. Conclusions

From the data summarized above it is clear that flow changes in the spanwise direction, which are commonly neglected, are of crucial importance in determining the nature of fluid flow in the wake-forming region behind a circular cylinder. For Reynolds numbers just below 10^5, where a definite vortex street exists, the maximum side force at the eddy frequency is comparable to the mean drag, C_K rising as high as 1·3 (confirming other results); but this is highly dependent on specific details of the end conditions. The breakdown of the periodic wake into a turbulent one, with large concurrent drops in both force coefficients, has long been connected with boundary-layer transition prior to separation; but here this has been explored further and specifically tied to the appearance of a particular kind of mixed flow. With threads on the cylinder surface, this becomes a stable spanwise pattern of cells in the boundary layer, and further hot-wire results have led to the conclusion that such cells, composed of turbulent fluid and of various and varying sizes, are for the bare cylinder the first sign of developing transition at critical Reynolds number.

This work forms part of a thesis submitted to Harvard University in partial fulfilment of the requirements for the Ph.D. degree; see Humphreys (1959). The helpful advice of Prof. R. E. Kronauer throughout the work is gratefully acknowledged.

REFERENCES

Birkhoff, G. & Zarantonello, E. 1957 *Jets Wakes and Cavities*, chapter 13. New York: Academic Press Inc.

Delany, N. & Sorenson, N. 1953 *NACA TN* 3038.

Den Hartog, J. P. 1954 *Proc. Nat. Acad. Sci., Wash.*, **40**, 3, 155.

Drescher, H. 1956 *Z. Flugwis*, **4**, 17.

Etkin, B., Korbacher, G. & Keefe, R. 1957 *J. Acoust. Soc. Amer.* **29**, 30.

Fung, Y. C. 1958 *Space Tech. Labs. Rep.* GM-TR-0165-00343, also 1960, *J. Aero. Sci.*, to be published.

Goldstein, S. 1938 *Modern Developments in Fluid Mechanics.* Oxford University Press.

Humphreys, J. 1959 *On a Circular Cylinder in a Steady Wind.* Harvard University Ph.D. Thesis in Mechanical Engineering.

Macovsky, M. 1958 *Vortex Induced Vibration Studies.* U.S. Navy Dept., D. Taylor Model Basin, Rep. 1190.

McGregor, D. 1957 *Experimental Investigation of Oscillating Pressures on a Circular Cylinder in a Fluid Stream.* University Toronto Inst. Aerophys., TN, no. 14.

Rosenhead, L. 1953 *Vortex Systems in Wakes*, p. 185. Adv. in Appl. Mech. III, Academic Press.

Roshko, A. 1954 On the Development of Turbulent Wakes from Vortex Streets. *NACA Rep.* 1191.

Third-order blast wave theory and its application to hypersonic flow past blunt-nosed cylinders

By R. J. SWIGART

Lockheed Aircraft Corporation, Missiles and Space Division, Palo Alto, California

(Received 14 July 1960)

The inviscid flow behind a cylindrical blast wave and its analogy with hypersonic flow past blunt-nosed cylinders is considered. Sakurai (1953, 1954) obtained a solution for the flow field behind a propagating blast wave by expanding the flow variables in power series of $1/M^2$, where M is the blast wave Mach number, and determining the coefficients of the first two terms in the series. Here the work is extended to include third-order terms. Third-order theory is shown to improve the prediction of shock wave shapes and surface pressure distributions on hemisphere-cylinder configurations at $M_\infty = 7{\cdot}7$ and $17{\cdot}18$.

1. Introduction

The purpose of this development is to extend Sakurai's solution (1953, 1954) for the unsteady flow field behind a propagating cylindrical blast wave to improve its accuracy at later times after the initial explosion. The case treated is that of a blast wave produced by an infinite line charge of constant energy per unit length.

Blast wave theory as developed by Taylor (1950) for spherical waves, Lin (1954) for cylindrical waves, and Sedov (1946) for spherical, cylindrical, and plane waves is applicable only when the blast wave is strong, i.e. for $\frac{1}{2}(\gamma-1)M^2 \gg 1$. Mel'nikova (1954) and Sakurai improved these solutions by expanding the flow variables in power series in $1/M^2$ of the form $\sum_{n=0}^{\infty} f^{(n)}(r/R)\,M^{-2n}$ where the $f^{(n)}$ are functions only of radial distance r non-dimensionalized with respect to the shock radius R as illustrated in figure 1. Sakurai obtained the series coefficients for $n = 0$, 1. The following development extends his work by obtaining the coefficients for $n = 2$, thus determining the third-order terms in the series expansions.

The analogy between steady hypersonic flow about a slender body with a corresponding unsteady flow in one less space dimension was first pointed out by Hayes (1947). This analogy applies between the constant energy flow behind a propagating cylindrical blast wave and the steady flow between the shock and outer edge of the entropy layer (Sychev 1960) on a blunt-nosed cylinder configuration.

The analogy may be illustrated as follows. Consider the blast wave produced by the explosion in a uniform atmosphere of an infinite line charge having finite constant energy per unit length. At some time after the explosion, the

cylindrical wave will have a radius R and a propagation velocity $U = dR/dt$. Since the phenomena possesses cylindrical symmetry, the flow in all meridian planes is identical and is characterized by a certain radial velocity, pressure, and density field. Further, consider the flow about a blunt-nosed slender body in high-speed flight (figure 2). For any transverse plane aft of the nose where the horizontal velocity component is approximately U_∞, the following relation holds

$$M_\infty \frac{dR}{dz} = \frac{U_\infty}{c}\frac{dR}{dt}\frac{dt}{dz} = \frac{1}{c}\frac{dR}{dt}, \tag{1}$$

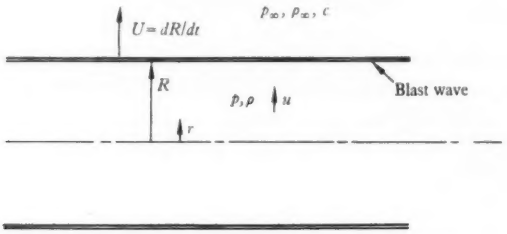

FIGURE 1. Cylindrical blast wave phenomena.

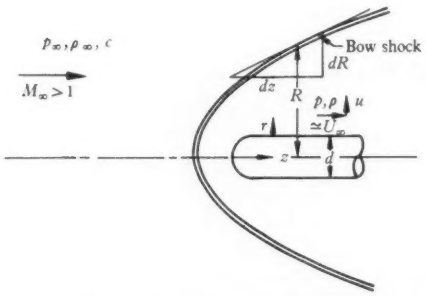

FIGURE 2. Flow about a blunt-nosed cylinder in steady flight.

where c is the speed of sound in the undisturbed stream. dR/dt, however, is analogous to the blast wave propagation velocity. Hence, (1) may be written as

$$M_\infty \frac{dR}{dz} = \frac{U}{c} = M. \tag{2}$$

Thus, if the radial velocity, pressure, and density behind the propagating blast wave are known functions of M and r/R, they are known through the above analogy in any given transverse plane aft of the nose of a blunt body whose flight Mach number and shock shape are known.

2. Mathematical analysis

Sakurai (1953, 1954) wrote the usual conservation equations of fluid mechanics in terms of the independent variables

$$x = \frac{r}{R}, \quad y = \left(\frac{c}{U}\right)^2, \tag{3}$$

and substituted into the differential equations and shock boundary conditions the following assumed power series expansions for particle velocity, pressure, and density.

$$u = U[f^{(0)}(x) + f^{(1)}(x)\,y + f^{(2)}(x)\,y^2 + \ldots], \tag{4}$$

$$p = p_\infty y^{-1}[g^{(0)}(x) + g^{(1)}(x)\,y + g^{(2)}(x)\,y^2 + \ldots], \tag{5}$$

$$\rho = \rho_\infty [h^{(0)}(x) + h^{(1)}(x)\,y + h^{(2)}(x)\,y^2 + \ldots]. \tag{6}$$

x	$\phi^{(2)}$	$\psi^{(2)}$	$\chi^{(2)}$
1·0	0	0	25
0·98	0·4229	−1·6187	0·4992
0·96	0·5285	−1·1517	− 8·0613
0·94	0·5481	−0·2062	− 9·4892
0·92	0·5400	0·6638	− 8·3281
0·90	0·5144	1·3174	− 6·1815
0·88	0·4680	1·7416	− 3·6955
0·86	0·3917	1·9716	− 1·3643
0·84	0·3053	2·0733	0·3793
0·82	0·2079	2·0837	2·2534
0·80	0·1031	2·0339	3·5950
0·78	−0·0049	1·952	4·8404
0·76	−0·1112	1·8527	5·6202
0·74	−0·2211	1·7468	6·6244
0·72	−0·3271	1·6422	7·1700
0·70	−0·4328	1·5441	7·8143
0·68	−0·5419	1·4549	8·1487
0·66	−0·6510	1·3759	8·5018
0·64	−0·7569	1·3317	8·8549
0·62	−0·8603	1·2469	9·2012
0·60	−0·9630	1·1963	9·4030
0·58	−1·0692	1·1519	9·9539
0·56	−1·1796	1·1137	10·1068
0·54	−1·2907	1·0815	10·5517
0·52	−1·4064	1·0551	10·6582
0·50	−0·5290	1·0342	10·7647
0·48	−1·6600	1·0174	—
0·46	−1·8008	1·0043	—
0·44	−1·9532	0·9937	—
0·42	−2·1231	0·9856	—
0·40	−2·3282	0·9802	10·75
0·30	—	0·9633	—
0·20	—	0·9571	—
0·10	—	0·9546	—
0·00	—	0·9478	—

TABLE 1. Numerical solutions for $\phi^{(2)}$, $\psi^{(2)}$, $\chi^{(2)}$

The equation of like powers of y then results in an infinite number of sets of equations for the series coefficients which may be solved successively. Further substitution of (4), (5), and (6) into the mathematical expression of equality of energy per unit length of the flow contained within the cylindrical shock and that of the original line charge results in the following expression for $R(y)$

$$y(R_0/R)^2 = J_0(1 + \lambda_1 y + \tfrac{1}{2}\lambda_2 y^2 + \ldots), \tag{7}$$

where $R_0^2 = E/p_\infty$, E being the energy per unit length of the original line charge, and J_0 and the λ_i's are constants.

The object of this work is to determine $f^{(2)}$, $g^{(2)}$, $h^{(2)}$, and λ_2 by solution of the set of equations resulting from equation of like powers of y^2. We define

$$f^{(2)}(x) = \{x - f^{(0)}(x)\}\,\phi^{(2)}(x), \tag{8}$$

$$g^{(2)}(x) = g^{(0)}(x)\,\psi^{(2)}(x), \tag{9}$$

$$h^{(2)}(x) = h^{(0)}(x)\,\chi^{(2)}(x), \tag{10}$$

and further, since $\phi^{(2)}$, $\psi^{(2)}$, and $\chi^{(2)}$ depend on λ_2, which cannot be obtained until $\phi^{(2)}$, $\psi^{(2)}$, and $\chi^{(2)}$ are known, we let

$$\phi^{(2)} = \phi_1^{(2)} + \lambda_2 \phi_2^{(2)}, \tag{11}$$

$$\psi^{(2)} = \psi_1^{(2)} + \lambda_2 \psi_2^{(2)}, \tag{12}$$

$$\chi^{(2)} = \chi_1^{(2)} + \lambda_2 \chi_2^{(2)}. \tag{13}$$

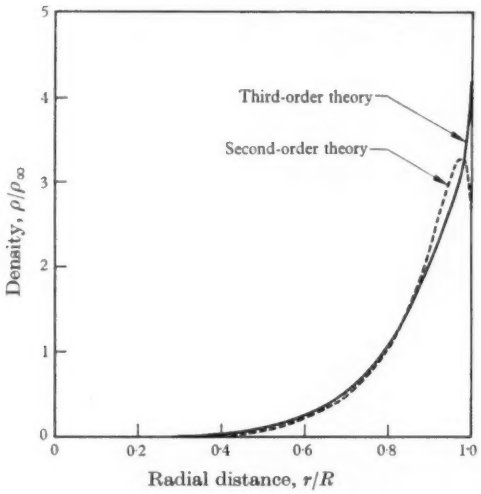

FIGURE 3. Density distribution comparison; $M = 3$, $\gamma = 1{\cdot}4$.

This leads, after some manipulation, to two pairs of coupled linear ordinary first-order differential equations for $\phi_1^{(2)}$, $\psi_1^{(2)}$, and $\phi_2^{(2)}$, $\psi_2^{(2)}$ whose coefficients derive from the previous approximations, together with appropriate boundary conditions. For details see Swigart (1960). These equations were integrated on a Rand 1103A computer utilizing the Runge–Kutta method. The results yield $\lambda_2 = 2{\cdot}7373$. The values of $\phi^{(2)}$, $\psi^{(2)}$, and $\chi^{(2)}$ then determined are given in table 1.

3. Blast wave results

Non-dimensionalized radial velocity, pressure, and density accurate to the third-order were obtained using equations (4)–(6) and the first- and second-order results given in Sakurai (1953, 1954). A typical result is given in figure 3 in which density distributions given by second- and third-order theory at a

shock Mach number of 3 are compared. Note that the physically incorrect maximum in the second-order curve is corrected by the third-order term. Further results indicate that the third-order term in the density expansion is negligible for M above 5, whereas terms higher than third-order may not be neglected for M less than 3. Corresponding results hold for radial velocity and pressure.

4. Blunt-body shock-wave shapes and surface-pressure distributions

As previously mentioned, an analogy exists between the constant-energy non-steady similar flow behind the blast wave and steady hypersonic flow about a blunt-nosed cylinder at zero incidence. For this case, the energy per unit length of the original line charge in the blast wave problem is identified with the nose drag, D, of the axisymmetric body.

Equation (7) is a differential equation relating the speed of the shock front $U = dR/dt$ with time t. Solution of this equation yields $R = R(t; E)$. Substitution of z/U_∞ for t and $(D/2\pi p_\infty)^{\frac{1}{2}}$ for R_0 yields an equation for the shock shape about a blunt-nosed slender body as a function of axial distance from the body nose and flight Mach number. The resulting third-order equation is

$$\frac{R}{d} = 0{\cdot}7951\,(C_D)^{\frac{1}{4}}\left(\frac{z}{d}\right)^{\frac{1}{2}}\left[1+\frac{1{\cdot}5730}{M_\infty^2\,(C_D)^{\frac{1}{2}}}\frac{z}{d}-\frac{5{\cdot}8037}{M_\infty^4\,C_D}\left(\frac{z}{d}\right)^2\right], \tag{14}$$

where C_D is the nose drag coefficient. Note that (14) is more general than the corresponding second-order equation reported by Lees & Kubota (1957) in that it depends parametrically on body nose-drag coefficient. Lees & Kubota's equation

$$\frac{R}{d} = 0{\cdot}78\left(\frac{z}{d}\right)^{\frac{1}{2}}\left(1+\frac{1{\cdot}62}{M_\infty^2}\frac{z}{d}\right) \tag{15}$$

has embodied in its derivation a nose-drag coefficient for a hemisphere at $M_\infty = 7{\cdot}7$ as determined by modified Newtonian theory

$$C_D = \frac{1}{\gamma M_\infty^2}\left(\frac{p_m}{p_\infty}+1\right), \tag{16}$$

where p_m is the pressure at the stagnation point.

For all Mach numbers above and slightly below 7·7, the neglect of the nose-drag variation with Mach number is justifiable. For nose geometries that differ considerably from a hemisphere, a value of C_D corresponding to the geometry should be used rather than (16). When the value for C_D obtained using (16) at $M_\infty = 7{\cdot}7$ is introduced in (14), the first two terms are identically equation (15).

A comparison with experimental data of the shock-wave shapes obtained using two and three terms of (14) is given in figure 4 for a hemisphere-cylinder at $M_\infty = 7{\cdot}7$. Although the second-order curve lies closer to the experimental points over the entire body length, third-order theory yields a more nearly parallel curve.

Differentiation of the third-order solution to (7) results in $U(t; E) = dR(t; E)/dt$. Substitution of this expression into (5) evaluated at $x = 0$ and use of the analogy

equalities results in the following third-order expression for surface-pressure distribution

$$\frac{P_b}{P_\infty} = 0{\cdot}0687\frac{M_\infty^2 (C_D)^{\frac{1}{2}}}{z/d} + 0{\cdot}405 + 0{\cdot}150\frac{z/d}{M_\infty^2 (C_D)^{\frac{1}{2}}}. \tag{17}$$

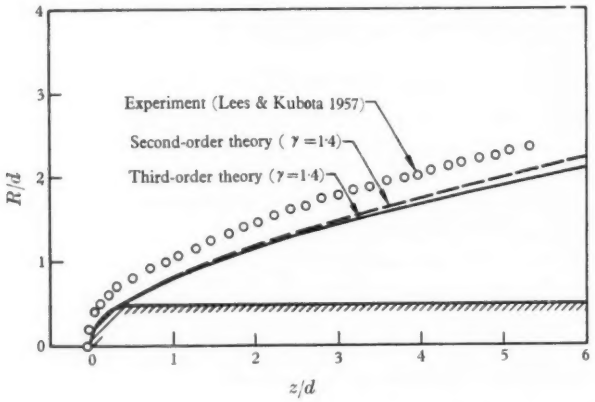

FIGURE 4. Shock shape about a hemisphere-cylinder; $M_\infty = 7{\cdot}7$.

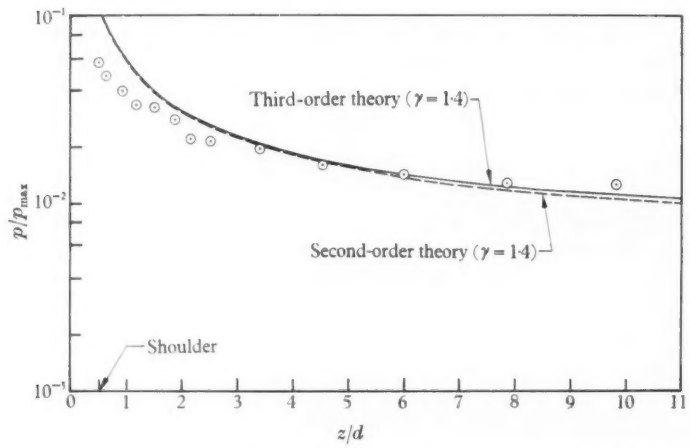

FIGURE 5. Surface pressure distribution on a hemisphere-cylinder; $M_\infty = 7{\cdot}7$.
⊙ Experiment (Lees & Kubota 1957).

The same comments regarding the nose-drag coefficient in (14) apply to (17) and the corresponding second-order expression for surface pressure distribution reported in Lees & Kubota (1957).

Comparisons of the results obtained using two and three terms of (17) with experimental data at $M_\infty = 7{\cdot}7$ (Lees & Kubota 1957) and with a numerical solution at $M_\infty = 17{\cdot}98$ (Feldman 1959) are given in figures 5 and 6. Note that the correction to the second-order curve increases with increasing z/d.

The significant contribution of third-order theory in both cases is, as with shock shape, the more accurate prediction of the slope of the pressure-distribution curve rather than correction of the value of the pressure at a given z/d. Indeed, depending on the z/d under consideration, third-order theory may be either more or less accurate than second-order theory in predicting the value of the pressure.

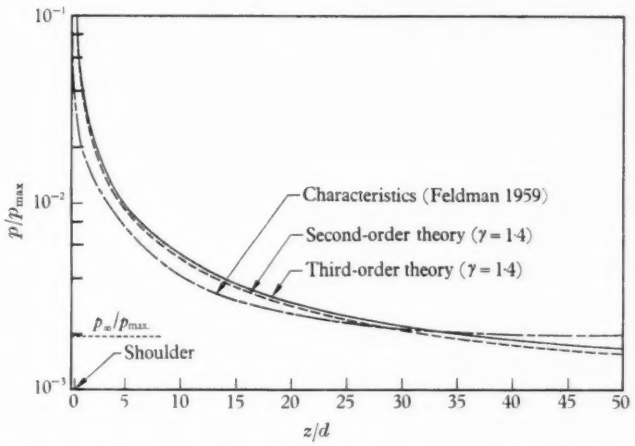

FIGURE 6. Surface pressure distribution on a hemisphere-cylinder; $M_\infty = 17{\cdot}98$.

Hence, since the predicted shoulder pressure is incorrect and changes very little between second- and third-order theories, application of one of the curve-shifting schemes to correct this deficiency (Casaccio 1959) will result in a more accurate pressure-distribution prediction by third-order theory than by second-order theory for the entire lengths of the bodies considered.

We might again point out that, due to the large entropy gradient in the vicinity of the body, the blast-wave analogy is not valid in this region. The pressure distribution obtained by the analogy actually applies on a body derived by taking the entropy layer into account (Sychev 1960). This fact accounts for some of the discrepancy between experimental or exact numerical results and blast wave theory.

REFERENCES

CASACCIO, A. 1959 Theoretical pressure distribution on a hemisphere-cylinder combination. *J. Aero Sci.* **26**, 63–4.

FELDMAN, S. 1959 A numerical comparison between exact and approximate theories of hypersonic inviscid flow past slender blunt-nosed bodies. *AVCO Everett Research Report* 71.

HAYES, W. P. 1947 On hypersonic similitude. *Quart. Appl. Math.* **5**, 105–6.

LEES, L. & KUBOTA, T. 1957 Inviscid hypersonic flow over blunt-nosed slender bodies. *J. Aero. Sci.* **24**, 195–202.

LIN, S. C. 1954 Cylindrical shock waves produced by instantaneous energy release. *J. Appl. Phys.* **25**, 54–7.

MEL'NIKOVA, N. S. 1954 *Zh. Mekhanika* **3**, 2535.

SAKURAI, A. 1953 On propagation and structure of the blast wave. I. *J. Phys. Soc. Japan*, **8**, 662–9.

SAKURAI, A. 1954 On propagation and structure of the blast wave. II. *J. Phys. Soc. Japan*, **9**, 256–66.

SEDOV, L. I. 1946 Propagation of strong blast waves. *Prikl. Mat. Mekh.* **10**, 241–50.

SWIGART, R. J. 1960 Third-order cylindrical blast-wave theory and its analogy to the flow about hemisphere-cylinder configurations in high speed flight. *Lockheed Missiles and Space Division Report* no. 288210.

SYCHEV, V. V. 1960 On the theory of hypersonic gas flow with a power-law shock wave. *Prikl. Mat. Mekh.* **24**, 518–23.

TAYLOR, G. I. 1950 The formation of a blast wave by a very intense explosion. *Proc. Roy. Soc.* A, **201**, 159–86.

The stability of a viscous fluid between rotating cylinders with an axial flow

By R. C. DIPRIMA

Department of Mathematics, Rensselaer Polytechnic Institute, Troy, New York

(Received 25 July 1960)

The stability of a viscous fluid between two concentric rotating cylinders with an axial flow is investigated. It is assumed that the cylinders are rotating in the same direction and that the spacing between the cylinders is small. The critical Taylor number is computed for small Reynolds number associated with the axial flow. It is found that the critical Taylor number increases with increasing Reynolds number.

1. Introduction

The stability characteristics of viscous flow between concentric rotating cylinders with an axial flow are of interest in several technical areas including paper making (Appel 1959), and the design of rotating electrical machinery (Kaye & Elgar 1957).

Goldstein (1937) considered this problem theoretically for the case of the outer cylinder at rest and the gap between the cylinders small compared to the mean radius. He found that the critical Taylor number T (associated with the angular velocity of the inner cylinder)* increases initially, as the Reynolds number R (associated with the axial velocity) increases from 0 to a value of about 20, and then decreases quite rapidly as R increases to about 25.

Cornish (1933) and Fage (1938) used pressure drop measurements to determine experimentally the critical angular velocity of the inner cylinder for given axial flows in the case in which the outer cylinder is at rest. The results of both of these investigations indicated that the critical Taylor number increases with increasing Reynolds number. However, the results of the two investigations are considerably different from one another. The results of Cornish (1933) give Taylor numbers larger by a factor of about three than those found by Fage (1938). Indeed an extrapolation of Cornish's results to the case of zero axial velocity gives a value of the critical Taylor number about three times larger than the known correct value. For this reason Goldstein (1937) concluded that Cornish was measuring a different phenomenon from that considered by himself. On the other hand, the results of Fage (1938), while giving the correct Taylor number when extrapolated to the case of zero axial velocity, show only a very slight increase of the critical Taylor number with increasing Reynolds number until fairly large values of R. More recently Kaye & Elgar (1957) have considered

* See equations (5) for a precise definition of the Taylor number and the Reynolds number.

this problem experimentally using an apparatus which allowed visual and photographic as well as hot-wire measurements. Their measurements (again, for the case of the outer cylinder at rest) show that the critical Taylor number increases fairly rapidly with increasing Reynolds number. Their results are in disagreement with the results of Cornish (1933) and Fage (1938).

This paper is concerned with a theoretical analysis of the stability of a viscous fluid between concentric rotating cylinders with a small axial flow. The characteristic value problem is formulated in §2 using the assumption that the spacing between the cylinders is small compared to the mean radius. In the case in which the cylinders are rotating in the same direction, the characteristic value problem is solved in §3 with the axial velocity replaced by its average value. Several methods of solving this problem are discussed. In §4 the same problem is treated using a parabolic axial velocity distribution and the results are compared with those of §3. It is found in both cases that the critical Taylor number increases rapidly (more rapidly for the latter case) from the correct value ($T \sim 1710$) at $R = 0$ to a value of abut 7000 at $R = 60$. The results further show that the frequency and wavelength of the distribution are sensitive to the approximation used for the axial velocity. In both cases the results of the present analysis are in complete disagreement with the work of Goldstein (1937), Cornish (1933) and Fage (1938) and in qualitative agreement with the work of Kaye & Elgar (1957).

2. The characteristic value problem

Consider two infinitely long concentric cylinders. Let (r, θ, z) be cylindrical coordinates, and let R_1, R_2, Ω_1 and Ω_2 denote the radii and angular velocities of the inner and outer cylinders, respectively. If u_r, u_θ, u_z denote the components of velocity in the increasing r, θ, and z direction and p denotes the pressure, the Navier–Stokes equations admit a steady solution of the form

$$u_r = 0, \quad u_\theta = V(r), \quad u_z = W(r), \quad \partial p/\partial z = \text{constant}. \tag{1}$$

Now superimpose on this steady motion a rotationally symmetric disturbance of a form such that the θ component of velocity is

$$u_\theta(r, z, t) = V(r) + v(r)\, e^{i(\sigma t + \lambda z)}. \tag{2}$$

In general σ will be complex. The motion will be stable or unstable as the imaginary part of σ is positive or negative, respectively. We shall be concerned in this paper with the case of neutral stability for which the imaginary part of σ is equal to zero. Notice this is different from the case for zero axial flow where the instability is of a stationary cellular nature and σ is set identically equal to zero. Substituting for u_r, u_θ, u_z and p in the Navier–Stokes equations and neglecting quadratic terms in the disturbance velocities leads to a sixth-order system of linear homogeneous differential equations. The requirement of no slip at the boundaries gives six homogeneous boundary conditions.

In the case that the distance between the cylinders, $d = R_2 - R_1$, is small compared to the mean radius, $R_0 = \frac{1}{2}(R_1 + R_2)$, this system of equations can be considerably simplified. Neglecting terms of order d/R_0, the angular velocity $\Omega = V/r$

and the axial velocity W can be approximated by linear and parabolic profiles. To the same order of accuracy the non-dimensional disturbance equations for neutral stability may be written as

$$(D^2-a^2)^2 u - i\{\beta - aRf(x)\}(D^2-a^2)u + 12iaRu = -a^2 Tg(x)v, \tag{3}$$

$$(D^2-a^2)v - i\{\beta - aRf(x)\}v = u, \tag{4}$$

where

$$\left.\begin{aligned} &r = R_0 + dx, \quad D = d/dx, \quad a = \lambda d, \quad \beta = \sigma_r d^2/\nu, \\ &W(x) = W_{av} f(x), \quad f(x) = 6(\tfrac{1}{4} - x^2), \quad \Omega(x) = \Omega_{av} g(x), \\ &g(x) = 1 - 2\frac{1-k}{1+k}x, \quad k = \Omega_2/\Omega_1, \quad k \neq -1, \\ &R = |W_{av}|\, d/\nu, \quad T = -4A\Omega_{av} d^4/\nu^2, \quad A = \frac{\Omega_2 R_2^2 - \Omega_1 R_1^2}{R_2^2 - R_1^2}. \end{aligned}\right\} \tag{5}$$

σ_r denotes the real part of σ, u has been redefined as $(2Ad^2/\nu)u$, and W_{av} and Ω_{av} denote the average axial and angular velocities, respectively. The parameter T associated with the angular velocity is commonly referred to as the Taylor number, and the parameter R associated with the axial velocity will be referred to as the Reynolds number. Equations (3) and (4) are identical with (25) and (27) given by Goldstein (1937); however the notation is different.

The boundary conditions are

$$u = v = Du = 0 \quad \text{at} \quad x = \pm\tfrac{1}{2}. \tag{6}$$

Notice that when there is no axial flow, $R = 0$, $\beta = 0$, (3) and (4) reduce to those for the classical Taylor problem as given by Chandrasekhar (1954); and when the cylinders are stationary, i.e. $T = 0$, the equations uncouple and (3) reduces to the Orr–Sommerfeld equation for the stability of a viscous flow between parallel plates. Thus for small values of T and large R we can expect an instability of the Tollmien–Schlichting type, and for small R and large T the instability will be of a non-stationary cellular nature. Kaye & Elgar (1957) have pointed out that there are four regions depending upon the values of R and T. This is illustrated qualitatively in figure 1. In this paper we shall only consider the case in which R is small. That is, we are interested in determining the lower left branch of the curves depicted in figure 1.

The system of equations (3) and (4) together with the boundary conditions (6) determine a non-self adjoint characteristic value problem for T as a function of R, a, β and k. Mathematically the problem is the following: for given real values of R and k we wish to find the minimum positive value of T with respect to real positive values of a and real values of β. This minimum value of T, T_c say, determines the value of Ω_1 at which a secondary motion will first occur; the corresponding values a_c and β_c give the wave number and the frequency of the secondary motion. The wave velocity $c = \sigma_r/\lambda$ can be conveniently expressed in dimensionless form by $c/W_{av} = \beta/aR$.

It is clear that the determination of T_c is a rather complicated four-parameter problem and we shall now restrict ourselves to the case in which the cylinders rotate in the same direction. In this case it is known that, for $R = 0$, $\Omega(x)$ can be approximated by its average value (even for $\Omega_2 = 0$) with only a very small error in the determination of T_c (see Chandrasekhar 1960). From the form of equation

(3) it can be anticipated that this will still be a satisfactory approximation for $R \geqslant 0$ as long as $k \geqslant 0$. Thus we replace $g(x)$ by its average value of unity in (3).

Even with this approximation the mathematical problem is still difficult because of the variable coefficients in (3) and (4) arising from the axial velocity. The possibility of approximating $W(x)$ by its average value is a much more

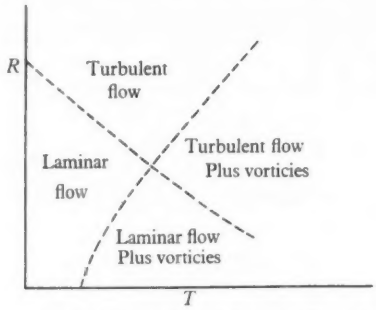

FIGURE 1. The four régimes of flow following Kaye & Elgar (1957).

delicate question than that of replacing $\Omega(x)$ by its average value for $k \geqslant 0$. Indeed from studies of the Orr–Sommerfeld equation we can expect that for large R the characteristic value will be very sensitive to variations in $W(x)$. However, for the case of small R considered here the situation should not be as serious, and in the next section we shall replace $W(x)$ by its average value in (3) and (4). With these approximations we obtain a characteristic value problem which can be solved accurately and fairly easily. In § 4 we shall treat by approximate methods the much more difficult problem where a parabolic profile is used for $W(x)$.

3. Case 1; W and Ω approximated by their average values

In this case we replace $f(x)$ and $g(x)$ each by unity and (3) and (4) reduce to

$$\{(D^2-a^2)^2 - i\xi(D^2-a^2) + 12iaR\}\, u = -Ta^2 v, \tag{7}$$

$$\{(D^2-a^2) - i\xi\}\, v = u, \tag{8}$$

where we have let $\xi = \beta - aR$. The characteristic value problem defined by the above equations and the boundary conditions (6) can be treated to a high degree of accuracy by convenient approximate techniques such as the Galerkin method or it can be solved exactly by the techniques used by DiPrima (1960) to treat similar problems. In this section we shall compare several such methods.

To solve the problem exactly, let $Z = T^{\frac{1}{2}}$, redefine u as $iaZu$ and define the functionals $\phi(u, v)$ and $\psi(u, v)$ by

$$\phi\ u, v) = \frac{1}{2}\int_{-\frac{1}{2}}^{\frac{1}{2}} \{[(D^2-a^2)\, u]^2 + i\xi[(Du)^2 + a^2u^2] + 12iaRu^2 - (Dv)^2 - a^2v^2 - i\xi v^2\}\, dx, \tag{9}$$

$$\psi(u, v) = \int_{-\frac{1}{2}}^{\frac{1}{2}} uv\, dx. \tag{10}$$

The above characteristic value problem is equivalent to the following variational principle: Among all functions u and v satisfying the boundary conditions (6), that set which makes the first variation of $I(u,v) = \phi(u,v) - iaZ\psi(u,v)$ vanish necessarily satisfy equations (7) and (8). The proof of this variational principle and the details of the solution are very similar to problems treated by DiPrima (1960) and hence only a brief summary of the method of solution will be given here.

To solve the variational problem we first note that the solution can be split into even and odd functions about $x = 0$. For the even solution we expand u and v in a complete set of even orthonormal functions on $-\frac{1}{2} \leqslant x \leqslant \frac{1}{2}$. Appropriate series are

$$u(x) = \sum_{n=1}^{\infty} a_n E_n(x), \quad v(x) = \sum_{n=1}^{\infty} b_n E_n(x), \tag{11}$$

where the $E_n(x) = 2^{\frac{1}{2}} \cos(2n-1)\pi x$. The boundary conditions $u = v = 0$ at $x = \pm\frac{1}{2}$ are automatically satisfied; the boundary conditions $Du = 0$ at $x = \pm\frac{1}{2}$ introduce the constraining condition

$$\Gamma = \sum_{n=1}^{\infty} (-1)^{n+1}(2n-1)a_n = 0. \tag{12}$$

Substituting the series for u and v in the expression for I and making use of the orthonormal properties of the $E_n(x)$ gives I as a function of the a_n and b_n. The vanishing of the first variation in I subject to the constraint (12) requires the vanishing of the partial derivatives of $I - \mu\Gamma$ with respect to the a_n and b_n. Here μ is a Lagrange multiplier. This leads to two simultaneous linear non-homogeneous equations for a_n and b_n. Solving for a_n and substituting in the condition $\Gamma = 0$ gives the following equation for T as a function of R, a, and ξ

$$\sum_{n=1}^{\infty} \frac{(2n-1)^2(A_n + i\xi)}{\{A_n(A_n + i\xi) + 12iaR\}(A_n + i\xi) - a^2T} = 0, \tag{13}$$

where $A_n = (2n-1)^2\pi^2 + a^2$. This equation after separation into its real and imaginary parts and some simple algebraic manipulations to improve the convergence of one of the series (the convergence is like $(2n-1)^{-4}$) can be solved by trial and error methods. For given values of R and a there are a sequence of pairs of real numbers (ξ, T) that satisfy the two equations. Choosing the smallest positive value of T and the corresponding value of ξ and then minimizing with respect to a determines T_c and the corresponding values of a and ξ. In carrying out the numerical computations a sufficient number of terms in the series were used to insure that there would be less than 1 % error in the determination of T_c. The results of the computations for $R = 5{\cdot}17$, $20{\cdot}67$, $25{\cdot}84$ and 100 are given in table 1. The odd solution which gives a larger value of T_c can be treated in a similar manner.

Although the above method can be used to determine the characteristic values as accurately as one wishes, satisfactory answers can be obtained by approximate methods that are easier to use. Also in solving equation (13) it is desirable to have first approximations to the roots as a starting point for the computations. Approximate solutions can be obtained conveniently by the Galerkin method. This method consists of expanding u and v in sets of complete functions, preferably orthogonal, that satisfy the boundary conditions and then requiring the

error in the equations for u and v to be orthogonal to the expansion functions for u and v. Thus for the even solution of equations (7) and (8) we write u and v as

$$u(x) = \sum_{n=1}^{M} a_n C_n(x), \quad v(x) = \sum_{n=1}^{M} b_n E_n(x), \tag{14}$$

Investigation	R	a	β	β/aR	T
1	0	3·10	0	—	1,728
4	0	3·10	0	—	1,715
1	1	3·11	2·53	0·814	1,730
2	1	3·11	2·53	0·814	1,710
1	2	3·11	5·06	0·814	1,734
2	2	3·12	5·08	0·814	1,714
4	5	3·1	12·6	0·813	1,753
1	5·17	3·12	13·13	0·816	1,769
2	5·17	3·13	13·16	0·813	1,750
3	5·17	3·1+	13·02	0·812	1,748
1	10·34	3·16	26·63	0·815	1,890
2	10·34	3·17	26·68	0·814	1,870
4	20·0	3·4	55·7	0·819	2,309
1	20·67	3·4	57·64	0·820	2,360
2	20·67	3·4	57·52	0·818	2,338
3	20·67	3·4	57·38	0·816	2,340
1	25·84	3·55	75·56	0·824	2,698
3	25·84	3·55	75·33	0·821	2,678
1	40	4·2	141·2	0·840	3,893
2	40	4·23	142·0	0·839	3,860
4	40	4·2	140·9	0·839	3,881
1	60	5·15	267·7	0·866	5,988
2	60	5·15	267·1	0·864	5,925
4	60	5·2	270·2	0·866	5,962
1	80	5·90	417·9	0·885	8,368
2	80	5·92	418·7	0·884	8,261
4	80	6·0	425	0·885	8,319
1	100	6·54	588·2	0·899	10,960
2	100	6·58	591·4	0·899	10,800
3	100	6·55	587·2	0·896	10,800
4	100	6·6	594·0	0·900	10,876

TABLE 1. Critical Taylor numbers and corresponding values of a and β and β/aR for assigned values of R. Investigation 1 refers to Galerkin method with $M = 1$; 2 refers to Galerkin method with $M = 2$; 3 is the exact solution; 4 refers to the results of Chandrasekhar (1960). (W and Ω are approximated by their average values.)

where the $E_n(x)$ are the functions defined earlier, and the $C_n(x)$ are even orthonormal functions* satisfying C_n and $DC_n = 0$ at $x = \pm\frac{1}{2}$. Substituting these series in equations (7) and (8), multiplying (7) by $C_j(x)$ and (8) by $E_j(x)$ for $j = 1, 2, \ldots, M$, and integrating from $-\frac{1}{2}$ to $+\frac{1}{2}$ gives $2M$ simultaneous

* The functions $C_n(x)$ are of the form $(\cosh \lambda_n x)/(\cosh \frac{1}{2}\lambda_n) - (\cos \lambda_n x)/(\cos \frac{1}{2}\lambda_n)$, where the λ_n are the positive roots of $\tanh \frac{1}{2}\lambda + \tan \frac{1}{2}\lambda = 0$. These functions have been tabulated by Reid & Harris (1958).

linear homogeneous equations for $a_1 \dots a_M$, $b_1 \dots b_M$. A determinantal equation of order $2M$ for T as a function of R, a, and ξ is obtained from the necessary condition that the determinant of the coefficients vanish. Computations have been carried out for $M = 1$ and 2 and the results are tabulated in table 1. The results for $M = 2$ are also shown graphically in figure 2. It is clear from table 1 that the results even for $M = 1$ are satisfactory, differing by about 1 % or less from the results for $M = 2$, and in close agreement with the results obtained from the exact computations. The success of the Galerkin methods with $M = 1$ for this problem rests essentially on the fact that there are no singular points in equations (7) and (8); hence the characteristic function corresponding to the smallest positive value of T can be easily approximated. Further, for $M = 1$ the computations are particularly easy, requiring only the evaluation of some simple integrals, Finally, it should be pointed out that the solution of the characteristic problem by the Galerkin method as it has just been described is completely equivalent to the substitution of the series given by (14) in the expressions for ϕ and ψ and then requiring I to be stationary as a function of the a_n and b_n.

When this work was nearly completed the author learned that Chandrasekhar (1960) had considered the characteristic value problem defined by equations (7) and (8) and the boundary conditions (6) with R replaced* by $-R$ and the variables u and v redefined so that the right-hand sides of equations (7) and (8) are v and $-Ta^2u$, respectively. The problem is solved by the methods developed and used by Chandrasekhar in a series of papers. The function $v(x)$ is expanded in a set of complete functions satisfying the boundary conditions $v = 0$ at $x = \pm \frac{1}{2}$, and equation (7) is then solved for (u) the four constants of integration being determined by the boundary conditions $u = Du = 0$ at $x = \pm \frac{1}{2}$. The series for u and v are then substituted in the second-order equation for v and a characteristic determinantal equation is obtained by requiring that the error in the differential equation be orthogonal to the original expansion functions. This method is an improvement on the Galerkin technique but it does require in this case a considerable amount of complex arithmetic. On the other hand, it should be pointed out that the size of the determinantal equation increases like M rather than $2M$ as was the case earlier. The results found by Chandrasekhar (1960) using one term in the series for v are in agreement with the results obtained by the Galerkin method and the exact solution. They are recorded in table 1.

4. Case 2; Ω approximated by its average value

In this case (3) and (4) may be rewritten as

$$(D^2-a^2)^2 u - i\{\xi + aR[1-6(\tfrac{1}{4}-x^2)]\}(D^2-a^2)u + 12iaRu = -Ta^2v, \quad (15)$$

$$(D^2-a^2)v - i\{\xi + aR[1-6(\tfrac{1}{4}-x^2)]\}v = u, \quad (16)$$

where again we have let $\xi = \beta - aR$. These equations are identical with (7) and (8) for case 1 except for the bracketed term $1-6(\frac{1}{4}-x^2)$. This term would be

* This simply means that the axial velocity is in the opposite direction to that chosen here, and hence since the disturbance velocities have the same form the values of σ (β in this paper) tabulated by Chandrasekhar in table 1 of his paper should be prefixed by a minus sign. This was a typographical error.

replaced by zero if we approximate the axial velocity by its average value. Because of the presence of this term the characteristic value problem defined by (15) and (16) and the boundary conditions (6) is considerably more difficult than the characteristic value problem of case 1. Neither the method used earlier for the exact solution nor the method suggested by Chandrasekhar is applicable here.

Approximate values of T can be found using the Galerkin method. Again the solution can be split into even and odd functions. For the even solution we use the series given in (14) for u and v and proceed in the manner described in the

Investigation	R	a	β	β/aR	T	T_1/T_2
1	1	3·11	3·63	—	1729	—
2	1	3·12	3·65	1·17	1710	1·01
3	1	3·11	2·53	0·814	1710	—
1	2	3·11	7·26	—	1732	—
2	2	3·12	7·30	1·17	1714	1·01
3	2	3·12	5·08	0·814	1714	—
1	5·17	3·11	18·77	—	1750	—
2	5·17	3·12	18·9	1·17	1744	1·003
3	5·17	3·13	13·16	0·812	1750	—
1	10·34	3·15	38·05	—	1815	—
2	10·34	3·13	37·8	1·17	1852	0·980
3	10·34	3·17	26·68	0·813	1870	—
1	20·67	3·28	79·40	—	2068	—
2	20·67	3·15	75·8	1·16	2293	0·902
3	20·67	3·40	57·52	0·818	2338	—
1	40	3·95	187·5	—	2887	—
2	40	3·2	147·7	1·15	4066	0·710
3	40	4·23	142·0	0·839	3860	—
1	60	4·73	342·6	—	3961	—
2	60	3·15	215·7	1·14	7563	0·524
3	60	5·15	267·1	0·864	5925	—

TABLE 2. Critical Taylor numbers and corresponding values of a and β and β/aR for assigned values of R. Investigations 1 and 2 refer to the Galerkin method with $M = 1$, and 2 with a parabolic profile used for W. 3 refers to the Galerkin method with $M = 2$ and W approximated by its average value. T_1/T_2 is the ratio of the values of T for investigations 1 and 2.

previous section. Actually the only new computations required are the evaluation of the integrals involving x^2. Computations have been carried out for $M = 1$ and 2, and the results are tabulated in table 2. The results from case 1 using the Galerkin method with $M = 2$ are also shown in table 2, and the results for cases 1 and 2 with $M = 2$ are given graphically in figure 2.

There are two points that should be made about these results. First, in case 2 as R increases beyond about a value of 20–30 there is an increasing difference between the results of the first and second approximations. This indicates that when the parabolic profile is used for the axial velocity the characteristic functions are more difficult to approximate. Practically speaking, since there is little difference between the first and second approximations up to values of $R \sim 20$, we might expect the second approximation to be satisfactory up to values of

$R \sim 40$. Of course, the only way we can be sure the second approximation is satisfactory is to compute a third approximation and compare the two. This would require the solution of a sixth-order determinantal equation with complex entries, which was not done in the present work. Further it should be noted that the two-term approximation predicts only a very slight increase of critical wave-number with increasing R up to values of about 40–50 and then a slight decrease. However, it would be dangerous to draw any conclusions about this decrease in a_c at $R = 60$ with the information available.

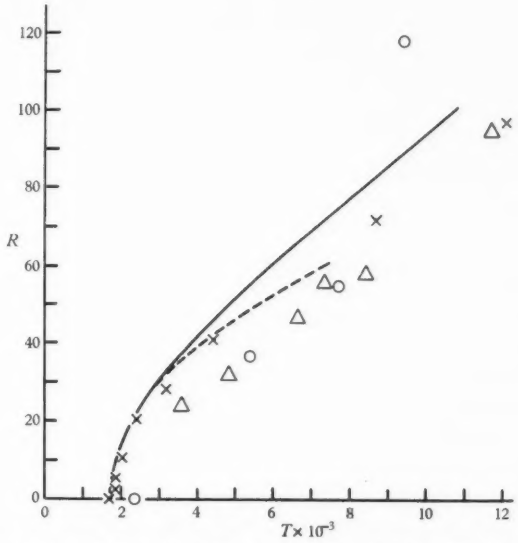

FIGURE 2. The variation of the critical Taylor number, T_c, as a function of the Reynolds number, R. Solid and dashed curves refer to the axial velocity approximated by its average value and by a parabolic profile, respectively. Values of T_c computed from the experimental data of Kaye & Elgar (1957), ○ for $d/R_0 = 0{\cdot}307$ and △ for $d/R_0 = 0{\cdot}198$; and Donnelly & Fultz (1960), × with $d/R_0 = 0{\cdot}0516$ are also shown.

The second point concerns the difference between the two-term approximations for the two cases. Even for very small values of R the results of case 2 (W approximated by a parabolic profile) give a frequency that is higher than that for the case 1 (W approximated by its average value). As R increases beyond a value of about 20–30 the values of T_c and a_c for the two cases also begin to diverge; T_c for case 2 grows more rapidly than for case 1, and a_c for case 2 remains nearly constant while increasing for case 1. These differences can be traced to the evaluation of the integrals

$$\int_{-\frac{1}{2}}^{\frac{1}{2}} \{1-6(\tfrac{1}{4}-x^2)\} C_n (D^2-a^2) C_m \, dx \quad \text{and} \quad \int_{-\frac{1}{2}}^{\frac{1}{2}} \{1-6(\tfrac{1}{4}-x^2)\} E_n E_m \, dx. \quad (17)$$

If $W(x)$ is approximated by its average value these integrals vanish; on the other hand, when the parabolic profile is used they take on values such that when multiplied by the factor aR they are of the same order of magnitude as the larger con-

tributions from other terms in the differential equations. Indeed for $n = m = 1$ and $a \sim 3$ the first integral in (17) is approximately 10, and when multiplied by aR for $R \sim 20$–60 gives a contribution of about 600–1800. This must be compared with the contributions from the integral of $C_1(D^2 - a^2)^2 C_1$ from $-\frac{1}{2}$ to $\frac{1}{2}$ which is about 700 for $a \sim 3$.

5. Discussion

The results of the present analysis show that when the cylinders are rotating in the same direction the critical Taylor number increases rapidly with increasing Reynolds number. Depending upon whether the axial velocity is approximated by its average values or by a parabolic profile, the results are slightly different. In the latter case, relative to the former the increase in T_c with increasing R is more rapid, the corresponding values of the frequency are greater, and the values of the wave-number are less. The ratio of the wave velocity to the mean average axial velocity is approximately constant up to values of $R \sim 40$ in each case but greater by a factor of about 1·17 in the latter case and less by a factor of about 0·82 in the former case.

In figure 2 the variation of T_c with R for the two cases is shown graphically and also compared with the recent experimental work of Kaye & Elgar (1957) and Donnelly & Fultz* (1960). For values of R up to about 20–30 the results of Donnelly & Fultz are in good agreement with the results for both cases; for larger values of R their measurements tend to confirm the more rapid increase in T_c with increasing R predicted by the use of a parabolic profile for the axial velocity. The results of Kaye & Elgar (1957) are also in qualitative agreement with the theoretical results found here. For small values of R the larger values of T_c that they find may be attributed, in part, to the larger values of d/R_0 that were used in their experiments. Indeed for $R = 0$ computation of the critical Taylor number as defined here for the case $k = 0$ and $d/R_0 = \frac{2}{3}$ using the critical value of Ω_1 found by Chandrasekhar (1958) gives a value of T_c of about 3100 in contrast to a value of about 1710 found using a small-gap approximation.

The question of the variation of the wave-number and frequency associated with the secondary motion with R requires more detailed measurements than have been carried out to date. However, Donnelly & Fultz (1960) did make one frequency measurement, finding $\beta \sim 5{\cdot}8$ at $R \sim 2{\cdot}7$. This value of β is below the value predicted in both cases 1 and 2. Also, though Kaye & Elgar (1957) did not make any measurements of λ, Elgar in a letter to the author pointed out that for the range of Reynolds numbers considered here it was his impression that the wavelength changed only slightly with increasing R. This would again tend to confirm the results found using a parabolic profile for the axial velocity.

The theoretical results of Goldstein (1937) which predict that T_c will increase with increasing R up to values of about 15–20 and then decrease rapidly with increasing R ($T_c \sim 763$ at $R = 25{\cdot}84$) are not shown in figure 2. As mentioned earlier, the characteristic value problem formulated here is identical with that

* Just as this manuscript was completed Mr Donnelly and Mr Fultz, in a private communication, were kind enough to furnish the author the preliminary data that are shown in figure 2.

treated by Goldstein (1937) Since the results found here in case 1 agree with those found independently and by a different method by Chandrasekhar (1960), it would appear that there must be a numerical error in Goldstein's computations. However, his computations were much too lengthy to check in detail. Also the experimental results of Cornish (1933) and Fage (1938) which are in disagreement with the theoretical results found here and the more recent experimental work are not shown in figure 2. For a comparison of these results with the experimental results of Kaye & Elgar (1957), see the latter paper.

Finally, this analysis shows clearly that the simpler characteristic-value problem with Ω and W approximated by their average values can be solved easily by several methods. The results of even a one-term approximation using the Galerkin method are satisfactory up to Reynolds number of at least 100. On the other hand, the more physically correct situation with W approximated by a parabolic profile leads to a much more difficult mathematical problem. In this case the use of the Galerkin method with two terms gives results that are acceptable only up to values of the Reynolds number of about 40–50.

The results presented in this paper were obtained in the course of research sponsored by the Mechanics Branch of the Office of Naval Research.

REFERENCES

Appel, C. 1959 *Tech. Assoc. Pulp & Paper Industry*, **42**, 767–73.
Chandrasekhar, S. 1954 *Mathematika*, **1**, 5–13.
Chandrasekhar, S. 1958 *Proc. Roy. Soc.* A, **246**, 301–11.
Chandrasekhar, S. 1960 *Proc. Nat. Acad. Sci.* **46**, 141–3.
Cornish, R. J. 1933 *Proc. Roy. Soc.* A, **140**, 227–40.
DiPrima, R. C. 1960 *Quart. Appl. Math.* (in the Press).
Donnelly, R. & Fultz, D. 1960 *Proc. Nat. Acad. Sci.* **46**, 1150–4.
Fage, A. 1938 *Proc. Roy. Soc.* A, **165**, 501–29.
Harris, D. & Reid, W. H. 1958 *Astrophys. J.* **3**, 429–53.
Goldstein, S. 1937 *Proc. Camb. Phil. Soc.* **33**, 41–61.
Kaye, J. & Elgar, E. C. 1957 *Trans. Amer. Soc. Mech. Eng.* **80**, 753–65.
Reid, W. & Harris, D. 1958 *Astrophys. J. Supp.* **3**, 429–52.

REVIEWS

The Gulf Stream: A Physical and Dynamical Description. By HENRY STOMMEL. University of California Press, 1959. 202 pp. 45*s*.

The intense current system in the western North Atlantic Ocean, called the Gulf Stream, is perhaps the best explored of all oceanic phenomena, although improving technique and instrumentation for research at sea are continually revealing features of major interest of the stream. The existence of the current has long been known from the directly observable surface velocities, and from the distinctly different properties, e.g. temperature, of the water masses on either side of the stream. The velocity structure and transport of the current have been inferred from observable profiles of density. From the Straits of Florida north to Cape Hatteras the current follows the coast of the United States; at that point it leaves the coast and flows to the north-east, holding together at least to the region of the Grand Banks. The stream is of the order of 100 km in width, and does not broaden appreciably after leaving the coast, although the position of the stream does become considerably more variable. In the region away from the coast, meanders (or loops in the stream) occur on a length scale of hundreds of kilometres (the downstream scale of the current itself is thousands of kilometres). In 1950, a multiple ship survey, lasting for 17 days, observed a meander to grow, to oscillate and finally to detach completely as an elongated eddy.

An intense western current system is not peculiar to the North Atlantic. Analogous currents are known to exist in the western parts of all oceans bounded by land masses which run roughly north to south. Most notable is the Kuroshio of the North Pacific. Moreover, the western current is not an isolated or local phenomenon, but is more appropriately described as the most striking feature of the total large scale current systems, i.e. of the so-called general circulation of an ocean.

The general oceanic circulation poses a highly complex problem of fluid mechanics, a problem which most fluid dynamicists will find somewhat unusual because of the unique manner in which the motion relative to the rotating earth is constrained by Coriolis accelerations. The accelerations due to the component of the earth's rotation parallel to gravity completely dominate those due to the normal component. Thus Coriolis effects vary from practically zero at the equator to a maximum at the poles. Correspondingly, there is a differential advection of vorticity relative to the earth by the basic rotational motion, which, over the main body of the ocean, almost entirely balances the curl of internal stresses caused by the atmospheric winds acting upon the upper free surface. The field of motion resulting from this balance has, however, a meridional component which is everywhere towards the equator. Since mass conservation does not permit a net transport across the ocean basin, a region in which some other process of vorticity transfer becomes dominant is necessary to complete the flow field. Because of the basic asymmetry of the rotational constraint, this singular region of intense poleward flow occurs along the western boundary of the ocean. In a simple but elegant paper in 1948, the author of *The Gulf Stream* first showed

the existence of the intense western current system to be intimately related to the latitudinal variation of Coriolis effects. This initiated a period of research and study which during the intervening years has produced sufficient understanding of the Stream to make this book feasible.

The stated purpose of the book is to communicate to physical scientists in general what is known about the intriguing natural phenomenon with which it deals. The chapter headings provide a good indication of the author's approach to this task. They are as follows: Historical introduction, Methods of observation, The geostrophic relationship, Large-scale features of the North Atlantic circulation, The wind system over the North Atlantic, Linear theories of the Gulf Stream, Non-linear theories of the Gulf Stream, Meanders in the Stream, Fluctuations in the currents, Role of the thermohaline circulation. The manner and level of discussion of the different topics vary throughout the book. The brief but scholarly historical section will be most enjoyable to those whose understanding of a subject is enhanced by a knowledge of the manner in which presently accepted ideas have evolved. The treatment of factual information and very basic theoretical ideas which follows is lucid and self-contained, and thus invaluable to the non-specialist. A higher level of mathematical sophistication is necessary for a full understanding of the theories of the mean current which are next presented in some detail.

The remaining chapters on time-dependent properties and the thermal circulation, which deal with features of the stream which are much less well understood, are probably of most value to the professional oceanographer. In particular, the discussion of meanders and fluctuations is suggestive rather than definitive. The reviewer feels that the usefulness of these sections is limited by the omission of theoretical calculations, the results of which are discussed at some length (e.g. the time-dependent problem of Veronis and Morgan and the stability analysis of Haurwitz and Panofsky). A full appreciation of Stommel's discussion can be achieved only by going to the original literature and then returning to the book.

Our knowledge of the thermohaline circulation of the oceans is advancing rapidly. The delay of four years between the writing and publication of the book has made this section already out-of-date, as may be inferred from the footnotes added in proof. The interested reader may wish to refer to two articles by Stommel and Arons, 'On the abyssal circulation of the world ocean' parts I and II, appearing this year in *Deep Sea Research*, which also contain references to relevant intervening work.

Throughout *The Gulf Stream* there persists a critical analysis of underlying assumptions and hypotheses which are made both in the interpretation of oceanographic observations and in the formulation of mathematical models. This constitutes a valuable contribution to oceanography. The book itself is attractively produced and the author's style is highly readable. The bibliography, data sources, diagrams and illustrations form a valuable collection. This short treatise is highly recommended to all scientists with a real curiosity concerning the Gulf Stream and the associated wealth of fascinating oceanographic phenomena.

ALLAN R. ROBINSON

Viscoelasticity: Phenomenological Aspects. Edited by J. T. BERGEN. New York: Academic Press, 1960. 150 pp. $6.00.

This book consists of seven papers given at a symposium in Pennsylvania organized by the Armstrong Cork Company in April 1958. The subject is phenomenological or macroscopic viscoelasticity; that is, the viscoelastic material is treated as a continuum and its response to stress or strain is described by equations whose elements are derived from the theories of continuum mechanics. Each paper is an up-to-date treatment of a particular aspect of the subject. The book is not a comprehensive treatise but, in the reviewer's opinion, provides an excellent introduction to the concepts of the subject to anyone prepared to read it through at least twice.

The first three papers treat linear viscoelasticity: they are 'Stress analysis for viscoelastic bodies' by E. H. Lee, 'The linear viscoelastic behaviour of rubber-like polymers and its molecular interpretation' by Robert S. Marvin, and 'Comparisons of viscoelastic behaviour in seven typical polymer systems' by John D. Ferry and Kazuhiko Nimomiya. The last four papers are concerned with non-linear viscoelasticity: 'The behaviour of certain viscoelastic materials in laminar shearing motions' by J. L. Ericksen, 'Constitutive equations for classes of deformations' by R. S. Rivlin, 'Stress relaxation of polymeric material in combined torsion and tension' by J. T. Bergen, and 'The normal stress effect in polymer solutions' by Hershel Markovitz. (If any stress $\sigma_1(t)$ produces strain $\epsilon_1(t)$ and any stress $\sigma_2(t)$ produces strain $\epsilon_2(t)$, then the material is said to be linear if stress $\sigma_1(t)+\sigma_2(t)$ produces strain $\epsilon_1(t)+\epsilon_2(t)$, t being time.)

The analyses of stress and strain (or strain rate) are common to all branches of continuum mechanics. It is the set of relationships between stress and strain which characterizes the different branches of the subject. For an isotropic linear viscoelastic material there are two independent functional relationships, the one connecting each deviatoric component of stress to the corresponding deviatoric component of strain and the other connecting the first invariant of stress to the dilatation; both relationships can be expressed in various equivalent forms. It is these forms, the means of converting one into another and the molecular interpretation of the model form, which Marvin treats in his paper. Experimentally it is possible to determine the complex modulus, the ratio of stress to strain at angular frequency ω when both are expressed in complex form $A\exp(i\omega t)$, for frequencies in the range 10^{-2} to 10^{10} radians per second. The creep function, strain against time at unit constant stress, can be measured for times greater than 1 sec. There is an overlap of about two decades, and it is possible to use either set of measurements to complete the time spectrum of the other set in the range where actual experimental measurement is not possible. The long-time end of the scale can frequently be extended by using the experimental fact that for many materials an increase in temperature casues a bodily shift of the real part of the complex compliance-frequency curve. The reviewer is rather doubtful, however, whether Marvin's extrapolation of the relaxation function to 10^{10} years is valid. (Complex compliance is the reciprocal of complex modulus and the relaxation function is the stress response to unit constant strain.)

Ferry and Nimomiya give the basic deviatoric viscoelastic functions for seven typical polymer systems. Five of the systems are amorphous polymers (i) of low molecular weight, (ii) of high molecular weight, (iii) of high molecular weight with long side groups, (iv) lightly vulcanized, and (v) below the glass transition temperature; the remaining systems are (vi) dilute polymer gel, and (vii) highly crystalline polymer. This list provides examples of actual materials to which the theory of linear viscoelasticity can be applied. Little experimental work appears to exist on the determination of dilatational viscoelastic functions.

Lee's paper is concerned with the solution of boundary value problems for linear viscoelastic materials. The governing differential equations are the strain-displacement equations, the equations of motion and the stress-strain relationships. It is frequently convenient to subject the time variable to an integral transform. The Laplace transforms of the stress-strain relationships involve the Laplace transforms of the creep or of the relaxation functions, while the Fourier transforms involve the complex moduli or compliances. If the boundary conditions are such that their transforms exist, then the transform approach is generally the best for that particular problem. The inverse transformation in general has to be evaluated numerically, although Lee gives examples where the stresses can be evaluated as explicit functions of space and time for the relatively simple case of a Maxwell material. For other problems it may be necessary to approximate to the stress-strain relationship by an equation of the form $P\sigma = Q\epsilon$, where P and Q are polynomials with constant coefficients in the operator d/dt; the fewer terms in P and Q, the easier the problem is to solve but the less accurate in general is the approximation. It is essential that such an equation be fitted to the experimentally measured viscoelastic functions over the time range which is significant for the particular problem considered.

It can be seen from the foregoing paragraphs that the theory of linear viscoelasticity is fairly comprehensive. This is not true of the non-linear theory. There is considerable diversity of opinion as to the form of the stress-strain relationship in the general case; in fact it is incorrect to talk of strain in this context, since workers in this field formulate relationships between the stress and the time derivatives of the displacement gradients. At present progress is being made by finding the stress, not for general displacement of a limited number of materials, but for particular classes of displacement of a wide range of materials.

Erickson starts by considering the postulate that the stress in simple shearing motion ($v_1 = Kx_2$, $v_2 = v_3 = 0$) is a function of certain symmetric tensors which appear in formulae for successive time derivatives of the distance between any two neighbouring particles. The components of stress can then be expressed as functions, in general arbitrary, of K and the time. The relationship thus formulated can be extended to any flow, which has the property that, in the neighbourhood of each point at any time, the flow can be reduced to the form $v_1 = Kx_2$, $v_2 = v_3 = 0$ by a rotation of axes. The rotation matrix in general depends on space and time. Such flows are called laminar shear flows. An interesting application is to flow through cylindrical pipes; it is the form of the arbitrary functions which decides whether linear flow, without secondary flow, is possible for a particular liquid through a pipe of arbitrary cross-section.

Rivlin investigates the stress-displacement gradient relationship for fixed displacements and for times large compared to the time at which the displacement was completed. The relationship contains the time explicitly. The form of the relationship is limited by two restrictions: (i) isotropy, and (ii) if the deformed body is subject to a rigid rotation, then the stress field is subject to the same rotation. The relationship is further simplified if the gradients are small. Rivlin calculates the torque and tension on a thin tube held at constant torsion and extension; the results contain one arbitrary function, a function of time and two invariants of the displacement gradient tensor.

Anyone who feels that Rivlin's paper is no more than an agreeable exercise in pure mathematics will be disillusioned by the paper that follows. Bergen carries out the experiments suggested by Rivlin on thin tubes of vulcanized rubber and of a type of polyvinyl chloride composition used for floor coverings. He finds that the arbitrary function mentioned above is of the form $\alpha(t)\beta(J)$, where J is the determinant of the classical strain matrix; he determines the functions α and β for these materials. In addition, by varying the rate at which the extension (without torsion) was initially applied, Bergen verifies Rivlin's initial hypothesis for these materials: if the time taken to apply the constant extension is T, then Bergen finds that the tension is independent of the rate of application at times later than $7T$ after the extension has become constant.

In the simple shearing motion considered by Ericksen, the normal deviatoric stress σ'_{22} is non-zero for most polymer solutions. Markovitz measures this stress experimentally with parallel plates, with cone and plate and with coaxial cylinders for various polymer solutions. He compares the measured stresses with those predicted by various rheological theories; the results are inconclusive.

D. R. Bland

Hypersonic Flow. Edited by A. R. Collar and J. Tinkler. Butterworth Scientific Publications, 1960. 70*s*.

This volume records the Proceedings of the Eleventh Annual Symposium of the Colston Research Society held in the University of Bristol in April 1959. The interests of the Colston Society are wide and varied and in past years subjects for symposia have been chosen in science and the arts, in medicine and administration; in 1959 Hypersonic Flow was chosen as an appropriate theme as this field of fluid dynamics is at present undergoing an interesting and active period of development.

Hypersonic conditions of flow correspond roughly to flows in excess of Mach number 5 and usually also imply high stagnation temperatures. In recent years the study of such flows has become important because of the rapid developments in rocket propulsion; such conditions obtain with long-range missiles, with artificial satellites and with space probes, particularly during the later stages of their launching period or during their re-entry into the Earth's atmosphere.

This meeting was attended by about one hundred members. Fifteen papers were presented and discussed at six half-day sessions. Five of the papers were

of a theoretical nature, and seven papers described a range of experimental facilities and recent results obtained in them; the remaining three papers dealt with design and operational aspects of hypersonic vehicles and propulsive units.

In the theoretical field, Guiraud of ONERA presents an extended examination of the Newtonian approximation when applied to the study of three-dimensional hypersonic flows. He derives formulae for the axial and normal forces and for the moment acting on a general body, and then more particularly for a cone and for a body of revolution at an angle of attack. The existence of a Ferri vortical layer on the surface of such a body is touched upon. Van Dyke of NASA describes some numerical methods of calculating the flow near the nose of a blunt body and in the neighbourhood of non-circular cones; marching techniques are used in both examples, starting from an assumed shock wave surface and terminating on the solid surface producing the disturbance. His results are generally satisfactory and compare well with similar results obtained by other investigators using slightly different methods. Mangler of the Royal Aircraft Establishment also describes a method of investigating the flow around a blunt body by a marching technique using specially chosen independent variables and describes some results obtained on an electronic computer. Miles of the University of California, Los Angeles, surveys methods of dealing with problems of unsteady flow at hypersonic speeds and examines various systems of approximation; he concludes that an adequate approximation to the unsteady aerodynamic pressure p' acting on bodies executing small motions in a hypersonic stream may be calculated from the plane wave relation $p' = \rho a v'$, where it is assumed that changes in entropy associated with the unsteady motion may be neglected. v' is the perturbation velocity normal to the perturbation wave front. In the fifth theoretical paper, Spence and Woods of the Royal Aircraft Establishment examine boundary layer and combustion effects that arise in a combustion-driven shock tube.

Of the seven papers dealing with experimental techniques and results, three describe recent work at the National Physical Laboratory. Henshall presents an account of measurements of shock speed and running time of their main shock tunnel; he also records measurements of the rate of heat transfer near a stagnation point and touches upon an investigation into the starting processes of the tunnel. In another paper Schultz describes investigations of gas ionization by an application of microwave techniques. Lapworth summarizes similarly recent results on the spectrograph measurement of gas temperatures in shock-tube flow for ranges of temperature below 10,000° K. Cox of the Armament Research and Development Establishment describes the development of light gas-gun tunnels at Fort Halstead; one of the main features of these tunnels is their longer running time when compared with that of the normal shock tube. He also touches upon the techniques used in these tunnels for measurements of pressure distributions, forces, heat transfer, etc., and describes a number of investigations designed to provide a comparison with other facilities. Bray of the University of Southampton reports a series of investigations designed to study the performance of their light gas-gun tunnel in considerable detail. This

work includes the recording of the motion of the piston, an analysis of the shock reflexion process and of the expansion conditions in the nozzle. Lobb of the U.S. Naval Ordnance Laboratory describes the expansion of the hypersonic test facilities at White Oak during recent years. This equipment includes wind tunnels, shock-tube tunnels and ballistic ranges. He also surveys the measuring techniques currently in use and presents a variety of results on real gas effects, on boundary-layer flow and on aerodynamic forces. Current hypersonic research at the Franco–German Institute (ISL) at Saint Louis is described by Oertel. This work includes the application of ballistic range techniques when carbon dioxide or carbontetrachloride is the working medium; use is also made of a shock expansion tube to obtain hypersonic flow of the order $M = 8$.

In the design field Eggers of NASA examines how future aircraft configurations, with adequate pay-load, can be made to attain intercontinental and global ranges and thus exploit the advantages of hypersonic speeds. He bases his investigations on the boost-glide form of flight path. His conclusions are that with increasing speed and range the trend will be first to more slender configurations with higher lift/drag ratios but that, for semi-global ranges and for speeds approaching that of satellites, the configurations should be more blunt and have higher lift and drag. Metcalfe of Bristol Aircraft also describes vehicle configurations for a number of flight conditions and for a range of operational tasks. He touches upon several problems of aerodynamic control. In the third paper of this group Jamison of Bristol Siddeley Engines surveys the problems of air-breathing propulsion devices for hypersonic flight and concludes that the maximum overall efficiency of a hydro-carbon fuelled ram-jet should be realized at around Mach 7. He outlines a project study of an aircraft designed for this speed and having a great circle range of 5000 miles.

Research on hypersonic flow has been built up steadily in the U.S.A. over the last 10 or 15 years, and in the United Kingdom mainly over the last 6 years. Although it does not aspire to give a comprehensive account of all the fields of activity in the U.S.A., the present volume does give a very adequate survey of most of the current lines of research in Western Europe. The present group of papers indicates a marked increase in research activity in Europe when compared with the work described at a similar symposium organized by AGARD at Scheveningen in July 1957. The proceedings of these two meetings, when studied alongside a systematic volume, such as that of Hayes and Probstein (*Hypersonic Flow Theory*, Academic Press, 1959) furnish a very good and broad introduction to this relatively new subject.

J. W. Maccoll

INDEX

BALL, F. K. Finite tidal waves propagated without change of shape, 506

BENJAMIN, T. BROOKE. Effects of a flexible boundary on hydrodynamic stability, 513

BLEVISS, Z. O. A study of the structure of the magnetohydrodynamic switch-on shock in a steady plane motion, 49

BOYER, D. W. An experimental study of the explosion generated by a pressurized sphere, 401

CHANG, I-DEE. Stokes flow of a conducting fluid past an axially symmetric body in the presence of a uniform magnetic field, 473

CONSTANTINE, T. On the movement of ships in restricted waterways, 247

DERGARABEDIAN, PAUL. Observations on bubble growths in various superheated liquids, 39

DIPRIMA, R. C. The stability of a viscous fluid between rotating cylinders with an axial flow, 621

DODD, K. N. On the disintegration of water drops in an air stream, 175

ELDER, J. W. An experimental investigation of turbulent spots and breakdown to turbulence, 235

ELDER, J. W. The flow past a flat plate of finite width, 133

GLAUERT, M. B. The method of images in shear flow, 561

GOODY, R. M. The influence of radiative transfer on the propagation of a temperature wave in a stratified diffusing atmosphere, 445

GREENSPAN, H. P. On longitudinal motion in a magnetic field, 455

GREGORY, N. and WALKER, W. S. Experiments on the effect of suction on the flow due to a rotating disk, 225

HASSAN, H. A. On unsteady laminar boundary layers, 300

HOWELLS, I. D. An approximate equation for the spectrum of a conserved scalar quantity in a turbulent fluid, 104

HUMPHREYS, JOHN S. On a circular cylinder in a steady wind at transition Reynolds numbers, 603

LAITONE, E. V. The second approximation to cnoidal and solitary waves, 430

LAUFER, JOHN and VREBALOVICH, THOMAS. Stability and transition of a supersonic laminar boundary layer on an insulated flat plate, 257

LIGHTHILL, M. J. Note on the swimming of slender fish, 305

LIGHTHILL, M. J. Note on waves through gases at pressures small compared with the magnetic pressure, with applications to upper-atmosphere aerodynamics, 465

LUDFORD, G. S. S. The propagation of waves along and through a conducting layer of gas, 119

MORTON, B. R. Weak thermal vortex rings, 107

PAIN, H. J. and SMY, P. R. The electrical conductivity of shock-ionized argon, 390

PHILLIPS, O. M. On the dynamics of unsteady gravity waves of finite amplitude. Part 1. The elementary interactions, 193

PHILLIPS, O. M. On the generation of sound by supersonic turbulent shear layers, 1

PROUDMAN, IAN. An example of steady laminar flow at large Reynolds number, 593

ROBINSON, A. R. On two-dimensional inertial flow in a rotating stratified fluid, 321

SAWYER, R. A. The flow due to a two-dimensional jet issuing parallel to a flat plate, 543

SHERCLIFF, J. A. One-dimensional magnetogasdynamics in oblique fields, 481

SMITH, D. H. and WINTLE, H. J. The propagation of sound in relaxing gases in tubes at low frequencies, 29

SMY, P. R. *See* PAIN, H. J.

STUART, J. T. On the non-linear mechanics of wave disturbances in stable and unstable parallel flows. Part 1. The basic behaviour in plane Poiseuille flow, 353

SWIGART, R. J. Third-order blast wave theory and its application to hypersonic flow past blunt-nosed cylinders, 613

TALWAR, S. P. Stability of a conducting rotating fluid of variable density, 581

TAYLOR, G. I. Deposition of a viscous fluid on a plane surface, 218

URSELL, F. Steady wave patterns of a non-uniform steady fluid flow, 333

VAGLIO-LAURIN, ROBERTO. Transonic rotational flow over a convex corner, 81

VINOKUR, M. Kinematic formulation of rotational gas flow, 533

VREBALOVICH, THOMAS. *See* LAUFER

WALKER, W. S. *See* GREGORY

WATSON, J. On the non-linear mechanics of wave disturbances in stable and unstable parallel flows. Part 2. The development of a solution for plane Poiseuille flow and for plane Couette flow, 371

WHITHAM, G. B. A note on group velocity, 347

WINTLE, H. J. *See* SMITH

WOODING, R. A. Rayleigh instability of a thermal boundary layer in flow through a porous medium, 183

YIH, CHIA-SHUN. A transformation for non-homentropic flows, with an application to large-amplitude motion in the atmosphere, 68

YIH, CHIA-SHUN. Exact solutions for steady two-dimensional flow of a stratified fluid, 161

REVIEWS

The Scientific Papers of G. I. Taylor. Vol. II: Meteorology, Oceanography and Turbulent Flow, 154

Advances in Geophysics. Vol. 6: Atmospheric Diffusion and Air Pollution, 156

Rheology: Theory and Applications. Vol. III, 158

Plasma Physics, 318

Units, Dimensions, and Dimensionless Numbers, 478

The Gulf Stream: A Physical and Dynamical Description, 632

Viscoelasticity: Phenomenological Aspects, 634

Hypersonic Flow, 636

JOURNAL OF FLUID MECHANICS

The JOURNAL OF FLUID MECHANICS exists for the publication of theoretical and experimental investigations of all aspects of the mechanics of fluids, and is issued in four parts per volume.

EDITOR

DR G. K. BATCHELOR

Department of Applied Mathematics and Theoretical Physics, University of Cambridge, Free School Lane, Cambridge, England

ASSISTANT EDITORS

DR T. B. BENJAMIN, DR I. PROUDMAN

Department of Applied Mathematics and Theoretical Physics, University of Cambridge, Free School Lane, Cambridge, England

ASSOCIATE EDITORS

PROF. G. F. CARRIER

Pierce Hall, Harvard University, Cambridge 38, *Massachusetts, U.S.A.*

DR W. C. GRIFFITH

Lockheed Missiles and Space Division, Palo Alto, California, U.S.A.

M. J. LIGHTHILL

Royal Aircraft Establishment, Farnborough, Hampshire, England

PROF. R. R. LONG

School of Engineering, The Johns Hopkins University, Baltimore 18, *Maryland, U.S.A.*

DR P. G. SAFFMAN

Department of Mathematics, King's College, London, W.C. 2, *England*

Authors wishing to have papers published in the JOURNAL should communicate them to any one of the persons named above, choosing one in their own country where possible.

Authors are urged to ensure that their papers are written clearly and attractively, in order that their work will be readily accessible to readers.

Manuscripts should be typed in double spacing on one side of the paper only, with references listed at the end in alphabetical order of authors. Drawings should be done on a large scale in Indian ink on tracing cloth or drawing paper, the lettering being shown clearly in pencil for reproduction by the printer; the list of captions should be typed at the end of the manuscript. Proofs of papers from overseas will usually be despatched to authors by airmail. There is no charge for publication. Authors are entitled to receive 50 offprints of a paper in the JOURNAL free of charge, and additional offprints can be purchased if ordered in advance.

SUBSCRIPTIONS

The subscription price for a volume of four parts is £5. 10*s*. net, post free, payable in advance; separate parts 30*s*. net, plus postage. Subscriptions may be sent to any bookseller, or to the Cambridge University Press, Bentley House, 200 Euston Road, London, N.W. 1.

Subscribers in the United States should send their orders to the Cambridge University Press, American Branch, 32 East 57th Street, New York 22. The subscription price per volume is $18.50, post free, payable in advance; separate parts $5.00, plus postage.

Quotations for available back volumes and parts may be obtained on application to the Cambridge University Press.

The Scientific Papers of Sir Geoffrey Ingram Taylor: II

Meteorology, Oceanography & Turbulent Flow

EDITED BY G. K. BATCHELOR

The second volume of *Scientific Papers* by Sir Geoffrey Taylor is the first of three devoted mainly to work on the mechanics of fluids. It will interest scientists concerned with fluid mechanics and also meteorologists, oceanographers and geophysicists. 526 *pages;* 167 *text-figures;* 3 *plates.*

75*s. net*

Turbulent Transfer in the Lower Atmosphere

C. H. B. PRIESTLY

Recent advances in the study of atmospheric disturbance near the ground are critically reviewed in this book. Much new material is included, and is relevant to fluid dynamics, oceanography and air pollution control as well as meteorology. UNIVERSITY OF CHICAGO PRESS. 28*s. net*

CAMBRIDGE STUDENTS' EDITIONS

An Introduction to Fourier Analysis & Generalised Functions

M. J. LIGHTHILL

10*s.* 6*d. net* (*cloth* 17*s.* 6*d. net*)

The Theory of Homogeneous Turbulence

G. K. BATCHELOR

18*s.* 6*d. net* (*cloth* 30*s. net*)

CAMBRIDGE UNIVERSITY PRESS

JOURNAL OF FLUID MECHANICS

Volume 9, Part 4 December 1960

CONTENTS

One-dimensional magnetogasdynamics in oblique fields
by J. A. SHERCLIFF *page* 481

Finite tidal waves propagated without change of shape
by F. K. BALL 506

Effects of a flexible boundary on hydrodynamic stability
by T. BROOKE BENJAMIN 513

Kinematic formulation of rotational gas flow
by M. VINOKUR 533

The flow due to a two-dimensional jet issuing parallel to a flat plate
by R. A. SAWYER 543

The method of images in shear flow
by M. B. GLAUERT 561

Stability of a conducting rotating fluid of variable density
by S. P. TALWAR 581

An example of steady laminar flow at large Reynolds number
by IAN PROUDMAN 593

On a circular cylinder in a steady wind at transition Reynolds numbers
by JOHN S. HUMPHREYS 603

Third-order blast wave theory and its application to hypersonic flow past blunt-nosed cylinders
by R. J. SWIGART 613

The stability of a viscous fluid between rotating cylinders with an axial flow
by R. C. DIPRIMA 621

REVIEWS

The Gulf Stream: A Physical and Dynamical Description 632

Viscoelasticity: Phenomenological Aspects 634

Hypersonic Flow 636

INDEX TO VOLUME 9 639

1651

Printed in Great Britain at the University Press, Cambridge
(Brooke Crutchley, University Printer)